Hydrogel Nanoparticles from Supercritical Technology for Pharmaceutical and Seismological Applications

by

Melinda Graham Hemingway

A dissertation submitted to the Graduate Faculty of
Auburn University
in partial fulfillment of the
requirements for the Degree of
Doctor of Philosophy

Auburn, Alabama
December 13, 2010

Keywords: Nanoparticles, Supercritical, Carbon Dioxide, High Pressure, Hydrogel, Miniemulsion Polymerization, Drying, Mesalamine, Zinc Oxide, Coating

Copyright 2010 by Melinda Hemingway

Approved by

Ram B. Gupta, Chair, Professor of Chemical Engineering
Christopher B. Roberts, Professor of Chemical Engineering
Elizabeth A. Lipke, Assistant Professor of Chemical Engineering
Jaychandra B. Ramapuram, Assistant Professor of Pharmacal Sciences

Abstract

This research focuses on hydrogel nanoparticle formation using miniemulsion polymerization and supercritical carbon dioxide. Hydrogel nanopowder is produced by a novel combination of inverse miniemulsion polymerization and supercritical drying (MPSD) methods. Three drying methods of miniemulsions are examined: (1) a conventional freeze drying technique, and (2) two supercritical drying techniques: (2a) supercritical fluid injection into miniemulsions, and (2b) the polymerized miniemulsion injection into supercritical fluid. Method 2b can produce non-agglomerated hydrogel nanoparticles that are free of solvent or surfactant (Chapter 2).

The optimized MPSD method was applied for producing an extended release drug formulation with mucoadhesive properties. Drug nanoparticles of mesalamine, were produced using supercritical antisolvent technology and encapsulation within two hydrogels, polyacrylamide and poly(acrylic acid-*co*-acrylamide). The encapsulation efficiency and release profile of drug nanoparticles is compared with commercial ground mesalamine particles. The loading efficiency is influenced by morphological compatibility (Chapter 3).

The MPSD method was extended for encapsulation of zinc oxide nanoparticles for UV protection in sunscreens (Chapter 4). ZnO was incorporated into the inverse miniemulsion during polymerization. The effect of process parameters are examined on absorbency of ultraviolet light and transparency of visible light. For use of hydrogel nanoparticles in a seismological application, delayed hydration is needed. Supercritical methods extend MPSD so that a hydrophobic coating can be applied on the particle surface (Chapter 5). Multiple analysis methods and coating materials were investigated to elucidate compatibility of coating material to polyacrylamide hydrogel. Coating materials of poly(lactide), poly(sulphone), poly(vinyl acetate), poly(hydroxybutyrate), Geluice 50-13, Span 80, octadecyltrichlorosilane, and perfluorobutane sulfate (PFBS)

were tested, out of which Gelucire, perfluorobutane sulfate, and poly(vinyl acetate) materials were able to provide some coating and perfluorobutane sulfate, poly(lactide), poly(vinyl acetate) delayed hydration of hydrogel particles, but not to a sufficient extent. The interactions of the different materials with the hydrogel are examined based on phenomena observed during the production processes and characterization of the particles generated. This work provides understanding into the interactions of polyacrylamide hydrogel particles both internally by encapsulation and externally by coating.

Acknowledgements

I would like to express my appreciation and gratitude to those who have assisted in my pursuit of this doctoral degree. Most notably, I would like to thank my professor, Dr. Ram B. Gupta, for his guidance, discussions, and support during this endeavor. His motivation and calm manner is much appreciated. I would like express sincere thanks to my committee members and my outside reader, Dr. Christopher Roberts, Dr. Elizabeth Lipke, Dr. Jaychandra Ramapuram and Dr. William Ravis for their valuable comments, encouragement, and suggestions. The work environment generated by prior laboratory colleagues Dr. Ganesh Sanganwar and Dr. Sandeep Kumar, and current colleagues Jin Heyang, Adam Byrd, Hema Ramsurn, Courtney Ober, and Dr. Lizhong Kong and undergraduate students for assistance and enjoyable moments during research is appreciated. I would like to thank Li Kang and Sateesh Sathigari for cooperation utilizing their laboratory equipment. I am grateful for the funding and support by the chemical engineering department and National Science Foundation. Thank you to Dr. Michael Miller and Brian Schweiker for technical assistance and amusing discussions. I am grateful to Aimee Poda for her friendship since my first semester on campus. I would also like to thank my parents, family and friends for providing comic relief and encouragement. Most sincerely, I thank my husband for his unwavering support, constant faith in me, and understanding, while laughing and enjoying life together through it all. At the end of the day, "my boys" make me smile.

One more check for our dreams' list. Let the adventures continue.

Table of Contents

List of Figures and Tables

1.0 INTRODUCTION

Supercritical fluid technology has extensive applications in diverse areas including particle formation, separation, and extraction. This dissertation research utilizes supercritical technology to solve problems in pharmaceutical and seismological applications as well as utilizing subjects such as hydrogels (Huglin 1986; Peppas 2000; Cai and Gupta 2002; Hynd 2007; Junginger 2007), polymerization (Daniels 1992; Antonietti and Landfester 2002; Rodriguez 2003), drying (Leuenberger 1987; Masters 1991; Broadhead 1992; Nail and Gatlin 1993; Giunchedi and Conte 1995; Pikal 2007), and coating (Hester 1990; Brock 2000; Bassett 2001; Goldschmidt and Streitberger 2003). This chapter introduces supercritical technology, nanoparticles and their formation by supercritical antisolvent technology, hydrogels and their formation by miniemulsion polymerization, drying, and coating with in-depth detail of projects presented in subsequent chapters. The key specific aims of this research are:

- produce surfactant and solvent free polyacrylamide nanopowder using miniemulsion polymerization and supercritical technology
- encapsulate material within hydrogel through processing with supercritical carbon dioxide providing insight into the interactions of hydrogel particles
- delay hydration of hydrogel particles by hydrophobic coating

1.1 Supercritical Fluids

A fluid becomes supercritical when heated and compressed beyond its critical point. The characteristic properties of supercritical fluids encountered in this region have similarities with both liquid and gas phases. Supercritical fluids have a lower viscosity than liquids with a high diffusivity similar to gases, which contributes to rapid mass and heat transfers. Characteristic diffusivity of a supercritical fluid is 10^{-3} cm^2/s compared to gases of 10^{-1} cm^2/s and 10^{-5} cm^2/s for liquids. The viscosity of a typical supercritical fluid is 10^{-4} g/cm/s, similar to gases, but 100-fold lower than typical viscosity of liquids. This combination of high diffusivity and low viscosity facilitates rapid equilibration. (Gupta 2005)

Phase diagrams provide a visual understanding of these unique characteristics for supercritical fluids. The critical point is the temperature and pressure at which a supercritical fluid is first incurred (Figure 1.1). Along the line from the triple point to the critical point, the density of the gas increases while the density of the liquid decreases until the critical point is reached where the two densities become equal to each other, leading to one phase termed as supercritical fluid. Temperatures and pressures greater than the critical point provide interesting phenomena: beyond this point greater compression cannot produce a liquid nor can added heat produce a gas. Examples of phase diagrams for water and carbon dioxide are shown in Figure 1.1.

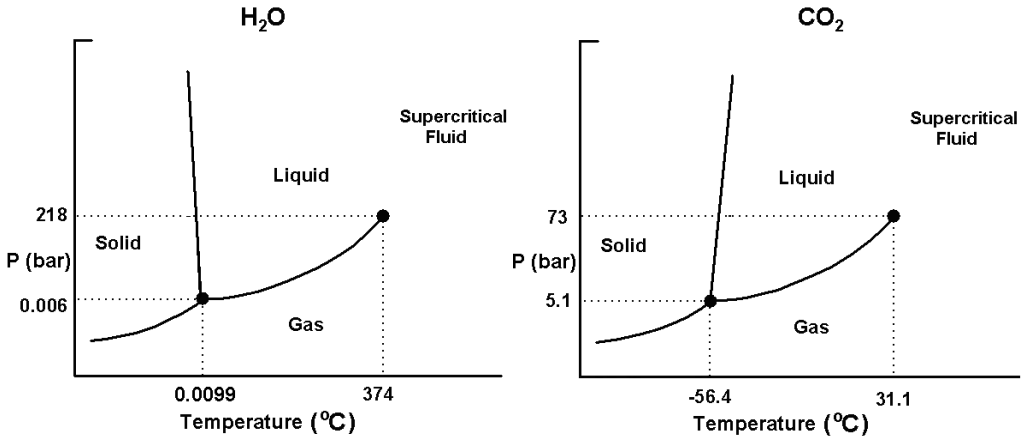

Figure 1.1 Phase diagrams of water (left) and carbon dioxide (right).

Small changes in pressure near the critical point can significantly affect fluid density, as shown in Figure 1.2; these phenomena can be beneficially utilized in a variety of applications. Comparing the different isotherms, the effect is more prominent closer to the critical point.

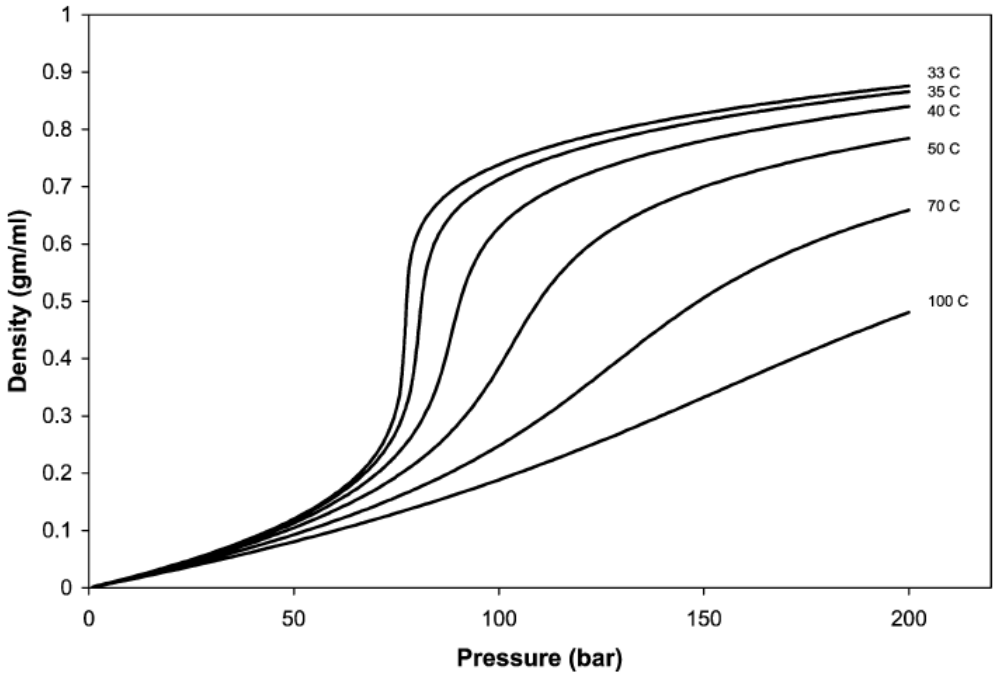

Figure 1.2 Density changes of carbon dioxide. (Gupta 2006)

Densities of common supercritical fluids, such as water or carbon dioxide, can be found at the *National Institute of Standards and Technology* webbook at *webbook.nist.gov/chemistry/(NIST).* Alternatively, the density, ρ, of carbon dioxide can be obtained from the following equation (Jouyban 2002) for a given temperature, T (K), and pressure, P (bars):

$$\rho = \frac{1}{44}\exp(-27.091 + 0.609\sqrt{T} + \frac{3966.170}{T} - \frac{3.445P}{T} + 0.401\sqrt{P} \quad \text{(Eq. 1.1)}$$

A list of selected supercritical fluids of interest given in Table 1.1.

Supercritical Fluid	T_c (˚C)	P_c (atm)	Safety hazard
Ethylene	9.3	49.7	Flammable gas
Ethane	32.3	48.2	Flammable gas
Chlorotrifluoromethane	28.9	38.7	—
Carbon Dioxide	31.1	72.8	—
Dinitrogen monoxide (laughing gas)	36.5	71.7	Not combustible but enhances combustion of other substances
Sulfur Hexafluoride	45.5	37.1	—
Propane	96.8	42.4	Extremely flammable
Ammonia	132.4	111.3	Flammable and toxic
Isopropanol	235.2	47.0	Highly flammable
Cyclohexane	280.3	40.2	Highly flammable
Toluene	318.6	40.6	Highly flammable
Water	374.0	212.7	—

Table 1.1 Supercritical solvent critical constants. (Gupta 2005)

Out of all these fluids, carbon dioxide is the supercritical fluid of choice in this work. Carbon dioxide is a relatively inexpensive, benign, and mild solvent to use for experimental and industrial applications. The critical point of carbon dioxide is mild for operational purposes at 73.8 bar and 31.1˚C. Carbon dioxide's non-flammable nature is advantageous over other more hazardous solvents, such as toluene or hexane to produce nanoparticles. Supercritical carbon dioxide is used in diverse applications ranging from natural product extraction, materials cleaning, and chemical reactions, to nanoparticle preparation and drying (Perrut 2000; Gupta 2006; Reverchon 2007; Gonen 2009).

Carbon dioxide (O=C=O) is a nonpolar molecule with some polarity due to its quadrapole moment. Solubility is a defining feature of how best to utilize supercritical carbon dioxide for a specific application. Small non-polar or slightly polar compounds are fully miscible with CO_2. Heavy and/or polar molecules are poorly soluble in

supercritical carbon dioxide, but the solubility of such compounds can be enhanced by adding a small amount (e.g., less than 10 wt.%) of cosolvent, such as acetone, methanol or ethanol (Dobbs 1987; Gupta 2005; Thakur and Gupta 2005). Solubility enhancement by using ethanol cosolvent in the extraction of fish oils at 60°C and 250 bar is shown in Figure 1.3 (Catchpole 2000; Gupta 2005).

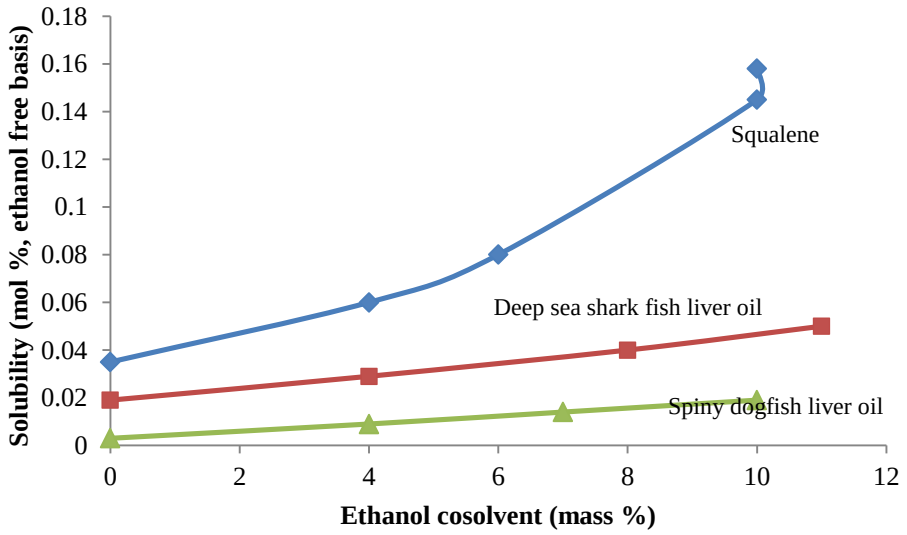

Figure 1.3 Enhancement of fish oil solubility in CO_2 by using ethanol cosolvent (adapted from (Catchpole 2000)

Carbon dioxide is the most widely studied and utilized supercritical fluid with significant industrial activity in the last 20 years (Beckman 2004). Cagniard de la Tour first discovered the supercritical phenomenon in 1822 and Hanney & Hogarth witnessed its solving power in 1879 (Eckert 1996). Supercritical fluids have found their way into a variety of commercial applications, including nicotine removal from tobacco, extraction of fragrances and flavors, dry cleaning, and plant wastewater treatment. Supercritical carbon dioxide ($scCO_2$) was first used for its extraction ability; one of the most commonly recognized is caffeine extracted from coffee beans to produce decaffeinated coffee.

1.2 Nanoparticles

Based on the definition from the National Nanotechnology Initiative (NNI 2009), a nanoparticle is deemed <100 nm in size, which is mostly applicable to hard inorganic substances, such as TiO_2 and ZnO. From a pharmaceutical prospective, nanoparticles can be viewed as particles less than 300 nm in size, as this is where the smaller particle size begins to increase the in-vivo bioavailability (Perrut 2003; Yasuji 2008). Pharmaceuticals, neutraceuticals, and polymers are "soft" materials and offer different challenges to form nanoparticles than the hard inorganic materials.

A fundamental enhancement over bulk material is that the nanoparticles have a higher surface area to volume ratio contributing to numerous unique properties suitable for many applications. In addition, the size reduction enables drug molecules to interact on a more appropriate sized level; comparable to rubbing an ant's leg with human fingers versus microscopic tweezers. These interaction scales of physical, chemical and biological phenomena become comparable to the size of the particle where new properties and phenomena emerge (Roco 1999). Nanoparticles can play a key role in poorly-water soluble drug, where many issues still exist due to the poor bioavailability (Perrut 2003).

Nanoparticles can be produced either by "top-down" or a "bottom-up" approach. In the top-down approach nanoparticles can be obtained by grinding, which has limitations to the smallest particle size and yield obtainable. Conventional grinding can lead to plasticizing of polymers through unintentional heating. Bottom-up approaches for producing nanoparticles include emulsification, homogenization, supercritical fluid precipitation, and wet synthesis.

1.3 Nanoparticle Production using Supercritical Carbon Dioxide Antisolvent

Supercritical carbon dioxide is commonly used in variety of techniques to generate nanoparticles. A defining feature of the chosen method to produce particles is the characteristic solubility of the drug in $scCO_2$, either as a solvent or an antisolvent. For compounds that are soluble in $scCO_2$, or solvent based $scCO_2$ techniques include rapid expansion of supercritical solution (RESS), rapid expansion of supercritical solution into liquid solvent (RESOLV), and rapid expansion of supercritical solution into aqueous suspension (RESAS). For the compounds that are insoluble in scCO2, antisolvent techniques include supercritical antisolvent (SAS), supercritical antisolvent with enhanced mass transfer (SAS-EM), and gas atomization system (GAS). Numerous articles are in the literature regarding these particle formation technologies (York 1999; Jung and Perrut 2001; Charbit 2004).

Supercritical carbon dioxide technology is utilized in antisolvent nanoparticle formation processes due to its innate ability to extract the solvents including methanol, acetone, dichloromethane, and dimethyl sulfoxide) that carry the drug compounds. A polymer can be coprecipitated along with the drug to obtain controlled release formulation (Martin 2002; Bandi 2004). The increased mass and heat transfer of supercritical fluids enables extraction of the carrier solvent in the antisolvent process (Werling and Debenedetti 1999; Mukhopadhyay and Dalvi 2004; Martín 2007).

Supercritical antisolvent techniques (GAS, SAS, SAS-EM, and SEDS) vary mostly by the way the drug solution is introduced to $scCO_2$ (Werling and Debenedetti 1999; Reverchon 2007). Supercritical antisolvent method is capable of producing nanosized particles depending on the process parameters (Reverchon and Adami 2006). SAS and SAS-EM utilize a countercurrent flow of $scCO_2$ to use the solving power of carbon dioxide with a polar liquid solvent (Figure 1.4). SAS-EM utilizes the injection nozzle in contact with the tip of an ultrasonic horn. The ultrasonication increases the mass transfer and dispersion compared to normal SAS and oftentimes produces smaller particles. Solution enhanced dispersion by supercritical fluids (SEDS) introduces carbon dioxide to the drug solution co-currently into a vessel. In all supercritical particle formation

methods, multiple parameters can be optimized to attain a desired particle size. Pressure, temperature, injection nozzle diameter, supercritical fluid flow rate, drug solution flow rate, drug solution concentration, and ultrasound amplitude (in case of SAS-EM) have an effect on the size of particles produced.

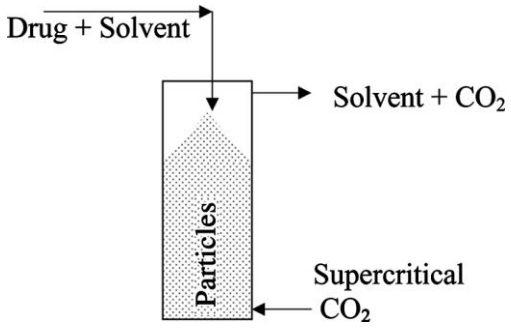

Figure 1.4 General SAS process. (Gupta 2006)

1.4 Hydrogels

A hydrogel is defined as "a hydrophilic polymer network that can swell and retain large amounts of water while maintaining its three dimensional shape" (Cai and Gupta 2002). Superabsorbent hydrogels can absorb up to 400 times its weight in water. The superabsorbent capability of hydrogels is a defining feature for utilization which is primarily controlled by the degree of crosslinking. The higher the crosslinkage the tighter the hydrogel is bound and the less swelling capability.

The ability to absorb significant amount of water contribute to hydrogel's diverse applications in diagnosis, drug delivery, separation, absorption, agriculture, waterproofing, and water retention (Cai and Gupta 2002). Hydrogels can be composed of naturally crosslinked materials, such as cellulose, starch, gelatin, and sodium alginate, polysaccharide, or synthetic polymers, such as poly(acrylamide) (PAM), poly(acrylic acid) (PAA), poly(methyl methacrylate) (PMMA), poly(ethylene glycol) (PEG), poly(vinyl alcohol), poly(*N*-vinyl 2-pyrrolidone) (PVP) and poly(hydroxy ethyl methacrylate) (pHEMA). Many hydrogels are approved by the US Food and Drug Administration (FDA) and a few by the Environmental Protection Agency (EPA) for use

in agriculture, consumer products and pharmaceuticals (Cai and Gupta 2002). Hydrogels are produced by various polymerizations techniques: emulsions, gaseous, bulk, suspensions, solution, and plasma. This research produces polyacrylamide and poly(acrylic acid) hydrogels through a miniemulsion polymerization technique.

1.5 Hydrogel Formation by Miniemulsion Polymerization

Miniemulsion polymerization is similar to emulsion polymerization where a disperse phase, continuous phase, and surfactant are present in the initial steps (Figure 1.6). The surface energy. E_S, of the droplets is related to the interfacial tension, σ, between the continuous and disperse phases by Equation 1.6

$$E_S = N\sigma\pi d^2 \qquad \text{(Eq. 1.6)}$$

where N is the number of droplets and d is droplet diameter of the disperse phase. Surface energy is also related to the volume of the dispersed phase, V_D, by substituting the relation of the number of droplets, $N = 6V_D/(\pi d^3)$ into Equation 1.6 yielding

$$E_S = \frac{6V_D\sigma}{d} \qquad \text{(Eq. 1.7)}$$

The overall particle size generated in miniemulsion is attributed to the ultrasonication shear forces and surfactant content. The limited use of surfactant reduces the interfacial tension of the two phases in minemulsions to about 40 mN/m; for comparison, the surface tension in microemulsions, utilizing heavy amounts of surfactants, are near zero. The incomplete surface coverage by surfactant in a miniemulsion generates a critically stabilized suspension. Most emulsions are metastable colloids, except for microemulsions which have zero surface tension and use excess surfactant above critical micellar concentration. The critical micelle concentration is the point where micelles are formed spontaneously and depends upon the type of surfactant.

Emulsions (miniemulsions, microemulsions, regular emulsions, and suspension emulsions) are not classified solely based on the particle size generated but also based on the process generating particles (Figure 1.5). Similar to suspension emulsions, the polymerized particles of miniemulsions maintained the size of the original droplets formed during the initial production process and are often considered microreactors. In microemulsions, complete surfactant coverage of monomer droplets coexist with empty micelles; with this complete coverage, initiation cannot be obtained in all droplets simultaneously. The first polymer chains are formed in some droplets leading to an increase of the droplet size, the formation of empty micelles, and secondary nucleation. In regular emulsions, the latex particle does not correspond to the primary emulsion droplet instead the monomer diffuses into larger monomer droplets through the continuous phase to micelles to sustain polymer particle growth until the monomer droplets have vanished; kinetic parameters such as the temperature, the amount of initiator, nucleation rate as well as nanoparticle stability play a predominant role. Microemulsions and regular emulsions are similar in that original droplet size is not the same as the polymer particle formed. Antonietti and Landfester (2002) provide an in-depth comparison of polymerization in microemulsions, miniemulsions, regular emulsions, and suspension emulsions.

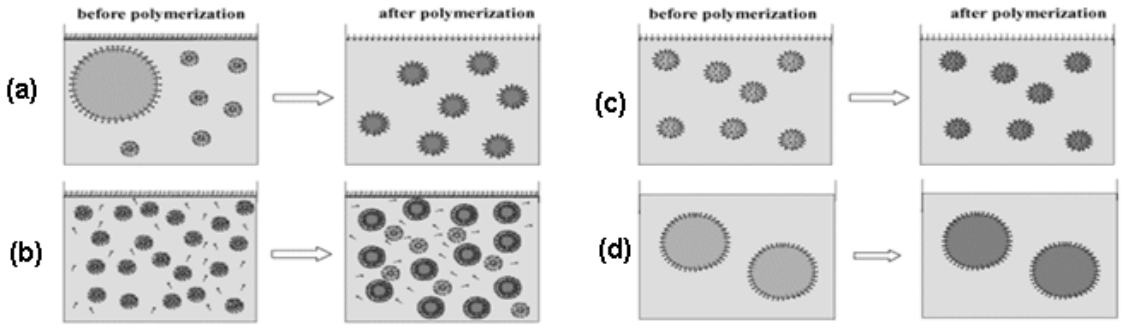

Figure 1.5 Emulsion overview: a) Emulsion (>100nm), b) Microemulsion (5-50nm), c) Miniemulsion (30-500nm), d) Suspension emulsion (1µm-1mm) (adapted from Antonietti and Landfester 2002)

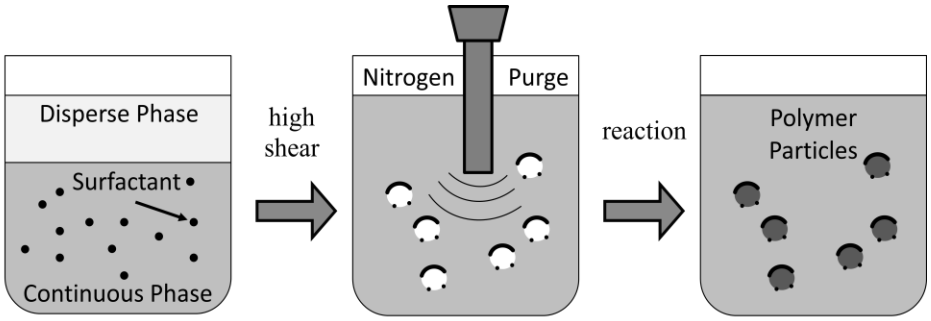

Step I Step II Step III

Figure 1.6 Miniemulsion process: Step I-Immiscible continuous and disperse phases with surfactant are mixed; Step II-High shear with an ultrasonication horn forms droplets with incomplete surfactant coverage; Step III-Reaction produces polymerized nanoparticles.

The miniemulsion polymerization (Figure 1.6) allows the formation of polymer particles with complex structures, such as nanoparticles, nanocapsules, and nanoprecipitates, and the encapsulation of many different materials (organic and inorganic pigments, magnetic and solid nanoparticles, hydrophobic and hydrophilic liquids, such as fragrances, drugs, or photoinitators (Antonietti and Landfester 2002; Xu 2004)). These interesting structures arise due to the placement of the components during polymerization. For example, nanoparticles which are more hydrophobic than the monomer can be dispersed in the monomer phase before miniemulsion polymerization. Miniemulsion copolymerization of hydrophobic and hydrophilic monomers located in different phases can occur with a surface active initiator (Landfester 2000; Willert and Landfester 2002; Blagodatkikh 2006). Otherwise, the initiation can be activated by heat, ultrasound, ultraviolet light, or redox chemical for production of free radicals to react with the monomers and crosslinkers to produce hydrogel.

Relevant to this work, poly(acrylamide) and poly(acrylic acid) hydrogel particles are formed by using an inverse-miniemulsion free radical vinyl polymerization by thermal initiation. Alternatives utilize a surfactant free emulsion method which is not suitable for thermally sensitive material (Yin and Chen 2004) or surface modification to prevent stickiness of the material (Jayasundera 2009). This work builds upon the prior studies

that have generated hydrogel particles of polyacrylamide and other polymers (Willert and Landfester 2002; Capek 2003; Xu 2004; Blagodatkikh 2006; Zhang and al. 2006).

1.6 Research Work

In Chapter 2, polyacrylamide hydrogels are produced using an inverse (water-in-oil, w/o) miniemulsion polymerization, but unlike previous research, this work develops a robust supercritical drying technique to obtain free flowing, non-agglomerated, surfactant-free nanoparticles. In Chapter 3, mesalamine particles generated by supercritical antisolvent process are encapsulated in hydrogel nanoparticles for sustained drug release. The Chapter 4 deals with the effects of hydrogel nanoparticles containing zinc oxide nanoparticles for sunscreen protection application. Chapter 5 deals with the hydrophobic coating of hydrogel nanoparticles so that the hydration can be delayed for proposed seismological application. Conclusions of this dissertation work are given in Chapter 6, and the possible future research ideas are listed in Chapter 7.

1.7 References

Antonietti, M. and K. Landfester (2002). "Polyreactions in miniemulsions." Progress in Polymer Science **27**(4): 689-757.

Bandi, N., R. Gupta, et al., Eds. (2004). Supercritical Fluid Technology for Drug Product Development. New York, Marcel Dekker.

Bassett, D. R. (2001). "Hydrophobic Coatings from Emulsion Polymers." The Journal of Coatings Technology **73(**912): 43.

Beckman, E. J. (2004). "Supercritical and near-critical CO2 in green chemical synthesis and processing." Journal of Supercritical Fluids **28**(2-3): 121-191.

Blagodatkikh, I., V. Tikhonov, et al. (2006). "New Approach to the Synthesis of Polyacrylamide in Miniemulsified Systems." Macromolecular Rapid Communications **27**(22): 1900-1905.

Broadhead, J., S. K. E. Rouan, et al. (1992). "The spray drying of pharmaceuticals." Drug Development and Industrial Pharmacy **18**(11): 1169-206.

Brock, T., M. Grotelaes, et al. (2000). European coatings handbook. Hannover, Germany, Vincent Verlag.

Cai, W. and R. B. Gupta (2002). Hydrogels. Kirk-Othmer Encyclopedia of Chemical Technology (5th Edition) **13:** 729-754.

Capek, I. (2003). Designed Monomers and Polymers **6**(4): 399-409.

Catchpole, O. J., J. B. Grey, et al. (2000). "Fractionation of fish oils using supercritical CO2 and CO2+ ethanol mixtures. ." Journal of Supercritical Fluids **19**(1): 25-37.

Charbit, G., E. Badens, et al. (2004). Methods of particle production. Supercritical Fluid Technology for Drug Product Development. Y. Peter, B. K. Uday and S. Boris. New York, Marcel Dekker**:** 367-410.

Daniels, E. S., E. D. Sudol, et al., Eds. (1992). Polymer Latexes - Preparation, Latexes, and Applications. ACS Symposium Series. Washington, D.C., American Chemical Society.

Dobbs, J. M., J. M. Wong, et al. (1987). "Modification of supercritical fluid phase behavior using polar cosolvents." Ind. Eng. Chem. Res. **26**(1): 56-65.

Eckert, C. A., B. L. Knutson, et al. (1996). Nature **383**.

Giunchedi, P. and U. Conte (1995). "Spray-drying as a preparation method of microparticulate drug delivery systems: an overview." S.T.P.Pharmaceutical Sciences **5**: 276-290.

Goldschmidt, A. and H.-J. Streitberger (2003). BASF Handbook on Basics of Coating Technology. Hannover, Germany, BASF Coatings AG.

Gonen, M., D. Balkose, et al. (2009). "Supercritical Carbon Dioxide Drying of Methanol-Zinc Borate Mixtures." Industrial & Engineering Chemistry Research **48**(14): 6869-6876.

Gupta, R. B. (2005). Supercritical Fluid Extraction. Encyclopedia of Chemical Processing, Marcel Dekker.

Gupta, R. B. (2006). Supercritical fluid technology for particle engineering. . Nanoparticle Technology for Drug Delivery. R. B. Gupta and U. B. Kompella, Drugs and the Pharmaceutical Sciences. **159** 53-84.

Hester, C. I., R. L. Nicholson, et al. (1990). Powder coating technology. Park Ridge, New Jersey, Noyes Data Corporation.

Huglin, M. B., M. M. A. M. Rehab, et al. (1986). "Thermodynamic interactions in copolymeric hydrogels." Macromolecules **19**(12): 2986-2991.
Hynd, M., J. A. Turner, et al. (2007). "Applications of hydrogels for neural cell engineering." J Biomater Sci. Polymer Edn **18**(10): 1223-1244
Jayasundera, M., B. Adhikari, et al. (2009). "Surface modification of spray dried food and emulsion powders with surface-active proteins: A Review." Journal of Food Engineering **93**: 266-277.
Jouyban, A. R., M., B. Y. Shekunov, et al. (2002). "Solubility prediction in supercritical CO2 using minimum number of experiments." Journal of Pharmaceutical Science **91**(5): 1287-1295.
Jung, J. and M. Perrut (2001). "Particle design using supercritical fluids: literature and patent survey." Journal of Supercritical Fluids **20**: 179-219.
Junginger, H. E., J. C. Verhoef, et al. (2007). Drug Delivery: Mucoadhesive Hydrogels. Encyclopedia of Pharmaceutical Technology**:** 1169-1200.
Landfester, K., M. Willert, et al. (2000). "Preparation of Polymer Particles in Nonaqueous Direct and Inverse Miniemulsions." Macromolecules **33**: 2370-2376.
Leuenberger, H. (1987). Process of drying a particulate material and apparatus for implementing the process. US, 4,608,764.
Martín, A., A. Bouchard, et al. (2007). "Mathematical modeling of the mass transfer from aqueous solutions in a supercritical fluid during particle formation." Journal of Supercritical Fluids **41**(1): 126-137.
Martin, T. M., N. Bandi, et al. (2002). "Preparation of budesonide and budesonide-PLA micropartilces using supercritical fluid precipitation technology." AAPS Pharm Sci Technol **3**(3).
Masters, K. (1991). Spray Drying Handbook. New York, John Wiley & Sons.
Mukhopadhyay, M. and S. V. Dalvi (2004). "Mass and heat transfer analysis of SAS: effects of thermodynamic states and flow rates on droplet size." The Journal of Supercritical Fluids **30**(3): 333-348.
Nail, S. L. and L. A. Gatlin (1993). Freeze drying: principles and practice. New York, Marcel Dekker, Inc.
NIST. "National Institute of Standards and Technology." from webbook.nist.gov/chemistry/.
NNI. (2009). "National Nanotechnology Initiative." from www.nano.gov.
Peppas, N. A., P. Bures, et al. (2000). "Hydrogels in pharmaceutical formulations. ." European Journal of Pharmaceutics and Bioplarmaceutics. **50**: 27-46.
Perrut, M. (2000). "Supercritical fluid applications: industrial developments and economic issues." Ind. Eng. Chem. Res. **39**(12): 4531- 4535.
Perrut, M. (2003). "Supercritical fluids applications in the pharmaceutical industry." STP Pharma Sciences **13**(2): 83-91.
Pikal, M. J. (2007). Freeze Drying. Encyclopedia of Pharmaceutical Technology. J. Swarbrick. Pinehurst, NC., Informa Healthcare USA, Inc. **1**.
Reverchon, E. and R. Adami (2006). "Nanomaterials and supercritical fluids. ." Journal of Supercritical Fluids **37** 1-22.
Reverchon, E., I. De Marco, et al. (2007). "Nanoparticles production by supercritical antisolvent precipitation: A general interpretation." J. Supercritical Fluids **43**: 126-138.

Roco, M. C. (1999). "Nanoparticles and nanotechnology research." J.ournal of Nanoparticle Research **1**(1): 1-6.
Rodriguez, F., C. Cohen, et al. (2003). Principles of Polymer Systems. New York, New York, Taylor & Francis Books, Inc.
Thakur, R. and R. B. Gupta (2005). "Rapid Expansion of Supercritical Solution with Solid Cosolvent (RESS-SC) Process: Formation of Griseofulvin Nanoparticles. ." Industrial & Engineering Chemistry Research **44**(19): 7380-7387.
Werling, J. O. and P. G. Debenedetti (1999). "Numerical modeling of mass transfer in the supercritical antisolvent process." J. Supercritical Fluids **16**: 167-181.
Willert, M. and K. Landfester (2002). "Amphiphilic Copolymers from Miniemulsified Systems." Macromolecular Chem. Phys. **203**: 825-836.
Xu, Z. Z., et al. (2004). "Encapsulation of nanosized magnetic iron oxide by polyacrylamide via inverse miniemulsion polymerization." Journal of Magnetism and Magnetic Materials. **277**: 136-143.
Yasuji, T., H. Takeuchi, et al. (2008). "Particle design of poorly water-soluble drug substances using supercritical fluid technologies." Adv Drug Delivery Reviews **60** 388-98.
Yin, N. and K. Chen (2004). "Ultrasonically initiated emulsifier-free emulsion copolymerization of n-butyl acrylate and acrylamide. Part I: Polymerization mechanism." Polymer **45**: 3587-3594.
York, P. (1999). "Strategies for particle design using supercritical fluid technologies." Pharmaceut. Sci. Technol. Today **2**: 430-440.
Zhang, D. and e. al. (2006). J. Phys. Chem B **110**: 9079-9084.

2.0 HYDROGEL NANOPOWDER PRODUCTION BY INVERSE-MINIEMULSION POLYMERIZATION AND SUPERCRITICAL DRYING

Hydrogel nanoparticles can be successfully produced by polymerization in inverse miniemulsions, for use in a variety of applications including diagnosis, drug delivery, separation, soil stabilization, and absorption. Unfortunately, conventional drying techniques result in agglomerated powder due to the sticky nature of the wet hydrogel particles. This work utilizes supercritical CO_2 drying to obtain free flowing hydrogel nanoparticles. Polyacrylamide hydrogel nanoparticles (~100 nm in diameter) are produced in an inverse miniemulsion composed of cyclohexane continuous phase, water dispersed phase, and a nonionic surfactant. The polymerized miniemulsion is dried by injecting into supercritical CO_2 which results in rapid removal of cyclohexane, water, and surfactant. The morphology, particle size and size distribution of the nanoparticles are determined using dynamic light scattering and scanning electron microscopy. The proposed miniemulsion polymerization supercritical drying (MPSD) method produces hydrogel nanopowder with much lower agglomeration or residual surfactant as compared to convention drying. In addition, the MPSD method produced solvent-free nanoparticles due to efficient extraction by supercritical CO_2.

2.1. Introduction

Hydrophilic polymeric networks of hydrogels can absorb water multiple times their own weight contributing to diverse applications in diagnosis, drug delivery, separation, absorption, agriculture, waterproofing, water retention, and soil stabilization (Cai and Gupta 2002). Environmentally benign, inexpensive, and readily available, hydrogels can be composed of naturally cross-linked materials, such as cellulose, starch, and sodium alginate, or synthetic polymers, such as poly(methyl methacrylate), poly(acrylic acid), poly(ethylene glycol), poly(hydroxy ethyl methacrylate), and polyacrylamide. Hydrogel nanoparticles can be synthesized using a miniemulsion polymerization, a technique that

utilizes less surfactant than in microemulsion polymerizations, instead the miniemulsion technique utilizes ultrasonication or intense mixing to create small droplets prior to polymerization (Antonietti and Landfester 2002; Anton 2008; Landfester 2009). Hence, the key difference from microemulsion is the microemulsion utilizes greater surfactant concentration (i.e., above the critical micelle concentration) to produce low surface tension enabling a stable emulsion. Studies so far have generated hydrogel particles of polyacrylamide and other polymers (Willert and Landfester 2002; Capek 2003; Xu 2004; Blagodatkikh 2006; Zhang and al. 2006), but did not develop a robust drying technique in order to obtain free flowing, non-agglomerated, surfactant-free nanoparticles.

Available methods for drying of emulsions include freeze-drying (Nail and Gatlin 1993; Pikal 2007; Packhaeuser 2009), spray-drying (Masters 1991; Broadhead 1992; Giunchedi and Conte 1995; Muller 2000; Gavini 2004; Lane 2005), or derivatives thereof, such as freeze-spray-drying (Merryman 1959; Leuenberger 1987; Heneczka 2006; Wang 2006). Unfortunately, these drying techniques when applied to nanoparticles result in particle agglomeration especially due to the sticky nature of the wet hydrogel nanoparticles (Brinker and Scherer 1990). Drying is an important step in determining particle agglomeration which contributes to bulk powder flow properties. In addition, the residual surfactant can affect the final hydrogel properties; for example, it can affect the drug release rates (Kapoor and Chauhan 2008). In addition, the existing methods do not completely remove the surfactant. To obtain surfactant-free product, either the emulsion without surfactant is utilized which results in large particle size, or the polymer is rinsed with a high amount of solvent in dialysis prior to drying.

Supercritical carbon dioxide (above 73.8 bar and 31.1 ^{o}C) has been utilized in a variety of extraction processes. Organic solvents and some non-ionic surfactants are readily soluble in supercritical CO_2 (Gupta and Shim, 2007), thus the products can be easily separated. For example, in supercritical fluid extraction of emulsion (SFEE), an oil-in-water (o/w) emulsion is injected into supercritical carbon dioxide producing an aqueous suspension of drug particles; the drug is first dissolved in the oil droplets (Shekunov 2006; Chattopadhyay 2007); the suspension is further freeze dried to obtain powder.

In this work, acrylamide monomer is polymerized in water-in-oil miniemulsion to produce hydrogel nanoparticles. The polymerized hydrogel nanoparticles are contained in the water droplets. The miniemulsion is then dried using supercritical CO_2. This work examines the proposed miniemulsion polymerization and supercritical drying (MPSD) method, specifically the effect of polymerization and drying conditions on the final hydrogel nanoparticles properties (i.e., size, morphology, particle flowability, and residual surfactant and solvent contents).

2.2. Materials and Experimental Methods

Electrophoresis grade (99+% pure) acrylamide and N,N-methylenebisacrylamide were obtained from Acros Organics. Azoisobutyronitrile (AIBN) and sorbitan monooleate were obtained from Sigma Aldrich. HPLC grade isopropanol, cyclohexane, and water were obtained from Fisher Scientific. All materials were used as received to produce hydrogel nanoparticles by a two-step procedure: inverse-miniemulsion polymerization followed by supercritical drying (MPSD), as described below.

2.2.1 - Step I: Inverse-miniemulsion polymerization

A schematic of the inverse-miniemulsion polymerization is shown in Figure 2.1. Here, the continuous phase consists of cyclohexane and sorbitan monooleate (Span 80) surfactant, and the dispersed phase is composed of water, acrylamide monomer, and N,N-methylenebisacrylamide (MBA) crosslinker. Disperse phase was dropwise added to the continuous phase with sonication at 10-14˚C. Subsequently, the initiator, azoisobutyronitrile (AIBN) was added and stirred at 150 rpm, and the emulsion is purged with nitrogen to remove dissolved oxygen which otherwise can scavenge free radicals needed for polymerization. Typical amounts used are: 24 g cyclohexane, 0.75 g Span 80, 2.25-3.0 g water, 2.25 g acrylamide, 22.5 mg MBA, and 75 mg AIBN. The miniemulsion is then heated to 65 ^{o}C to decompose AIBN (which occurs at 60 ^{o}C) producing free radicals. As shown in Figure 2.2, the polymerization mechanism begins with the initiator thermally decomposing into free radicals which then react with the vinyl

group in the acrylamide monomer for free radical polymerization. The reaction proceeds for 2 hours with stirring at 150 rpm. Several factors, such as the solubility of the polymer, the type and concentration of the surfactant, agitation speed, and drop wise addition rate, can affect the final properties of emulsified polymer particles.

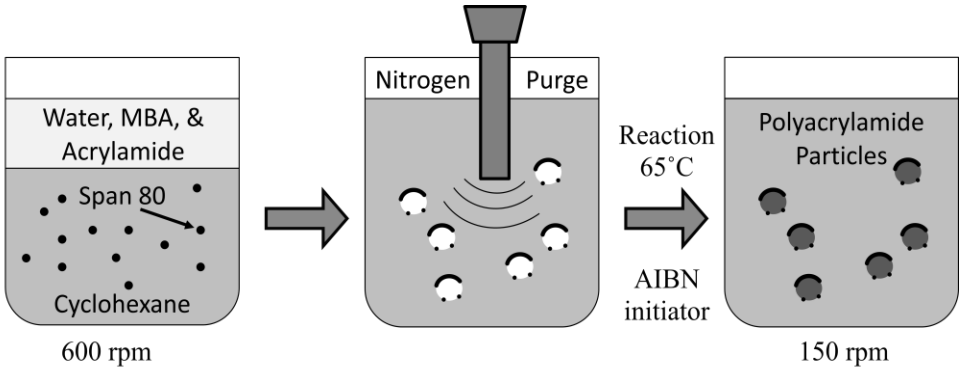

Figure 2.1. Inverse-miniemulsion polymerization to produce hydrogel nanoparticles

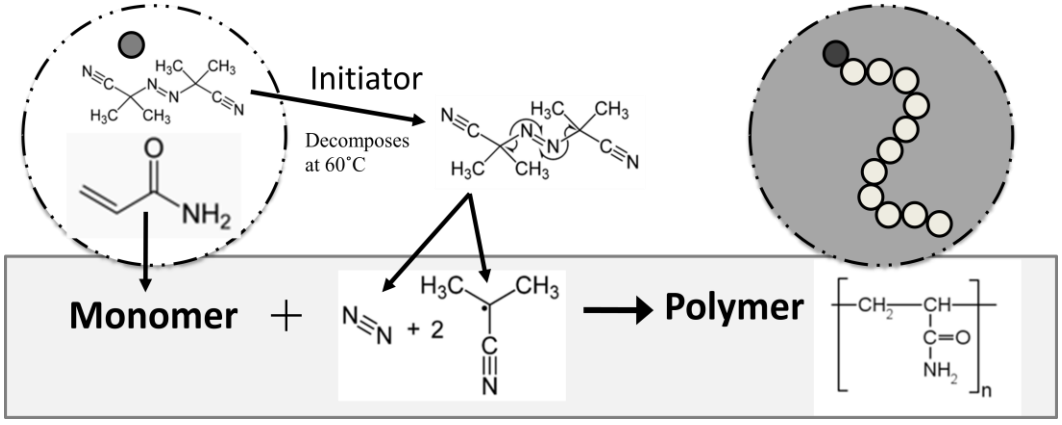

Figure 2.2. A free radical polymerization reaction mechanism

2.2.2 - Step II: Supercritical drying

Three different methods of drying the synthesized hydrogel nanoparticles were tested as shown in Figure 2.3: (a) conventional freeze drying, (b) supercritical CO_2 injection into the miniemulsion, and (c) miniemulsion injection into supercritical CO_2. Freeze-drying was carried out in a manifold drying apparatus for a minimum of 24 hours and maximum of 48 hours. The supercritical drying is shown in Figure 2.4. Supercritical CO_2 flowed through the 100 ml high pressure vessel continuously and maintained at 40˚C. A double fluoropore membrane filter (0.025 µm and 0.2 µm pore sizes) was mounted on the outlet line from the high pressure vessel to prevent loss of dried hydrogel powder. A heated back pressure regulator was used to maintain 1600 psi pressure in the system. A vent nozzle of 150 µm internal diameter was utilized to sustain slow depressurization at a maximum rate of 2.5 ml/min after flushing with carbon dioxide. For supercritical drying by miniemulsion injection, the polymerized suspension was loaded on one side of the injection vessel while pressure is applied to the other side of the piston to inject the contents into the high pressure vessel through a PEEKsil nozzle. For supercritical CO_2 injection into the miniemulsion, the injection system was not utilized, as CO_2 was directly injected into the preloaded miniemulsion in the vessel.

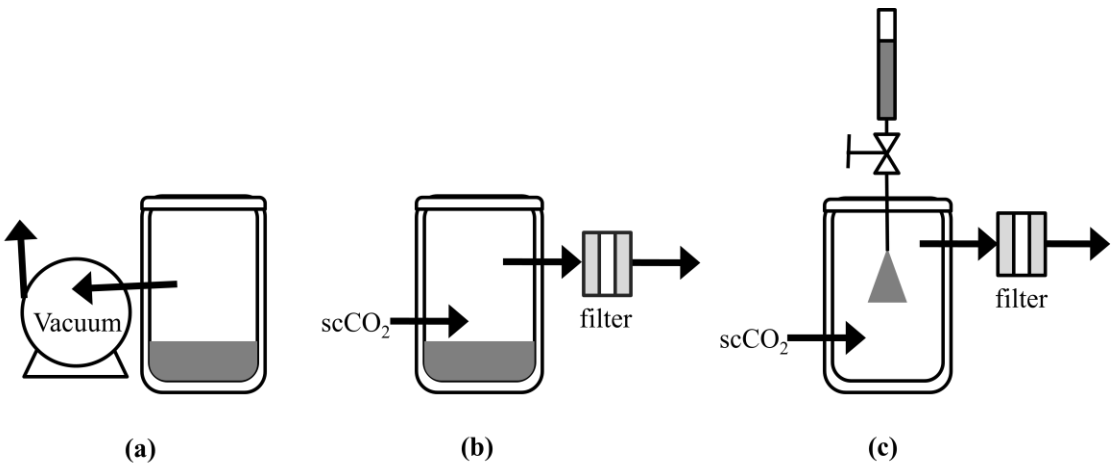

Figure 2.3. Drying of miniemulsion polymerization (a) Freeze-drying, (b) Drying by supercritical CO_2 injection into miniemulsion, and (c) Drying by miniemulsion injection into supercritical CO_2 (supercritical drying)

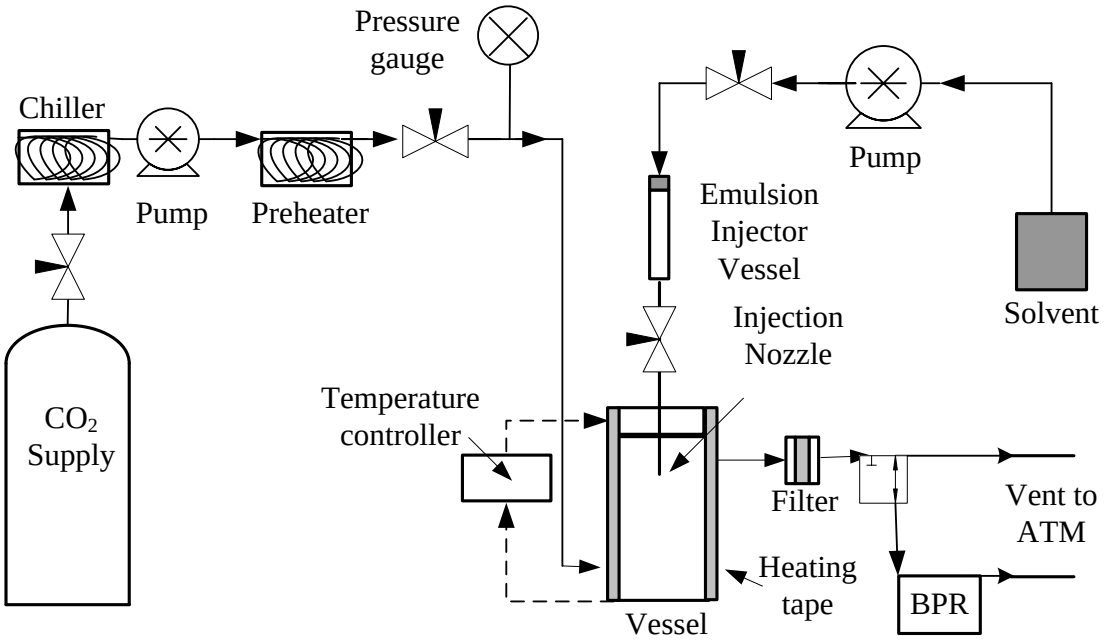

Figure 2.4. Supercritical drying process flow diagram

2.2.3. Hydrogel particle characterization.

Nicolet IR100 Fourier transform infrared (FTIR) spectrometer was utilized to confirm polymerization of acrylamide to polyacrylamide. NICOMP 380 (Particle Sizing System) dynamic light scattering (DLS) instrument was used to determine the hydrodynamic diameters of particles. Zeiss EVO 50 scanning electron microscope (SEM) was used to obtain micrographs of particles that were sputter coated with a 15 nm layer of gold by an EMS 550X gold sputter coater. Residual solvent in the particles was measured using a QIR 5000 thermogravimetric analyzer which is coupled with a mass spectrometer and NIST version 2005 spectral library. Residual surfactant in the particles was measured using a Waters HPLC system with a UV dual absorbance detector.

2.3. Results and Discussion

This study investigates the effect of various process parameters on hydrogel nanopowder production, specifically the particle size and morphology, and residual solvent and surfactant contents.

2.3.1. Miniemulsion polymerization. Confirmation of polymerization during miniemulsion polymerization can be inferred from the FTIR spectra shown in Figure 5. The functional group C=C in the monomer acrylamide vibrates at 980 cm^{-1} wavelength showing two peaks in this region. Upon polymerization, both of these peaks disappear confirming the conversion of the vinyl groups. Additional peaks shown are due to C=O at 1630-1700 cm^{-1}, NH_2 deformation at 1550 cm^{-1}, and primary amides at 1420-1400 cm^{-1}.

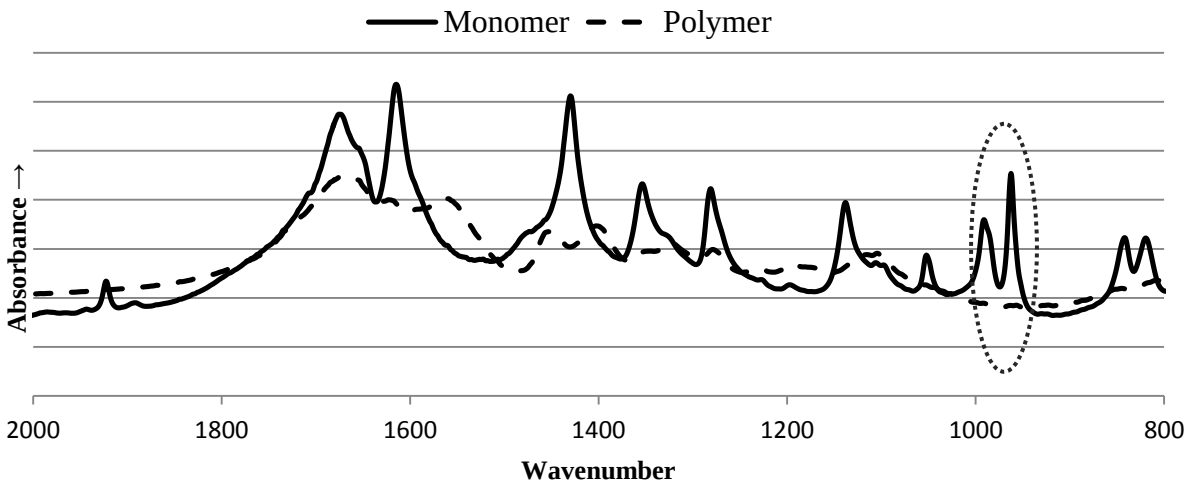

Figure 2.5. FTIR spectra of acrylamide monomer and polyacrylamide polymer

The emulsion droplet size can be influenced by the extent of shear and the amount of surfactant used. A sonicator set at 10% amplitude (about 60 W power) was used for 20 minutes in both continuous and pulsed (5 second off and 5 second on cycle) modes utilizing two different tips (12.7 and 19 mm diameters). The effects of ultrasonic tip size in a control study consisting of 3g water, 24g cyclohexane, and 0.75g surfactant found the 12.7-mm tip used in pulsed mode produced smallest and most consistent particles

(316.4 nm in size) compared to the 19-mm tip (435.7 nm in size) in a control study. During sonication the miniemulsion was kept in the chilled water bath maintained at 12 ^{o}C to remove heat produced. The duration of sonication did not significantly change particle size from 15 minutes to 20 minutes.

The particle size was observed to reduce significantly with an increase in the surfactant amounts with respect to disperse phase, consistent with the previous studies (Antonietti and Landfester 2002; Anton 2008; Landfester 2009). The effect of surfactant was tested at 1%, 3.3% and 5 wt% concentrations which gave volume-averaged particle size of 899, 411, and 150 nm, respectively. A recipe consisting of 0.75 g surfactant and 2.25 g water produced desired particle size of less than 200 nm; hence this recipe was preferred for most of the experiments. Hydrodynamic sizes of the polyacrylamide particles prior to drying using the preferred recipe was 74 nm (number average) and 155 nm (volume average) as shown in Figure 6. The particle size distribution shows two peaks attributed to the presence of either a small degree of clustering of the smaller particles or a few larger particles as seen in the number weighted distribution where the second peak is minimal (1.4%) as compared to the volume weighted average (38.9%). The effect of water content was tested at two levels. When the amount of water was reduced from 3.0 to 2.25 g keeping 0.75 g surfactant constant, the particle size reduced significantly from 133 to 74 nm in number-average or 356 to 155 nm in volume-average. In fact, out of all the steps and variables involved in the process, the surfactant amount with respect to water content in the disperse phase appears to be the most influential parameter determining particle size.

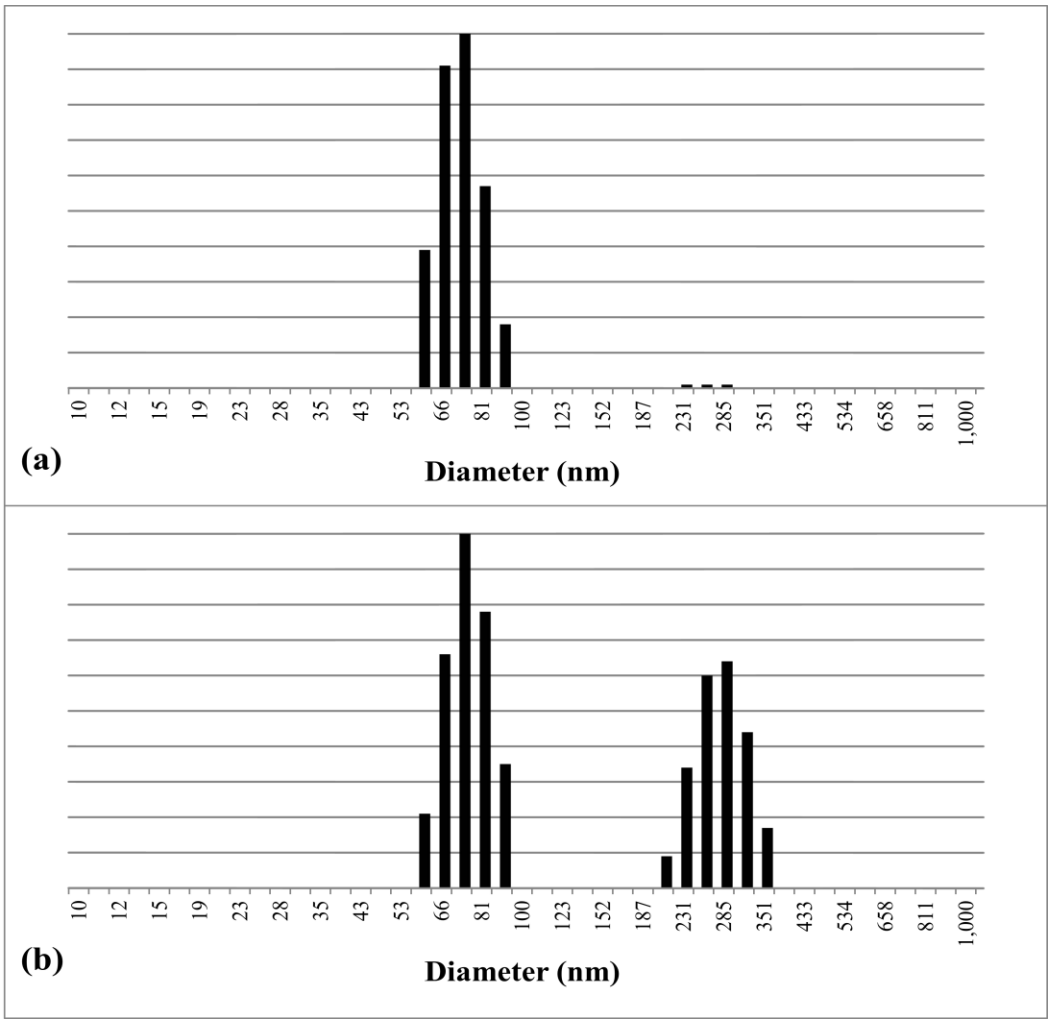

Figure 2.6. Hydrogel particle size distribution prior to drying, from dynamic light scattering: (a) number-weighted and (b) volume-weighted

2.3.2. Drying of polymerized miniemulsion. In the case of freeze drying technique, the emulsion was freeze-dried for a minimum 24 hours directly after polymerization. The particles obtained appear to be molded and fused together as a film (Figure 7a). Individual particles were not observed due to the presence of surfactant. The bulk samples were sticky and clumpy with a distinct yellow coloration due to visible surfactant. The powder is not free flowing.

When using supercritical CO_2 injection into the emulsion, the particles are also fused together, as shown in Figure 7b. In this technique, polymerized emulsion is first placed in the vessel and then the vessel is pressurized with supercritical CO_2. The precipitation

of particles from the emulsion occurs gradually as CO_2 expands cyclohexane. The precipitated particles are still wet when they come in contact with each other, causing particle fusion. The features of individual particles can be seen more clearly here than those from freeze drying. However the powder is still not free flowing and a portion is in the form of a film. As the cyclohexane extraction by CO_2 continues, hard films are formed giving mass transport resistance to the remaining interior material. The residual surfactant softened and fused the particles together.

In the case of miniemulsion injection into supercritical CO_2 (supercritical drying), the injection nozzle atomizes the liquid into small droplets from which cyclohexane, water and surfactant are rapidly extracted by CO_2. The fast extraction causes the particles to harden before coming into proximity, avoiding fusion. The final product is obtained as individual particles (Figure 7c), with excellent particle flow characteristics. Particles obtained by varying the nozzle diameter (254, 384, 502 μm internal diameter) did not significantly influence the particle size. However, in some experiments 254 μm nozzle clogged and 502 μm nozzle produced aggregated needle-like structures composed of polymerized spheres. Due to the lack of jet breakup in the 502 μm nozzle, needle-like particles were produced that were of the similar diameter as the nozzle internal diameter. The 384 μm nozzle generated the best powder consistently without obstruction and was thus utilized for subsequent evaluation of other process parameters. The emulsion flow rates of 0.25, 0.5, and 0.8 ml/min were tested and did not show any effect on the particle size. It was observed that a CO_2 to emulsion mass flow ratio of about 20:1 should be maintained to obtain hydrogel nanoparticles of good quality.

The general characteristics of the hydrogen particles obtained from the three drying methods are compared and summarized in Table 1.

Drying technique	Characteristics
Freeze drying	Surfactant film present Poor flow properties Sticky powder Particles are not distinct
Supercritical CO_2 injection into the miniemulsion	Surfactant film present Poor flow properties Some distinct particles underneath film
Miniemulsion injection into supercritical CO_2	No visible surfactant film Good flow properties Spherical particles

Table 2.1. Characteristics of the hydrogel powders obtained from three drying techniques

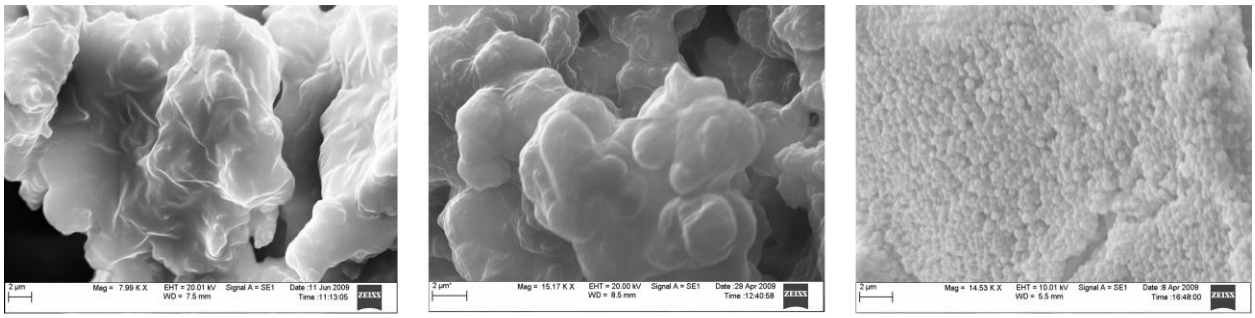

(a) **(b)** **(c)**

Figure 2.7. Hydrogel particles obtained from (a) freeze-drying, (b) supercritical CO_2 injection into miniemulsion, and (c) miniemulsion injection into supercritical CO_2 (supercritical drying)

2.3.3. Removal of solvent and surfactant. Solvent and surfactant are removed by supercritical CO_2 extraction. Cyclohexane and the small amount of water (about 7.6 wt.% of total materials utilized present in the inverse miniemulsion) are easily extracted by CO_2. The solubility data for the Span 80 surfactant is not available in the literature. To evaluate if this surfactant can be extracted along with cyclohexane, a controlled miniemulsion consisting of only cyclohexane, water, and surfactant was injected at 0.5 ml/min into the high pressure vessel with carbon dioxide flowing continuously at 15 g/min. At the end of extraction, out of 238 mg of surfactant injected, only 2.8 mg remained in the vessel providing confidence that supercritical carbon dioxide can extract the surfactant.

The hydrogel powder obtained from the supercritical drying (i.e., miniemulsion injection into CO_2 method), was analyzed for residual solvent by thermogravimetric analysis with mass spectrometer (TGA-MS). The temperature was ramped initially at 85˚C for 20 minutes and later 110˚C for 10 minutes (Figure 8). In the attached mass spectrometer, cyclohexane, if present, would show up at 84, 56, or 41 m/e ratios. As shown in Figure 9, there was no detectable amount of cyclohexane in the powder. The peak at 18 m/e is due to moisture present in the hydrogel. Even the powders that were oven dried and then subject to TGA-MS analysis showed this peak for water, which could be attributed to the facts that hydrogel quickly absorbs water from humid laboratory air prior to the analysis due to its strong hygroscopic nature, and the high sensitivity of the TGA-MS instrument.

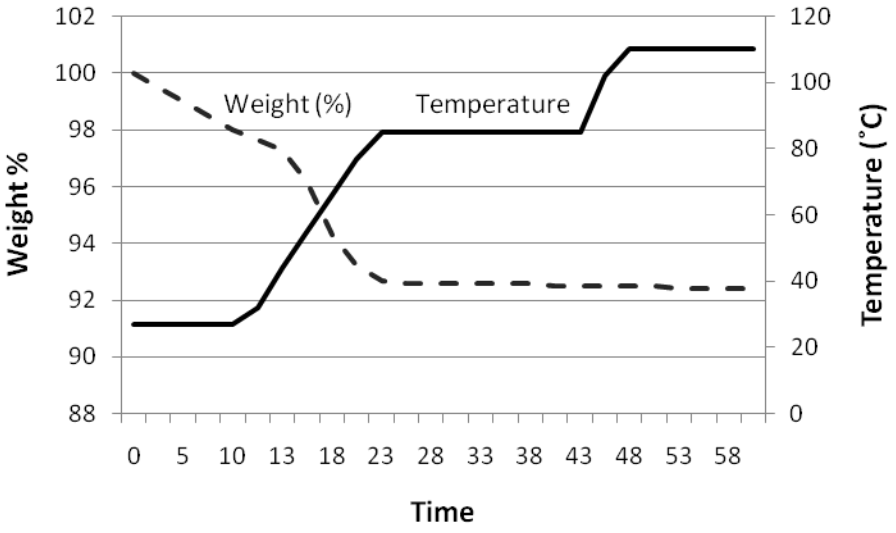

Figure 2.8. Thermogravemetric analysis of the hydrogel nanoparticles

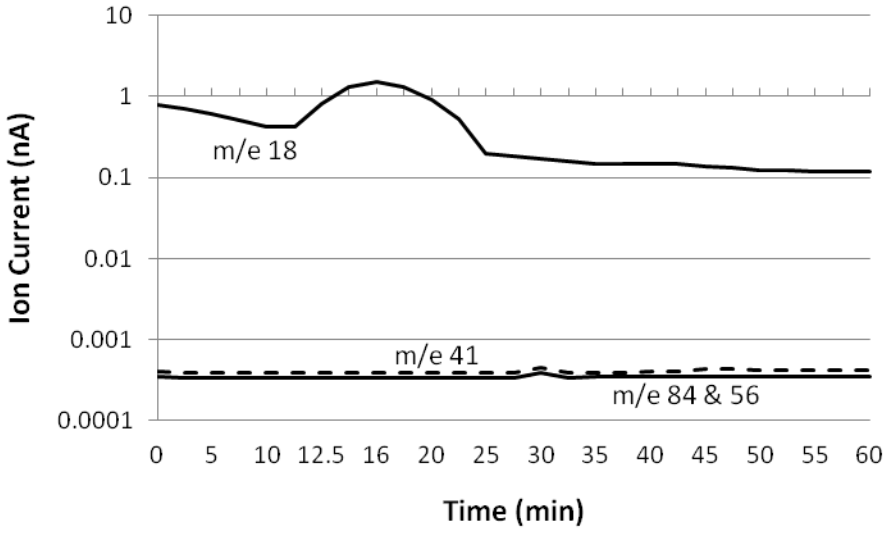

Figure 2.9. Mass-spectrometer data for residual solvent analysis

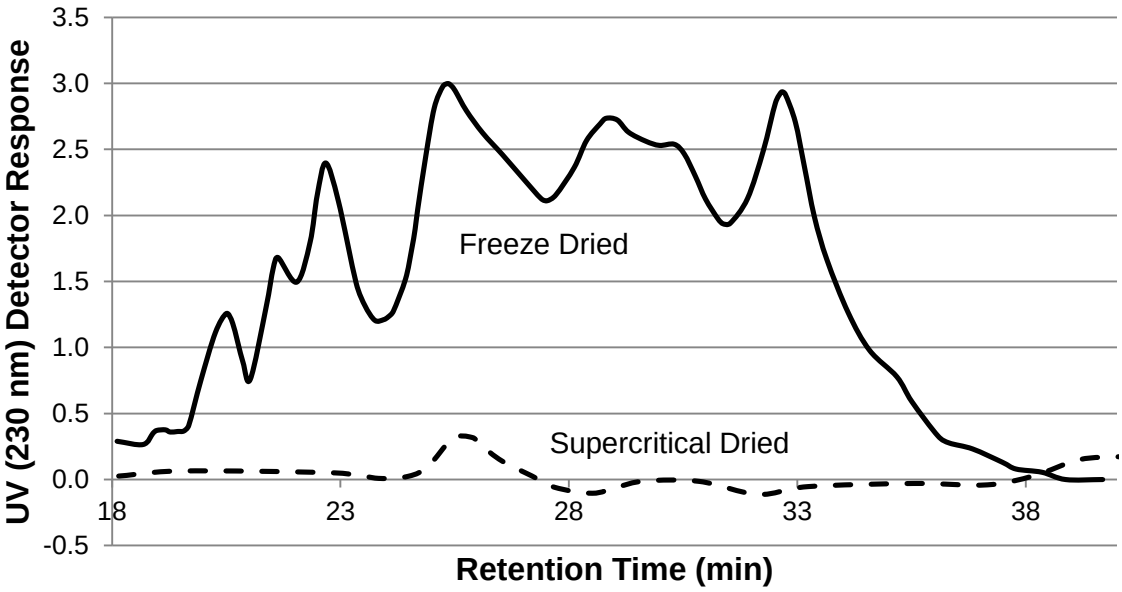

Figure 2.10. Typical HPLC results for surfactant remaining in (a) freeze-dried powder, and (b) supercritical-dried powder.

The residual surfactant in the hydrogel powder was analyzed using high-pressure liquid chromatography using isopropanol-water (60:40 vol%) mobile phase flowed at 0.5 ml/min through an Inertsil ODS 2 column (4.6x250mm) at 35˚C. Span 80 is made up of monoesters, diesters, triesters, and tetraesters components which create multiple peaks in the HPLC chromatogram; the standard calibration was based on the 230 nm absorbance peak area present in 18-35 minute retention time corresponding to the diester fraction of commercial Span 80. The dried hydrogel powder was washed with isopropanol to leach out surfactant. The supernatant was filtered by 0.2 μm filter to remove any suspended particles before injection into HPLC. As evident from the HPLC resultant data in Figure 10, the samples obtained from freeze drying showed a high surfactant content (area under curve of 1747.3 units), whereas supercritical CO_2 dried powder has a negligible surfactant amount (area under curve of 7.2 units). The efficient extraction of non-ionic Span 80 surfactant can be attributed to good solubility in supercritical CO_2 modified with cyclohexane present in the miniemulsion itself.

When applying the MPSD method to other water-in-oil (w/o) miniemulsions, a key aspect to consider is solubility of the combined surfactant and the organic continuous

phase in carbon dioxide. MPSD technology is expected to work well for the non-ionic surfactants which typically are more soluble in supercritical CO_2 than ionic surfactants(Gupta and Shim 2007).

2.4. Conclusions

Polyacrylamide hydrogel nanoparticles were successfully produced by the inverse miniemulsion polymerization and supercritical drying (MPSD) method. By injecting the polymerized miniemulsion into supercritical carbon dioxide, rapid removal of cyclohexane, water, and surfactant occurs, yielding a dry nanopowder. The produced nanopowder has better flow properties and lower agglomeration than those obtained from freeze-drying or CO_2 injection into miniemulsion method. In addition, the produced nanopowder is free of solvent and surfactant.

2.5 Literature Cited

(1) Cai, W.; Gupta, R. B. Hydrogels in *Kirk-Othmer Encyclopedia of Chemical Technology (5th Edition)* **2002,** *13*, 729-754.

(2) Landfester, K. Miniemulsion Polymerization and the Structure of Polymer and Hybird Nanoparticles. *Angewandte Chemie International Edition* **2009,** *48*, 4488-4507.

(3) Anton, N.; Benoit, J.-P.; Saulnier, P. Design and production of nanoparticles formulated from nano-emulsion templates - a review. *Journal of Controlled Release* **2008,** *128*, 188-199.

(4) Antonietti, M.; Landfester, K. Polyreactions in miniemulsions. *Progress in Polymer Science* **2002,** *27*, (4), 689-757.

(5) Xu, Z. Z.; Wang, C. C.; Yang, W. L.; Deng, Y. H.; Fu, S. K. Encapsulation of nanosized magnetic iron oxide by polyacrylamide via inverse miniemulsion polymerization. *Journal of Magnetism and Magnetic Materials* **2004,** *277*, 136-143.

(6) Capek, I. *Designed Monomers and Polymers* **2003,** *6*, (4), 399-409.

(7) Blagodatkikh, I.; Tikhonov, V.; Ivanova, E.; Landfester, K.; Khokhlov, A. New Approach to the Synthesis of Polyacrylamide in Miniemulsified Systems. *Macromolecular Rapid Communications* **2006,** *27*, (22), 1900-1905.

(8) Zhang, D.; Song, X.; Liang, F.; Li, Z.; Liu, F. *J. Phys. Chem B* **2006,** *110*, 9079-9084.

(9) Willert, M.; Landfester, K. Amphiphilic Copolymers from Miniemulsified Systems. *Macromolecular Chem. Phys.* **2002,** 203, 825-836.

(10) Nail, S. L.; Gatlin, L. A. *Freeze drying: principles and practice.* 2nd. ed.; Marcel Dekker, Inc.: New York, **1993**; Vol. 2.

(11) Pikal, M. J. Freeze Drying in *Encyclopedia of Pharmaceutical Technology*, 3rd ed.; Swarbrick, J., Ed. Informa Healthcare USA, Inc.: Pinehurst, NC., **2007**; Vol. 1.

(12) Packhaeuser, C. B.; Lahnstein, K.; Sitterburg, J.; Schmehl, T.; Gessler, T.; Bakowsky, U.; Seeger, W.; Kissel, T. Stabilization of Aerosolizable Nano-carriers by Freeze-Drying. *Pharmaceutical Research* **2009,** *26*, (1), 129-138.

(13) Lane, M. E.; Brennan, F., S.; Corrigan, O. I. Comparison of post-emulsification freeze drying or spray drying for the microencapsulation of plasmid DNA. *Journal of Pharmacy and Pharmacology* **2005,** *57*, (7), 831-838.

(14) Broadhead, J.; Rouan, S. K. E.; Rhodes, C. T. The spray drying of pharmaceuticals. *Drug Development and Industrial Pharmacy* **1992,** *18*, (11), 1169-206.

(15) Giunchedi, P.; Conte, U. Spray-drying as a preparation method of microparticulate drug delivery systems: an overview. *S.T.P.Pharmaceutical Sciences* **1995,** *5*, 276-290.

(16) Masters, K. *Spray Drying Handbook.* John Wiley & Sons: New York, 1991.

(17) Gavini, E.; Chetoni, P.; Cossu, M.; Alvarez, M. G.; Saettone, M. F.; Giunchedi, P. PLGA microspheres for the ocular delivery of a peptide drug, vancomycin using emulusification/spray-drying as the preparation method: in vitro/in vivo studies. *European Journal of Pharmaceutical Science* **2004,** *57*, 207-212.

(18) Muller, C. R.; Bassani, V. L.; Pohlman, A. R.; Michalowski, C. B.; Petrovick, P. R.; Guterres, S. S. Preparation and Characterization of Spray-Dried Polymeric Nanocapsules. *Drug Development and Industrial Pharmacy* **2000,** *26*, (3), 343-347.

(19) Wang, Z. L.; Finlay, W. H.; Peppler, M. S.; Sweeney, L. G. Powder formation by atmospheric spray-freeze-drying. *Powder Technology* **2006,** *170*, 45-52.

(20) Heneczka, M.; Baldyga, J.; Shekunov, B. Y. Modeling of spray-freezing with compressed carbon dioxide. *Chemical Engineering Sciences* **2006,** *61*, 2880-2887.

(21) Merryman, H. T. *Science* **1959,** *130*, 628-629.

(22) Leuenberger, H. Process of drying a particulate material and apparatus for implementing the process. **1987**.

(23) Brinker, C. J.; Scherer, G. W. *Sol-Gel Science: The Physics and Chemistry of Sol-Gel Processing*. Academic Press Inc.: San Diego, CA, **1990**; 501− 509.

(24) Kapoor, Y.; Chauhan, A. Drug and surfactant transport in Cyclosporine A and Brij 98 laden p-HEMA hydrogels. *Journal of Colloid and Interface Science* **2008,** *322* (2), 624-633.

(25) Shekunov, B. Y.; Chattopadhyay, P.; Seitzinger, J.; Huff, R. Nanoparticles of Poorly Water-Soluble Drugs Prepared by Supercritical Fluid Extraction of Emulsions. *Pharmaceutical Research* **2006,** *23* (1), 196-204.

(26) Chattopadhyay, P.; Shekunov, B. Y.; Yim, D.; Cipolla, D.; Boyd, B.; Farr, S. Production of solid lipid nanoparticle suspensions using supercritical fluid extraction of

emulsion (SFEE) for pulmonary delivery using the AERx system. *Advanced Drug Delivery Reviews* **2007,** *59*, 444-453.

(27) Gupta, R. B.; Shim, J.-J. *Solubility in Supercritical Carbon Dioxide*. Taylor & Francis Group: Boca Raton, FL, **2007**.

3.0 HYDROGEL NANOPARTICLES CONTAINING MESALAMINE DRUG

Hydrogel nanopowders with mesalamine, a drug commonly utilized to treat ulcerative colitis, were produced by polymerization in inverse miniemulsions and supercritical drying. Microparticles and nanoparticles of mesalamine produced from supercritical antisolvent technology were attempted to encapsulate into two types of hydrogels, poly(acrylamide) and a copolymer of poly(acrylic acid) and poly(acrylamide), and evaluated for encapsulation efficiency by high performance liquid chromatography. Complete polymerization was determined using Fourier transform infrared analysis. The morphology, particle size and size distribution of the nanoparticles were determined using dynamic light scattering and scanning electron microscopy. This study investigates details of a three step process to create mesalamine containing hydrogel nanopowders and the interactions between the hydrogels, the drug, and the effects of process parameters. These nanoparticles have a potential to improve local drug delivery to the affected areas within the colon utilizing the proven mucoadhesive properties of the hydrogel.

3.1. Introduction

Mesalamine is the first line therapy to treat mild to moderate colitis; ulcerative colitis affects between 250,000-500,000 in the United States each year (Cohen 2006). Mesalamine dosage forms include rectal enema, rectal suppository, extended-release oral capsule, and delayed-release capsule (based on Rowasa, Asacol, Pentasa, Lialda) (U.S. Food & Drug Administration 2010); however, rectal administration, though effective, is less appealing to general population and less adhered to than oral administration which is more natural, less invasive, and less expensive. Mesalamine has poor absorption into the colon with exception of the distal colon; this issue is not well understood but is thought to explain the low bioavailability. Over 80% of the rectally administered mesalamine ends

up excreted by urine. A longer exposure of the affected area to mesalamine could increase its therapeutic effect. To alleviate painful symptom flair-ups and minimize multiple dosages, this research examines two nanoparticle morphologies for localized delivery of mesalamine to the colon.

Forming drugs into nanoparticles can increase bioavailability by providing a high surface area, dissolution rate, and chemical potential while minimizing side effects (Jounela 1975; Liversidge and Cundy 1995; Rasenack and Muller 2002; Merisko-Liversidge and Liversidge 2008). Scientists are constantly trying to develop new technologies to increase the bioavailability of poorly water soluble drugs (Kharb 2006). Drug nanoparticles can be produced by supercritical technology (Gupta 2006; Reverchon 2007; Pasquali 2008), specifically, supercritical antisolvent (SAS) methods. Supercritical carbon dioxide has a mild critical point (73.8 bar and 31.1 ^{o}C), is relatively inexpensive, and offers easy removal by simple depressurization. Prior work produced tetracycline nanoparticles by supercritical antisolvent with enhanced mass transfer (SAS-EM) utilizing ultrasonication at the injection nozzle (Gupta and Chattopadhyay 2003). This research extends the injection duration from a smaller batch injection to a longer duration injection in SAS-EM to produce mesalamine nanoflakes and avoids potential overheating of the vessel by extended usage of ultrasonication.

Nanoflakes of mesalamine can be incorporated into a mucoadhesive material for extended drug release in the colon increasing localized therapeutic effect. A large number of studies examined mucosal potential of structural requirements of polymers for successful adhesion (Robinson and Park 1984; Park and Robinson 1985; Peppas and Buri 1985). Small particles may take advantage of mucosal membrane irregular surface morphology (cracks and crevices) while requiring only small adhesive interactions (Thairs 1998; Jackson 2000; Takeuchi 2001). Smart explains general mucoadhesion theory which occurs in two stages: 1) contact/wetting and 2) consolidation establishment of the adhesive interaction (Smart 2005). The adsorption is key for dosage, while consolidation is more important for high-stress environments.

Mucoadhesive materials are hydrophilic macromolecules containing numerous hydrogen bond forming groups (Smart 2005). Due to hydrogen bonding, poly(acrylic acid) provides a good mucoadhesion in the gastrointestinal tract. For example, poly(acrylic acid) particles (1-10 μm in diameter) have been found to widen the intercellular spaces of caco-2 cell monolayers (commonly used for evaluation of mucoadhesion) allowing improved transport into the mucus layer and potential drug delivery of the drug sulforhodamine (Kriwet and Kissel 1996). The mechanisms of mucoadhesion of poly(acrylic acid) and poly(acrylic acid-co-acrylamide) were investigated by Park and Robinson (1987) and for mucoadhesion to occur, polymers must have a minimum threshold of hydrogen bond ability (80% for vinyl concentration) and for poly(acrylic acid) with the presence of the carboxylic groups to obtain a critical quantity of hydrogen bonds 80% of carboxylic groups should be in the protonated state. Compared to polyacrylamide, poly(acrylic acid) will have more hydrogen bonding potential due to the presence of carboxyl groups. A higher crosslinked density of polymers exhibited a lower mucoadhesive capability (Park and Robinson 1987), thus a low crosslinkage amount was pursued in this work. In poly(acrylic acid-co-acrylamide) copolymers, the acrylic acid to acrylamide ratios of 80:20 or 75:25 provides a mucoadhesive similar to poly(acrylic acid), but drastically reduces at a 66:34 ratio, thus a copolymer ratio of 75:25 or higher was investigated for loading of mesalamine.

Copolymers such as poly(N-vinyl-2-pyrrolidone) and poly(acrylamide-co-maleic acid) oriented in cylindrical matrices showed promise for colon specific oral drug delivery of Vitamin B (Bajpai and Sonkusley 2002). Synthesis of bioadhesive poly(acrylic acid) microparticles using an inverse emulsion polymerization method for the entrapment of hydrophilic drug yielded promising results (Kriwet 1998). Macromolecules containing silyl groups of HEMA and MAA with crosslinkers BVPE and DVB were synthesized for colon specific drug delivery by Galehassadi though no particle size indications were mentioned but thorough dissolution profiles were studied (Galehassadi 2007). Mesalamine was incorporated into poly(N-vinyl-2-pyrrolidone, β-Cyclodextrine, and polyethylene glycol through a solid kneading method (Yadav and Yadav 2008). None of these studies show incorporation of drug nanoparticles within hydrogel nanoparticles.

Hydrogel nanoparticles produced in this research would have an increased probability to make contact and adhere to the mucosal lining of the wall, as nanoparticles flow closer to this surface than larger microparticles (Silebi and DosRamo 1989; Florence 2006). Hydrogel interacting with the mucosa lining prolong their residence time at the delivery location (Huang 2000; Peppas 2000). Peppas et. al provides a good review article for hydrogels in pharmaceutical applications. (Peppas 2000).

Targeting of mesalamine nanoparticles to the colon by the use of mucoadhesive hydrogel nanoparticles is the key feature for this study. The overall process to produce this novel drug delivery system involves three steps: 1) form mesalamine nanoparticles, 2) embed drug into hydrogel nanoparticles during polymerization, and 3) produce nanopowder by supercritical drying. This technology can be applied to drugs that can be wetted by water provided they are not soluble in the continuous phase solvent (i.e., cyclohexane or toluene) or supercritical carbon dioxide. Supercritical technology is employed twice in the process, final result yielding a water wetting drug embedded in a mucoadhesive hydrogel nanopowder matrix. The effects of adding mesalamine into this system, the efficiency of loading, and the interactions of two mesalamine morphologies with two polymers are examined.

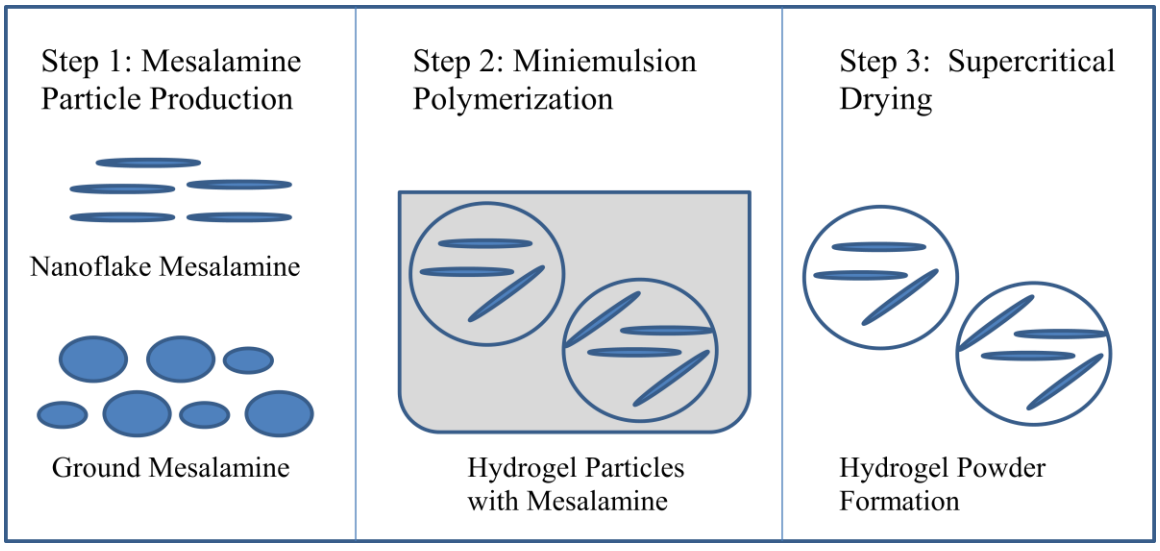

Figure 3.1. Mesalamine encapsulation process steps.

3.2 Materials and Analysis Methods

3.2.1 Materials

Materials for experiments were used as received from Fisher Scientific: cyclohexane (HPLC grade), water (HPLC grade), sorbitan monooleate (Span 80), azoisobutyronitrile (AIBN), N,N-methylbisacrylamide (MBA), acrylamide (99.9% electrophoresis grade), methanol (HPLC grade), hydrochloric acid, and potassium bromide. Micronized mesalamine USP was obtained from a pharmaceutical company. Bone dry carbon dioxide and nitrogen were obtained from AirGas. Acrylic acid 99.5% extra pure with 200 ppm monomethyl ether hydroquinone (MEHQ) was obtained from MP Biomedical. Additional HPLC materials include 1-heptanoic sulfuric acid sodium salt, acetonitrile (HPLC grade), methanol (HPLC grade), and KH_2PO_4. Primary materials of interest, mesalamine and monomers, are listed in Table 3.1.

Material	MW g/mol	T_m (˚C)	Structure
Mesalamine	153.13	283	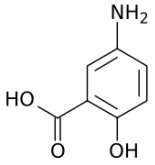
Acrylamide	71.08	84.5	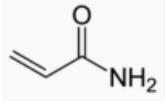
Acrylic Acid	72.06	14	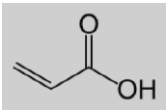

Table 3.1. Material structures and characteristics.

3.2.2 Analysis Methods

A NiComp 380 Particle Sizing System was used to obtain hydrodynamic particle distributions by dynamic light scattering. A Nicolet IR100 Fourier transform infrared (FTIR) spectrometer was utilized to confirm polymerization of vinyl monomer to polymer in potassium bromide (KBr) pellets. Zeiss EVO 50 scanning electron microscope (SEM) was used to obtain micrographs of particles that were sputter coated

with a 15 nm layer of gold by an EMS 550X gold sputter coater provided visual morphology and particle size. A NOVA 2200e by Quantachrome Instruments was utilized to obtain a 5-point BET analysis of mesalamine surface area after degassing samples overnight at 75°C.

For mesalamine encapsulation analysis, an HPLC method was developed based on Kersten's work (Kersten 1991). A mobile phase of KH_2PO_4 and heptanoic sulfuric sodium salt (890 ml), methanol (50 ml), and acetonitrile (30 ml) flowed at 1.2 ml/min through a Hypersil C8 column as stationary phase; 50 µL aliquots were injected and analyzed by UV at 220 nm wavelength. A calibration curve was established for mesalamine in a 10% 1*N* HCl solution from concentration range of 1 to 100 ppm. Potential residual interferences (monomer, crosslinker, initiator, surfactant, and polymer) were also evaluated. Mesalamine solutions were prepared by extracting mesalamine from the hydrogel powder using various 1*N* HCl solution, centrifuging (2 min at 3400 rpm), and filtering (0.2 µm syringe filter); these processed solutions were evaluated using this HPLC method. (Appendix E)

3.3 Experimental Methods

The production of the novel drug delivery system is composed of three steps:
1) nanoparticle production using supercritical antisolvent with enhanced mass transfer,
2) hydrogel production through miniemulsion polymerization while embedding drug nanoparticles, and 3) supercritical drying in carbon dioxide to produce nanopowder.

3.3.1- Step 1: Mesalamine Nanoflake Production

Three types of methods were employed to generate mesalamine particles: a supercritical antisolvent (SAS), a supercritical antisolvent with enhanced mass transfer (SAS-EM), and grinding with mortar and pestle. Supercritical antisolvent experiments were carried out using a small 100 ml high pressure vessel in a semi-continuous mode with a constant flow rate of carbon dioxide and batch injection of drug solution. Carbon dioxide flow rate during injection and purging ranged from 0.5 to 2 ml/min controlled by a T-valve. Total carbon dioxide volume flushed for purging was at minimum 350 ml at 1550 psi. A

5 ml injector vessel loaded with drug solution on one side of a piston and a methanol manual pump to induce 500 psi pressure gradient on the other side of injected the solution through the capillary nozzle. The drug solution injected was a 1.8 mg/ml concentration in a 5:1 by volume methanol:acetone solvent. A capillary nozzle of 100 µm was employed to inject the drug solution into the pressurized vessel. Multiple injections of the drug solution can be made in a given experiment from the 5 ml batch injector to increase drug production.

Continuous SAS-EM technology was employed to generate smaller nanoparticles in a high yield (Figure 3.2). Experiments consisted of multiple injections of the drug solution at a flow rate of 1 ml/min in the vessel maintained at 1600 psi and 35-42˚C. A 75 µm nozzle was utilized to continuously inject the mesalamine solution (1.8 mg/ml concentration in a 5:1 methanol:acetone by volume) unto a ¾" ultrasound tip while carbon dioxide flowed at 8-12 ml/min. Ultrasound was applied at constant 25% amplitude by a Sonics Vibra Cell Model VCX750. Batches of 40 ml solutions were injected allowing for a high production of nanopowders and the vessel flushed with CO_2 between batches. A back pressure regulator maintained pressure and was heated to prevent freezing and clogging of the outlet. With the utilization of continuous ultrasound as the nozzle injects the drug solution directly onto the ultrasonic horn tip, temperature monitoring was imperative for experiments during injection as dissipated ultrasound energy can increase the fluid temperature. The carbon dioxide was pumped with a Thar supercritical high pressure pump from a siphon tube tank to a series of coils submerged in a heated water bath of 35˚C. The 80 ml high pressure vessel equipped with two sapphire windows was maintained at 35˚C by an external heating tape, insulation, and temperature controller with a thermocouple located inside the vessel.

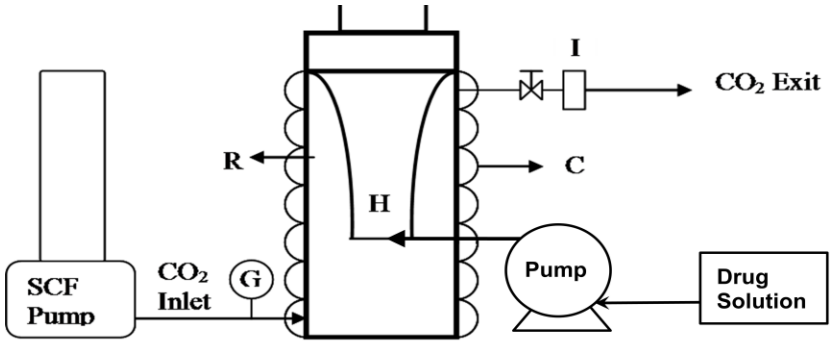

Figure 3.2. Supercritical antisolvent method. R: Precipitation chamber; SCF Pump: Supply of supercritical CO_2; I: Inline filter; H: Ultrasonic horn; G: Pressure gauge; C: Heating coil with temperature controller (Gupta 2006).

3.3.2 - Step 2: Inverse-Miniemulsion Hydrogel Formation

Successful polyacrylamide polymerization has been achieved in this laboratory (Hemingway 2010). The process and amounts are similar to the experimental design in Chapter 2 to produce nanoparticle hydrogel particles through inverse miniemulsion polymerization: continuous phase of 24 g cyclohexane and 0.75 g Span 80 with a disperse phase of 2.25 g water, 2.25 g monomer, 22.5 mg MBA, 75 mg AIBN and 0.112g mesalamine. Mesalamine particles were suspended in the dispersed aqueous phase by short ultrasonication (3 minutes total of 5s active and 5 s rest pulses 10% amplitude) in chilled water prior to drop wise addition into the continuous phase. Ultrasonication of 30 min (5 s active and 5 s rest 10% amplitude) completed the miniemulsion and heating to 65°C form polymer particles (Figure 3.3). Mesalamine is water wettable and not soluble in cyclohexane allowing for the incorporation of mesalamine into this process possible. Potential issues in this thermally initiated polymerization were avoided as mesalamine is a light sensitive and darkens with exposure to light.

Two separate monomers, acrylamide and acrylic acid, as well as a mixture of these monomers were evaluated for the production of hydrogel particles encapsulating mesalamine. Deviations in the above technique were not required for poly(acrylic acid) or poly(acrylic acid-*co*-acrylamide) (75:25) as their vinyl monomers are similarly polymerized by a free radical initiation based mechanism. The acrylic acid contains

monomethylether hydroquinone (MEHQ) to stabilize the monomer. MEHQ retards the rate of polymerization; however, Cutie et al mentions adding more initiator to overcome this phenomenon (Cutie 1996). The initiator amount of 75 mg AIBN was deemed to overcome the MEHQ in acrylic acid.

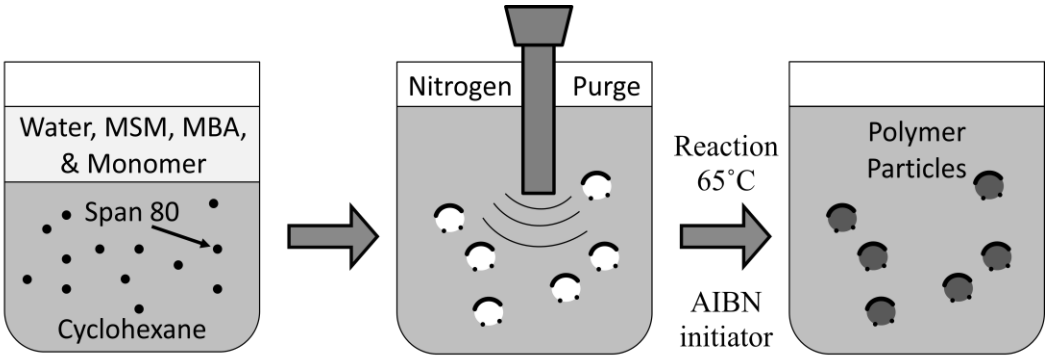

Figure 3.3. Miniemulsion process: Step 1-Immiscible continuous and disperse phases with surfactant are mixed; Step 2-High shear with an ultrasonication horn forms droplets with incomplete surfactant coverage; Step 3-Reaction produces polymerized particles.

3.3.3-Step 3: Supercritical Drying

Supercritical drying experiments were carried out in a 100 ml vessel similar to the methods and the optimized conditions determined in chapter 2 (40˚C, 1600psi, 384µm injection nozzle). Injection flow rate of solution was 0.5 ml/min with carbon dioxide flow rate greater than 18 ml/min for at least 2.5 hrs per injection. Pressure was maintained using a back pressure regulator (BPR) with slight heating to prevent freezing over of the outlet fluid (Figure 3.4).

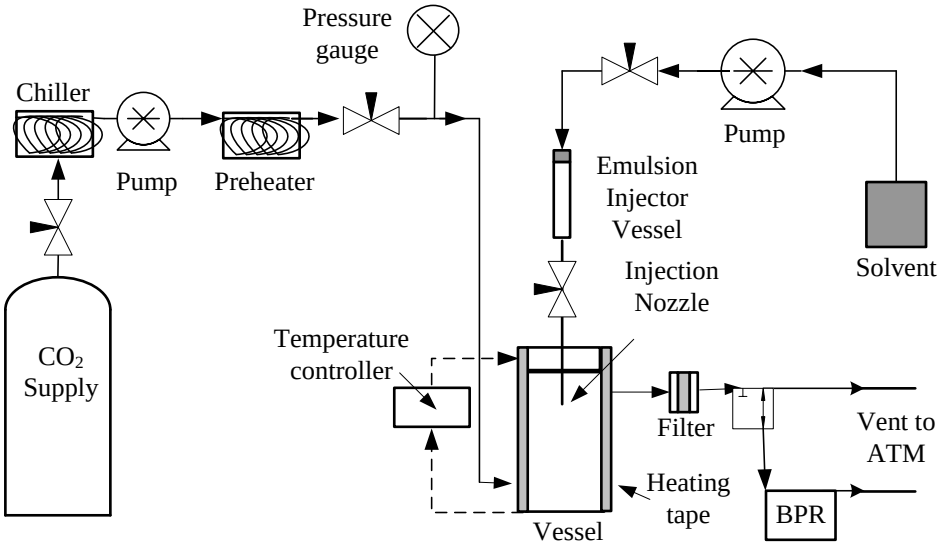

Figure 3.4. Supercritical drying process flow diagram

3.4. Results & Discussion

The production of mesalamine nanoparticles and the utilization of these in inverse miniemulsion polymerizations and supercritical drying of hydrogel particles are investigated. The effects of mesalamine on polymerization and efficiency of encapsulation within hydrogel particles are examined.

3.4.1 Mesalamine Nanoparticles from Supercritical Antisolvent Process

Particles produced by SAS-EM were smaller than those by SAS as evident by the SEM images in Figure 3.5. The nanoparticles produced by SAS are on average 5 μm in length and 250 nm in thickness which is larger than the SAS-EM nanoflakes at 1.1 μm in length and 98 nm in thickness. The jetting of the mesalamine solution through the nozzle onto the ultrasonic horn tip disperses the droplets more efficiently producing smaller particles (Chattopadhyay and Gupta 2002; Gupta and Chattopadhyay 2003). In this work a continuous operation is utilized instead of batch operation in the previous studies. In continuous operation, temperature control was an issue as ultrasonication can produce heat; this was managed by controlling the heating equipment. The temperature was maintained above critical temperature of CO_2 in the range 35- 42˚C. Ultrasound energy

utilization is expected to produce results similar to those of (Gupta and Chattopadhyay 2003). The majority of the mesalamine produced by SAS-EM was collected on the filter membrane as the CO_2 flow patterns carried small-sized particles to the exit line.

Surface area analysis of the mesalamine particles were conducted using a 5 point BET method. The SAS-EM nanoflakes had two analyses performed based on the location of sample collection in the vessel. First location of collection was from the filter membrane where the carbon dioxide exits. These nanoflakes were used for encapsulation in hydrogel and had 21.93 m^2/g surface area per mass; the particles are very long and flat. Other mesalamine particles were collected on the bottom of the vessel after multiple SAS-EM experiments and had a surface area to mass ratio of 11.65 m^2/g. Thus, the smaller particles generated flowed with the carbon dioxide to collect on the filter. These smaller nanoflakes were utilized for miniemulsions polymerization encapsulation.

The distinction between the morphology of the ground mesalamine and the nanoflakes is seen in Figures 3.5 and 3.6. The ground mesalamine consists of larger pieces as well as micronized pieces of indiscriminate shape whereas the mesalamine generated through SAS-EM are nano-thin flakes. Ground particles were generated by using a mortar and pestle on the commercial mesalamine. The average length and width of the smaller ground mesalamine particles are 350 nm and 225 nm, respectively; however, the overall ground mesalamine particles appear random in shape and size. The overall surface area of the ground particles is 7.54 m^2/g by BET. Simplified estimations are provided of the two mesalamine particle geometries for nanoflakes as flat elliptical cylinder and smaller ground particles as long rounded rods (Figure 3.7).

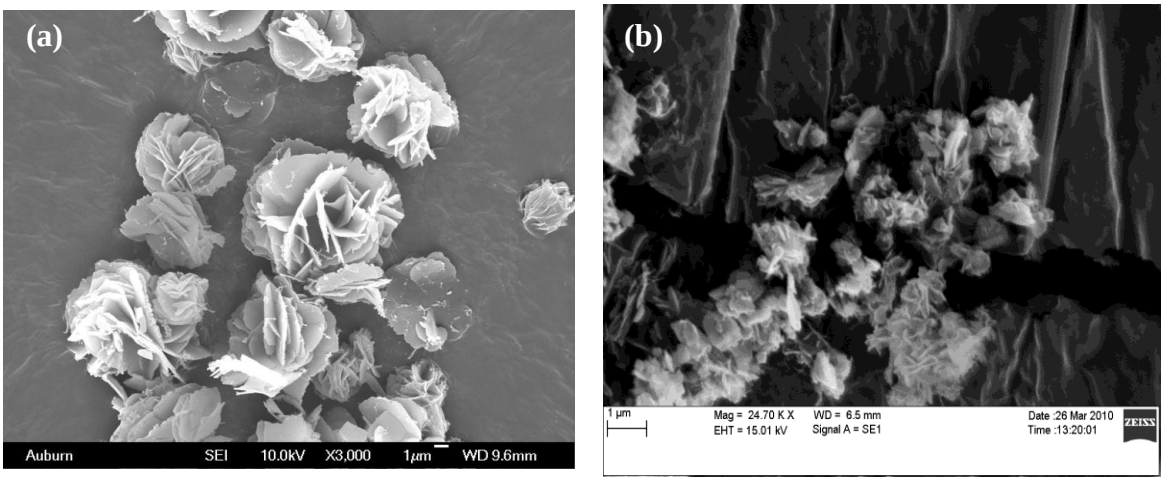

Figure 3.5. Mesalamine particles produced via supercritical antisolvent processes: a) SAS and b) SAS-EM

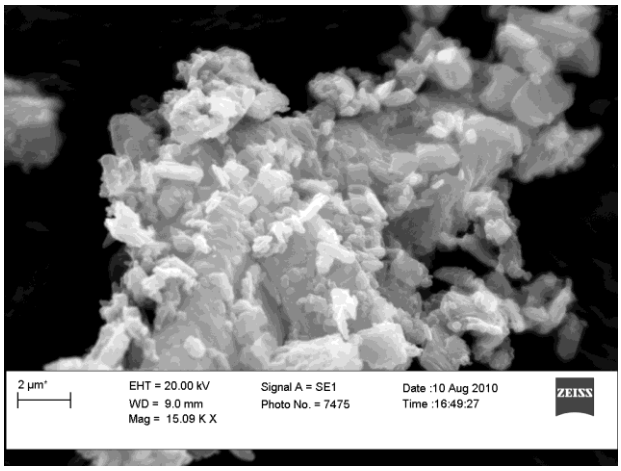

Figure 3.6. Ground commercial mesalamine particles.

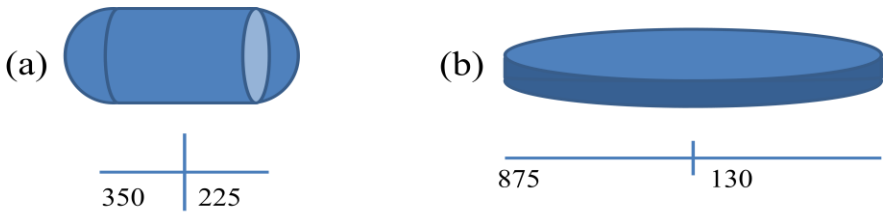

Figure 3.7. Mesalamine morphologies (nm): a) small ground particles and b) nanoflake particles.

3.4.2 Formation of Hydrogel Nanoparticles Containing Mesalamine

Various formulations of drug in the hydrogel are listed in Table 3.2.

No.	Experiment	MSM%	AA%	AM%	MBA%
I	PAM	0	0	99	<1
II	PAA	0	99	0	<1
III	PAA-AM	0	75	25	<1
IV	nMSM-PAM	4.8	0	0	<1
V	gMSM-PAM	4.8	0	0	<1
VI	gMSM-PAA-PAM	4.8	71.4	23.8	<1
VII	nMSM-PAA-PAM	4.8	71.4	23.8	<1

Table 3.2. Experimental ratios of main components: mesalamine (MSM), acrylic acid (AA), acrylamide (AM) and methylbisacrylamide (MBA).

Confirmation of polymerization during miniemulsion polymerization can be inferred from the FTIR spectra. Monomers, acrylamide and acrylic acid, have the vinyl functional group C=C that vibrates at 980 cm^{-1} wavelength showing two peaks in this region. Upon polymerization, both of these peaks disappear confirming the complete conversion of the vinyl groups. Additional peaks shown are due to C=O at 1630-1700 cm^{-1}, NH_2 deformation at 1550 cm^{-1}, and primary amides at 1420-1400 cm^{-1}, which are attributed to the amide group in polyacrylamide and mesalamine and the C=O in polyacrylamide, polyacrylic acid, and mesalamine. In summary, the polymerization is successful with the disappearance of the vinyl peaks for polyacrylamide, poly(acrylic acid), and the copolymer in Figures 3.10-3.13.

Polymerizations of the acrylic acid or copolymer did not follow similar visible trends to that observed of polyacrylamide. In the case of polyacrylamide, after the initial drop wise addition and ultrasonication the solution turns white into emulsion status. In the case of poly(acrylic acid), the initial yellowed translucence changes to white upon reaction initiation. The translucence of solution until the reaction was also obtained with polyacrylamide polymerization in the presence of 1*N* HCl and copolymer. The dried poly(acrylic acid) powder has faint yellow coloration compared to the white of polyacrylamide. For PAA, the attractive forces were strong enough to collapse the dried

particles into a disc-like form (Figure 3.8). Upon initial manipulation, the disc was hard and coarse, but after application of mild force, the disc turned easily into powder form.

Two types of mesalamine, ground and nanoflakes, were utilized for encapsulation. After the initial ultrasonication and during dropwise addition of the aqueous phase of the copolymer, the disperse phase was visibly heterogeneous with ground mesalamine precipitating to the bottom which was not obvious during the nanoflake mesalamine hydrogel synthesis. Hence, mixing was used with the pipette to counteract this phenomenon, thus the droplets that were created may not have been homogenous. After ultrasonication, suspension of the majority of mesalamine was not achieved and subsequently yielded a good amount of mesalamine collected in the bottom of the reaction vessel. In the industrial scale operation, the mesalamine that fell from solution can be recycled into the next batch for encapsulation.

The coloration of the mesalamine reaction is a good indicator of exposure to light and heat. The reaction time was minimized from 2 hours, 1 hour, to 30 minutes as the extra time did not have any impact on the extent of polymerization but the extended exposure to heat did have an effect on the discoloration. Attempts were made to prevent light exposure which discolors mesalamine by using amber vials and aluminum foil. The heating process for thermally initiated polymerization does alter the original coloration, for example, white, tan, chocolate milk, and dark chocolate colors, light purple, and purple colors were observed in different experiments. The color indicative nature of this drug allows for visible assessment of the extent of exposure; based on pharmacists recommendations of drugs containing mesalamine (Asacol, Pentasa, Rowasa), if color change has occurred, the drug is still considered active until dark brown, though the discoloration may elicit rejection by potential consumers.

Without mesalamine, the polyacrylamide and copolymer suspensions appear white. In the presence of mesalamine, the copolymer suspension exhibited purple hues. The color darkened to deeper tones of purple as the reaction time and exposure to heat are extended. The mesalamine in polyacrylamide appears white initially then with exposure to light will discolor.

When handling these powders, the electrostatic interactions are obvious by the adherence to the glass and the mobile nature of the powder without physically touching (Figure 3.9b). The copolymer poly(acrylic acid-*co*-acrylamide) experiments have the most electrostatic interactions, this is due to the carboxylic group of the acrylic acid as well as the smaller size particles. The differences in the bulk density are shown in Figure 3.9a where the same quantity of powder (100 mg) from each experiment is compared side by side. Samples from experiments VI and VII with the copolymer have double the bulk density of other samples.

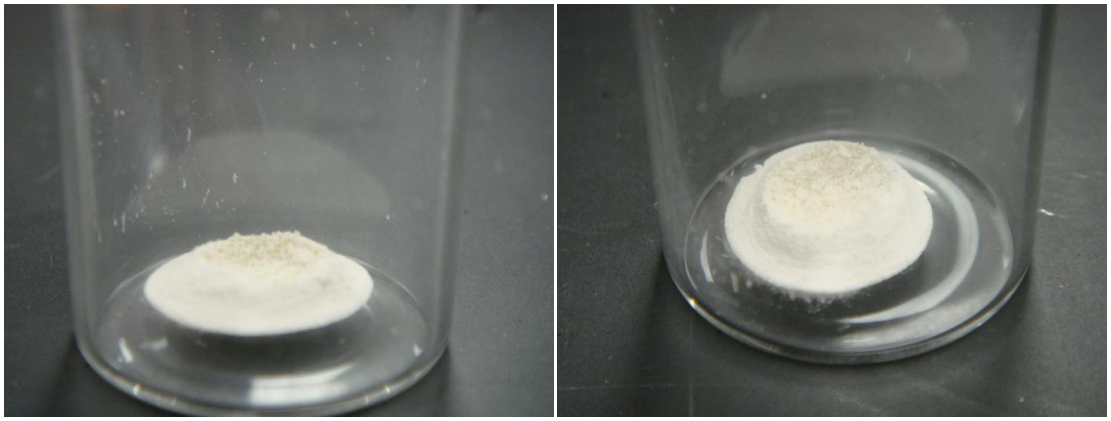

Figure 3.8. Poly(acrylic acid) powder disk shape formed overnight after collection.

(a) 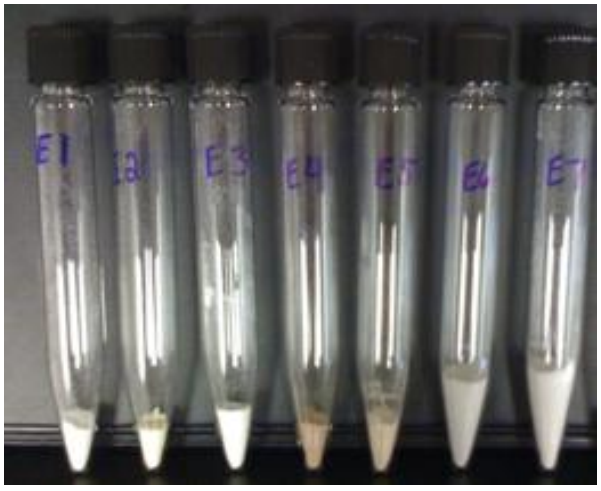 (b) 

Figure 3.9. Powder produced a) side by side comparisons of 100 mg of powder produced for experiments I-VII and b) electrostatic interactions of nanopowder (Expt VII).

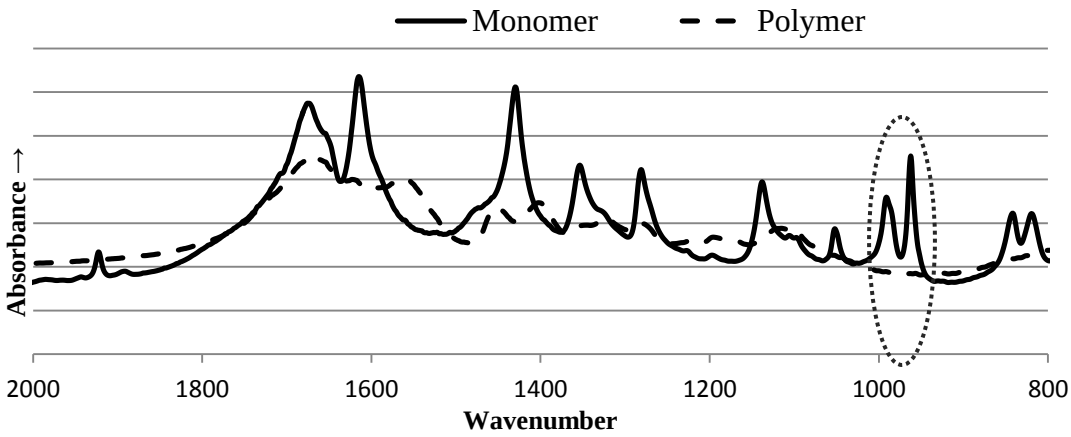

Figure 3.10. Acrylamide monomer present at the vinyl 980 cm^{-1} wavelength disappears upon polymerization.

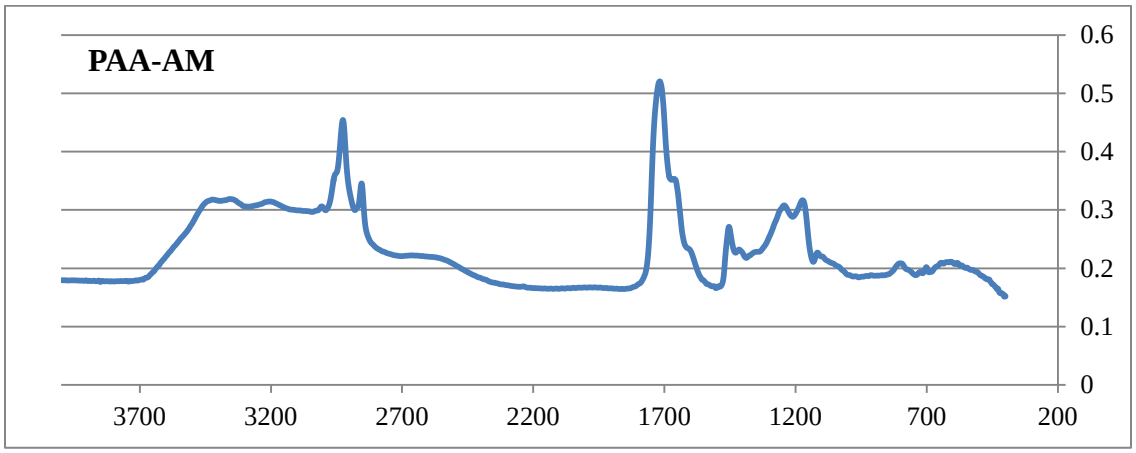

Figure 3.11. FTIR of sample from experiment III PAA-AM.

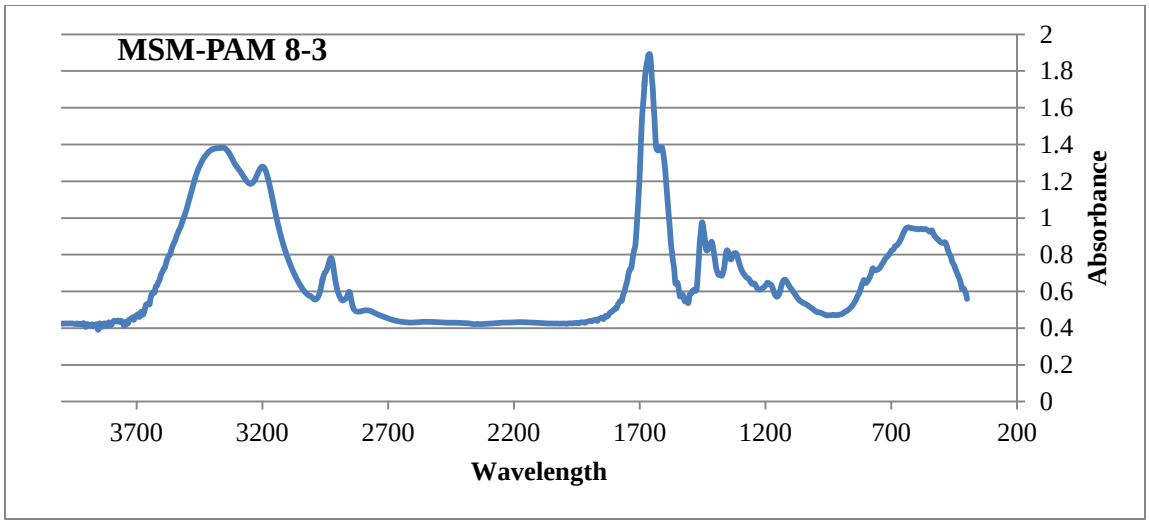

Figure 3.12. FTIR of sample from experiment V gMSM-PAM.

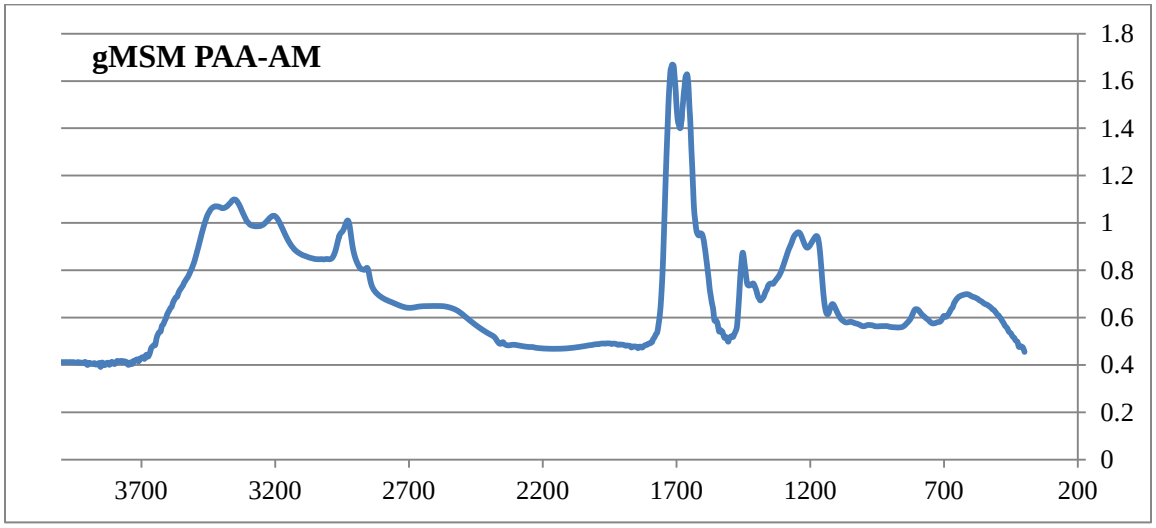

Figure 3.13. FTIR of sample from experiment VI gMSM-PAA-AM.

Polyacrylamide and poly(acrylic acid) have notably spherical or rounded morphology (Figures 3.14-15). To compare the morphology, mesalamine was physically mixed with polyacrylamide nanoparticles and observed in SEM. The distinctive morphology of mesalamine nanoflakes contrasts with the polyacrylamide spheres as evident in Figure 3.16; here polyacrylamide is on the left and mesalamine is on the right side of the image. No mesalamine nanoflakes were seen in samples IV-VII (Figures 3.17-18). Hydrogel miniemulsion polymerization and supercritical drying was not as effective with mesalamine present hence the spheres typical of both polyacrylamide and poly(acrylic acid) particles are not as easily visible in the images and particles appear fused and agglomerated. The droplet dispersion of supercritical drying was not as efficient as compared to the MPSD system in Chapter 2 without mesalamine.

The ground mesalamine appeared more difficult to encapsulate into the hydrogel particles. The disperse phase separated during the dropwise process as the ground mesalamine was drastically different in size compared to the nanosized mesalamine. The interactions prior to introduction of the surfactant and cyclohexane are similar for both nanosized and microsized mesalamine particles, but the degree of separation was smaller for nanoparticles. The monomers acrylamide and acrylic acid have excellent solubility in water compared to mesalamine (0.8 mg/ml) so the encapsulation efficiency is due to the amount of particles contained within the aqueous droplets. Increasing water content and surfactant to maintain surface tension prior to addition to the continuous phase could potentially prevent visible settling of mesalamine and maintain higher particles within the droplets; however, increasing ultrasonication duration and amplitude even with extra measures of cooling water bath and pulsatile mode will over heat the mesalamine drug and increase discoloration.

Mesalamine with acrylamide in the aqueous phase did not have similar interactions as the system with acrylic acid. To elucidate interactions, these three main components were evaluated on their pH (Table 3.3). In aqueous phase, acrylamide is neutral (7), whereas acrylic acid is acidic <1.2 with high instability suggests either the amount of hydronium ions present is higher than should be used with the pH system or the data exceeded the 4 point calibration range of instrument (2, 4, 6, and 8). Mesalamine in water (0.05g/ml) is

slightly acidic 4.17 pH. A mixture of mesalamine and monomer produces a pH similar to the most acidic component in the mixture. As a stronger acid is introduced more hydronium ions are present to create a more acidic solution. The similarities of acidity between acrylic acid and mesalamine suggested improved compatibility over acrylamide; however, based on the observations of disperse phase, the neutral acrylamide was better suited for compatibility with mesalamine. The acrylic acid and mesalamine were competing for water molecules present as a Lewis base in the mixture.

Material	Mesalamine	Acrylic acid	Acrylamide	MSM + AM	MSM + AA
pH	4.24	<1.2	7	4.24	1.19

Table 3.3. pH of three main components: mesalamine (MSM), acrylamide (AM), and acrylic acid (AA)

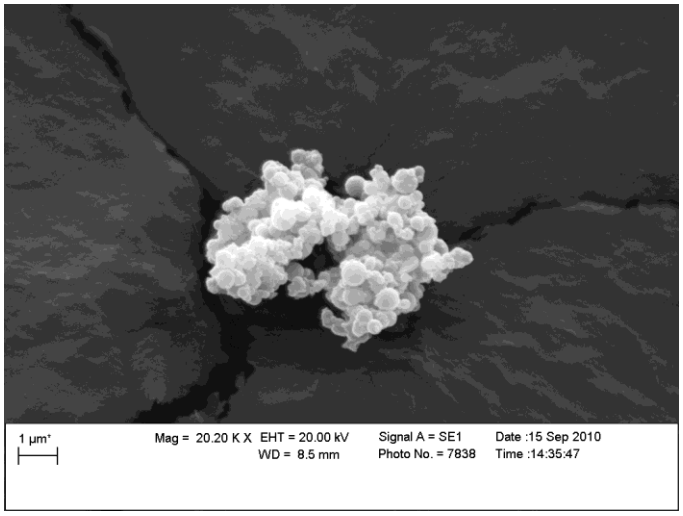

Figure 3.14. SEM micrograph of polyacrylamide nanoparticles Experiment I.

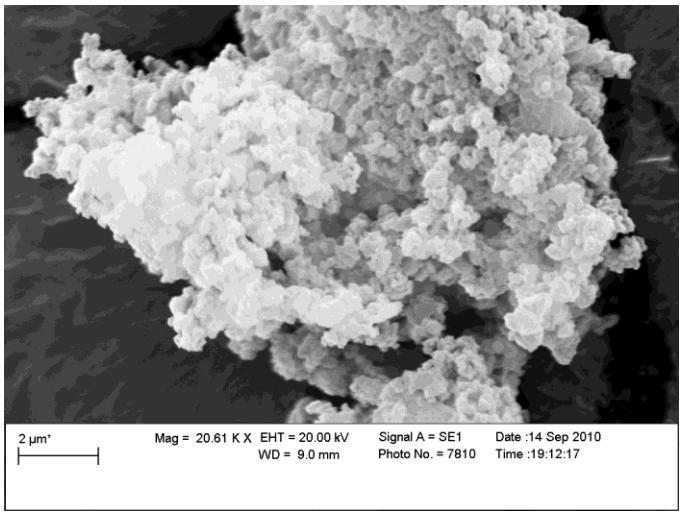

Figure 3.15. SEM micrograph of poly(acylic acid) Experiment II.

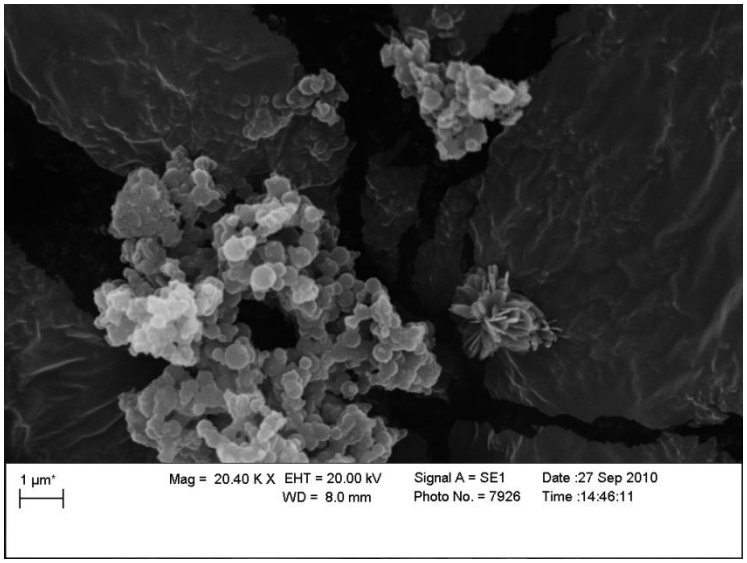

Figure 3.16. Physically mixed PAM-NP and MSM-NP.

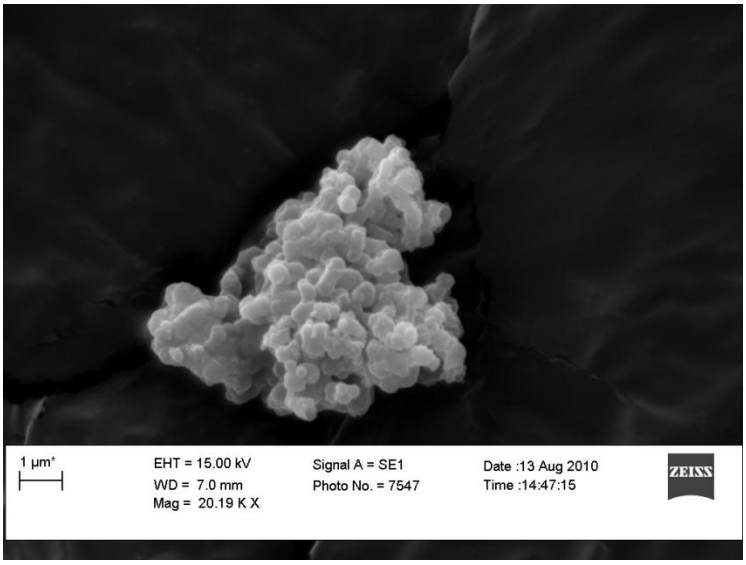

Figure 3.17. SEM micrograph of Experiment V gMSM-PAM.

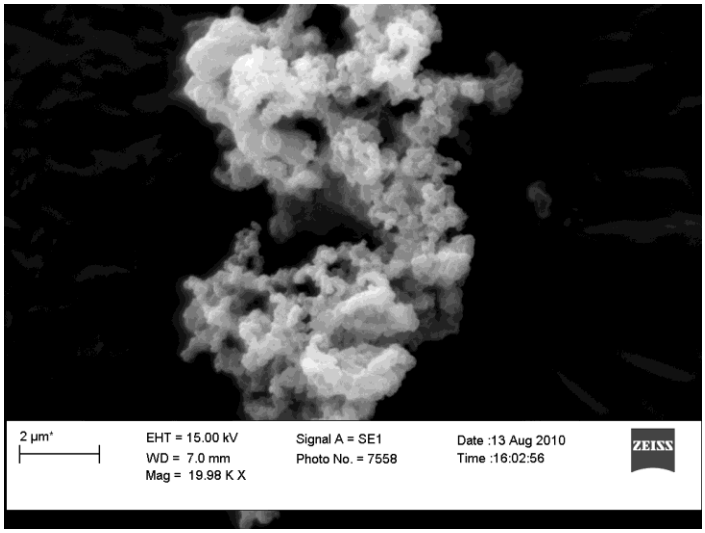

Figure 3.18. SEM micrograph of Experiment VI gMSM-PAA-AM.

3.4.3 Particle Size Distributions

Before supercritical drying, size distribution of the polymer particles was measured by dynamic light scattering (Figures 3.19-25). The control polymerizations without mesalamine (experiments I-III) yielded larger particles than those with mesalamine (experiments IV-VII). Polyacrylamide experiment with mesalamine nanoflakes (IV) yielded surprisingly small particles 31nm number weighted average compared to the ground mesalamine in polyacrylamide 64 nm (V), double the size. In the copolymer with mesalamine experiments, the small particle sizes in experiments VI and VII (10.7 nm and 25.4 nm, respectively) can be attributed to the precipitation of the majority of mesalamine during the polymerization leaving the smaller particles. Poly(acrylic acid) has the highest average number weighted particle size of 680 nm, this could be attributed to small particles agglomerated in the cyclohexane suspension medium and their non-spherical rounded shape as the calculations for light scattering data are based on spherical particles and depend on the orientation of the particles in the path of the laser. The particle size distribution data is compared in Table 3.4.

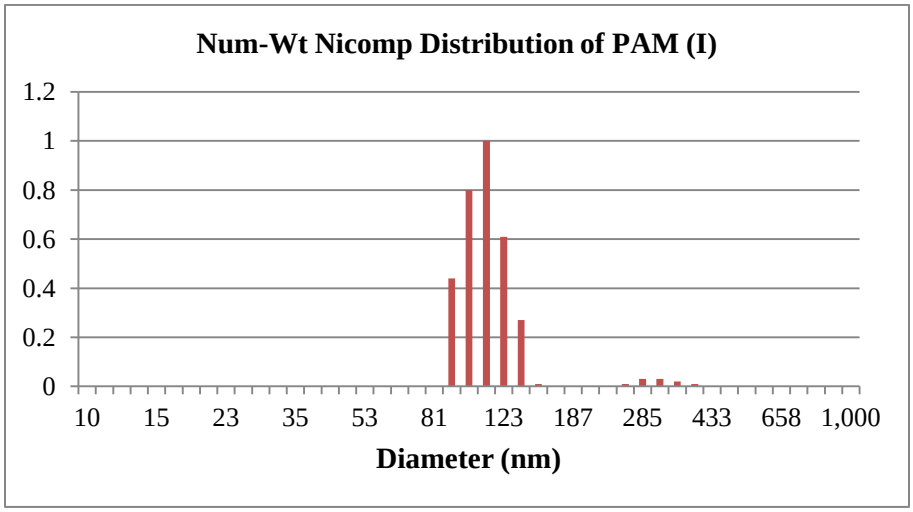

Figure 3.19. Particle size distribution of polyacrylamide.

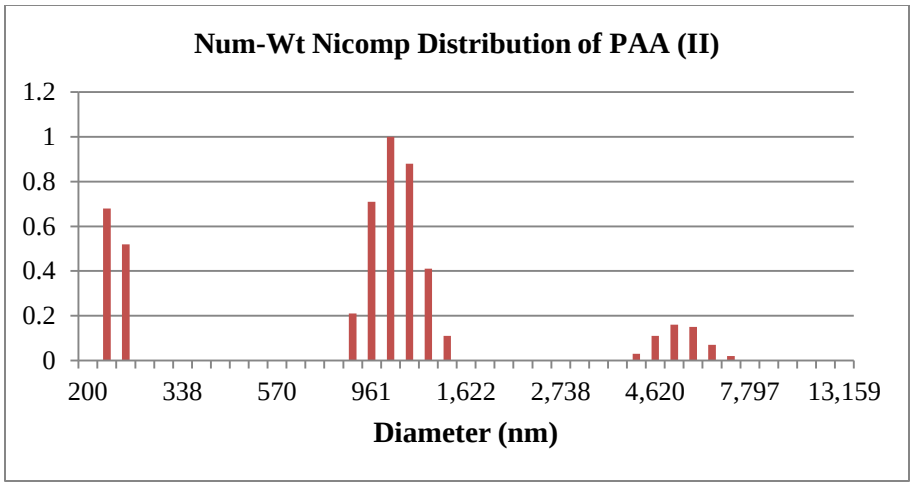

Figure 3.20. Particle size distribution of poly(acrylic acid).

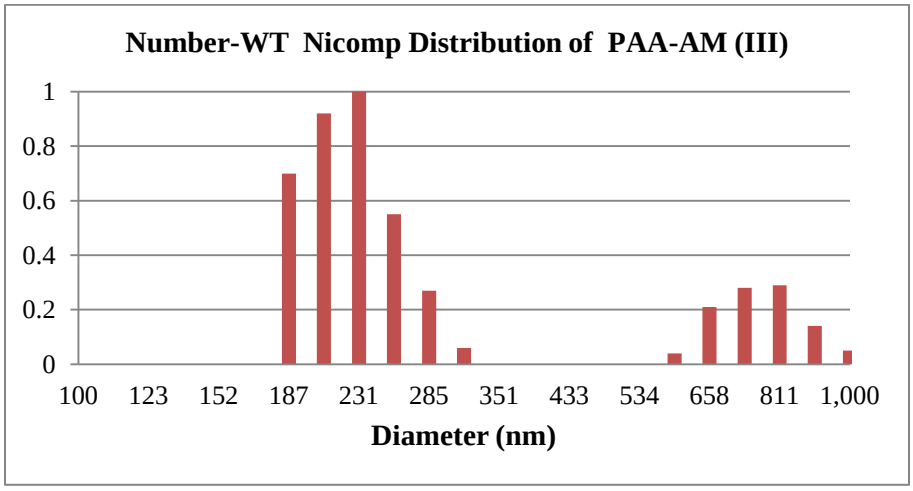

Figure 3.21. Particle size distribution of poly(acrylic acid-co-acrylamide).

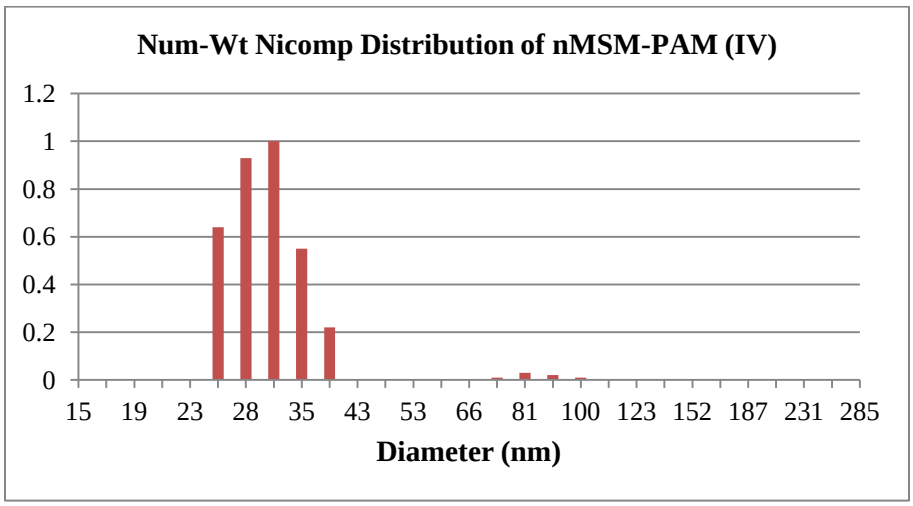

Figure 3.22. Particle size distribution of nMSM-PAM (IV)

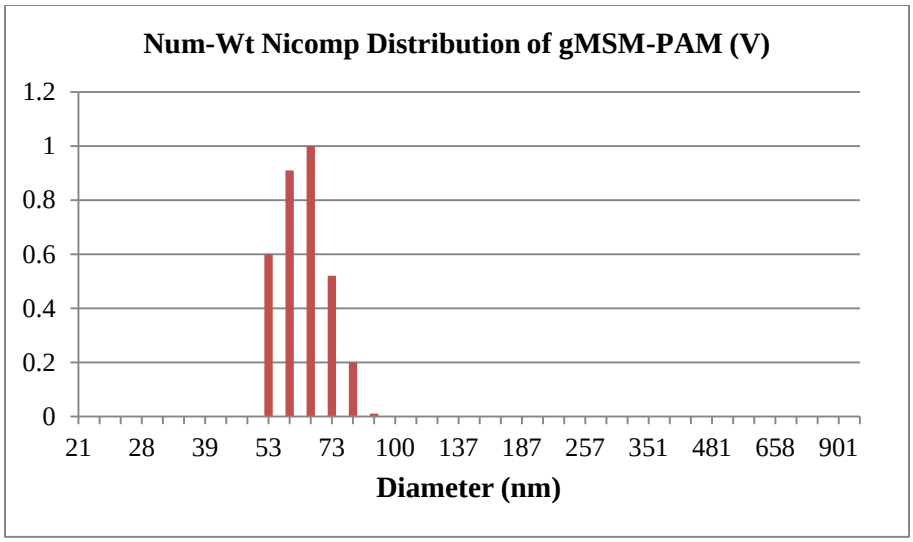

Figure 3.23. Particle size distribution of gMSM-PAM

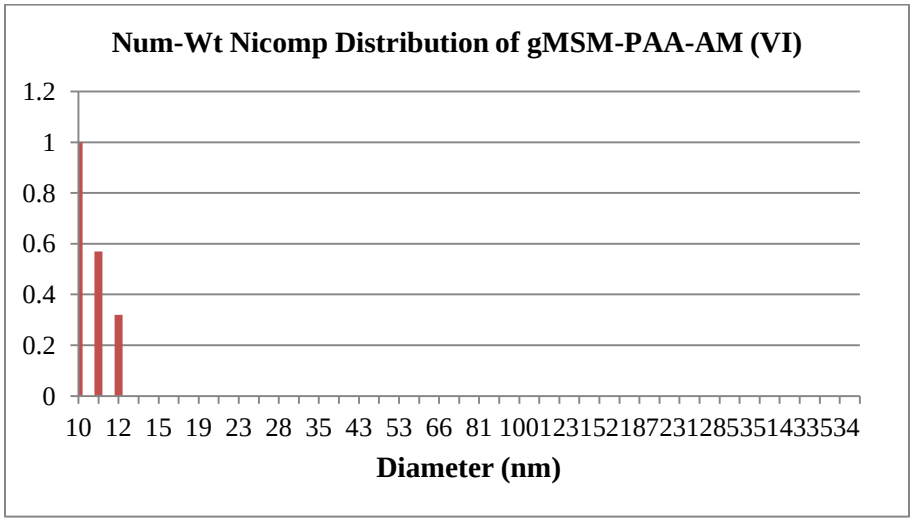

Figure 3.24. Particle size distribution of gMSM-PAA-AM

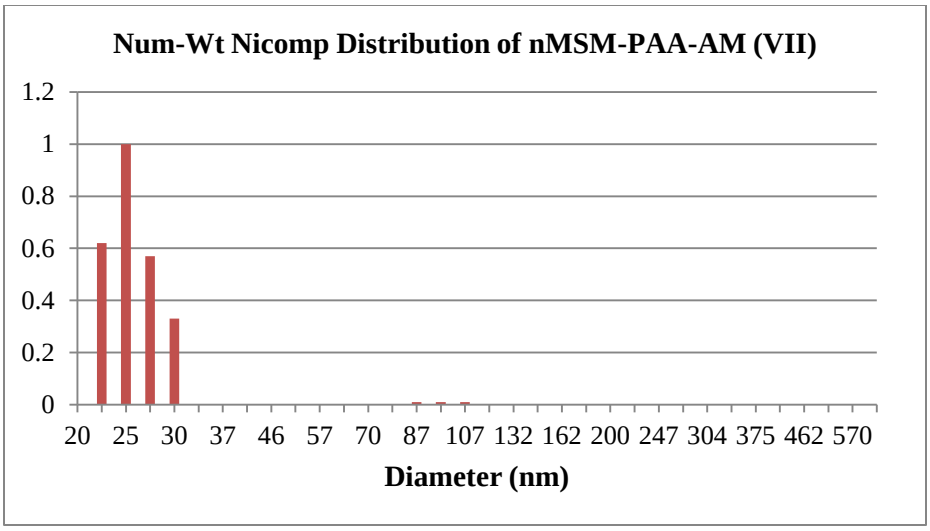

Figure 3.25. Particle size distribution of nMSM-PAA-AM

No.	Experiment	Peak 1 (nm)	%	Peak 2 (nm)	%	Avg
I	PAM	109.9	97.5	312.2	2.5	115
II	PAA	232.7	37.1	1094.9	54.3	680.8
III	PAA-AM (75:25)	224.2	77.4	779	22.6	349.6
IV	nMSM-PAM	30.6	97.5	86	2.5	31
V	gMSM-PAM	63.8	100	--	--	--
VI	gMSM-PAA-PAM	10.7	100	--	--	--
VII	nMSM-PAA-PAM	25.4	99.2	--	--	--

Table 3.4. Summary of number weighted NICOMP particle distributions.

3.4.4 HPLC Analysis

Mesalamine concentrations were determined by HPLC after extracting the mesalamine from the hydrogel powder. To determine the best solution to rapidly extract the mesalamine, multiple solutions were tested on pure mesalamine: ACN:water (50:50), methanol: (ACN:water (50:50)) (80:20), 10% 1 *N* HCl in methanol, 10% 1*N* HCl in water, 50% 1 *N* HCl in water, 75% 1 *N* HCl in water, and pure 1 *N* HCl prior to applying to polymer samples. The solutions with HCl most rapidly dissolved mesalamine as mesalamine has improved solubility in dilute acid. HPLC sample preparation involved exposing samples to dissolution solution, sonicate in a water bath for 2 minutes, shake for 30 minutes, sonicate again, and either wrist-shaking for another 45 minutes and sonicate again or let sit overnight. Samples were centrifuged for 2 minutes at 3400rpm to minimize suspended particles and the supernatant filtered through a 0.2 μm syringe filter was analyzed via the HPLC method.

Stability of mesalamine in 1 *N* HCl was found to be within tolerable range. Pure mesalamine exposed to 1 *N* HCl was evaluated multiple times on HPLC to determine if degradation occurred. Over two days of constant high HCl acid exposure, the peak area was maintained. The mesalamine 101 ppm standard in 10% 1 N HCl solution was evaluated throughout the process as a standard. The recovery of these standards was 98.0% with a standard deviation of 2.16%. Polyacrylamide displayed no peaks in the mesalamine retention time (H5 and 141). Mesalamine alone with the shorter extraction time recovered 93% of expected mesalamine (H6 and 143).

The extraction solution and exposure time were determined by control samples as to whether dilute HCl in water or methanol and extraction times of 1.5 hrs or overnight. Control samples consisted of pure mesalamine and of physically mixed polyacrylamide and mesalamine to establish reliability in sample preparation. Water was deemed better than methanol as the hydrogel will swell more exposing more mesalamine quicker to dissolve in the HCl despite slightly higher results for experiment IV in methanol than in water by 0.52% but is within standard deviation of the HPLC method. Control samples of known mesalamine content were physically mixed with polyacrylamide and had noticeable

differences on HPLC compared to pure mesalamine. Concentrations using a shorter extraction time of 1.5 hrs and 10% 1 *N* HCl were low at 77% recovery (H7, 142, and Expt. 9) for physically mixed, and pure mesalamine recovered using the same extraction method was 93% of expected mesalamine (H6 and 143). Recovery from the physically mixed mesalamine and PAM was 100% (C1) using a longer extraction time overnight and stronger acid content 75% 1 *N* HCl solution. This leads to conclude another phenomenon and interaction of mesalamine with polyacrylamide is occurring even without going through the polymerization process. Polyacrylamide and mesalamine both have amide groups that increase their compatibility. Details of the calibration curve, peak areas, concentrations, and select chromatographs are available in Appendix E.

Samples of the other components in polymerization process were evaluated on HPLC to establish if any interference in peak detection and area could be attributed to MBA, AM, AIBN, and Span 80. Retention times for MBA, AM, and AIBN were prior to that of the mesalamine peak (~35min); these materials being more polar are not retained on the C8 column. The crosslinker MBA (22.5 mg), at such low concentrations (less than 1%), comparatively did not appear to play a role in the interactions observed with the components in the greater quantities: MSM, AM, and AA. The surfactant however does have a peak after mesalamine in (~38min). For some copolymer results, separation of these peaks was difficult to analyze for samples with greater HCl concentration and longer time.

Some mesalamine drug was loaded into the hydrogel through the inverse miniemulsions polymerization process (Table 3.5). In all cases, the actual quantity loaded was much lower that the theoretical maximum of 5 g of mesalamine per 100 g of polymer. Mesalamine encapsulated in the polyacrylamide was higher than that in the poly(acrylic acid-*co*-acrylamide). Polyacrylamide experiments IV & V (11.4 and 54.3 wt%, respectively) encapsulated more mesalamine which was higher than the copolymer, poly(acrylic acid-*co*-polyacrylamide), in experiments VI & VII (<9%).

As experiment IV utilized the mesalamine nanoparticles and experiment V utilized ground mesalamine, approximately 42% more mesalamine was encapsulated in experiment V with the ground mesalamine. This can be attributed to the different surface areas of the different

mesalamine morphologies. Mesalamine with amide groups had higher encapsulation in polyacrylamide which also has amide groups, thus leading to conclude mesalamine is more compatible with acrylamide than with acrylic acid. The smaller surface area per mass (7.54 m^2/g) of ground mesalamine contributes greater loading efficiencies of the drug whereas nanoflakes with 21.93 m^2/g has nearly 3 times the surface area, so for a constant mass of mesalamine nanoflake mesalamine would have more interactions with the monomers of hydrogel than the ground mesalamine.

The surface does not solely explain why ground mesalamine encapsulated within polyacrylamide with higher efficiency than the other experiments. The recovery ratio 4.7 of 54.3% (V) to 11.4% (IV) is disproportionate to the surface area/mass ratio 2.9 and another explanation is needed. The polymer solution tested with DLS yielded double the size of polymer particles with the ground mesalamine experiment V (63nm) as for the nanoflake experiment IV (31nm). The large length dimension 1.1 μm of the mesalamine nanoflakes was difficult for the spherical polymer particles to maintain mesalamine within the small droplets. An analogy for this is a foot long hot dog in a mini-sized bun; the bun does cannot hold the hot dog. The ground mesalamine with polyacrylamide had the most loading efficiency of all experiments due to general chemical compatibility with polyacrylamide as a neutral material and physical size compatibility of the mesalamine ground particles.

The extent of mesalamine encapsulated in poly(acrylic acid-*co*-acrylamide) was less than 9%. The lowest calibration point for reliable detection limit of the HPLC instrument was at 1 ppm of mesalamine. The general reliability of the HPLC results is ±2.16% given deviations in mesalamine standards without polymer present. Given this variation the experimental results from VI overlaps experiment VII and VI results in the minimum and maximum, respectively, applying this variation. The extraction of VI having no mesalamine content was only for a 1.5 hr time period and an 8.8% recovery was with greater HCl content and time; the mesalamine encapsulated may have been more difficult to extract and require the longer time. With the addition of acrylic acid in the polymerization process with its carboxylic group has increased attraction to water by hydrogen bonding in such a manner that the mesalamine is displaced from the aqueous phase. This conclusion drawn from the behavior observed during polymerization where the mesalamine was

difficult to stay suspended in the disperse phase. The morphological differences of mesalamine cannot be determined for copolymer experiments based on the variation efficiency of encapsulation.

However, exhibited by the disc formation of the poly(acrylic acid) powder without mesalamine present the self-attractive forces of acrylic acid is very strong. The smallest grounded mesalamine particles were comparable to the mesalamine nanoflakes and thus elicited similar encapsulation efficiencies. With assistance by ultrasound prior to polymerization, the monomers could wedge between nanoflakes surrounding the drug mesalamine and size fractionation of the smaller drug nanoflakes were incorporated into the hydrogel. The mesalamine ground particles showed a fractionating of the smaller rounded mesalamine particles begin incorporated into the hydrogel during the polymerization process. Greater surfactant quantities or increasing aqueous phase content might overcome this issue, but is dependent upon the self attractive nature of acrylic acid. Mesalamine to some extent is compatible with this polymerization process. Instead, the repulsive interaction between the mesalamine and the acrylic acid brought on by the increased attractive forces between water and acrylic acid pushed the mesalamine out of the suspension.

No.	Experiment	Mesalamine loading efficiency (%)
IV	nMSM-PAM	11.5 ± 2.16
V	gMSM-PAM	54.3 ± 2.16
VI	gMSM-PAA-PAM	8.8± 2.16
VII	nMSM-PAA-PAM	4.7± 2.16

Table 3.5. HPLC results of mesalamine loaded into different hydrogels.

3.5 Conclusions

Using miniemulsion polymerization and supercritical drying, hydrogel nanoparticles containing mesalamine drug were produced. Smaller polymer particles were produced with mesalamine than without mesalamine. The interactions of the acrylic acid in the aqueous phase displaced the larger mesalamine flakes limiting incorporation into the hydrogel.

Mesalamine experiments yielded incorporation of some mesalamine into the polymers. The efficiencies were lower than the theoretical maximum for all experiments. The mesalamine ground particles showed a fractionating of the smaller mesalamine particles which are incorporated into the hydrogel during the polymerization comparable to the nanoflakes. The ground mesalamine with polyacrylamide had the most loading efficiency of all experiments due to general chemical compatibility with polyacrylamide and improved morphological compatibility of the mesalamine ground particles compared to nanoflakes.

3.6 References

Bajpai, S. K. and S. J. Sonkusley (2002). "Hydrogels for Colon-specific Oral Drug Delivery: An In Vitro Drug Release Study (II)." Iranian Polymer Journal **11**(3).

Chattopadhyay, P. and R. B. Gupta (2002). "Protein Nanoparticles Formation Using Supercritical Antisolvent with Enhanced Mass transfer." AIChE J. **48**: 235-244.

Cohen, R. D. (2006). "Review article: evolutionary advances in the delivery of aminosalicylatese for the treatment of ulcerative colitis. ." Ailment Pharmacology and Therapeutics. **24**: 465-74.

Cutie, S. S., D. E. Henton, C. Powell, R. E. Reim, P. B. Smith and T. L. Staples (1996). "The Effects of MEHQ on the Polymerization of Acrylic Acid in the Preparation of Superabsorbent Gels." Superabsorbent Gel Preparation

Florence, A. T., Ed. (2006). Nanoparticulates as drug carriers. Nanoparticle Flow: Implications for Drug Delivery. Danvers, MA, Imperial College Press.

Galehassadi, M., M. Mahkam and F. Hosseinzadeh (2007). "Synthesis and characterization of new macromolecule systems for colon specific drug delivery." e-Polymers **028**.

Gupta, R. B. (2006). Supercritical fluid technology for particle engineering. . Nanoparticle Technology for Drug Delivery. R. B. Gupta and U. B. Kompella, Drugs and the Pharmaceutical Sciences. **159** 53-84.

Gupta, R. B. and P. Chattopadhyay (2003). Method of forming nanoparticles and microparticles of controllable size using supercritical fluids with enhanced mass transfer. United States. **6620351**.

Gupta, R. B. and P. Chattopadhyay (2003). Method of forming nanoparticles and microparticles of controllable size using supercritical fluids with enhanced mass transfer. **US Patent 6620351.**

Hemingway, M. G., R. B. Gupta and D. J. Elton (2010). "Hydrogel Nanopowder Production by Inverse-Miniemulsion Polymerization and Supercritical Drying." Ind. Eng. Chem. Res.

Huang, Y., W. Leobandung, A. Foss and N. A. Peppas (2000). "Molecular aspects of muco- and bio-adhesion: tethered structures and site-specific surfaces." J. Control. Release.

Jackson, S. J., D. Bush, N. Washington and A. C. Perkins (2000). "Effect of resin surface charge on gastric mucoadhesion and residence time of cholestyramine." International Journal of Pharmaceutics **205**: 173-181.

Jounela, A., P. Pentikainen and A. Sothmann (1975). "Effect of particle size on the bioavailability of digoxin. ." Eur J Clin Pharmacol **8**(365-70).

Kersten, B. S., T. Catalano and Y. Rozenman (1991). "Ion-pairing high-performance liquid chromatographic method for the determination of 5-aminosalicyclic acid and related impurities in bulk chemical." Journal of Chromatography **588**: 187-193.

Kharb, V., M. Bhatia, H. Dureja and D. Kaushik. () 82, 6,8, 90-2. (2006). "Nanoparticle technology for the delivery of poorly water soluble drugs." Pharm Technol. **30**

Kriwet, B. and T. Kissel (1996). "Poly(acrylic acid) Microparticles Widen the Intercellular Spaces of Caco-2 cell monolayers: an examination by confocal laser

scanning microscopy." European Journal of Pharmaceutics and Biopharmaceutics. **42**(4): 233-240.
Kriwet, B., E. Walter and T. Kissel (1998). "Synthesis of bioadhesive poly(acrylic acid) nano- and microparticles using an inverse emulsion polymerization method for the entrapment of hydrophilic drug candidates." Journal of Controlled Release **56** 149-158.
Liversidge, G. G. and K. C. Cundy (1995). "Particle size reduction for improvement of oral bioavailability of hydrophobic drugs: absolute oral bioavilability of nanocrystalline danzol in beagle dogs." Int J Pharm. **125** 91-97.
Merisko-Liversidge, E. M. and G. G. Liversidge (2008). "Drug nanoparticles: formulating poorly water-soluble compounds. ." Toxicol Pathol. **36** 43-8.
Park, H. and J. R. Robinson (1985). J Controlled Release **2**: 257-275.
Park, H. and J. R. Robinson (1987). "Mechanisms of mucoadhesion of poly(acrylic acid) hydrogels." Pharmaceutical Research **4**(6): 457-64.
Pasquali, I., R. Bettini and F. Giodano (2008). "Supercritical fluid technologies: An innovative approach for manipulating the solid-state pharmaceuticals." Advanced Drug Delivery Reviews **60**: 399-410.
Peppas, N. A., P. Bures, W. Leobandung and H. Ichikawa (2000). "Hydrogels in pharmaceutical formulations. ." European Journal of Pharmaceutics and Bioplarmaceutics. **50**: 27-46.
Peppas, N. A. and P. A. Buri (1985). J Controlled Release **2**: 257-275.
Rasenack, N. and B. W. Muller (2002). "Dissolution rate enhancement by in situ micronization of poorly water-soluble drugs." Pharm Res. **19** 1894-900.
Reverchon, E., I. De Marco and E. Torino (2007). "Nanoparticles production by supercritical antisolvent precipitation: A general interpretation." J. Supercritical Fluids **43**: 126-138.
Robinson, J. R. and H. Park (1984). Int J Pharm. **19**: 107-127.
Silebi, C. A. and J. G. Dosramo (1989). "Separation of submicrometer particles by capillary hydrodynamic fractionation (CHDF)." Journal of Colloid and Interface Science **130**: 14-24.
Smart, J. D. (2005). "The basics and underlying mechanisms of mucoadhesion." Adv. Drug Delivery Reviews **57**: 1556-1568.
Takeuchi, H., H. Yamamoto and Y. Kawashima (2001). "Mucoadhesive microparticulate systems fo peptide drug delivery." Drug Delivery Reviews **47**: 39-54.
Thairs, S., S. Ruck, S. J. Jackson, R. J. C. Steele, L. C. Feely, C. Washington and N. Washington (1998). "Effect of dose size, food and surface coating on the gastric residence and distribution of ion exchange resin." Int J Pharm. **176**: 47-53.
U.S. Food & Drug Administration, F. (2010). "Orange Book: Approved Drug Products with Therapeutic Equivalence Evaluations." Retrieved March 5, 2010, 2010, from www.accessdata.fda.gov.
Yadav, A. V. and V. B. Yadav (2008). "Improvement of physicochemical properties of mesalamine with hydrophilic carriers by solid dispersion (kneading) method." Research J. Pharm. and Tech. **1**(4).

4.0 HYDROGEL NANOPARTICLES CONTAINING ZINC OXIDE FOR ULTRAVIOLET PROTECTION

4.1 Introduction

Long term ultraviolet exposure is commonly linked to skin cancer. According to the American Cancer Society (2009), skin cancer is the most common of all cancers accounting for nearly half of all cancers in the United States. In the year 2009 alone, more than 1 million cases are non-melanoma skin cancer type most of which are considered to be sun-related, and melanoma, the most serious type of skin cancer, accounted for about 68,720 cases and 11,590 deaths.

Prevention of skin cancer utilizes topical application of sunscreen with ingredients able to block out most of UVA and UVB rays. Current broad spectrum ingredients approved by the Food and Drug Administration (2009) includes benzophenones (oxybenzone), cinnamates (octinoxate cinoxate), sulisobenzone, salicylates, titanium dioxide, zinc oxide, and avobenzone (Parsol 1789). Cosmetics containing alpha-hydroxy acids increase sun sensitivity and susceptibility to sunburn. Sunscreens that contain physical broad spectrum ingredients, such as zinc oxide, are non-irritating and non-allergenic; flake-like zinc oxide provides more comfortable feeling for sunscreen cosmetics (Haishi 1992). Sensitivity and allergic reactions are more common with chemical sunscreens (Bryden 2006; Rodríguez 2006), and safety issues surfaced with oxybenzone (Hanson 2006; SCCP 2006; Sutton 2008).

Zinc oxide is one of the world's most commonly used nanoparticles of which the most common usage is for protection from ultraviolet exposure. Zinc oxide is found in many common personal care products, including lotions, cosmetics, as well as paint, rubber, and paper coating. In addition, zinc oxide nanoparticles have demonstrated interesting antibacterial properties (Yamamoto 2004; Li 2007; Wahab 2010).

Zinc oxide usage as sunscreen is a well depicted 1980s icon of white noses walking around the beach. Ultraviolet (UV) radiation is composed of three types: UV-A at 320-400 nm, UV-B at 280-320 nm, and UV-C at 100-280 nm. Of the global UV radiation at the ground, which varies based on altitude and latitude, the majority 90-95% is UV-A, 10-6% is UV-B, and UV-C is absorbed completely in the stratosphere by ozone. According to the World Health Organization (2010), UV radiation damages DNA after surpassing the small amount promoting vitamin D generation. A recent change in sun protection factor (SPF) labeling based on only UVB protection has mandatory disclosure of "No UVA" protection if the product is not a broad spectrum product.

For industrial applications, zinc oxide has been incorporated into various polymer materials for UV protection. For example, composite sheets of poly(methyl methacrylate) with ZnO nanoparticles (100 and 300 nm) reduced transmittance of UV light (290, 320, and 360 nm) from 90.1 to 0% when greater than 0.1% ZnO is utilized (Anzlovar 2008). The UV absorbance of ZnO/poly(amic acid) composite solution in dimethylacetamide was found to be larger than that of its components taken separately due to capping of the linear organic chains for better dispersion (Levine 2004). Modified ultrafine flake-like zinc oxide with silica and trimethyl siloxane produces particles that are highly transparent in the visible range and still provide UV protection (Cao 2009). Modified zinc oxide with poly(vinylpyrrolidone) as the capping agent was investigated for optical response (Guo 2000).

Microfine zinc oxide demonstrates superior protection compared to microfine titanium dioxide, another physical sunscreen, in long-wave UVA range (340 and 380 nm) and is less white at similar concentrations (Pinnell 2000). The whiteness of ZnO can be further reduced by reducing particle size to nanoscale. UV protection relates with the scattering and/or absorbance of ZnO particles. The scattering property plays an important role in shielding of UV irradiation (Klein 2004). Nanoparticle ZnO would provide an improved UV absorption if dispersed well throughout a sample allowing for improved surface coverage and increased probability that UV light will encounter a ZnO particle. A method to prevent growth of ZnO nanoparticles is quenching by adsorption of a ligand, such as octanethiol (Pesika 2002).

Several techniques synthesize zinc oxide in a wide range of particle sizes and shapes using solution chemistry and calcinations (Bahnemann 1987; Spanhel and Anderson 1991; Al-Hilli and Willander 2006; Wang 2006). Zinc oxide ultrafine particles' surface and photocatalytic properties are investigated by Jing (2001). Zinc oxide nanoparticles for transdermal penetration was explored by Cross (2007).

Numerous industrial patents and some literature articles emerge on zinc oxide encapsulated polymers. Most recently, zinc oxide rods (200-300 nm diameters) were conjugated to poly(N-isopropylacrylamide) hydrogel for bioimaging (John 2010). Zinc oxide was dispersed in oil phase of water-in-oil for cosmetic usage (Michiya 2007). An oil-in-water type with a triazine and silicone compound is patented for photoprotecting the skin by L'Oreal (Allard and Gombert 2001). Kanagawa, Japan-based researchers for Shiseido have patented a development process of zinc oxide that is UV protective and transparent for cosmetic and sunscreen usage.

Zinc oxide has been encapsulated in multiple polymers, for example, polystyrene, amphiphilic *N*,*N*-dimethylacrylamide (DMAA) (Sakohara and Mori 2008), inorganic siloxane compounds Inoue JP 04161245 1992, poly(N-vinyl lactam)-polysaccharide for antimicrobial applications (Gruening 2005) or surface functionalized (Khrenov 2005). Zinc oxide in polyurethane decreased adhesion of astroglia neuronal cells (Seil and Webster 2008). Zinc oxide hydrogels can be employed in wound healing and food packaging due to antimicrobial effects.

ZnO-hydrogel nanoparticles provide an alternative for safe, non-penetrating, transparent, topical sunscreen formulations. Zinc oxide nanoparticles within hydrogel nanoparticle improve the individual properties for use within a sunscreen; zinc oxide particles are employed in sunscreens and polyacrylamide as a thickening agent. This work limits agglomeration of nanoparticles into microparticles reducing the white appearance while improving dispersion of nanoparticles improving absorbance of UV light. Utilizing physical sunscreen in a biocompatible hydrogel would be advantageous over chemical sunscreens for consumers with sensitive skin. The hydrogel portion provides compatibility with sweat though the nanoparticle-hydrogel is not tested water-proof

usage. Chemical sunscreens have higher sensitivities thus utilizing the physical broad spectrum sunscreen generates a non-irritating product and improving the physical broad spectrum ingredient dispersion reduces the visible white appearance; both advantageous for consumers.

This work produces zinc oxide-embedded hydrogel nanoparticles by inverse miniemulsion polymerization and supercritical drying for potential topical applications. Two types of zinc oxide (about 1 μm and 50 nm in size) are encapsulated into hydrogel of crosslinked polyacrylamide in this work by means of an inverse miniemulsion polymerization process and supercritical carbon dioxide drying to create nanopowder. Effect of various process parameters, the size of zinc oxide and the amount of ultrasonication applied are examined on their effectiveness to absorb UV while transmitting visible light.

4.2 Materials and Methods

Acrylamide and N,N-methylenebisacrylamide, both biochemistry electrophoresis grade 99+% pure, were obtained from Acros Organic. Azoisobutyronitrile (AIBN), sorbitan monooleate (Span 80), ZnO microparticles (99% <1μm), and ZnO nanoparticles (97% <50nm) were obtained from Sigma Aldrich. HPLC grade isopropanol, cyclohexane, and water were obtained from Fisher Scientific.

4.2.1 Step 1: Inverse-miniemulsion ZnO-hydrogel formation

Method for ZnO-hydrogel formation is similar to that for synthesizing polyacrylamide hydrogel as mentioned in Chapter 2. Zinc oxide particles were suspended in the aqueous phase with monomer and crosslinker by ultrasonication. This disperse phase was added to the continuous phase and the reaction method was continued per the method in Chapter 2.

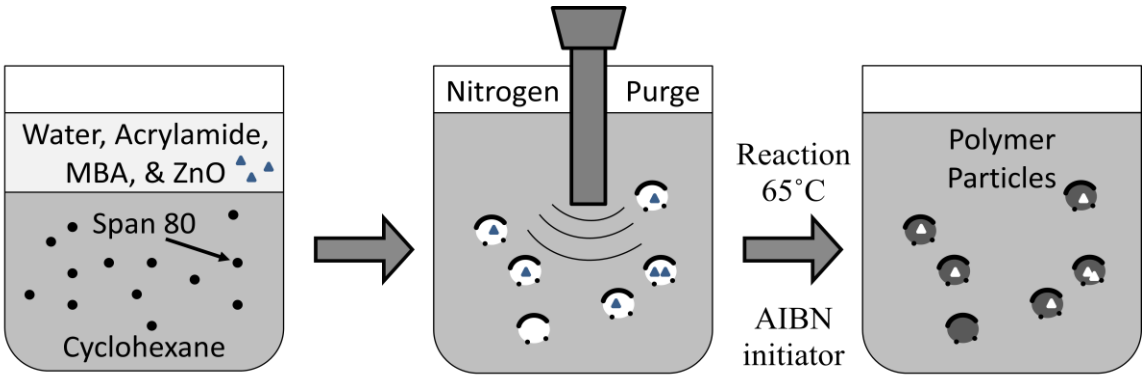

Figure 4.1. Inverse-miniemulsion polymerization to produce hydrogel-ZnO nanoparticles

4.2.2 Step 2: Supercritical drying

Supercritical drying experiments were carried out in 100 ml vessel with identical methods employed in Chapter 2. A reproduction of the process flow diagram set-up is provided.

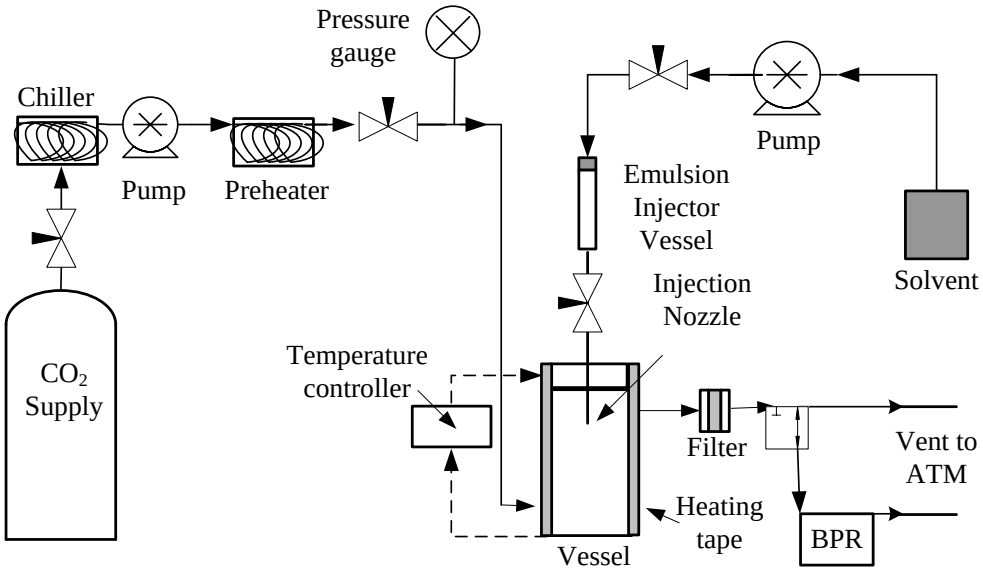

Figure 4.2. Supercritical drying process flow diagram

4.2.3 Particle characterization.

Nicolet IR100 Fourier transform infrared (FTIR) spectrometer was utilized to confirm polymerization of acrylamide to polyacrylamide. NICOMP 380 (Particle Sizing System) dynamic light scattering (DLS) instrument was used to determine the hydrodynamic diameters of particles. Zeiss EVO 50 transmission electron microscope (TEM) was used to obtain micrographs of particles that were suspended in cyclohexane and dried on 300 mesh copper grids. Zinc oxide-hydrogel particles blended in petroleum jelly were evenly spread onto microscope slides then analyzed by light microscopy before and after exposure to water.

4.2.4 Ultraviolet Transmittance.

Ultraviolet/visible spectroscopy is utilized to discern absorption of light from 200 to 800 nm where visible light is from 400 to 800 nm. Ultraviolet (UV) radiation having wavelengths less than 200 nm is difficult to handle, thus is seldom used as a routine tool for analysis. A modified method developed by Cao et al. (2009) was used to analyze UV and visible light transmission. In this method, the powder was added to melted white petrolatum (65°C), ultrasonication of sample (short or long duration of time), then placing melted dispersed sample between quartz plates with a polyethylene spacer, pressed and allowed to cool to room temperature (Figure 4.3). Analysis of UV/Visible transmission on a Genesis 2 Spectrometer was carried out at four points: 290, 320, and 360 nm to encompass UVA and UVB radiations, and visible light at 500 nm (Figure 4.4).

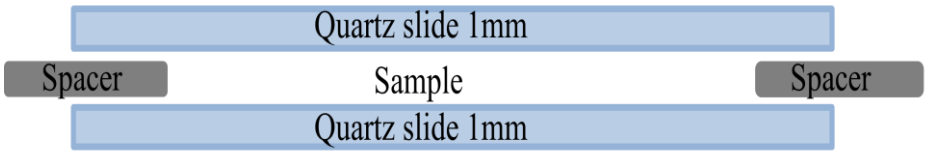

Figure 4.3. Diagram of the apparatus for UV transmission.

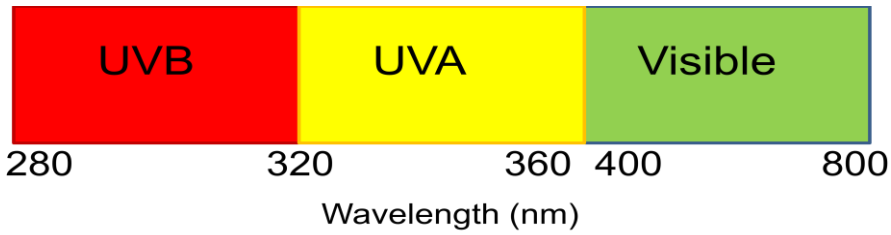

Figure 4.4. Diagram of ultraviolet and visible light detection points.

4.3 Results & Discussion

Hydrogel blanks, pure ZnO nanoparticles, and ZnO loaded-hydrogel particles were evaluated for UV and visible light transmittance. Experiments were performed at varying concentrations (1, 2, and 5 wt%) of zinc oxide with respect to the monomer (acrylamide) amount used (Table 4.1). Confirmation of polymerization by FTIR, particle size distributions by dynamic light scattering, transmission electron microscopy images, and UV/Vis transmission results are examined.

Expt.	ZnO Size	ZnO amount wt%
A	---	0
B	<50nm	1
C	<50nm	2
D	<50nm	5
E	<1um	2

Table 4.1. Experimental loading of ZnO quantity (wt% to monomer amount).

Confirmation of polymerization during miniemulsion polymerization can be inferred from the FTIR spectra shown in Figure 4.6. The functional group C=C in the monomer acrylamide vibrates at 980 cm^{-1} wavelength showing two peaks in this region. Upon polymerization, both of these peaks disappear confirming the conversion of the vinyl groups. Additional peaks shown are due to C=O at 1630-1700 cm^{-1}, NH_2 deformation at 1550 cm^{-1}, and primary amides at 1420-1400 cm^{-1}.

The polymerization process produces a white miniemulsion. As such, the incorporation of zinc oxide into the disperse phase proved difficult to detect any dissonance with the polymerization process.

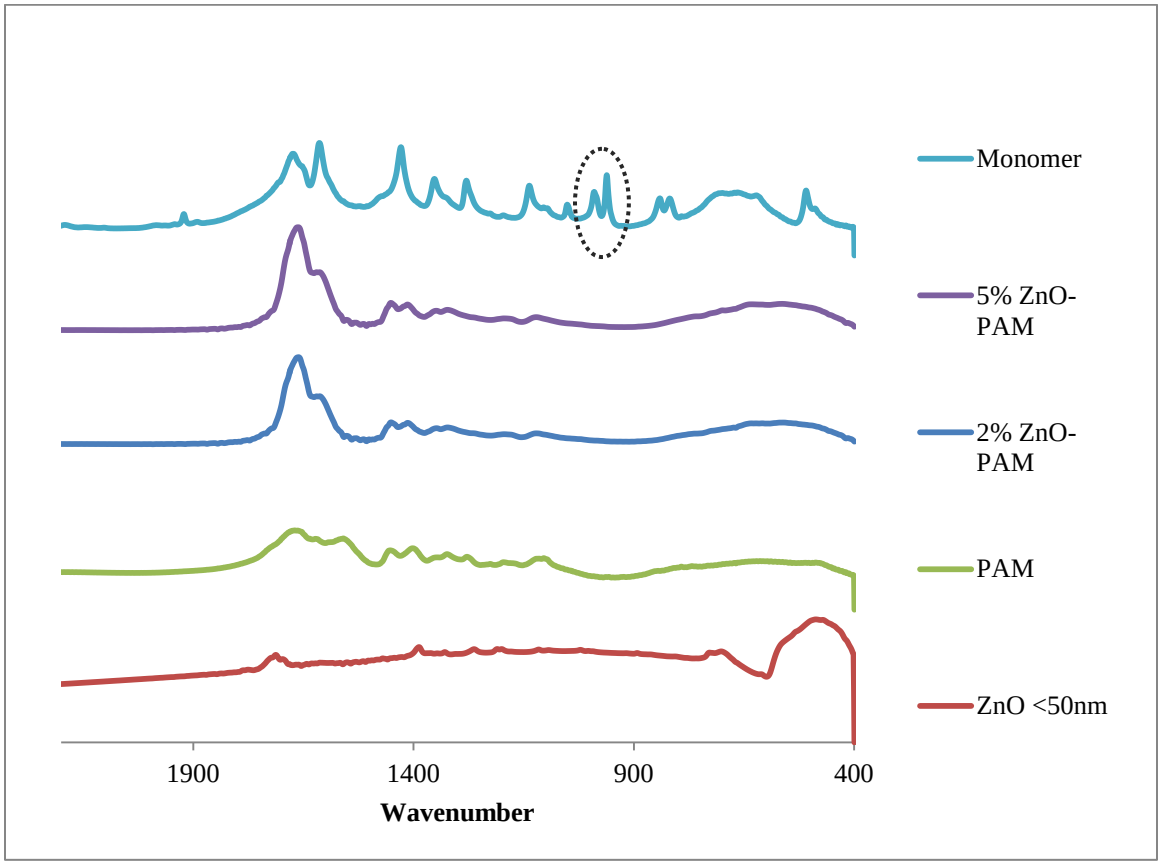

Figure 4.5. FTIR spectra of ZnO experiments: ZnO < 50nm, polyacrylamide (PAM), 2% ZnO-PAM, 5% ZnO-PAM, and acrylamide monomer, circled is the vinyl group.

4.3.1 Transmission Electron Microscopy Images

The spherical morphology of polyacrylamide nanoparticles produced remains constant with and without zinc oxide present. Zinc oxide microparticles are very dense and allow no transmission of electrons. The ZnO nanoparticles are not entirely opaque on transmission electron microscope images (TEM) (Figure 4.6) but the distinct shape compared to spherical PAM allows for clear differentiation between the two types of particles.

The larger PAM particles absorb more electron charge in TEM than the smaller spheres causing difficulty distinguishing if a darker shape within the sphere is a zinc oxide particle or the overlap of another polymer particle. The occurrence of the smaller less dense PAM particles increased when decreasing the water content of the miniemulsion process to 2.25 g thus creating smaller PAM particles; here some larger polyacrylamide particles are still present. All scale bars are 200 nm unless otherwise marked.

As demonstrated by the TEM images, not every polymer particle contains zinc oxide. From the images, there appears an improved ability to encapsulate the <50nm than the <1µm ZnO nanoparticles. Circles indicate the ZnO embedded within the hydrogel in Figures 4.8-10. The larger zinc oxide particles (Expt. E) were difficult to fully encapsulate due to the similarity in size to the polymer particles (Figure 4.7). The zinc oxide tends to be on the outer portions of the polymer particles. This is attributed to the curvature of the water droplet and cohesive forces in the polymerization process prior to drying. The zinc oxide that is not encapsulated in the polymer may have been partially encapsulated on the outer portion of the particle and after supercritical drying the zinc oxide was worked loose by shear forces from the soft loosely crosslinked hydrogel; increasing the crosslinker amount could overcome this. The smaller zinc oxide particles with polyacrylamide appear to be well separated compared to the images of the physically mixed sample (Figure 4.11) and petrolatum (Figure 4.12). The zinc oxide in these images forms larger agglomerates than the zinc oxide encapsulated with polyacrylamide.

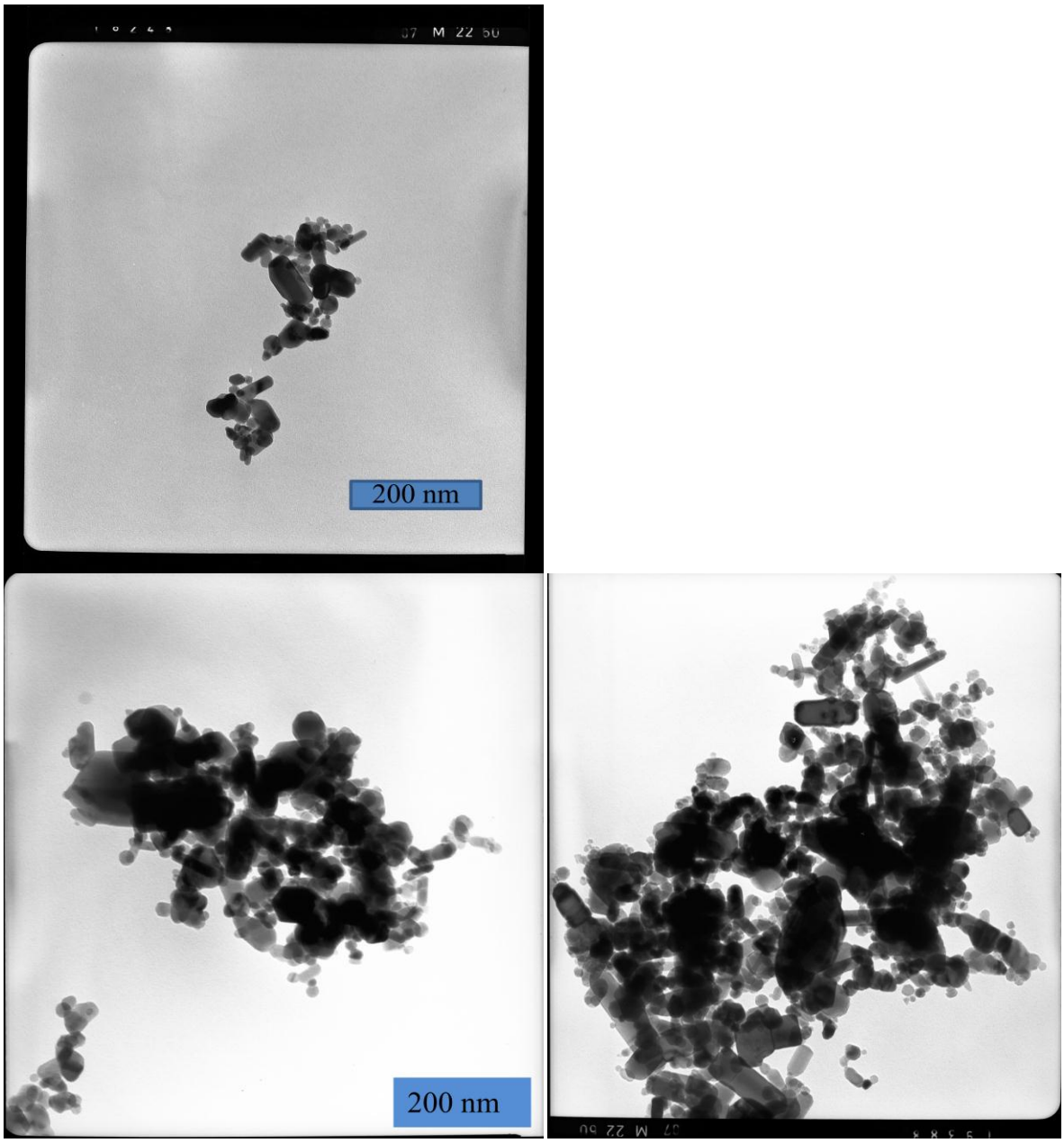

Figure 4.6. TEM image of ZnO nanoparticles. Magnification, 100k.

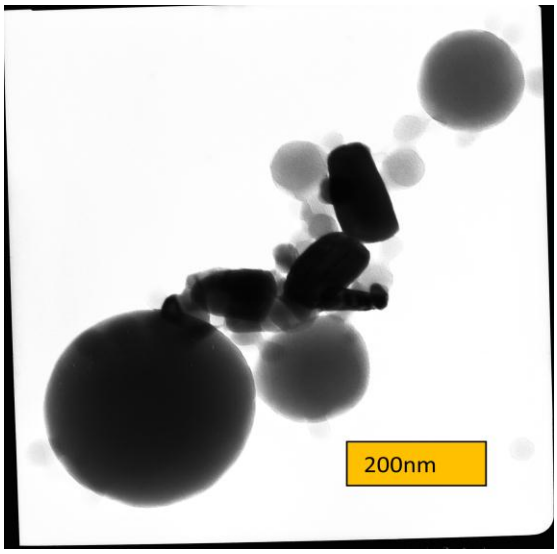

Figure 4.7. TEM image 2% ZnO microparticles in PAM. Magnification, 100k.

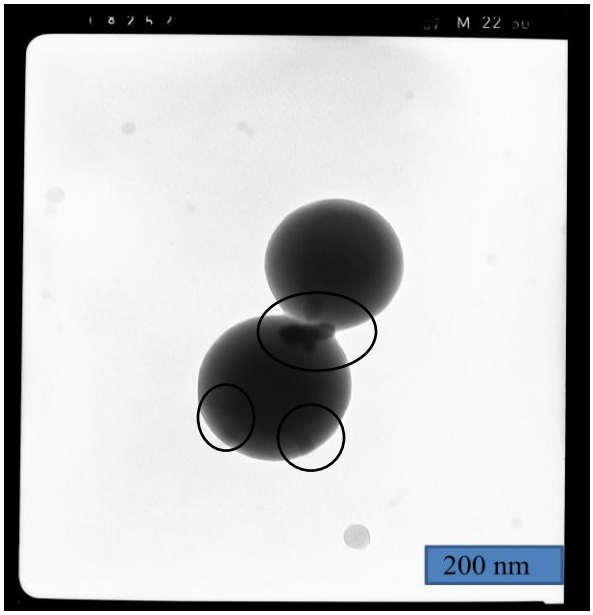

Figure 4.8. TEM image: 2% ZnO nanoparticles in PAM: circles indicate locations of ZnO within the PAM: scale bar is 200 nm. Magnification, 100k.

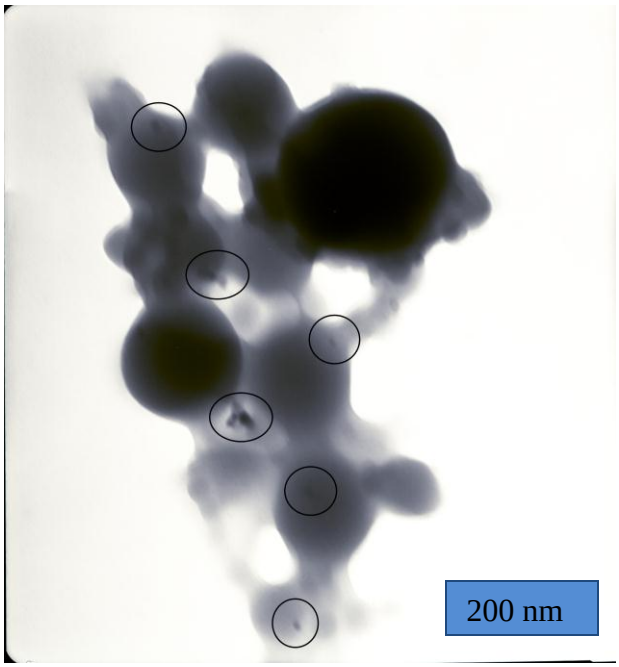

Figure 4.9. TEM image: 2% ZnO nanoparticles in PAM. Magnification, 100k.

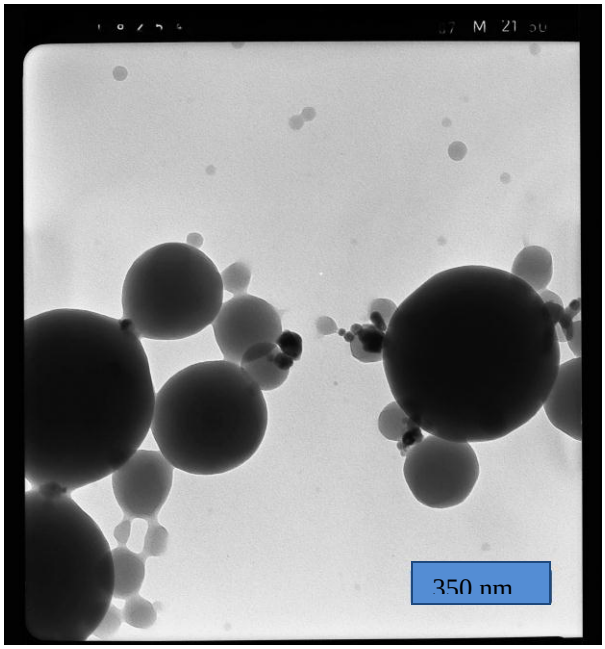

Figure 4.10. TEM image: 2% ZnO nanoparticles in PAM. Magnification, 80k.

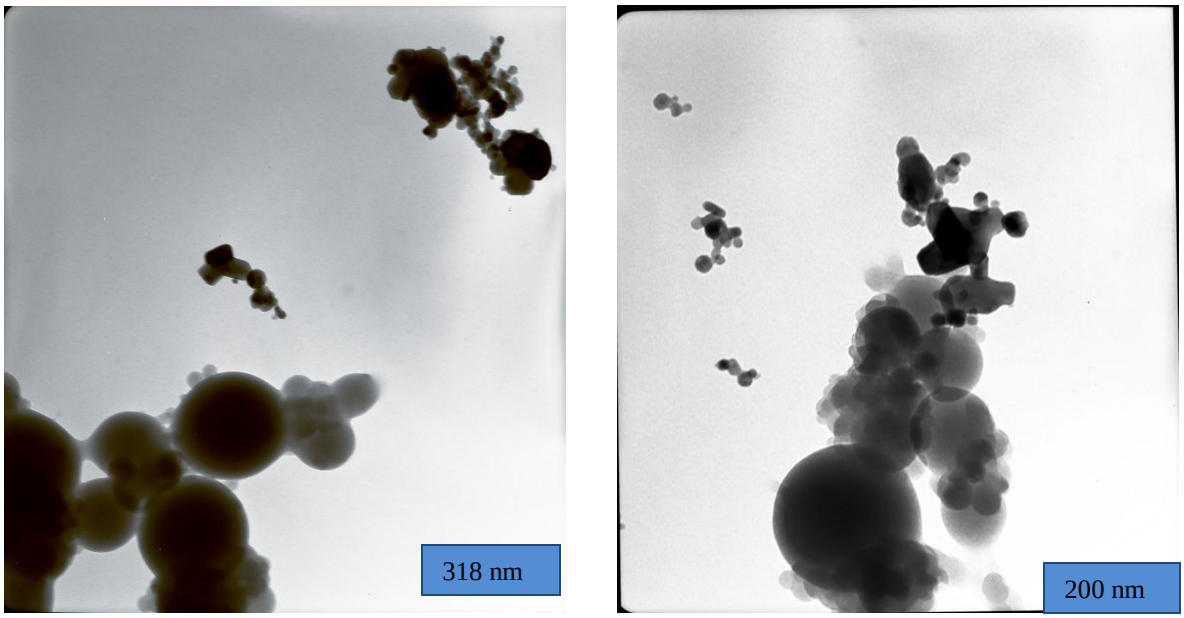

Figure 4.11. Physically mixed ZnO nanoparticles and PAM nanoparticles. Magnification, 63 k (left) and 100 k (right).

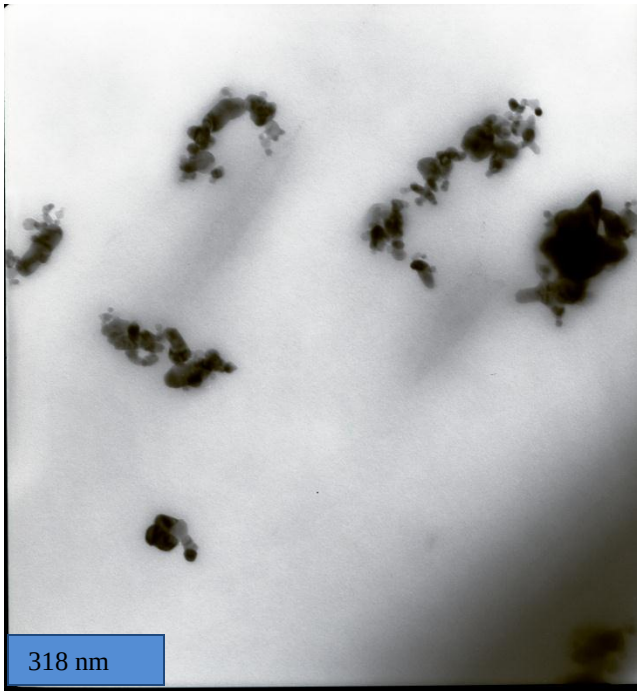

Figure 4.12. TEM ZnO nanoparticles in petrolatum. Magnification, 63k.

4.3.2 Dynamic Light Scattering

Two types of particle size distributions, number weighting (NMD) and volume weighting (VMD), are obtained (Table 4.2). Number weighted mean diameter of polyacrylamide was steadily around 100 nm, consistent with sizes in the TEM images. Zinc oxide within aqueous phase is easier to disperse into individual particles with ultrasound as seen with the DLS graphs (Figures 4.13-18). The original zinc oxide samples were evaluated in water. Viewing the NMD the zinc oxide is near the vendor assessment of <50 nm and the VMD is bimodal with 50 nm and 250 nm, most likely a complex of three particles together. All particles produced have NMD near 100 nm.

DLS data was obtained for pure zinc oxide samples in petrolatum heated to 65˚C. This data produced interesting results (Figures 4.19-20). When mixed with petrolatum, the interactions between the petrolatum and zinc oxide (<50nm) were minimized by the aggregation of zinc oxide yielding large clusters identified by DLS volume weighted average of 872 nm and the number weighted average 180 nm. This leads to the strong likelihood that the zinc oxide remained in the aqueous disperse phase droplets prior to polymerization and would have a stronger attraction to staying inside the polyacrylamide.

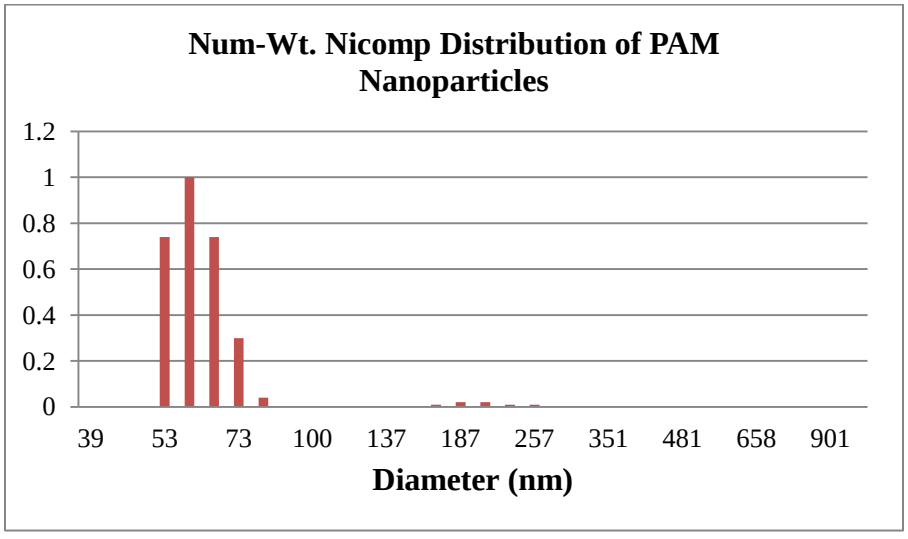

Figures 4.13. Number-weighted hydrogel particle size distribution.

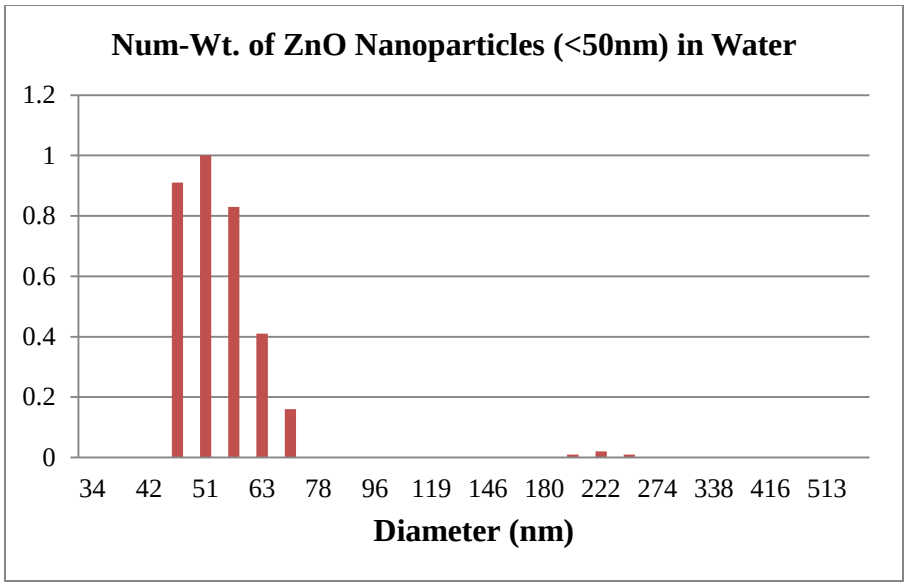

Figures 4.14. Number-weighted hydrogel particle size distribution.

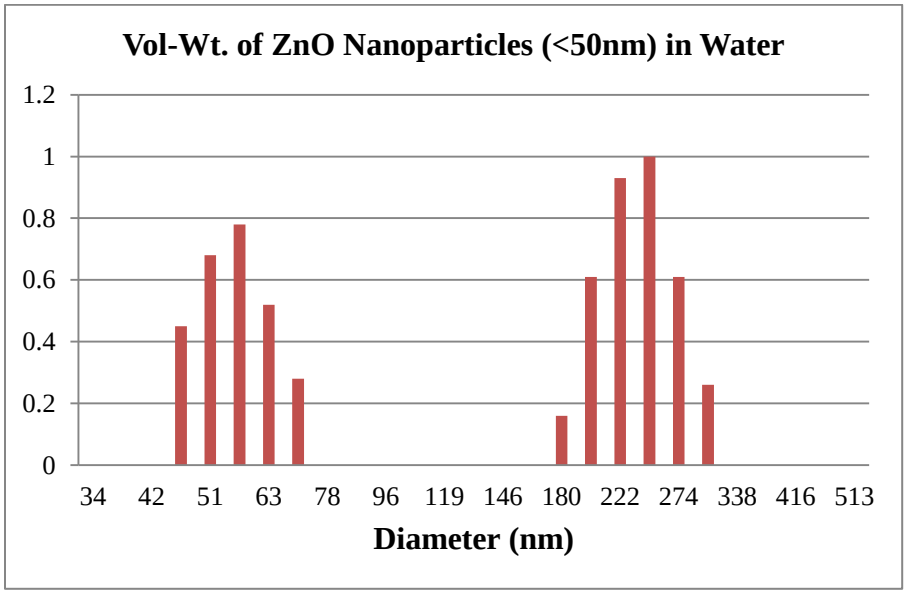

Figures 4.15. Volume-weighted hydrogel particle size distribution.

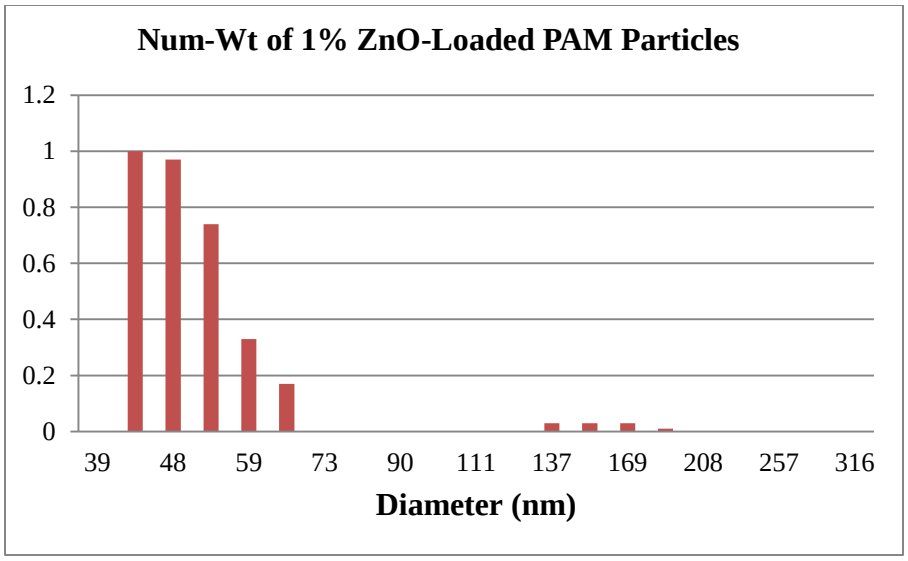

Figures 4.16. Number-weighted hydrogel particle size distribution.

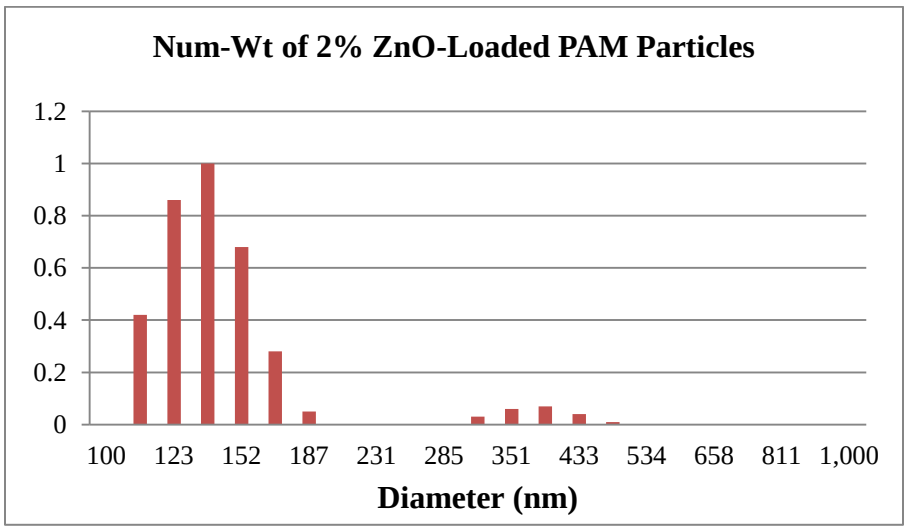

Figures 4.17. Number-weighted hydrogel particle size distribution.

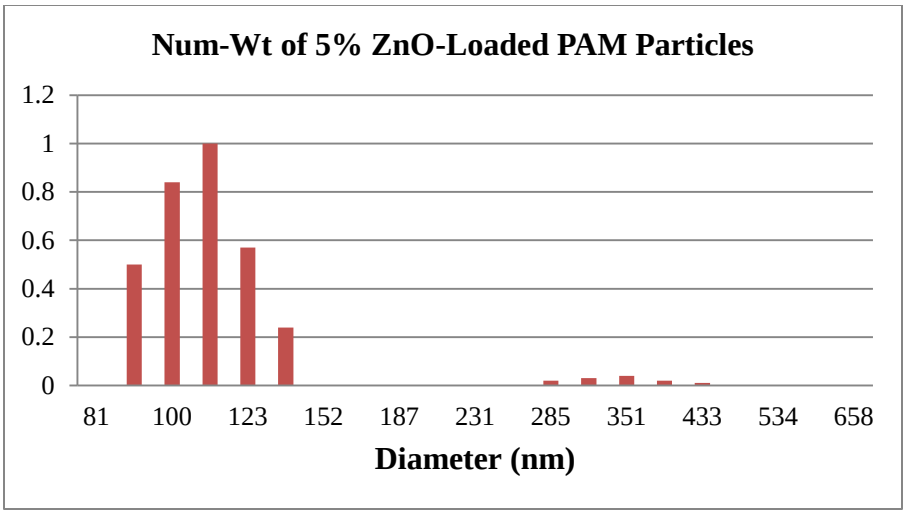

Figures 4.18. Number-weighted hydrogel particle size distribution.

Expt.	ZnO Size	ZnO%	Avg NMD	Avg VMD
A	---	0		
B	<50nm	100	55.8	160
C	<50nm	1	51.3	115.8
D	<50nm	2	141.7	301.2
E	<50nm	5	74.3	154.5
F	<1um	2		

Table 4.2. Size distribution of zinc oxide-hydrogel particles: number weighted average (NMD) and volume weighted average (VMD) with ZnO in weight % to monomer.

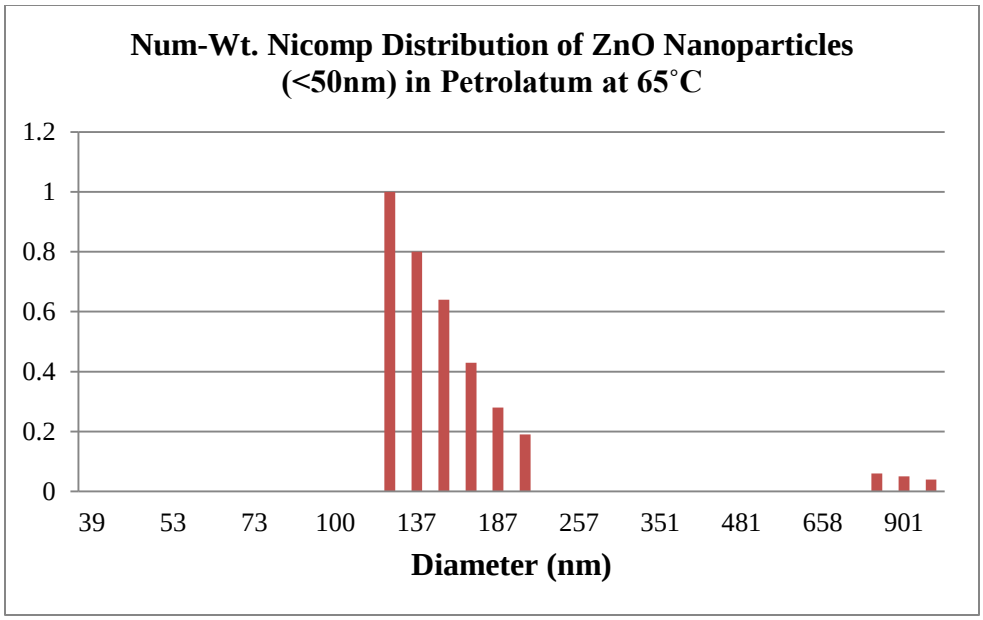

Figure 4.19. Zinc oxide in petrolatum.

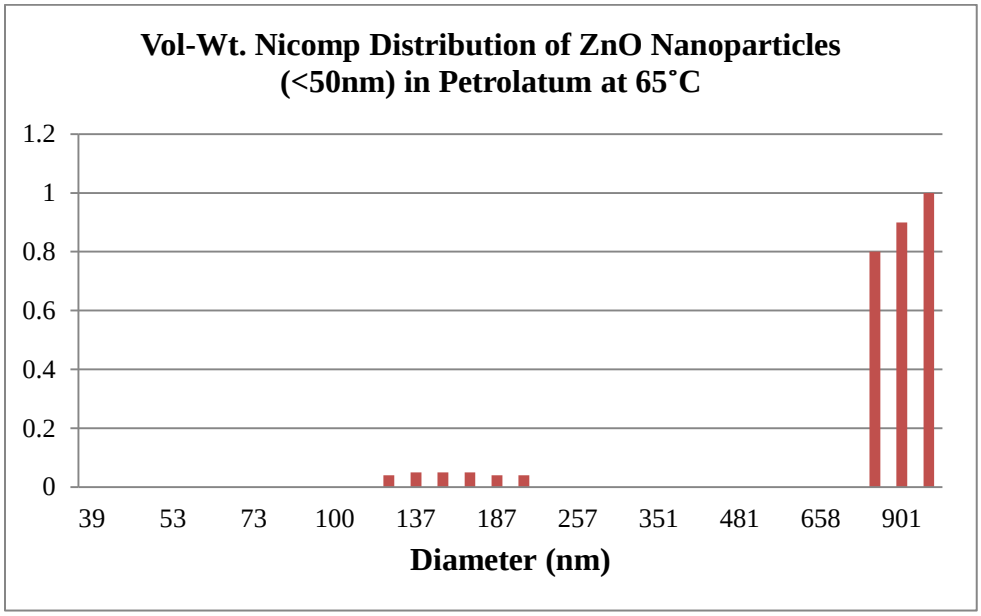

Figure 4.20. Zinc oxide in petrolatum.

4.3.3. Ultraviolet Transmittance

The desired formulation should have maximum transmission of visible light and minimum transmission of ultraviolet light. The light transmission was tested using a modification of the method developed by Cao et al. (2009), in which particles are mixed with melted petrolatum and then applied onto quartz plates for UV/Visible analysis.

Multiple concentrations of zinc oxide in petrolatum were investigated as well as various exposures to ultrasonication to determine the optimum time. The zinc oxide agglomerates in the petrolatum (Figure 4.21) and to overcome this ultrasonication of the zinc oxide in the petrolatum was utilized. Increments of 2 minutes, 3 minutes, 20 minutes and 30 minutes ultrasonication (US) were applied by an ultrasonication horn at 10% amplitude. The short duration is compared to the long duration (Figure 4.23). The smaller the concentration of zinc oxide loading, for example 0.5%, the less ultrasound duration was required to achieve a similar absorbance as a higher concentration of zinc oxide with less ultrasound exposure. Further sample analysis employed longer duration ultrasonication to improve the dispersion of the particles.

When analyzed separately, both petrolatum and polyacrylamide absorb light. Petrolatum has transmissions of 45% at 290 nm and 85% at 500 nm. Polyacrylamide shows a more linear trend than petrolatum across the four wavelengths examined: 3.8% at 290 nm, 9.4% at 320 nm, 14.3% at 360 nm, and 25.5% at 500 nm.

To study water uptake, petrolatum that contained 13% polyacrylamide particles was spread upon a microscope slide. Water droplets were placed at various locations on the slide and observed for visible separation over time. After 6 hours, no separation was detected; hence in the presence of water the hydrogels maintain their original location. The hydrogel particles will be a conduit of compatibility between the skin and aqueous perspiration as hydrogels can absorb larger amounts of water. As hydrogel absorbs water, they become more transparent as the refractive index becomes nearly that of water.

The amount and size of zinc oxide loaded into polyacrylamide nanoparticles has an effect on the amount of UV absorbed and visible light transmitted. To have absorption greater

than that of polyacrylamide by itself, more than 2% zinc oxide must be loaded into the hydrogel (Figure 4.25). When utilizing the same amount of zinc oxide material, nanoparticle ZnO can yield greater surface area coverage compared to larger ZnO particles as the probability a UV beam interacting with zinc oxide nanoparticle goes up (Figure 4.22). By zinc oxide nanoparticles being embedded within the hydrogel improvement of separation between zinc oxide nanoparticles was achieved preventing agglomerations and decreasing the amount of UV light transmitted. This could be attributed to the larger surface area available generated by the embedded nanoparticles and distributed throughout the sample. Improved distribution within the petrolatum enhances the transmission as seen in Figure 4.23. Higher concentrations of nanoparticles loaded into the petrolatum demonstrate generally lower transmission of ultraviolet light. Hence, the ZnO nanoparticles reduce transmission of UV light while maintaining a low absorption of visible light (Figure 4.24).

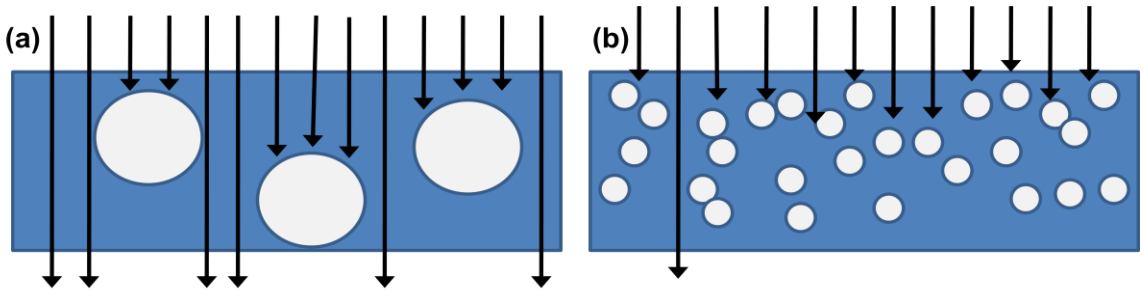

Figure 4.21. Diagram of different surface coverage by same mass of zinc oxide particles a) ZnO microparticles and b) ZnO nanoparticles.

Disparity in the sample thickness between slides can contribute to variations in the results; the measurement error of the thickness was to the nearest 40 μm. Concentration gradient was sometimes evident and visible from the slide preparation and yielded varied results, hence multiple samples were prepared to confirm results. The average thickness of all slides was 130 μm with a standard deviation of 60 μm. Thickness deviations in the individual slides are minor but present which correlated to slight differences in transmission. To avoid this bias, measurements were made for samples at three positions on the slide: center, left and right.

Trends of UV light transmission is slightly linear until the visible light where a drastic increase of transmittance occurs with constant powder loadings of 200 mg of varying percentages of zinc oxide (Figure 4.22). The amount of powder loaded into the petrolatum was maintained constant at 13.1 wt% with the zinc oxide concentration varied (1, 2, and 5% in the polymer) and long ultrasound duration was applied to all samples for mixing with petrolatum. The addition of zinc oxide to polyacrylamide began to overcome the initial absorption by polyacrylamide itself at 5% loading. The 0.5% loading with high ultrasonication time (25 minutes) produced the most drastic difference in transmission at visible light compared to ultraviolet.

The same percentage (2 wt%) of the two types of zinc oxide particles are compared in Figure 4.24. The difference between the UV and visible transmittance is larger for the nanoparticles than microparticle. Embedded within polyacrylamide, the smaller zinc oxide nanoparticles are not hindered from absorbing UVB but appear to have a lower UVA absorption. Zinc oxide particles polymerized with hydrogel are still capable of absorbing UV light, but absorbs UVB slightly better than UVA.

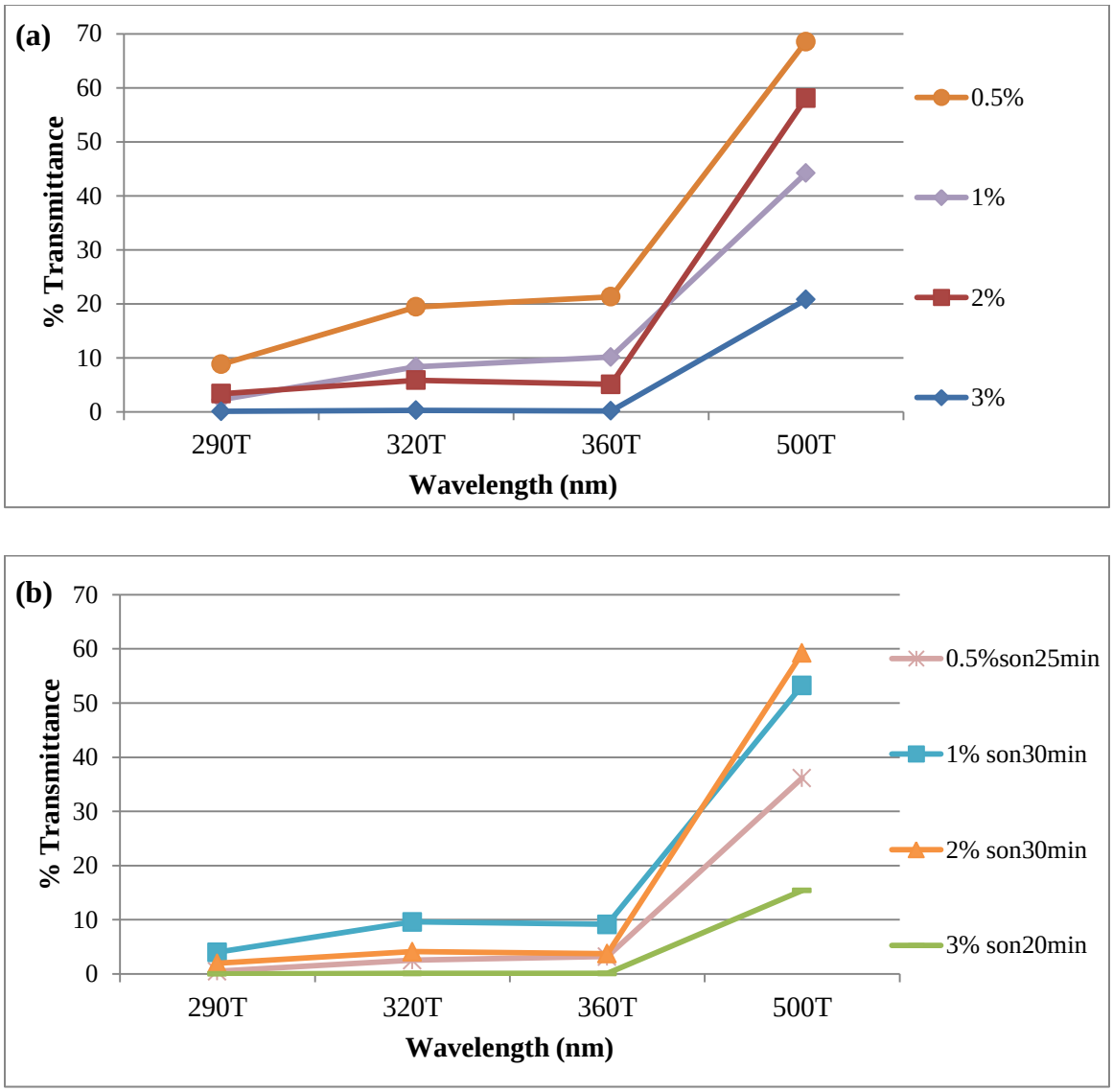

Figure 4.22. Two ultrasonication durations: a) (2-3min) and b) (20-30min), applied to zinc oxide (<50nm) in petrolatum.

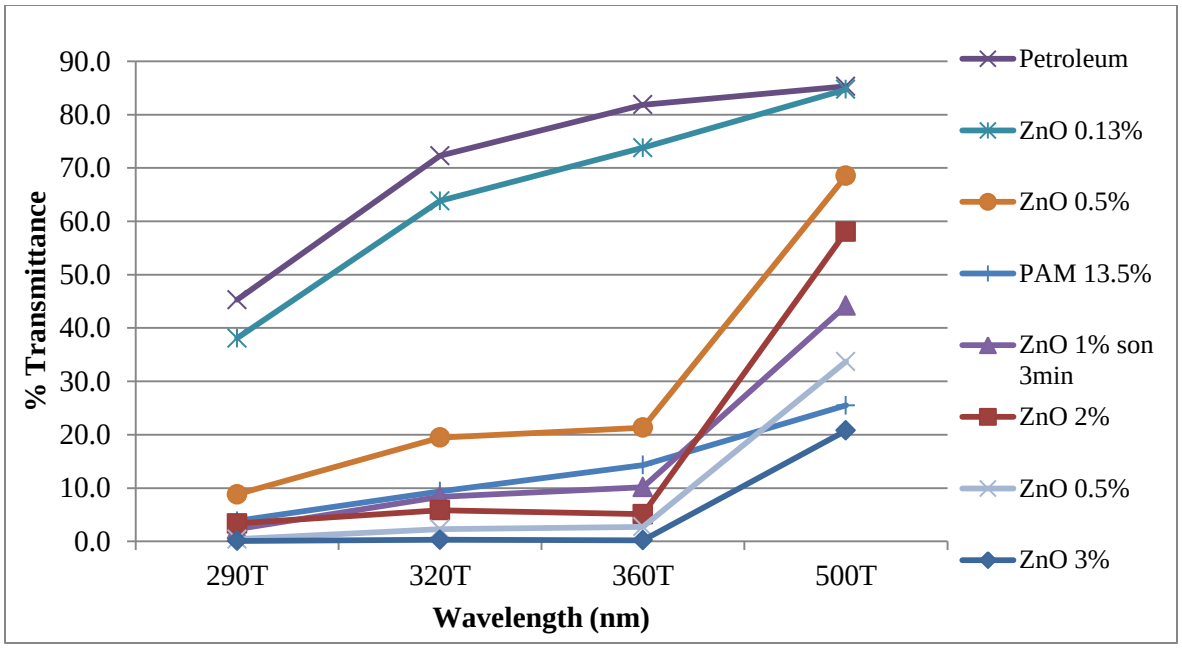

Figure 4.23. Varying concentration of zinc oxide (<50nm) in petrolatum.

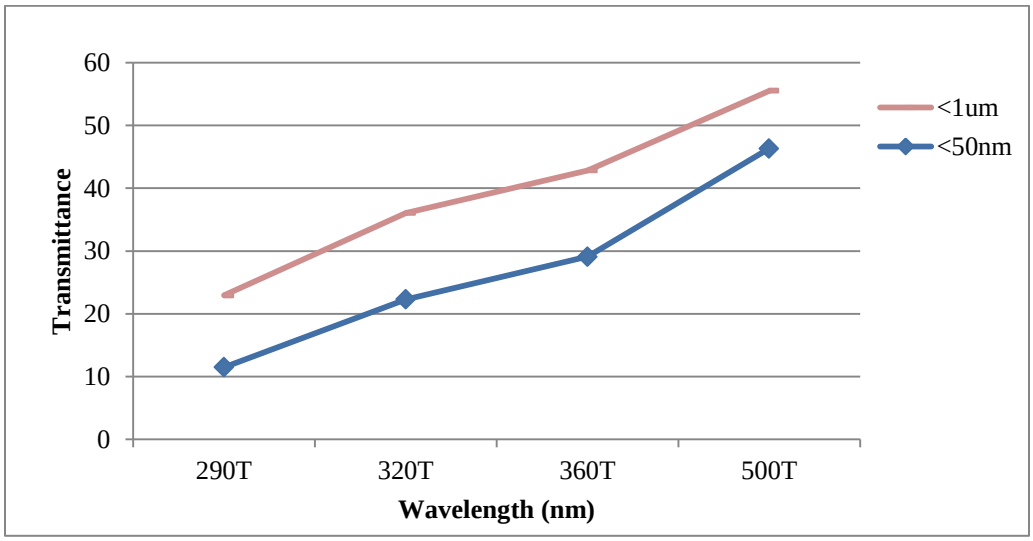

Figure 4.24. UV transmission between 2% zinc oxide hydrogel particles <50nm and <1µm.

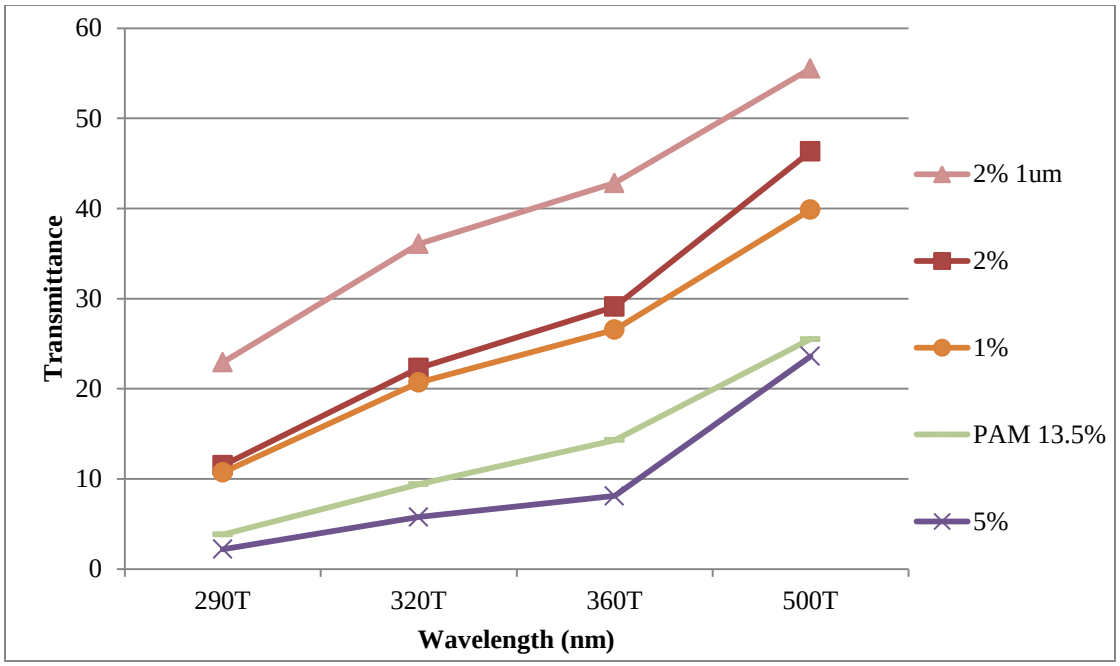

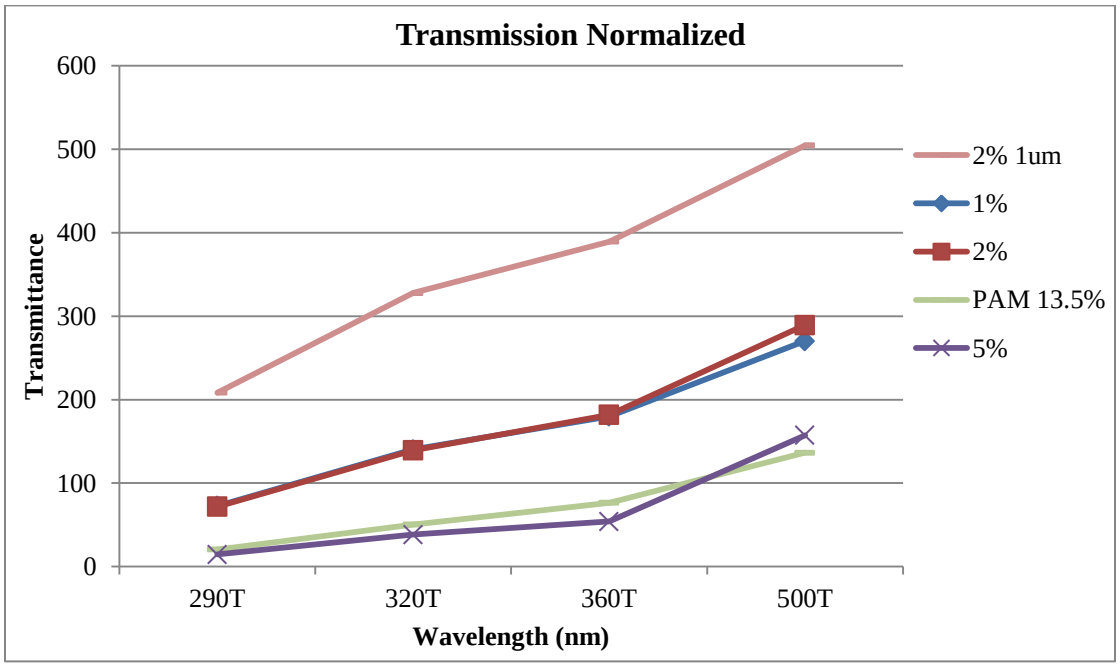

Figures 4.25. UV transmission of zinc oxide hydrogel nanoparticles (200mg).

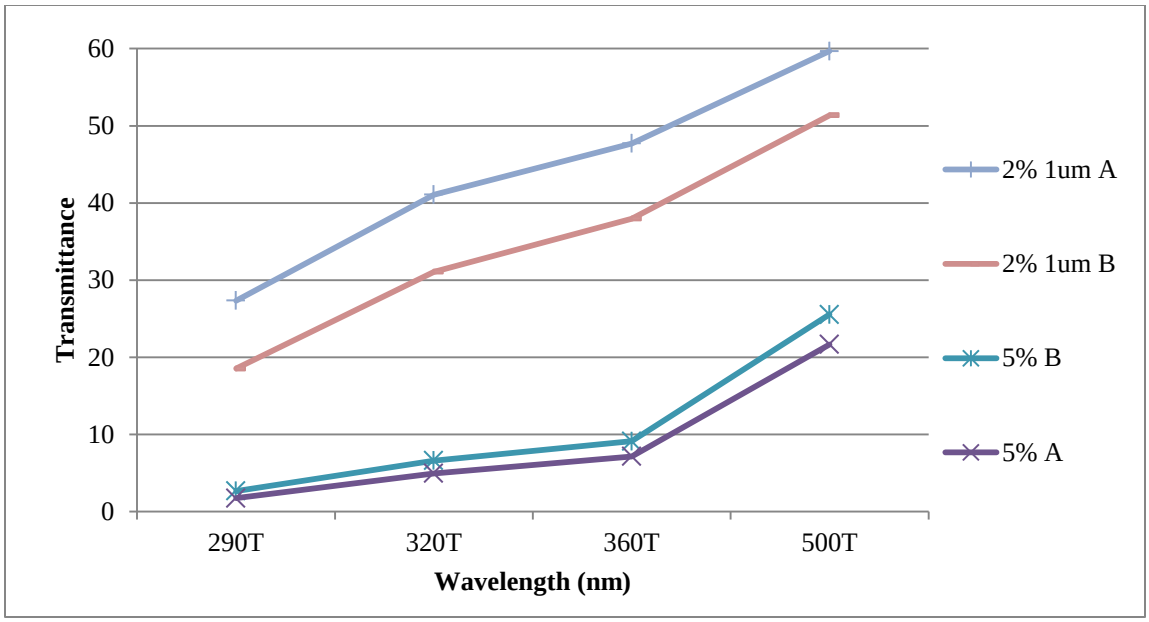

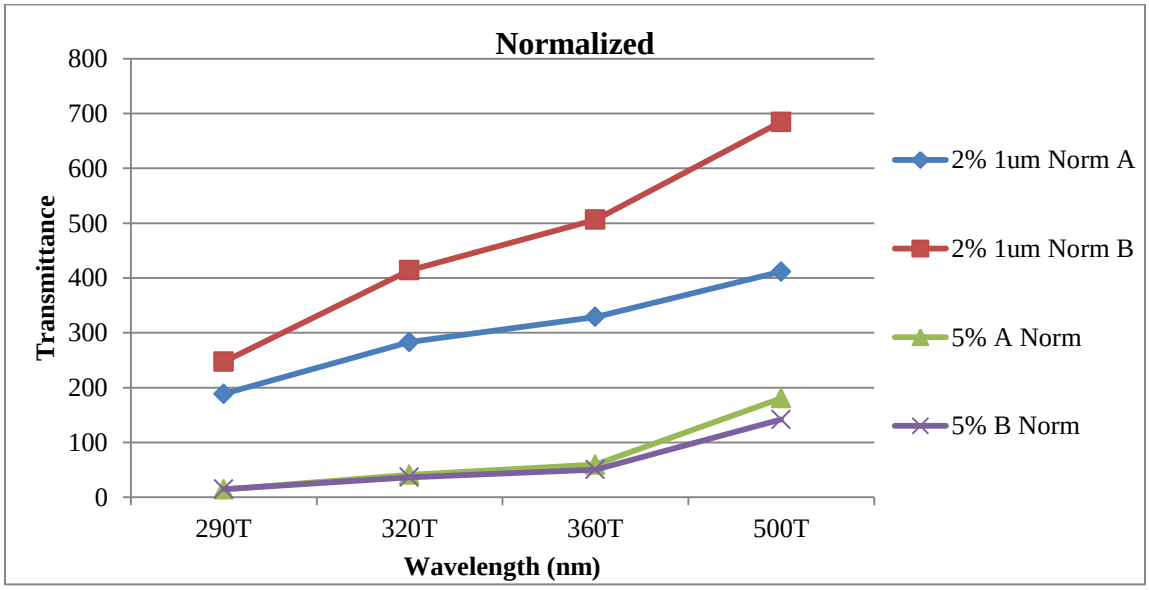

Figure 4.26. UV transmission between two samples on different slides compared to their normalized.

4.5 Conclusions

Zinc oxide nanoparticles were successfully loaded into hydrogel nanoparticles. The compatibility of zinc oxide in water allowed for incorporating the metal oxide into the aqueous phase prior to polymerization. UV absorption can be enhanced by an increase in the concentration of zinc oxide and/or an increase in the dispersion of particles in the petrolatum jelly by ultrasonication. The morphology of polyacrylamide nanoparticles produced with and without zinc oxide present remains spherical. Zinc oxide nanoparticles have improved separation with the presence of polyacrylamide preventing agglomerations. At a fixed weight loading of ZnO in hydrogel, when compared to microparticles, zinc oxide nanoparticles show higher absorption of UV light and a lower absorption of visible light.

4.6 References

Al-Hilli, S. M. and M. Willander (2006). "Optical properties of zinc oxide nano-particles embedded in dielectric medium for UV region: Numerical simulation." Journal of Nanoparticle Research **8**: 79-97.

Allard, D. and C. Gombert (2001). Synergistically UV-photoprotecting triazine/silicone compositions. Societe L'Oreal S.A. United States. **6,171,579**.

Anzlovar, A., Z. C. Orel, et al. (2008). "Nanocomposites with nano-to-sub-micrometer size zinc oxide as an effective UV absorber." Polymeri **29**: 84-87.

Bahnemann, D. W., C. Kormann, et al. (1987). "Preparation and Characterization of Quantum Size Zinc Oxide: Fluoresence and Non Linear Optical Effects." J. Phys. Chem B **91**: 3789-3798.

Bryden, A. M., H. Moseley, et al. (2006). "Photopatch testing of 1155 patients-results of the U.K. multicentre photopatch study group." British Journal of Dermatology **155**(4): 737-747.

Cao, Z., Z. Zhang, et al. (2009). "Synthesis and UV shielding properties of zinc oxide ultrafine particles modified with silica and trimethyl siloxane." Colloids and Surfaces A: Physiochem. Eng. Aspects **340**: 161-167.

Cross, S. E., B. Innes, et al. (2007). "Human Skin Penetration of Sunscreen Nanoparticles: In-vitro Assessment of a Novel Micronized Zinc Oxide Formulation." Skin Pharmacology and Physiology **20**(3): 148-154.

FDA. (2009). "Food and Drug Administration. Radiation-Emitting Products - Sunscreen." Retrieved 3/2010, from http://www.fda.gov/Radiation-EmittingProducts/RadiationEmittingProductsandProcedures/Tanning/ucm116445.htm.

Gruening, R., D. J. Perschbacher, et al. (2005). Anti-infectious hydrogel compositions. I. Hydromer, USA. United States.

Guo, L., S. Yang, et al. (2000). "Synthesis and Characterization of poly(vinylpyrrolidone)-Modified Zinc Oxixde Nanoparticles." Chemical Materials **12**: 2268-2274.

Haishi, T., E. Sakamoto, et al. (1992). Flaky powder of zinc oxide and its composition for external use. United States.

Hanson, K. M., E. Gratton, et al. (2006). "Sunscreen enhancement of UV-induced reactive oxygen species in the skin." Free Radical Biology and Medicine **11**(8): 1205.

Jing, L., Z. Xu, et al. (2001). "The surface properties and photocatalytic activities of ZnO ultrafine particles." Applied Surface Science **180**: 308-314.

John, S., S. Marpu, et al. (2010). "Hybrid zinc oxide nanoparticles for biophotonics." Journal of Nanoscience and Nanotechnology **10**(3): 1707-12.

Khrenov, V., M. Klapper, et al. (2005). "Surface Functionalized ZnO Particles Designed for the Use in Transparent Nanocomposites." Macromolecular Chemistry and Physics **206**(1): 95-101.

Klein, K. (2004). "Using zinc oxide in sunscreen products." Cosmetics & Toiletries **199**: 22-25.

Levine, K. L., J. O. Iroh, et al. (2004). "Synthesis and properties of the nanocomposite of zink oxide and poly(amic acid)." Applied Surface Science **230** 24-33.

Li, Q., S. L. Chen, et al. (2007). "Durability of nano ZnO antibacterial cotton fabric to sweat." Journal of Applied Polymer Science **103**(1): 412-416.
Michiya, T., K. Matsuyama, et al. (2007). Oily particles containing zinc oxide particles, hydrogel particles containing the same, and manufacture thereof. E. P. Office.
Pesika, N. S., Z. Hu, et al. (2002). "Quenching of Growth of ZnO Nanoparticles by Adsorption of Octanethiol " J. Phys. Chem. B **106** (28): 6985-6990.
Pinnell, S. R., D. Fairhurst, et al. (2000). "Microfine zinc oxide is a superior sunscreen ingredient to microfine titanium dioxide." Dermatologic Surgery - American Society for Dermatologic Surgery **26**(4): 309-14.
Rodríguez, E., M. C. Valbuena, et al. (2006). "Causal agents of photallergic contact dermitis diagnosed in the national institute of dermatology of Columbia." Photodermatol Photoimmunol Photomed **22**(4): 189-192.
Sakohara, S. and K. Mori (2008). "Preparation of ZnO nanoparticles in amphiphilic gel network." Journal of Nanoparticle Research **10**(2): 297-305.
SCCP (2006). "Opinion on Benzophenone-3." European Commission - Scientific Committee on Consumer Products.
Seil and Webster (2008). Int J Nanomedicine **3**(4): 523-31.
Society, A. C. (2009, 2009). "Skin Cancer Facts." from www.acs.org.
Spanhel, L. and M. A. Anderson (1991). "Semiconductor clusters in the sol-gel process: quantized aggregation, gelation, and crystal growth in concentrated zinc oxide colloids." Journal of the American Chemical Society **113**(8): 2826-2833.
Sutton, R. (2008). "CDC: Americans Carry Body Burden of Toxic Sunscreen Chemical - Environmental Working Group (EWG)." Environmental Working Group Science Analysis, from www.ewg.org/analysis/toxicsunscreen.
Wahab, R., A. Mishra, et al. (2010). "Antibacterial activity of ZnO nanoparticles prepared via non-hydrolytic solution route." Applied Microbiology and Biotechnology **87**(5): 1917-1925.
Wang, Z. L. (2006). "Novel Zinc Oxide Nanostructures Discovery by Electron Microscopy." Journal of Physics: Conference Series **26**: 1-6.
WHO. (2010). "Ultraviolet radiation and the INTERSUN Programme." World Health Organization Retrieved 3/2010, from http://www.who.int/uv/en/.
Yamamoto, O., M. Komatsu, et al. (2004). "Effect of lattice constant of zinc oxide on antibacterial characteristics." Journal of Materials Science: Materials in Medicine **15**(8): 847-851.

5.0 COATING OF HYDROGEL PARTICLES USING SUPERCRITICAL CO_2

5.1 Introduction

Coating technologies have numerous applications in pharmaceutical, food, fertilizer, cosmetics, electronic, and biomedical fields (Cao 2008). Encapsulating and coating particles are commonly carried out using organic solvent-based processes, such as coacervation, solvent evaporation, emulsification, homogenization, spray drying, and hot melt extrusion; many of these processes can result in low yields, high residual solvent, and thermal degradation of the active substance (Majerik 2007).

When supercritical carbon dioxide is utilized for coating, typically the residual solvent is very low. Supercritical technology has been utilized to coat pharmaceutical particles, by a variety of methods for delayed drug release. In the rapid expansion from supercritical solution (RESS) process, the material is first dissolved in $scCO_2$ with or without a co-solvent. The solution is then expanded rapidly through a nozzle to form coated drug particles. For example, Tom et al. showed that RESS could be used to encapsulate microparticles (Tom and Debenedetti 1991; Tom 1993); Kim et al. (1996) used RESS to encapsulate naproxen in poly(L-lactic acid); and Dos Santos (2002) coated protein microparticles with lipid compounds Dynassan® 114 and Gelucire® 50-02 utilizing a multi-step process.

When CO_2 cannot dissolve the coating material, an organic solvent can be utilized to dissolve the material and the solution is then injected into $scCO_2$ using a variety of processes including gas antisolvent precipitation (GAS) which involves injecting CO_2 into an organic solvent, supercritical antisolvent precipitation (SAS), precipitation by compressed antisolvent (PCA), aerosol solvent extraction system (ASES), and solution enhanced dispersion by supercritical fluids (SEDS). Most of these processes have focused on encapsulating pharmaceutical compounds in biodegradable polymers. For

example, GAS was used by Elvassore et al. (2001) to prepare insulin/PEG in poly(L-lactic acid) (PLA) nanoparticles. Young et al. (1999) and Falk and Randolph (1998) encapsulated lysozyme and gentamycin, respectively, in biodegradable polymers via PCA. Bleich et al. (1994) used ASES to encapsulate drugs in poly(L-lactic acid). The use of coaxial nozzles in supercritical antisolvent methods can produce and encapsulate nanoparticles simultaneously (Wang 2004). Sze Tu et al. (2002) used ASES to encapsulate para-hydroxybenzoic acid in poly(L-lactic acid). Ghaderi et al. used SEDS to encapsulate hydrocortisone into poly(L-lactic acid). Davies, Cooper, and Cocero review applications of supercritical CO_2 in the encapsulation/co-precipitation systems (Cooper 2000; Cocero 2008; Davies 2008). Supercritical antisolvent with enhanced mass transfer (SAS-EM) utilizes ultrasonication to produce nanoparticles (Chattopadhyay and Gupta 2002; Gupta and Chattopadhyay 2003).

None of above efforts have focused on utilizing supercritical technology to produce a protective shell/coating around hydrogel particles to delay hydration, which a focus of this work. Coated hydrogel particles (Figure 5.1) are recommended to prevent liquefaction in patent PCT/US2008/009398 (Elton and Gupta), details in Appendix G. The coating must be water insoluble, water wettable, biodegradable and delay hydration.

Coating polyacrylamide hydrogel particles using supercritical technology is explored using two methods: A) carbon dioxide as an antisolvent for the coating material, and B) carbon dioxide as a solvent for the coating material.

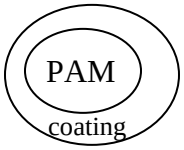

Figure 5.1. Target particle structure.

The crystalline and amorphous nature of coating materials can be a factor in selecting the suitable materials. Coating material, such as ethyl cellulose, that has a more amorphous and plasticizable nature increases the likelihood of the coating material to cover the entire core particle surface. In the coating process, enough time should be allowed for the shell to harden prior to interacting with the other particles, to reduce aggregation.

5.2 Experimental Materials & Methods

5.2.1 Core Hydrogel Particles

Commercial polyacrylamide (Soil Moist from JRM Chemical) was ground and sieved to collect various distributions: >75 µm, 45-75 µm, 25-45 µm, and <25 µm. The smaller particle distributions of less than 25 µm and 25-45 µm were utilized as the core hydrogel particles. Detailed grinding procedure is presented in Appendix F.

5.2.2 Coating (Shell) Materials

Chemical	**Structure**	**MW (g/mol)**	**Solubility Parameter and Density**
Polyacrylamide (PAM) CAS No.: 9003-05-8	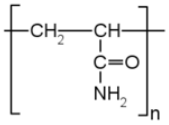	Crosslinked	
Poly(vinyl acetate)PVAc CAS No.: 9003-20-7	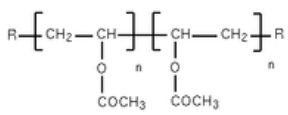	100000	δ 19.7MPa$^{1/2}$ 1.19 g/ml amorph at 25˚C
Polysulfone PSF CAS No.: 25135-51-7	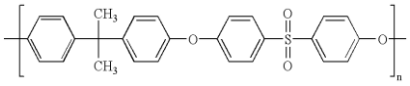	M_w 35000 M_n 16000	δ 20.3 MPa$^{1/2}$ 1.24 g/ml
Poly(L-lactide) PLA CAS No.: 26161-42-2	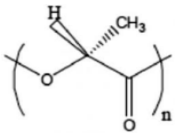	50000	2 dl/g
Poly(hydroxybutyrate) PHB CAS No.: 26063-00-3	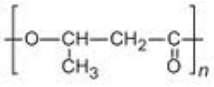	M_w 437,000 M_n 300,000	
Gelucire 50-13 CAS No.: 121548-05-8	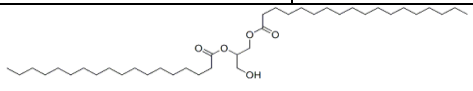		

Table 5.1. Coating material structures and properties.

Coating materials, poly(L-lactide), poly(hydroxybutyrate), poly(vinyl acetate), and poly(sulfone), were obtained from Sigma Aldrich and used as received. Gelucire 50-13 samples, composed of stearoyl polyoxylglycerides with minimum T_m of 50°C with a midrange hydrophilic-lipophilic balance (HLB) of 13 were donated by Gattefossé SAS based in France.

5.2.3 Hydration Analysis

Coated PAM particles were evaluated for delayed hydration. This simple and cheap testing was executed by adding 10 mg sample to 1.5 ml of deionized water or adding 20 mg sample to 5 ml of deionized water. As the hydrogel hydrates, the viscosity of the mixture drastically increases; hence visual inspection of the flow is taken as the measure of hydration either as no hydration, immediate, delayed, or complete hydration.

5.2.4 Coating Methods A and B

Two coating methods were explored in which supercritical carbon dioxide served as an (A) anti-solvent and (B) solvent. The anti-solvent method is utilized for the coating materials that are not soluble in carbon dioxide, and the solvent method us utilized for the coating materials that are soluble in carbon dioxide. Both utilize a high-pressure vessel equipped for ultrasonication (Figure 5.2). Suspension of polyacrylamide particles in $scCO_2$ was achieved by both ultrasonication and continuous CO_2 flow in Method A, and by ultrasonication in Method B.

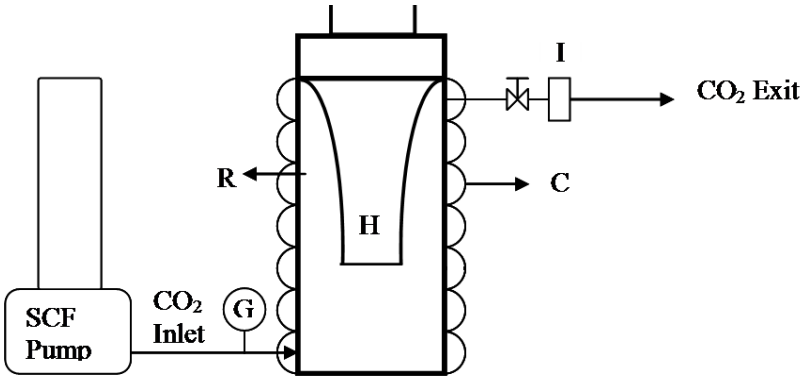

Figure 5.2. Apparatus for coating using supercritical CO_2. R: Precipitation chamber; SCF Pump: Supply of supercritical CO_2; I: Inline filter; H: Ultrasonic horn; G: Pressure gauge; C: Heating coil with temperature controller.

5.2.4.1 Method A: Carbon Dioxide as Anti-solvent

The method A (SAS-EM-Coating method) employs suspending particles in supercritical carbon dioxide with ultrasonication and utilizing an optimum carbon dioxide flow rate to aid suspension. Polyacrylamide particles (<25µm) were preloaded into a high-pressure vessel in 250 or 500 mg quantities. The coating experiments were carried out using a 500 ml high-pressure vessel (design shown in Appendix A) at 40˚C and 120 bar equipped with a 3/4" ultrasound tip and Vibra Cell sonicator or a stirring impellar at 400 rpm. Carbon dioxide flowed continuously at a minimum rate of 15 g/min by Thar P-Series pump. Multiple experiments were performed with injecting the coating solution unto the ultrasound tip while hydrogel particles were suspended in carbon dioxide. Coating materials polyvinyl acetate (PVAc), poly(L-lactide) (PLA), and polysulphone (PSF) were investigated with this method.

5.2.4.2 Method B: Carbon Dioxide as Solvent

This method investigates a coating process that utilizes $scCO_2$ and ultrasonication. Figure 5.2 shows the supercritical coating batch process apparatus with ultrasonic horn attached to the vessel. The supercritical phase, which has both liquid-like and gas-like properties, provides increased mass transfer and solubility of the coating material. Organic solvents are not used in this new process; hence organic-solvent sensitive

particles such as proteins can be safely processed avoiding denaturation. The process exploits the difference between the core and shell material solubility in $scCO_2$; for example, PHB and Gelucire are soluble in $scCO_2$, while PAM is not soluble. Solubility of PHB in CO_2 as a function of pressure and temperature is shown in Figure 5.3. The biodegradable polymers poly(β-hydroxybutyrate) (PHB) and Gelucire (50-13), composed of fatty acid glycerides, are investigated as shell coating material in this method.

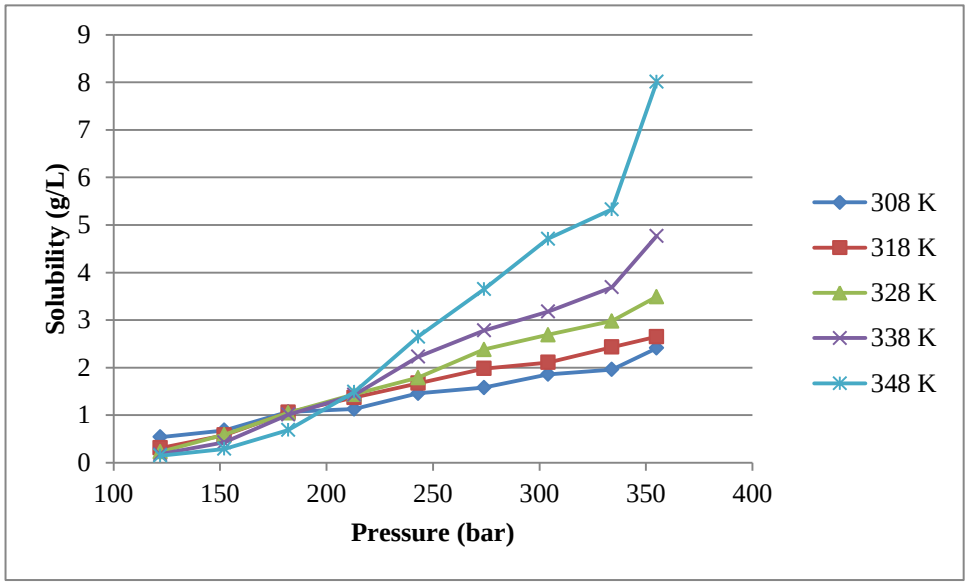

Figure 5.3 Poly(β-hydroxybutyrate) (MW=800,000) solubility in carbon dioxide (Gupta and Shim 2007).

The overall process has four steps, as sketched in Figure 5.4. In sketches A and B, the vessel is depicted with electrical heating tape and insulation on its exterior and a sonication horn centered inside the chamber. PAM particles are depicted by the white shapes and the coating material by black shapes. The dashed rectangle represents a pouch (more details are provided in the appendix) made of Grade 1 filter paper (pore size 11 μm) housing the coating materials. The pouch allowed dissolved coating material in $scCO_2$ to leave the pouch, and retained any excess coating material from entering the main vessel. Figure 5.4 depicts steps of the solvent coating process. In Step A, PAM was loaded into the vessel: half of the coating material was loaded into the vessel, and other half of the coating material was loaded into the filter pouch. Operational conditions of 45˚C and 182 bar are reached as the vessel is heated and pressurized with carbon

dioxide. Step B had the same temperature and pressure as in Step A, but PAM was intimately mixed with the dissolved coating material by the use of sonication. In Step B, the sonication horn was utilized in 5 or 2 second pulses for a total sonication of 20 minutes spread throughout 3 hours. In Step C, the insulation and electrical heating tape were removed and a fan was aimed at the vessel to aide in cooling the vessel by convection using ambient air. The temperature was allowed to decrease to ambient temperature. This process took approximately 1.5 hours and the pressure remained above the critical pressure such that liquid carbon dioxide and precipitation of the coating material occurred. For mixing while precipitating, the ultrasonication was used in 5 or 2 second pulses for a total of 12 minutes spread throughout the 1.5 hours; coating accumulated on the white PAM particles. In Step D, the vessel was depressurized, which changed the CO_2 to the gas phase. Complete depressurization of the vessel took approximately 1 to 2 hours. The final particles were collected from the bottom of the vessel.

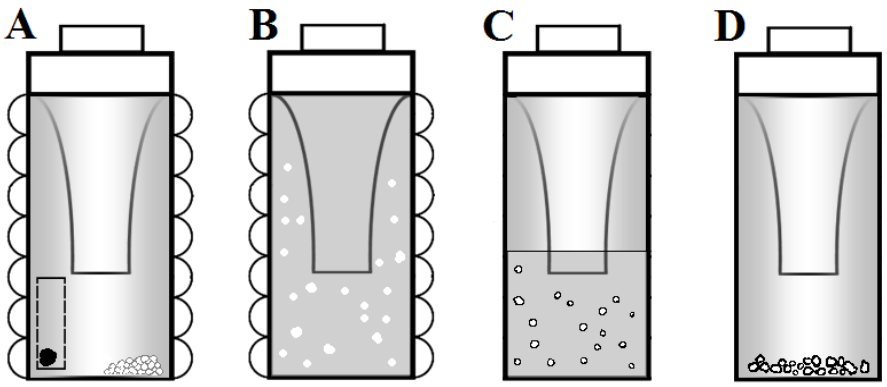

Figure 5.4. Supercritical fluid solvent coating process: A-coating (black) and PAM (white) preloaded into vessel; B-coating dissolved in $scCO_2$ and PAM suspended by ultrasonication horn; C-slow dissolution of coating; D-depressurization and precipitation.

Experiments were designed to investigate the effects of polyacrylamide amount, initial polyacrylamide particle size, and sonication method on the coating outcomes. The temperature and pressure were held constant at 45˚C and 182 bar, respectively. In addition, the amount of PHB was held constant at 100 mg. The experimental parameters included polyacrylamide amount (100 mg or 50 mg), initial PAM particle size (25-45 or

<25 micron), and sonication methods include traditional (5 s on and 5 s off) and extended rest (2 s on and 8 s off) for total sonication time of 2 minutes.

5.3 Results

The morphology of ground commercial polyacrylamide microparticles is irregular yet smooth as shown in Figure 5.5.

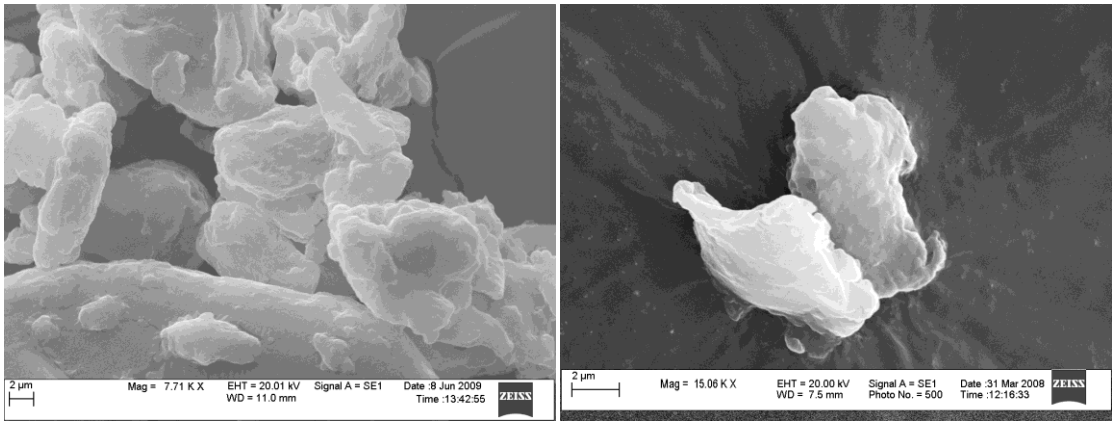

Figure 5.5. Polyacrylamide microparticles.

Rheometry was utilized to analyze the flow characteristics to differentiate fully coated particles from uncoated particles. Samples were evaluated with an Anton Paar Physica MCR 301 rotational rheometer in plate mode. Shear rate was varied from 0.1-100 s^{-1} and viscosity was calculated from the measured torque and shear stress. Data with torque below 0.5 µNm was below detection limits and not utilized in data analysis. The size increments of particles are those less than 25 µm, 25-45 µm, 45-75 µm, and greater than 75 µm. The viscosity of hydrated ground polyacrylamide added to water drastically changes with size (Figure 5.6). With increasing size, viscosity increased due to the decreased ability of particles to flow over one another. The larger particles are less likely to move around each other than smaller ones. Hydrating uncoated polyacrylamide of different size ranges results in an obvious viscosity difference if same water content is added. Hydration in a vial at concentrations around 10 mg/1.5 ml was the primary

method to ascertain coating of the hydrogel. When shear was applied in the rheometer, the nonspherical particles aligned with the flow of the water.

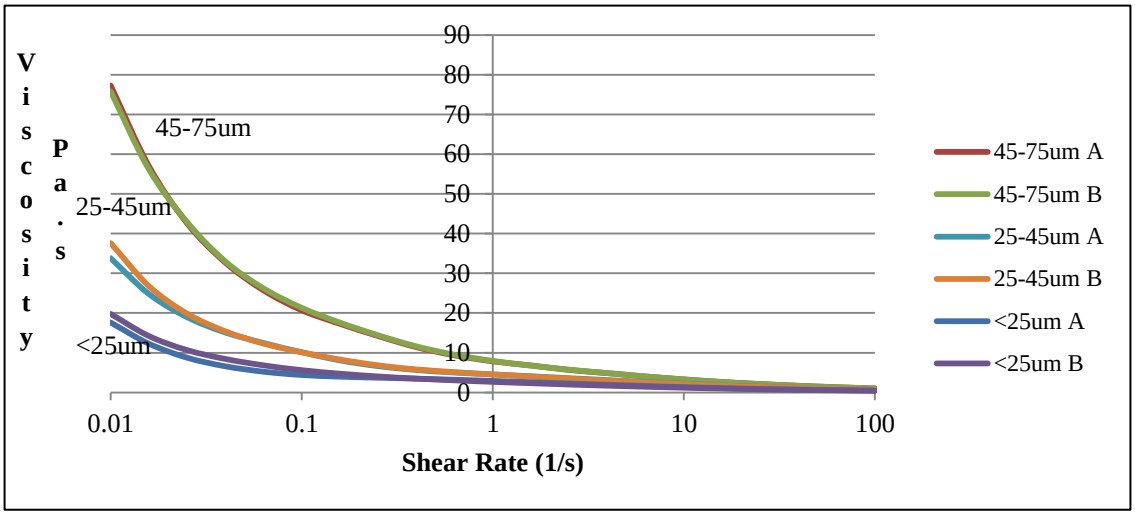

Figure 5.6. Viscosity of dependence of the size of polyacrylamide in water at 2.5 mg/ml concentration.

5.4 Supercritical Antisolvent with Enhanced Mass Transfer for Coating

Supercritical antisolvent with enhanced mass transfer (SAS-EM) produced nanoparticles as described in Chapter 3 and in prior research (Chattopadhyay and Gupta 2002; Gupta and Chattopadhyay 2003). This method for coating hydrogel particles employed supercritical antisolvent technology for coating with PLA, PSF, and PVAc.

Expt	Type of Coating	ratio of shell/core	Loaded PAM (mg)	Vessel Type	Coating Conc. (wt%)	Solvent
1	PVAc	no PAM	0	SAS-EM	5	Acetone
2	PVAc	1 to 3	250	SAS-EM	1	Acetone
3	PVAc	1 to 5	500	SAS-EM	1	Acetone
4	PVAc	1 to 6	250	SAS-EM	1	Acetone
5	PVAc	1 to 8	500	SAS-EM	1	Acetone
6	PVAc	1 to 15	500	SAS-EM	1	Acetone
7	PLA	1 to 5	250	impeller	1	DCM
8	PLA	no PAM	0	SAS-EM	5	DCM
9	PSF	no PAM	0	impeller	5	DCM

Table 5.2. Antisolvent Coating Experiments.

The PLA and PSF formed particles around the PAM in a coprecipitation manner. To improve the PLA coverage on the PAM particle surface, heating of the composite particles to anneal coating was investigated. The PLA particles did encompass the hydrogel microparticles (Figure 5.8). A delay in hydration was observed for some samples, but only by a few minutes compared to hydration of the uncoated polyacrylamide.

Polyvinyl acetate forms a film in the vessel under supercritical carbon dioxide. Samples from the SAS-EM Coating experiments were easily hydrated despite the increasing concentrations of coating material. A coating experiment utilizing the impellar high pressure vessel with 1:8 PVAc:PAM ratio also hydrated (15 mg/2.5 ml) similar to the other samples. Foaming issues were also encountered with PVAc coating in supercritical carbon dioxide.

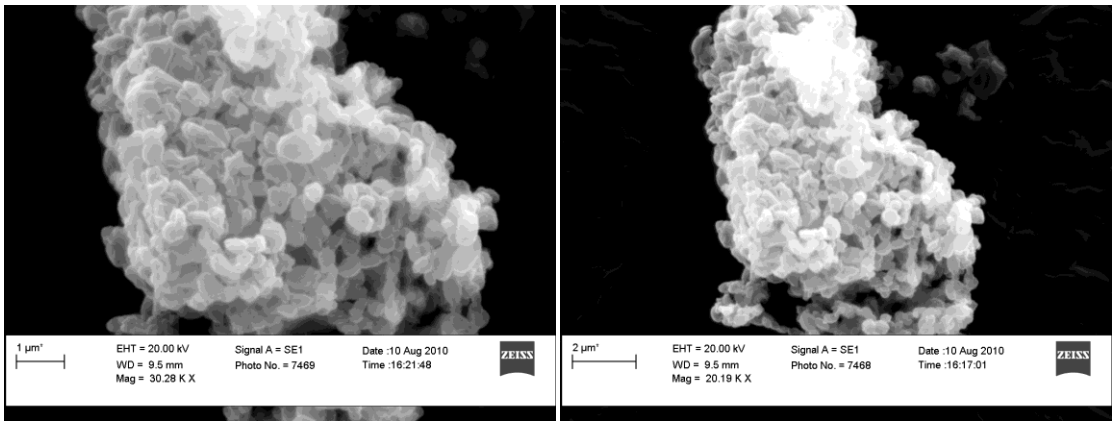

Figure 5.7. PLA particles produced by SAS-EM using $scCO_2$.

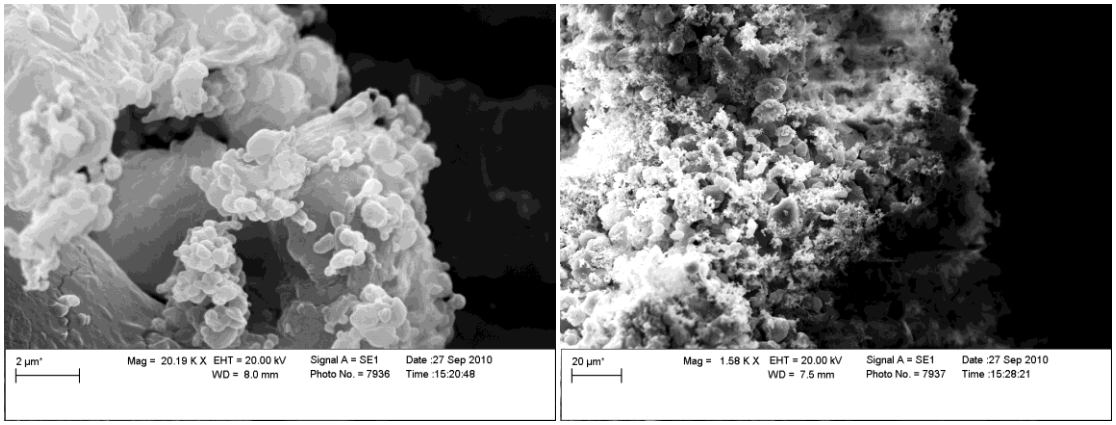

Figure 5.8. PLA nanoparticles on PAM microparticles.

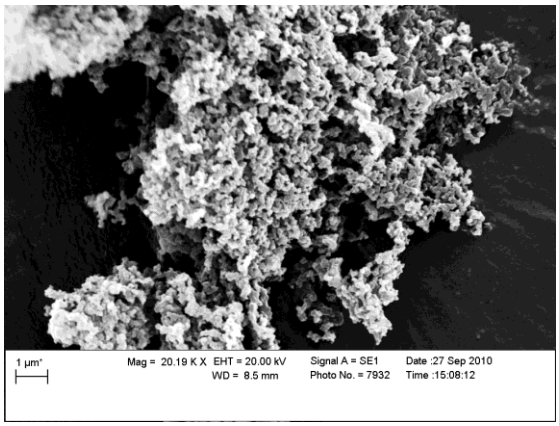

Figure 5.9. Polysulfone produced by particles by SAS-EM.

5.4.1 Compatibility

To determine compatibility of polyacrylamide with coating material, millimeter sized polyacrylamide granules were covered with a film of coating dissolved in a solvent and left to air dry. Multiple layers were placed on the granule as well as granules submerged in a 5 wt% solution. Hydration of granules was tested to evaluate the extent of protection by the polymer coatings. The start of hydration was defined as the edges of the polyacrylamide changing from opaque to clear as water diffuses into the polymer matrix. With these granules, the degree of swelling is very evident.

Coating Material	**% Loading in solution**	**Solvent**
PVAc	1, 5	Acetone
PLA	5	DCM
PSF	5	DCM

Table 5.3. Coating of PAM by material dissolved in a solvent and then air drying.

Uncoated polyacrylamide instantaneously swells when contacted with water. PAM granules (1 mm) were immersed in the above solution (listed in Table 5.3), air dried, and evaluated by the time hydration starts. With PVAc and PSF, the hydration was delayed, only for about 15 minutes. With PLA, hydration delayed for less than 5 minutes. PSF coating hydrated within 10 minutes. Interestingly, the samples in the corners took about 1.5 times longer to hydrate than granules in the center of the vial; thus, more polymer content generates a thicker polymer matrix that takes longer for the water to penetrate.

5.4.2 *Annealing of Polymers*

To minimize or eliminate pores in the polymer matrix in which water could penetrate, polymer solutions air dried on microscope slides are compared to those heated in an oven (65˚C, 85˚C, 100˚C) for three hours (images in Appendix H). In the case of heat treatment, the polymer will either not change surface morphology, the polymer will spread, or the polymer *(PLA, PSF, PVAc)* will coalesce into larger beads. The coating of the PAM surface that spreads will fill in incomplete coverage areas to coat the entire hydrogel surface, thus protecting the surface of the polyacrylamide from water. As water reaches the hydrogel and initiates swelling, the shell-coating is displaced causing a rapid increase in hydration.

The polymers heated on the microscope slides were compared to those not heated. Poly(vinyl acetate) remained a clear film before and after heating. Polysulfone at 100˚C for 3 hours exhibited change from smaller dried droplets to larger droplets. This demonstrates a behavior of self-attraction against the glass microscope slide instead of the desired effect of spreading and reduction of void spaces within the polymer. Coalescing allows the interfacial area to reduce thus decreasing the free energy of the system (Yuan and Favis 2004), producing a pronounced increase in size of a PS-PLA co-blend observed upon annealing; the morphology can also be affected by the thermal history.

Granules of PAM were placed in coating solutions, air dried, then heated to 100˚C. Heated PLA-coated PAM delayed hydration by only 10 minutes. Initial hydration was observed with PVAc within 15 minutes and PSF within 10 to 22 minutes dependent on initial amount of coating solution added. During heating to 100˚C, PSF expanded and doubled in size, no decrease in size occurred within 1 hour at returning to room temperature. This expansion improved coverage of the hydrogel particles however pores were still open allowing water access for hydrogel. Overall, annealing of polymer coating did slightly extend the delay of hydration.

5.4.3 Depressurization Issues

The PVAc foams with CO_2 depressurization and the depressurization rate plays a critical role in the resulting polymer coating. A rapid depressurization (183 bar to ambient) in less than 5 minutes creates an high foaming (Figures 5.10b,c); whereas, a slow depressurization develops film on the vessel walls. To ensure film-like coating of the particles, a slow depressurization rate that took > 2 hours was utilized. For illustration, PVAc beads (Figure 5.10a) were exposed to $scCO_2$ for 30 minutes, during which the beads plasticized PVAc to a clear film. With depressurizing over 50 minutes, the foam (Figure 5.10b) is generated when the pressure is around 600 psi as the dissolved carbon dioxide in the polymer expanded.

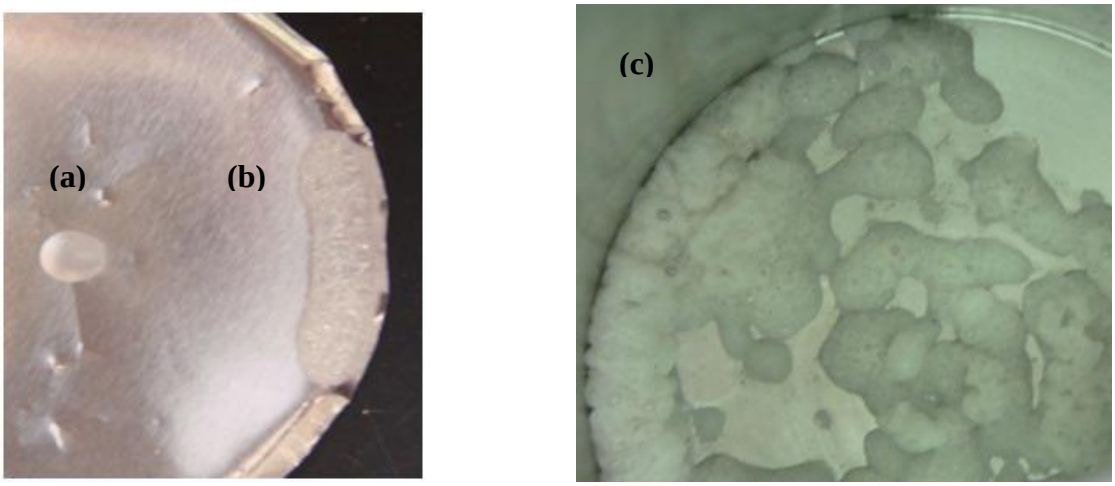

Figure 5.10. Polyvinyl acetate $scCO_2$ foaming: a) original bead, b) bead after exposure to $scCO_2$ and rapid depressurization (15 min), c) fast depressurization (45 min) with PVAc and PAM in vessel

5.5 Supercritical Carbon Dioxide as Solvent for Coating

Two coating materials, poly(hydroxybutyrate) (PHB) and Gelucire 50-13, are utilized with this method. Experimental variables for PHB are shown in Tables 5.4 and 5.5 and that for Gelucire in Table 5.6. Initial experiments C1 through C4 with PHB evaluated parameters of interest to design experiments and formulate the mechanics of the different stages: pressurization, solubility, cooling, and depressurization. These were carried out with PAM (<75 μm) prior to the sieves 25 μm (No. 500), 45 μm (No. 325), and 75 μm (No. 200) refining the size ranges as <25 μm, 25-45 μm, 45-75 μm, and >75 μm of ground polyacrylamide, respectively (more details are provided in Appendix F). The pouch for delivery of coating material was used in these experiments (i.e., loading 50 mg into the pouch and 50mg directly into the vessel).

Experiment	PAM Size, μm	PAM, mg	PHB, mg	T (˚C)	P (bar)
PHB-PAM c1	<75	500	50	45	150
PAM c1	<75	500	0	45	150
PHB c1	<75	0	200	45	150
PHB-PAM c2	<75	500	250	45	150
PHB-PAM c3 colored	<75	100	100	45	182
PHB-PAM c4 colored	<75	100	50	45	182

Table 5.4. Experiments of Method B.

Experiment	Sonication Method	PAM Size, um	PAM, mg
5-1	120 s 5s on 5s off	25-45	100
5-2	120 s 5s on 5s off	25-45	50
5-3	120 s 5s on 5s off	<25	100
5-4	120 s 5s on 5s off	<25	50
5-5	120 s 2s on 8s off	25-45	100
5-6	120 s 2s on 8s off	25-45	50
5-7	120 s 2s on 8s off	<25	100
5-8	120 s 2s on 8s off	<25	50

Table 5.5. Experiments of Method B with 100 mg PHB.

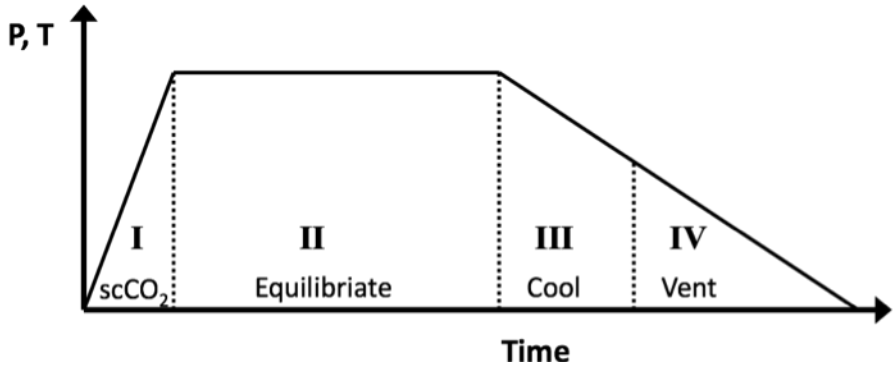

Figure 5.11 Stages in antisolvent coating process (Method B): I supercritical conditions of carbon dioxide, II allow coating material to solubilize in scCO2 conditions, III cool vessel to allow coating material to precipitate while suspending hydrogel particles, and IV venting and depressurizing to atmospheric conditions.

The samples were tested for hydration by mixing 20 mg in 5 ml water giving following results: PAM 1 clear and viscous, PAM C1 semi-clear, C1 semi-cloudy less viscous than PAM 1, and C2 cloudy with water like viscosity. From these results, the ratio of 2:1 coating to core in C2 produced the best quality of powder; this ratio was used in the following experiments. By lowering the polyacrylamide quantities in the vessel suitable for the amount of coating material that can be dissolved in the CO2 present in the vessel. At 45˚C, solubility of PHB in $scCO_2$ is 0.58 g/l at 150 bar and is 1.06 g/l at 182 bar. The material loading was based on the solubility at 45˚C and 182 bar.

The surface morphology of PAM to the surface morphology of coating material was compared using SEM. PAM has an irregular but generally smooth surface with random smaller pieces, whereas coating material PHB is composed of many smaller particles. Figure 5.12 shows the PHB morphology at low magnification and at a higher magnification where PHB is a collection of spheres that when looked at from a lower magnification resembles a fuzzy texture. All images showed evidence of PHB and PAM agglomeration.

From the SEM images and hydration studies with PHB (Appendix X), these particles were not coated but simply agglomerated mixtures. The best operating conditions for a slower hydration was using <25 µm PAM initial size and 50 mg of PAM with sonication, (experiment 5-4); however, this gave the least amount of hydrogel in the smallest size range yielding the least viscosity in hydration test. Experiment 2 appeared to have a low hydration viscosity contributed to the small PAM size <25 µm. The conditions for Experiment 4 are the basis for future experiments when testing other coating polymers where the overall ratio of coating to core (2:1) is preserved.

In water, small PHB particles float and large particles sink. All PHB-PAM samples hydrated in the presence of water and solution thickened with the floating of white PHB particles on top confirming lack of coating.

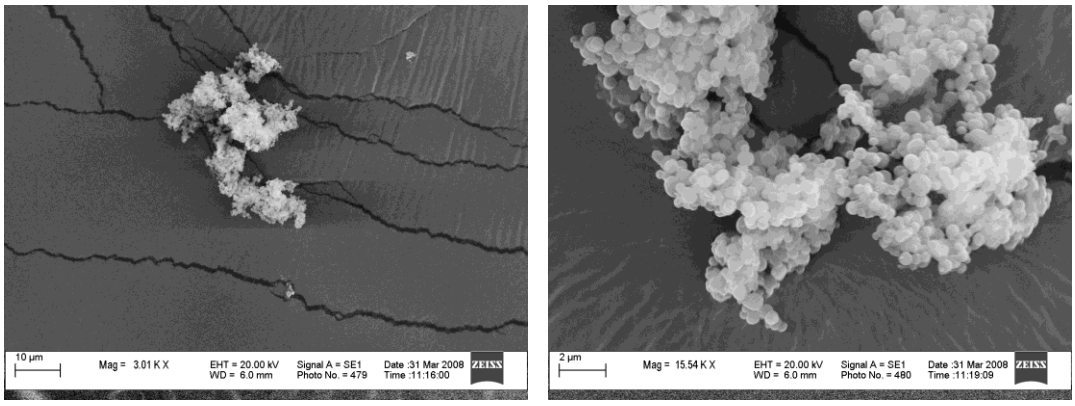

Figure 5.12. poly(β-hydroxybutyrate) (PHB) from supplier.

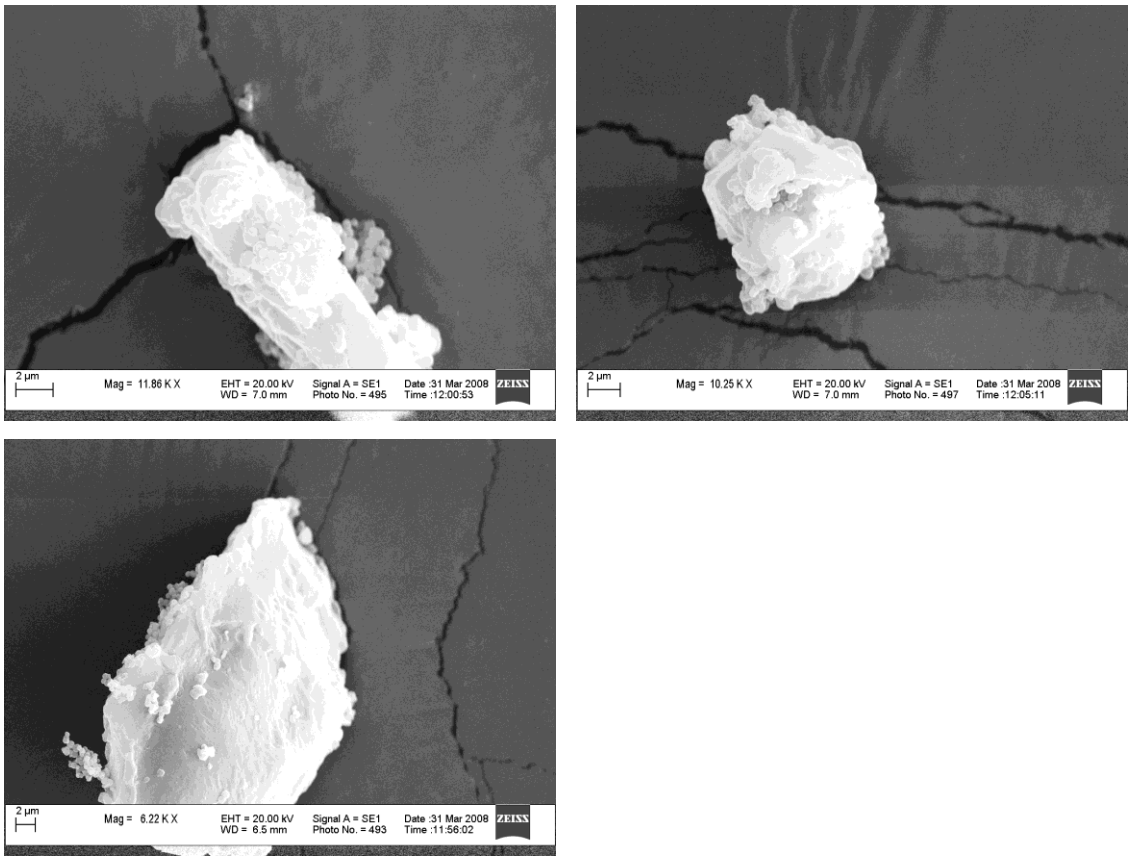

Figure 5.13. PAM-PHB C1

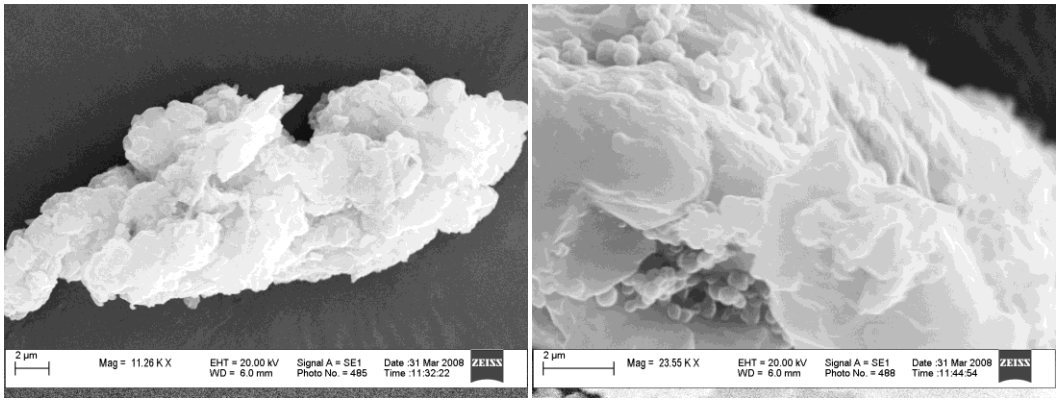

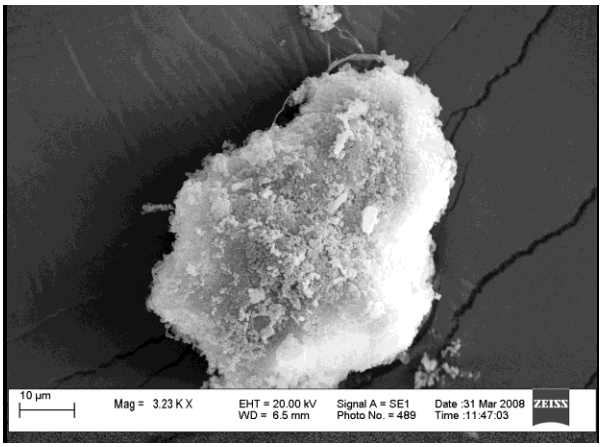

Figure 5.14. PHB-PAM C2.

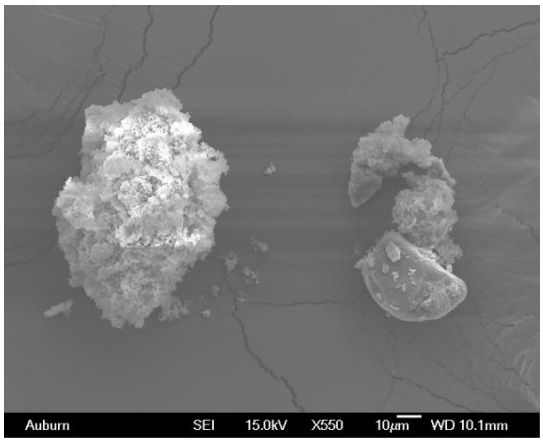

Figure 5.15. PHB is on the left and PAM is on the right.

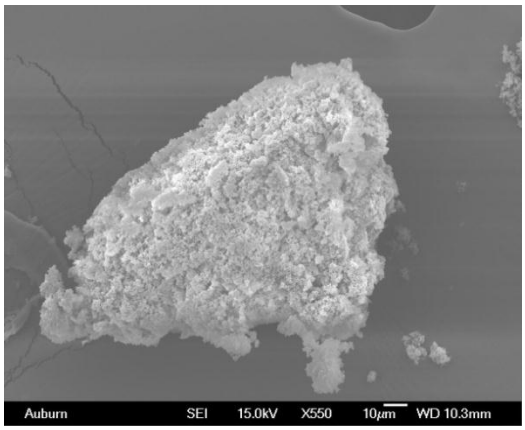

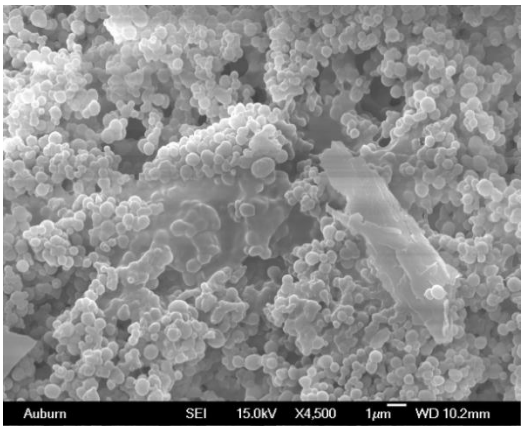

Figure 5.16. Experiment 5-2.

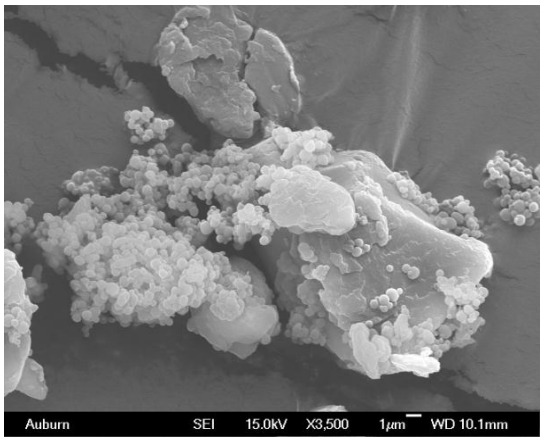

Figure 5.17. Experiment 5-3.

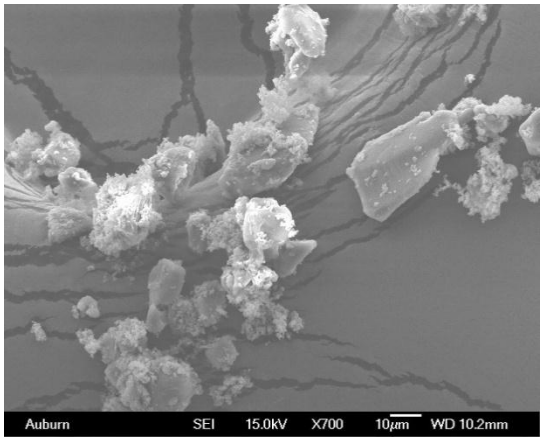

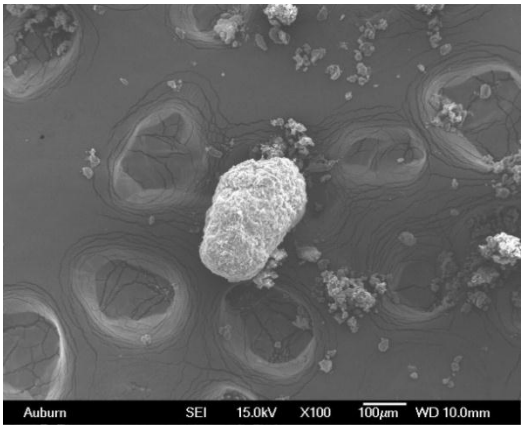

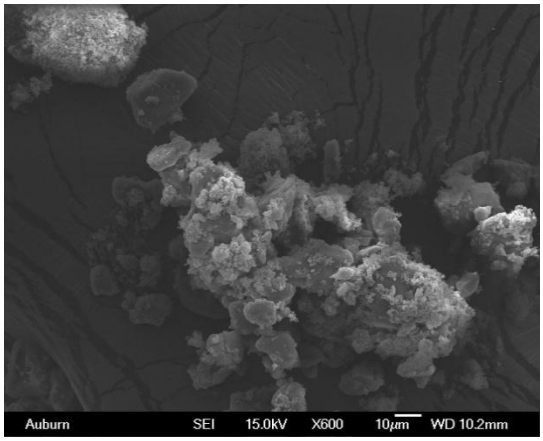

Figure 5.18. Experiment 5-4.

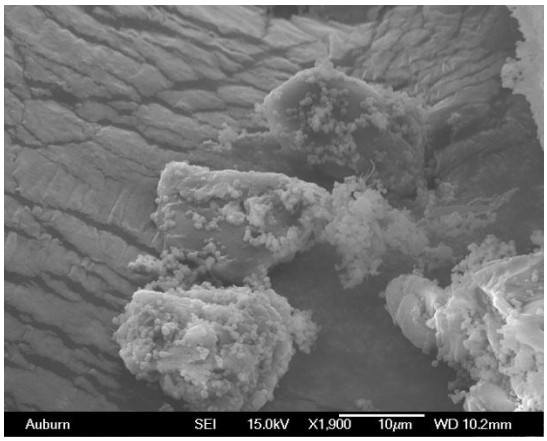

Figure 5.19. Experiment 5-5.

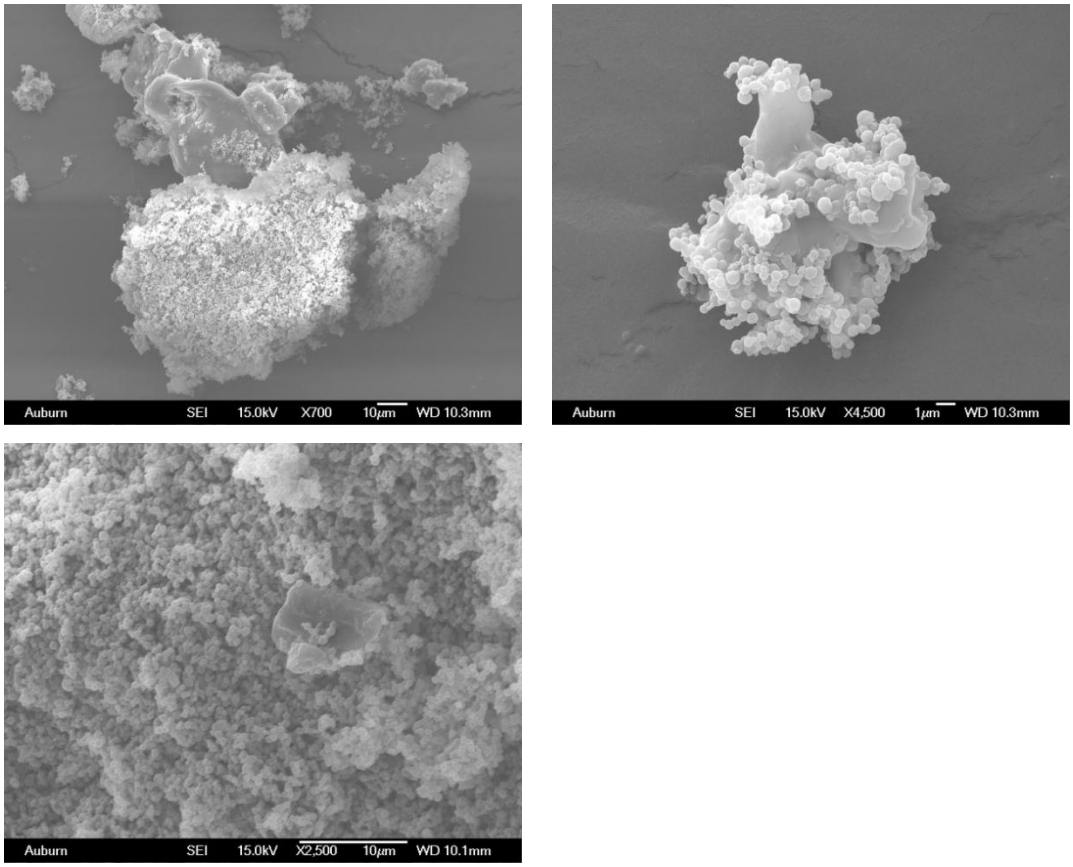

Figure 5.20. Experiment 5-6.

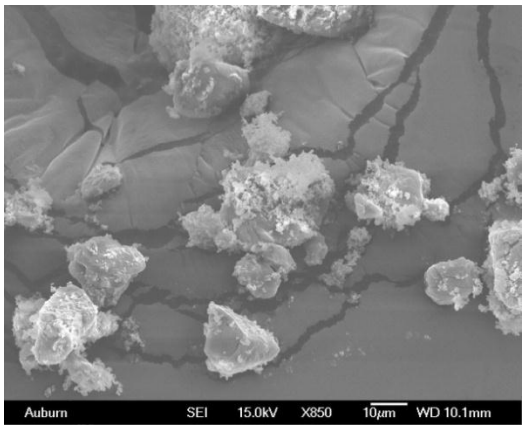

Figure 5.21. Experiment 5-7.

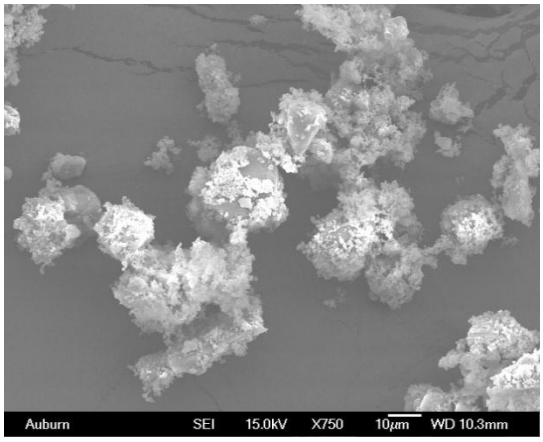

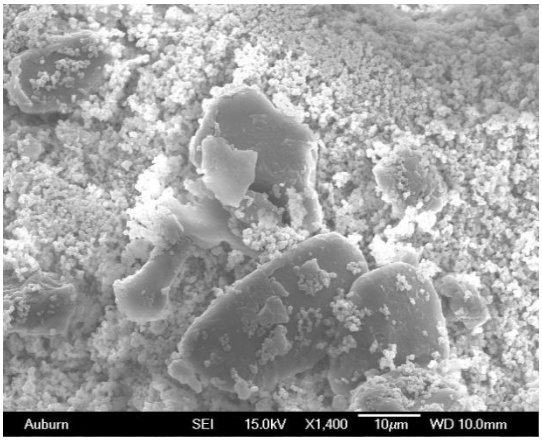

Figure 5.22. Experiment 5-8.

Experiments with Gelucire 50-13 were performed using ultrasound in a pulse mode with 5s on and 5 s off cycles. Gelucire pellets, composed of stearoyl macrogolglycerides, were ground and loaded half inside the vessel with the PAM (50 mg and <25 μm) and another half (50 mg) inside the pouch. Experiments were carried out at two temperatures: 35 and 45°C. Gelucire melts at 50°C and has hydrophilic-lipophilic balance (HLB) of 13 as indicated by the nomenclature 50-13 from the supplier Gattefosse. This mid-range HLB value was to offer compatibility onto the hydrogel without being too lipophilic. The original Gelucire has flake-like morphology.

Experiment	Sonication Method	T (°C)	PAM Size, μm	PAM, mg
1	120 s 5s on 5s off	45	<25	50
2	120 s 5s on 5s off	35	<25	50

Table 5.6. Experiments for Method B with Gelucire (100 mg).

The morphology the original Gelucire and coated samples were examined by SEM. Based on these images, the Gelucire at 45˚C was softened due to proximity to melting temperature at 50˚C along with carbon dioxide aided plasticization to help spread on the hydrogel particles. Despite the promising coating based on SEM images, Gelucire 50-13 did not delay hydration of the hydrogel. When mixed with water, Gelucire particles self agglomerate giving an appearance of cloudiness.

An experiment with Gelucire (50 mg) and PHB (50 mg) with no pouch at 35°C was carried out to determine the interaction. The final powder in the vessel was clumped on the bottom with little on the sides of the vessel. Upon hydration Gelucire-PHB sample clouded the water and the PHB particles floated on the water. The following SEM images (Figures 5.23-27) are obtained from the powder produced.

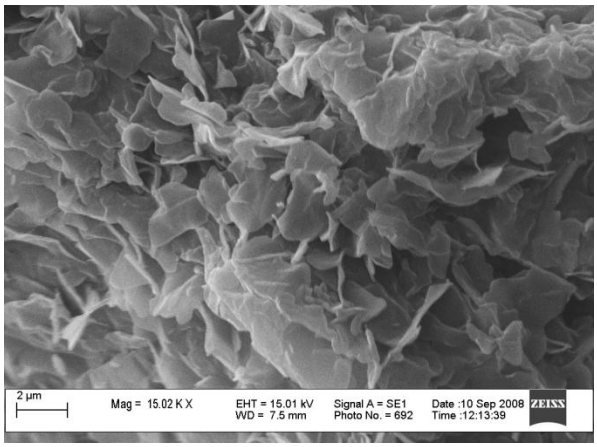

Figure 5.23. Gelucire from supplier.

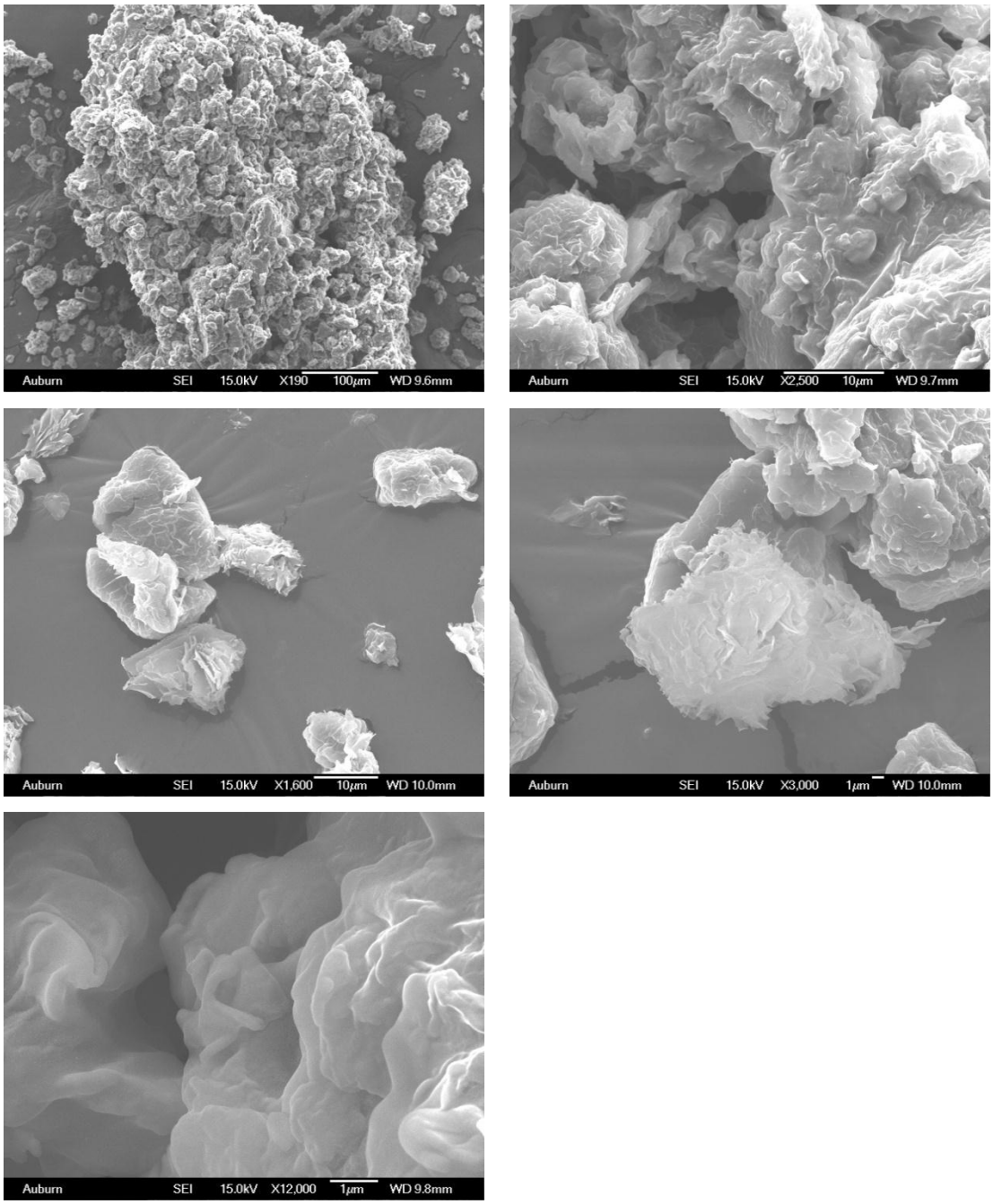

Figure 5.24. Gelucire –PAM (45˚C).

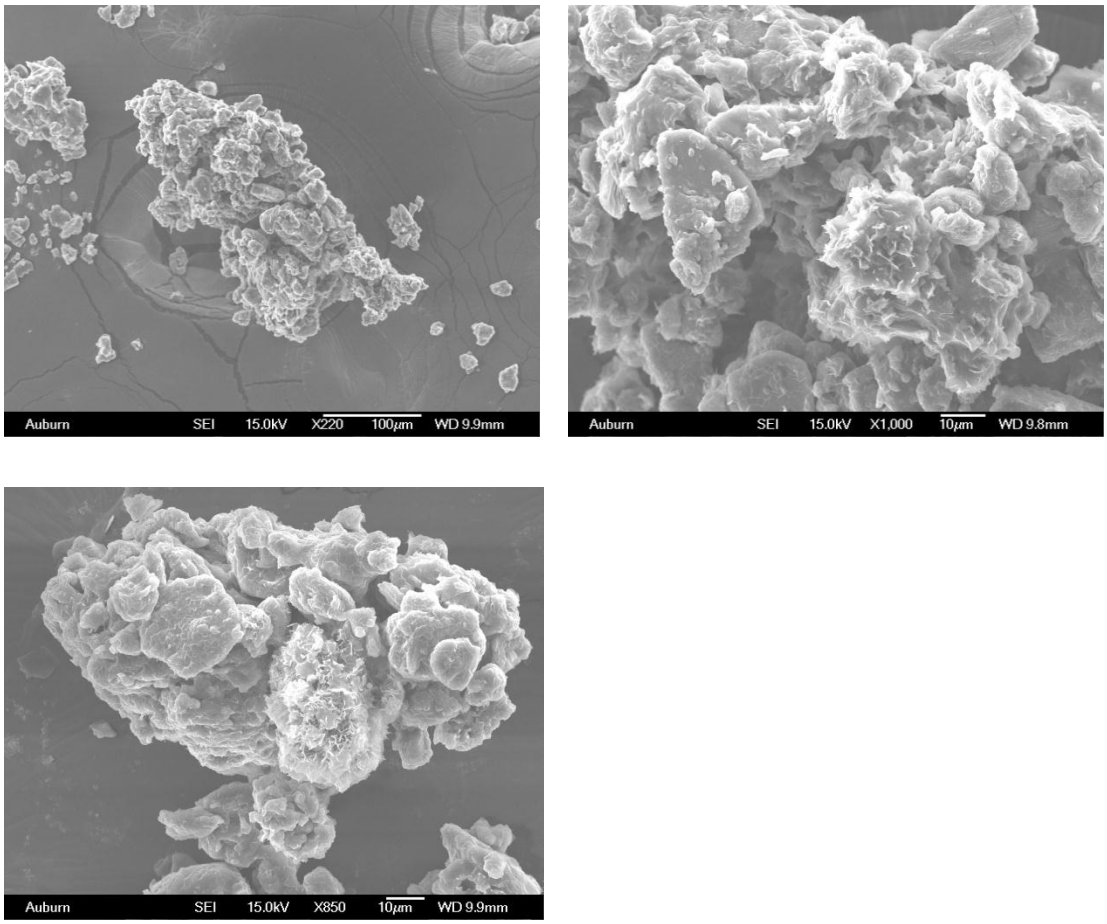

Figure 5.25. Gelucire – PAM (35˚C).

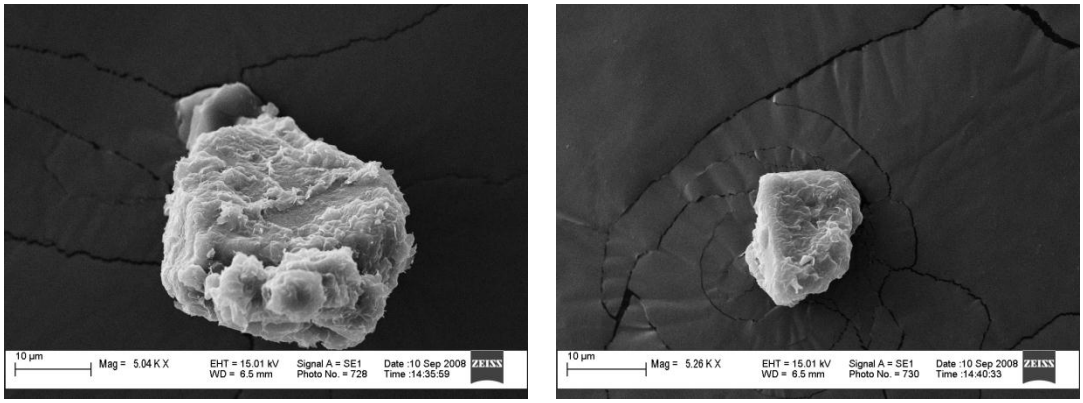

Figure 5.26. PAM-Gelucire.

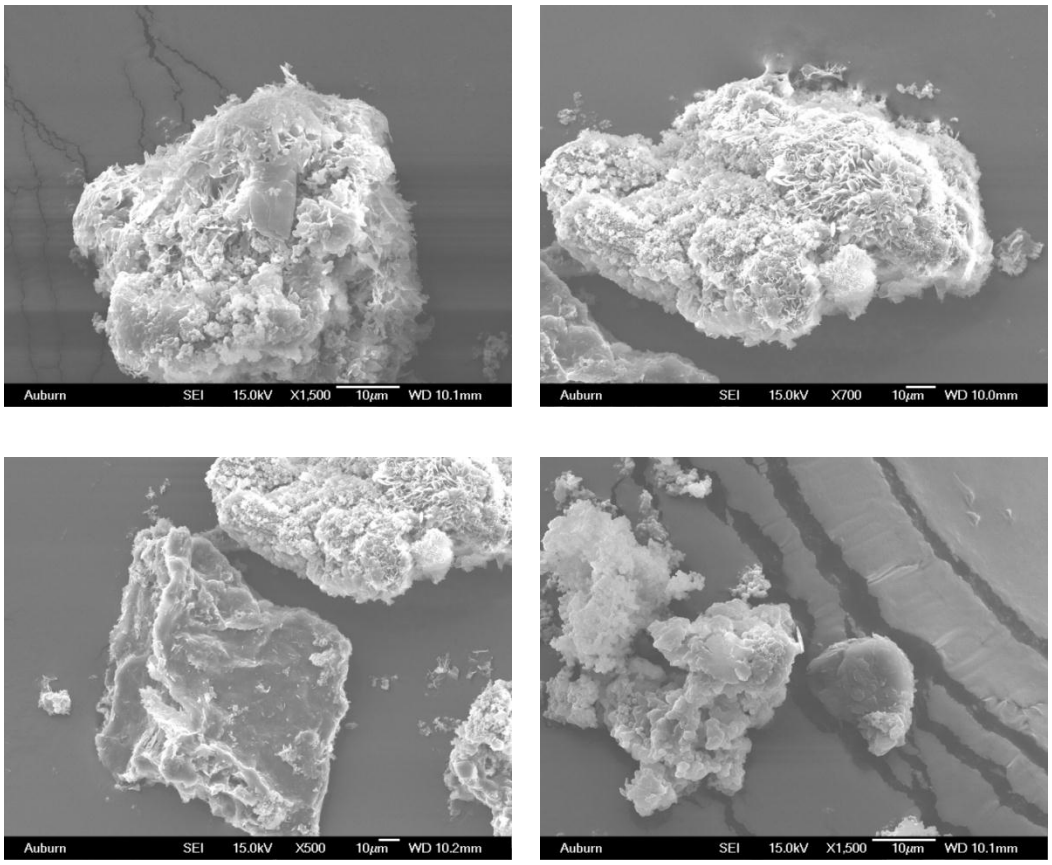

Figure 5.27. Gelucire and PHB.

Neither Gelucire nor PHB in coating was successful in extended delay of the hydration of polyacrylamide particles.

5.6 Alternative Coating Methods

Several liquid-based methods were tested for coating PAM as follows:

5.6.1 Coating by Coacervation

Coating of polyacrylamide with polyvinylacetate (PVAc) by coacervating in miglyol 840 was investigated. Miglyol provides a viscous material to suspend the polyacrylamide particles, and then as an acetone-polyvinylacetate solution is added, the acetone dissolves into miglyol causing PVAc to precipitate/coacervate onto the polyacrylamide particles. In these experiments, PVAc does precipitate from acetone when a threshold concentration is reached; the extent of PVAc precipitating on PAM versus vessel wall was unresolved.

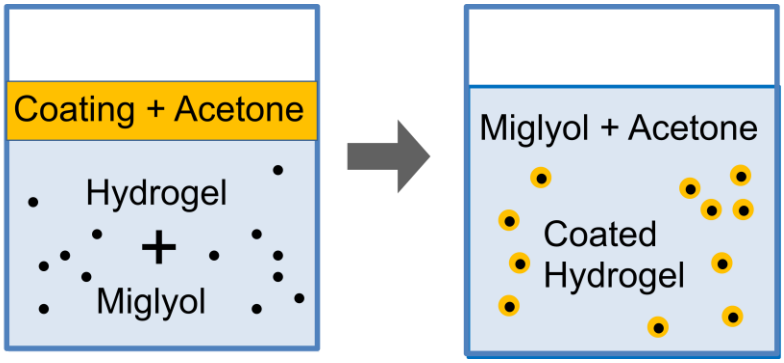

Figure 5.28. Coacervation process.

Experiment No	PVAc Concentration	Base Solution Migylol	Added Solution PVAc/ Acetone	
	mg/ml	ml	ml	mg/ml
MPA 1	1.67	5	1	10
MPA 2	2.86	5	2	10
MPA 3	28.57	5	2	100

Table 5.7. Coacervation quantities.

Label	Addition Method	Agitation	Outcome
MPA 1	Rapid	wrist shaker	miscible
MPA 2	DW 1.4ml/min	open to air for 2.5 hrs	precipitated on wall
MPA 3	DW 0.16ml/min	open to air for 3 hrs	big clump

Table 5.8. Coacervation method and results.

5.6.2 Coating by Solvent Evaporation

Multiple materials were employed to determine compatibility with polyacrylamide by adding a coating solution onto polyacrylamide particles and evaluate the effectiveness against hydration.

5.6.2.1 Span 80

The ability of Span 80, already employed for the creation of hydrogel nanoparticles in Chapter 1, to protect polyacrylamide from hydration was investigated as coating material. If the original surfactant contributed to protecting the hydrogel from hydration, it in itself would be advantageous. Several recipes of coating commercial ground polyacrylamide with surfactant Span 80 were attempted. The 45-75 μm PAM particles were employed to visually determine whether the particles would swell in water after the coating. Table 5.9 lists variables for these coating experiments.

Coating Experiment Parameters							
Expt. No.	**PAM mass (mg)**	**Span 80 + Cyclohexane volume(mL)**	**Span 80 mass (mg)**	**%loading**	**Stirring**	**Stirring Time**	**Stirrer RPM**
1	70.00	1	24	34.29	No	---	---
2	140.02	2	48	34.28	Yes	overnight	100
3	140.03	1	24	17.14	Yes	2 hrs-cap	100
4	140.52	1	24	17.08	Yes	1.5 hrs	200
5	140.40	1	24	17.09	Yes	1.5 hrs	200
6	140.16	1	24	17.12	Yes	1.5 hrs	200
7	140.22	2	48	34.23	Yes	1.5 hrs	200

Table 5.9. Coating quantities and methods utilizing Span 80.

Experiments 1 and 2 were unsuccessful in that the power swelled immediately when placed in water. Experiment 3 resulted in a less viscous, cloudy hydrogel when contacted with water indicating a partial coating. Experiments 4, 5, 6, and 7 also resulted in partial coating with even less viscous hydrogels.

5.6.2.2 Octadecyltrichlorosilane

Octadecyltrichlorosilane (OTS) has a long hydrophobic chain that is often used in MEMS devices for its self-assembling monolayer capability on silicon dioxide substrates. Its hydrophobic nature is well documented as the primary active component in Rain-X®. Octadecyltrichlorosilane was added to a cyclohexane suspension of PAM particles (45-75 µm and 1-2 mm) by three methods. First, OTS was directly added to the PAM suspension. The next two techniques applied a silicon dioxide base on the dry polyacrylamide particles for OTS to attach: vapor deposition of trimethylsilanol and a seeding layer. These treated PAM particles were then suspended in cyclohexane and the OTS solution then added. The suspensions were then vacuum filtered and dried. To evaluate this material, some treated particles were added to water to test hydration. All techniques proved incomplete coverage with immediate hydration of particles when subjected to water.

5.6.2.3 Perfluorobutane Sulfate

Perfluorobutane sulfate (PFBS), the active ingredient in Scotchguard®, was tested for its functional ability to repel water and protect the particles from hydration. A solution of perfluorobutane sulfonate, isopropanol, and acetone, was sprayed on 45-75µm polyacrylamide particles and granules. As the coating dried the particles were gently rotated and sprayed again every hour for a day, allowing approximately 12 coating applications. When introduced to water, the particles resisted initial swelling. The paper towel underneath coated with PFBS solution also showed very good water resistance ability. After 1 hour of submersion in water, however, the paper towel was wetted and the particles were hydrated. Hence, this material was unsuccessful in significantly delaying the hydration.

5.6.2.4 Polyvinyl Acetate

PAM (<25 µm in diameter) particles were coated with polyvinyl acetate in acetone. The powder was initially added to cyclohexane, sonicated for 2 minutes, and dropwise addition of various percentages of the coating solution while agitating at 200 rpm for 1.5hrs. While adding the acetone coating solution of 5mg/ml or 10mg/ml to the cyclohexane-polyacrylamide mixture, the powder precipitated out due to the interaction between cyclohexane and acetone where acetone is a stronger interferrant than cyclohexane. When cyclohexane is added to a larger volume of acetone the interaction is minimized. These samples were then dried overnight. The samples formed film on the bottom of the vial which were detached and broken up into powder. These were analyzed via SEM, rheometry, and light microscope. Filming commonly occurred with all solvent evaporation samples with higher percentages of PVAc loading giving a higher probability of filming.

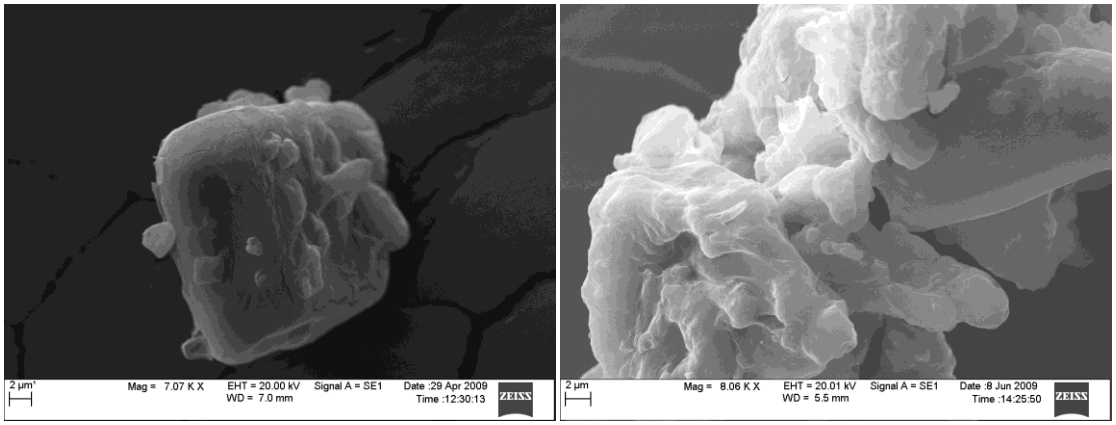

Figures 5.29. SEM image: a) 5% PVAc and b) 10% PVAc <25um PAM.

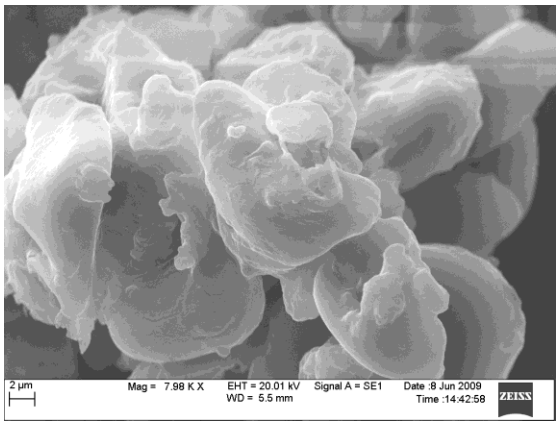

Figure 5.30. 12.5% PVAc <25um PAM.

5.7 Alternative Analysis Results

5.7.1 Rheometry

Varying weight percentages of polyvinyl acetate were utilized to coat polyacrylamide via the solvent evaporation method. These samples were mixed with water and run on an Anton Paar Physica MCR 301 rotational rheometer in plate mode. Shear rate was varied from 0.1-100 s^{-1} and viscosity was calculated from the measured torque and shear stress. Upon visual assessment, 5% PVAc sample behaved thicker like polyacrylamide with no coating. The 12.5% and 15% PVAc coated particles behaved similarly upon visual inspection. Both flowed like water and appeared to have particles suspended; however, these samples became thicker with time as hydrogel hydration increased.

As illustrated in the Figure 5.31, the viscosity is not linear with shear rate which is attributed to the asymmetry of the commercially ground particles. The nonspherical morphology was more pronounced than any coating differences; as greater shear is applied, the particles orient themselves toward the path of least resistance in the flow direction. Initially, the particles are in a more chaotic state and with increasing shear align in the direction of flow lending to a more linear relation. The distinction between coating percentages influencing the viscosity is not clear (Figure 5.32).

Other issues regarding rheometry for these samples are particle settling and comparisons of samples to control of water. The sample with 6% coating does not show any settling even after 15 hours as opposed to the 15% PVAc coating (Figures 5.33-34). The greatest difference amongst the coated particles occurs in the lower shear rates; however, the sample data for DI water is not reliable below 15.8 s^{-1} shear rate due to the low torque required to sustain the experiment. In the mid-range shear rate, coated particles do not follow a trend relating to PVAc content (Figure 5.35).

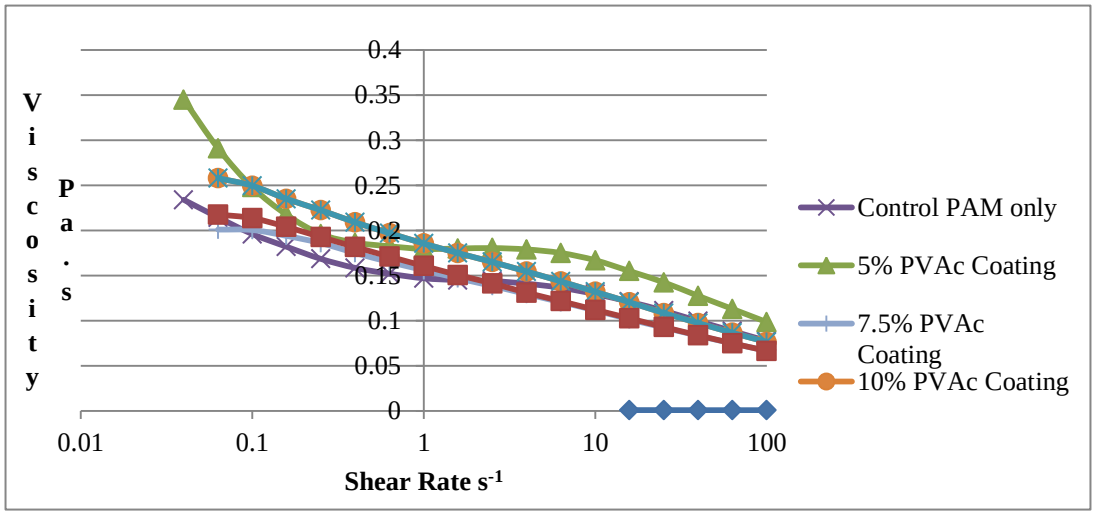

Figure 5.31. Solvent evaporation rheometry results: PAM <25um coated varying percentages of PVAc.

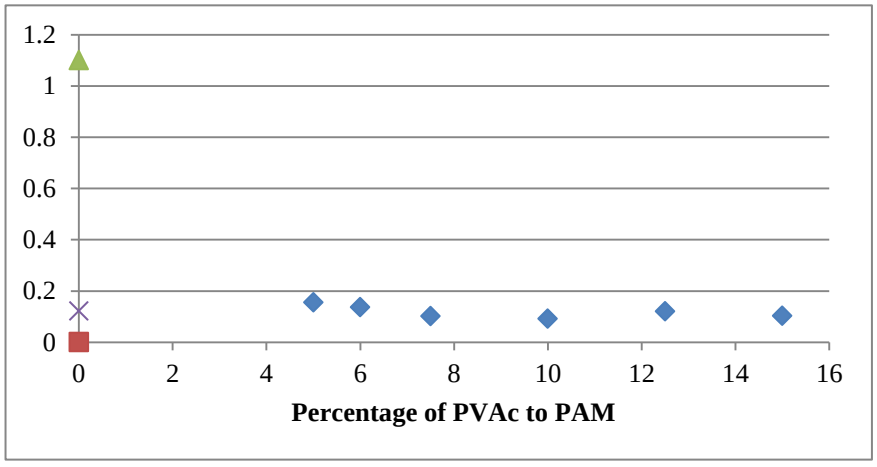

Figure 5.32. Rheometry results at constant shear rate of 15.8s^{-1}.

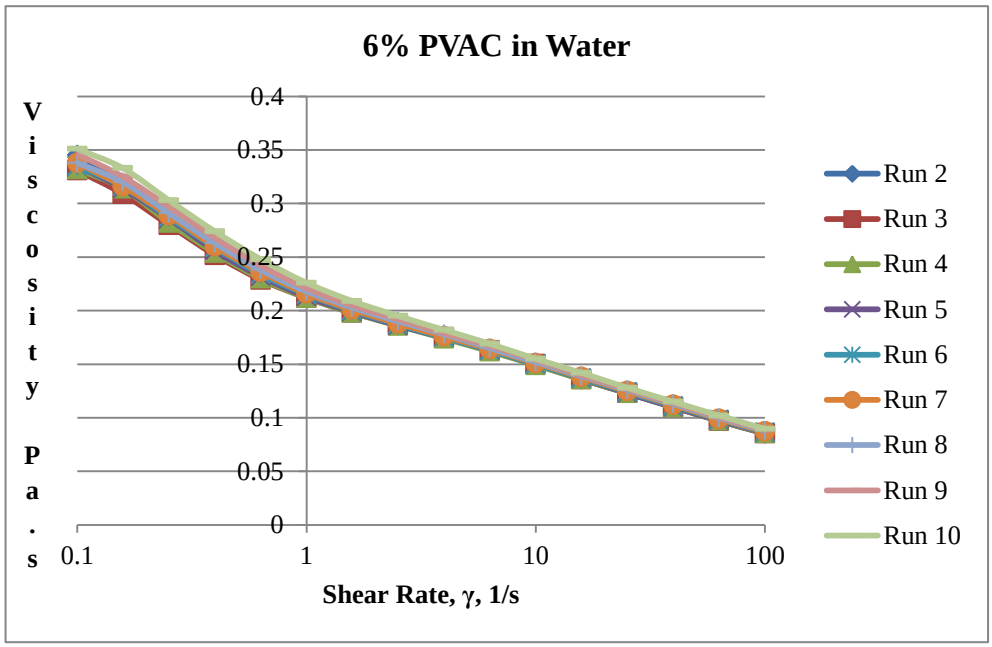

Figure 5.33. 6% PVAc solvent evaporation experiment - durability evaluation.

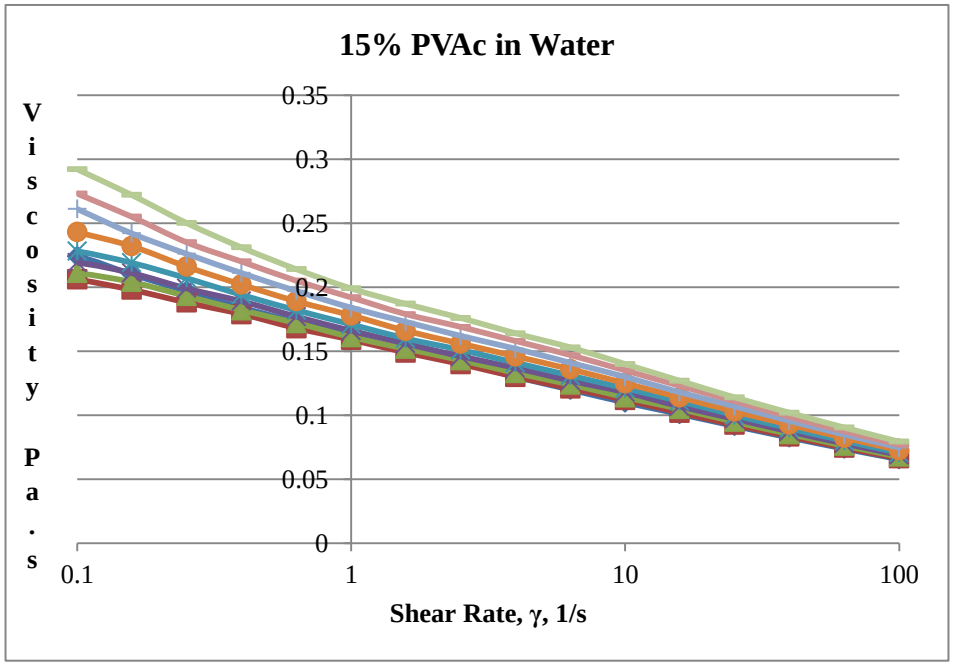

Figure 5.34. 15% PVAc solvent evaporation experiment - durability evaluation.

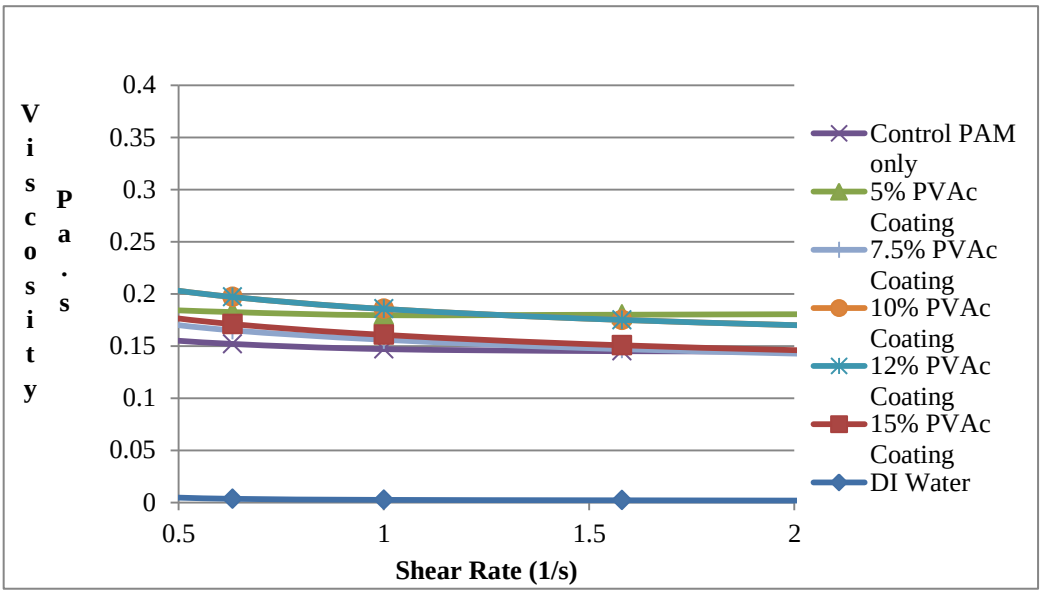

Figure 5.35. Rheometry results of PAM (<25um) PVAc with shear rate 0.5 to 2 s^{-1} range.

5.7.2 Contact Angle

To test the hydrophobicity due to the coating, contact angle with water droplet was measured. The powder was compressed into a pellet to form a smooth surface. However, the surface was not smooth enough which resulted in the erroneous angle measurements.

5.7.3 Light Microscope

Hydration of ground particles can be visibly detected under a light microscope. This technique was used to evaluate coating of particles. The diverse particle distribution average mean size prior to and after hydration did not provide reliable results as the individual particles were difficult to track. The coating slows the rate of swelling but the precision between initiation and completion of swelling for rate determination was difficult by this method. A dye was further added to aid in visualization. The polyacrylamide particle (Figure 5.36) swelled to approximately 140% its original size when placed in water.

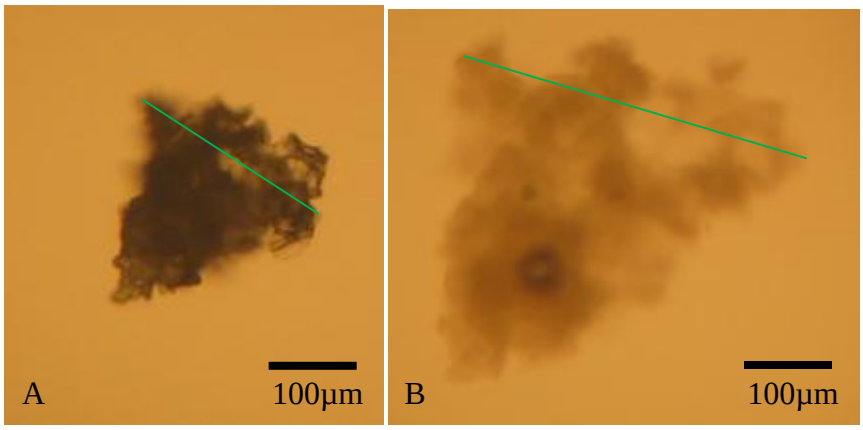

Figures 5.36. Light microscopic views of samples at 40x: A) dry commercial polyacrylamide B) swollen polyacrylamide with water.

5.7.4 Humidity Tests

Another method to analyze the extent of coating was to place samples of hydrogel into a saturated humidity vessel and detect the increase in weight for the amount of water absorbed from the air (Table 5.10). Samples were placed in a sealed oven at 35˚C with water container to saturate the air. The samples were left for durations of time and periodically analyzed for change in weight. The twelve control samples of various weights of hydrogel proved this method was highly variable and would not provide more insight applied to coating material. The diffusion of the water from the air into the sample is highly dependent on how the samples were spread on the aluminum plates. The sample was placed on the aluminum plate and tapped to spread powder. Similar sample amounts produced variable percentages of water content: for example, 20 mg were 8.5%, 11%, and 27.8%, 50 mg were 36%, 46%, and 48.8%, and 100 mg were 50.13% and 35.5%.

	T	Ctrl 1	Ctrl 2	Ctrl 3	Ctrl 4	Ctrl 5	Ctrl 6
sample		0	0	10.79	21.35	20.34	20.38
dry 16-Jun	33	982.96	981.22	982.22	983.63	983.04	983
18-Jun	31	982.86	981.2	993.52	1006.65	1005.96	1006.66
difference		-0.1	-0.02	11.3	23.02	22.92	1006.66
water content				0.51	1.67	2.58	986.28
water %				4.73	7.82	12.68	4839.45

21-Jun	31	982.94	981.24	993.71	1007.46	1006.3	1006.06
difference		-0.02	0.02	11.49	23.83	23.26	23.06
water content				0.7	2.48	2.92	2.68
water %				6.49	11.62	14.36	13.15
24-Jun	31	982.85	981.23	993.63	1006.79	1005.62	1009.04
difference		-0.11	0.01	11.41	23.16	22.58	26.04
water content				0.62	1.81	2.24	5.66
water %				5.75	8.48	11.01	27.77
8-Jul	31	982.48	981.29				
difference		-0.48	0.07				
	T	**Ctrl 7**	**Ctrl 8**	**Ctrl 9**	**Ctrl 10**	**Ctrl 11**	**Ctrl 12**
sample		50.98	51.14	50.41	101.9	101.23	0
dry 24-Jun		979.74	984.02	986	986.72	987.2	986.96
		979.7	983.94	985.9	986.76	987.18	987.03
		979.67					
	Avg	979.7033	983.98	985.95	986.74	987.19	986.995
29-Jun	31	1046.47	1055.3	1057.73	1133	1133.42	0.9869
difference		66.76667	71.32	71.78	146.26	146.23	0.9869
water content		15.78667	20.18	21.37	44.36	45	0.9869
water %		30.97	39.46	42.39	43.53	44.45	--
8-Jul	31	1035.54	1041.57	1046.02	1114.08	1125.15	986.73
difference		55.84	57.55	60.02	127.36	137.95	-0.23
water content		4.86	6.41	9.61	25.46	36.72	-0.23
water %		9.53	12.53	19.06	24.99	36.27	--
14-Jul		1055.58	1059.29	1054.56	1139.72	1124.39	986.76
difference		75.88	75.31	68.61	152.98	137.20	-0.24
water content		24.90	24.17	18.20	51.08	35.97	-0.24
water %		48.84	47.26	36.10	50.13	35.53	--

Table 5.10. Polyacrylamide humidity tests.

5.7.5 Hydrate and Filter with Centrifuge

To evaluate hydration of coating samples, a method hydration polyacrylamide particles then filtering by centrifuging was designed and evaluated. Control samples of uncoated polyacrylamide (<25 µm) were placed in centrifuge filter tubes, hydrated with 3 ml of water, then centrifuged to remove excess water. Commercial filter-centrifuge tubes (Centricon YM-10 and VectaSpin 3) proved difficult to remove excess water from samples even with increased rpm (3460 to 5000) and time (1 hour); thus, a custom system (Figure 5.37) with polypropylene filter (AN06) of pore size 0.6 µm was designed. Most samples maintained higher than 100% water content which is expected for hydrogel. However, results in Table 5.11 demonstrate varying percents of hydration based on the quantity PAM utilized and centrifuge time with weight steadily decreasing concluding issues of incomplete removal of excess water, or removal of absorbed water by compression of hydrogel subjected to the centrifugal forces.

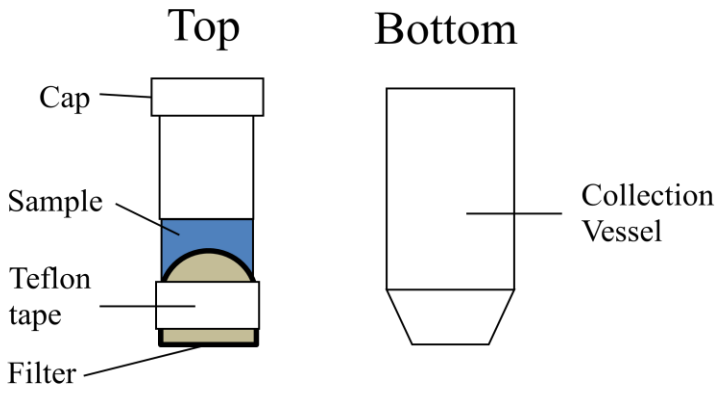

Figure 5.37. Centrifuge filter.

Hydrate and Filter with Centrifuging			Ctrl #1	Ctrl 2	Ctrl 3	Ctrl 4
		PAM mg	10.112	15.08	20.05	15.1
		Water	3	3	3	3
Date	**Water content % Hydration**	**Centrifuge time**				
6/18		dry	2404.5	2549.5	2524.5	2474.2
		0.6um				
6/21		15	4442.8	4865.8	5050.4	4650.1
	water content mg		2028.188	2301.22	2505.85	2160.8
	%hydration		200.57	152.60	124.98	143.10
		3	4372.8	4814.3	5009.2	4594.1
	water content mg		1958.188	2249.72	2464.65	2104.8
	%hydration		193.65	149.19	122.93	139.39
		10	4242.5	4687.3	4919.1	4468.5
	water content mg		1827.888	2122.72	2374.55	1979.2
	%hydration		180.76	140.76	118.43	131.07
		5	4158.5	4628.8	4850.8	4412.6
	water content mg		1743.888	2064.22	2306.25	1923.3
	%hydration		172.46	136.88	115.02	127.37
		2	4121.8	4596.1	4827	4392.3
	water content mg		1707.188	2031.52	2282.45	1903
	%hydration		168.83	134.72	113.84	126.03
		3	4058.1	4551.8	4787.6	4346
	water mg		1643.488	1987.22	2243.05	1856.7
	%hydration		162.53	131.78	111.87	122.96
6/23		0	3900.3	4430.9	4712.5	4268.8
	water mg		1485.688	1866.32	2167.95	1779.5
	%hydration		146.92	123.76	108.13	117.85
		5	3774.3	4307.8	4587.4	4146
	water mg		1359.688	1743.22	2042.85	1656.7
	%hydration		134.46	115.60	101.89	109.72
		5	3689.5	4221	4509.4	4069.2
	water mg		1274.888	1656.42	1964.85	1579.9
	%hydration		126.08	109.84	98.00	104.63

		5	3621.30	4139	4420	3998.4
	water mg		1206.688	1574.42	1875.45	1509.1
	%hydration		119.33	104.40	93.54	99.94
		2.5	3591.4	4109.8	4397.2	3972.1
	water content mg		1176.788	1545.22	1852.65	1482.8
	%hydration		116.38	102.47	92.40	98.20
		2.5	3562.3	4083.9	4380	3951.2
	water content mg		1147.688	1519.32	1835.45	1461.9
	%hydration		113.50	100.75	91.54	96.81

Table 5.11. Results of polyacrylamide hydration with filtration by centrifuging.

5.7.6 Moisture Analysis

A Denver Instruments moisture analyzer IR 35 was utilized to measure the degree of swelling various sizes of polyacrylamide. In Tables 5.12-15, three solvents (methanol, acetone, and water) were compared to elucidate the extent of solvent absorbed on polyacrylamide (PAM). Moisture percentage contained within the hydrogel (% M), the solid residual (% S), and the (% MS) were obtained. The final solid mass after drying requires being above the scale minimum detection limit. Methanol swells the polymer up to 15%, whereas acetone swells the polymer less at 8%. Water swells the hydrogel the most absorbs around 100%. The instrument generates errors (Err01) when the percent moisture is over 100%.

PAM (25-45 μm)in Water							
Run	T (˚C)	Starting Mass (g)	%M	%S	%MS	Residual Wt. (g)	time (min)
1	110	0.501	101.68	-1.68	Err 01	0.004	25
2	110	0.513	99.81	0.19	51400.0	0.001	27
3	110	0.508	95.87	4.13	2319.05	0.021	26
4	110	0.522	100.19	-0.19	Err 01	-0.001	23
5	110	0.503	100.99	-0.99	Err 01	-0.005	20
6	110	2.068	100.00	0	Err 01	0.001	37
7	110	2.085	99.62	0.38	25962.5	0.008	39
8	110	2.044	100.2	-0.2	Err 01	-0.004	34

Table 5.12. Moisture content of polyacrylamide.

PAM (>75 µm) in Water							
Run	T (˚C)	Starting Mass (g)	%M	%S	%MS	Residual Wt. (g)	time (min)
1	105	2.076	97.11	2.89	3361.67	0.060	43
2	140	2.158	96.94	3.06	3170.77	0.065	44

Table 5.13. Moisture content of polyacrylamide.

PAM (>75 µm) in Acetone							
Run	T (˚C)	Starting Mass (g)	%M	%S	%MS	Residual Wt. (g)	time (min)
1	105	2.249	7.19	92.81	7.74	2.079	4.2
2	105	2.030	8.38	91.62	9.15	1.858	9.0
3	105	2.059	4.86	95.14	5.10	1.959	7.4

Table 5.14. Moisture content of polyacrylamide.

PAM (>75 µm) in Methanol							
Run	T (˚C)	Starting Mass (g)	%M	%S	%MS	Residual Wt. (g)	time (min)
1	105	2.770	14.55	85.45	17.03	2.366	5.0
2	105	2.209	8.69	91.31	9.52	2.017	5.0
3	105	2.221	6.03	93.97	6.42	2.087	5.8

Table 5.15. Moisture content of polyacrylamide.

5.8 Discussion

Multiple methods and coating materials proved to not be successful in delaying the hydration of hydrogel particles.

Incomplete coverage can explain the results evident from SAS-EM coating shown in Figure 5.38. The SAS-EM coating demonstrated properties more similar to coprecipitation. Higher material loading of PLA and PSF provides a thicker quantity of coating particles that increases the time for diffusion of water through the coating particle layer, but unless they bind to each other by annealing or use of secondary coating material that is plasticizable polymer by $scCO_2$, hydration of PAM hydrogel will occur.

Another material utilized in SAS-EM-Coating, PVAc despite the ability to easily form film in supercritical carbon dioxide, higher quantities injected had an increased rate of foam formation. Carbon dioxide easily diffuses into PVAc, and upon depressurization generates sponge structure. The pores generated by carbon dioxide diffusing out of the polymer even with slow depressurization would create access paths to hydrate hydrogel.

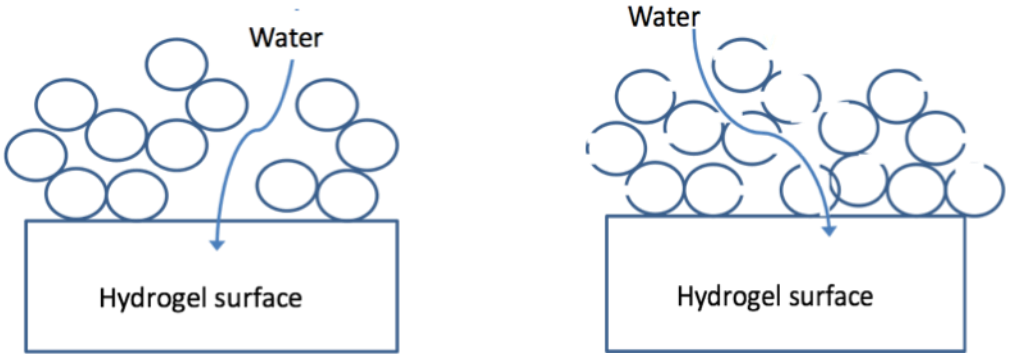

Figure 5.38. Water access to hydrogel a) incomplete coverage and b) open pore access

With the supercritical carbon dioxide solvent method, Gelucire 50-13 and PHB did not delay hydration of the hydrogel particles. Gelucire coating appeared to mold to the surface of polyacrylamide better than the other coatings. This could be attributed to the processing temperature (45˚C) being close to the original melting temperature (50˚C) and the additional effect of carbon dioxide reduces melting temperature (Kazarian 2002; Verreck 2006; Li 2008). Gelucire increased solubility in carbon dioxide at this higher

temperature allowed for more material to precipitate onto hydrogel particles. However, Gelucire did not provide enough hydrophobicity to delay hydration.

A highly lipophilic coating, such as PFBS and OTS, does not bind well to the polyacrylamide hydrogel due to the repulsive surface interactions. Drying by slow evaporation can lead to capillaries forming or direct pore access to the core hydrogel that small water molecules can easily maneuver. Fundamental compatibility is necessary for physical adherence of one to the other. Large molecular weights utilized (PLA 100,000 g/mol and PVAc 50,000 g/mol) that are not very polydisperse contributed to the open pores accessible by water; however, utilizing smaller molecular weights leads to higher solubility in carbon dioxide. Exploration into the combinations of processing conditions, coating material, and molecular weights, by eliminating potential coating materials of polyacrylamide was achieved. A combination of various molecular weights and materials should be pursued to achieve longer delay of hydrogel hydration.

Surface interactions between the hydrogel and the coating material are vitally important. Looking at the molecular structures in the materials table (Table 5.1) demonstrates some of the incompatibilities. The acetate group (CH_3CO_2-) in the poly(vinyl acetate) may be too hydrophobic with the methyl group blocking the oxygen for physical adherence to the polyacrylamide with ketone (=O), alcohol (-OH), and amine groups (RNH_2) off the polymer carbon backbone. The benzyl backbone of polysulfone may repel water and produce hydrophobicity gradient in the molecule, and the sulfur dioxide group contributes to its water wettable nature. More than likely it is due to the physical open pore formations by the particles themselves allowing water access to the hydrogel core. During solvent evaporation experiments, the coating material adheres to the polyacrylamide but the slow evaporation leads to capillaries that deeper solvent creates by diffusing to evaporate through the dried material closer to the surface.

5.9 Conclusions

Multiple methods and coating materials were investigated to delay hydration of polyacrylamide hydrogel particles. These methods were unsuccessful in this pursuit due to incompatibility of the material with the hydrogel. Coating of Gelucire, perfluorobutane sulfate, and poly(vinyl acetate) occurred; however, some delay of hydration occurred with the antisolvent coating materials, PVAc, PLA, and PFBS but not sufficiently. The solvent method did not delay hydration of the hydrogel particles.

5.10 References

Bleich, J., P. Kleinebudde and B. W. Muller (1994). "Influence of gas-density and pressure on microparticles produced with the ASES process." International Journal of Pharmaceutics **106**(1): 77-84.

Cao, L., L. Chen, P. Cui and J. Wang (2008). "Synthesis of PNIPA/PDMS-g-PAA Core-Shell Composites in Supercritical Carbon Dioxide. ." Journal of Applied Polymer Science. **108** 3843-3850.

Chattopadhyay, P. and R. B. Gupta (2002). "Protein Nanoparticles Formation Using Supercritical Antisolvent with Enhanced Mass transfer." AIChE J. **48**: 235-244.

Cocero, M. J., A. Martin, F. Mattea and S. Varona (2008). "Encapsulation and co-precipiation processes with supercritical fluids: Fundamentals and applications." J. Supercritical Fluids.

Cooper, A. (2000). "Polymer synthesis and processing using supercritical carbon dioxide." J. Material Chemistry **10** 207-234.

Davies, O., A. Lewis, M. Whitaker, H. Tai, K. Shakesheff and S. Howdle (2008). "Applications of supercritical CO2 in the fabrication of polymer systems for drug delivery and tissue engineering." Advanced Drug Delivery Reviews. **60** 373-387.

Elton, D. and R. B. Gupta WATER STABILIZATION USING MICROPARTICLES. PCT/US2008/009398. United States. **WO/2009/020594**.

Elvassore, N., A. Bertucco and P. Caliceti (2001). "Production of insulin-loaded poly(ethylene glycol)/poly(L-lactide) (PEG-PLA) nanoparticles by gas antisolvent techniques." Journal of Pharmaceutical Sciences **90**(10): 1628-1636.

Falk, R. F. and T. W. Randolph (1998). "Process variable implications for residual solvent removal and polymer morphology in the formation of gentamycin-loaded poly(L-lactide) micropaticles." Pharmaceutical Research **15**(8): 1233-1237.

Gupta, R. B. and P. Chattopadhyay (2003). Method of forming nanoparticles and microparticles of controllable size using supercritical fluids with enhanced mass transfer. **US Patent 6620351.**

Gupta, R. B. and J.-J. Shim (2007). Solubility in Supercritical Carbon Dioxide. . Boca Raton, FL., Taylor & Francis Group.

Majerik, V., G. Charbit, E. Badens, G. Horvath, L. Szokonya, N. Bosc and E. Teillaud (2007). "Bioavailability enhancement of an active substance by supercritical antisolvent precipitation." J. Supercritical Fluids **40** 101-110.

Sze Tu, L., F. Dehghani and N. R. Foster (2002). "Micronisation and microencapsulation of pharmaceuticals using a carbon dioxide antisolvent." Powder Technology **126**(132-149).

Tom, J. W. and P. G. Debenedetti (1991). "Formation of bioerodiable polymeric microspheres and microparticles by rapid expansion of supercritical solutions." Biotechnol. Prog. **7**: 403-411.

Tom, J. W., X. Kwauk, S.-D. Yeo and P. G. Debenedetti (1993). "Rapid expansion of supercritical solutions (RESS): fundamentals and applications." Fluid Phase Equil. **82**.

Wang, Y., R. N. Dave and R. Pfeffer (2004). "Polymer coating-encapsulation of nanoparticles using a supercritical anti-solvent process." Journal of Supercritical Fluids **28**: 85-99.

Young, T. J., K. P. Johnston, K. Mishima and H. Tanaka (1999). "Encapsulation of lysozyme in a biodegradable polymer by precipitation with a vapor-over-liquid antisolvent." Journal of Pharmaceutical Science **88**(6): 640-50.

Yuan, Z. and B. D. Favis (2004). "Macroporous poly(L-lactide) of controlled pore size derived from the annealing of co-continuous polystyrene/PLA blends." Biomaterials **25**: 2161-2170.

6.0 CONCLUSIONS

This research pertains to hydrogel nanoparticle formation using miniemulsion polymerization and supercritical carbon dioxide drying. Hydrogel nanopowder is produced via a novel inverse miniemulsion polymerization and supercritical drying (MPSD) method by injecting the polymerized miniemulsion solution into supercritical carbon dioxide. Due to efficient extraction by $scCO_2$, the powder obtained is free of residual solvent or surfactant. This work analyzed the processes of generating hydrogel nanopowder and the effect the addition of an inorganic (zinc oxide) material, an organic drug (mesalamine), and polymer coatings have on the hydrogel. These experiments provide understanding of interactions of the hydrogel with these materials.

The spherical particle morphology generated by the polymerization method is robust as the supercritical fluid and additional materials do not significantly affect overall hydrogel particles formed. The smaller disperse phase droplet size limits the additional particle type to be encapsulated as the ground mesalamine with polyacrylamide had the most loading efficiency of all experiments due to general chemical and morphological compatibilities. Also, the self-attraction of the acrylic acid monomers in the aqueous phase displaces the larger mesalamine particles limiting incorporation into the hydrogel.

Zinc oxide, being ionic, resides within the water droplets more easily than the non-polar cyclohexane phase. Also, zinc oxides amphoteric nature as an acid or base is comparable to interactions of mesalamine. Polyacrylamide with an amine group versus poly(acrylic acid) with carboxylic groups interacts with the addition of another substance in water differently. The nature of the material determines the extent of interference in the hydrogen bonds formed in water with the monomer and thus relates to the encapsulation ability of the process. This work has provided insight into the interactions of polyacrylamide hydrogel particles both internally by encapsulation and externally by coating.

7.0 FUTURE WORK

This research leads to the following suggestions for future work:

Nanoparticle hydrogel coating can be pursued using the large (0.5 L) high pressure vessel (Appendix A). Experiments can now be accomplished with double injection onto the ultrasound horn tip in supercritical conditions. Coating hydrogel nanoparticles from the miniemulsion solution is suggested after either supercritical drying or precipitating the polymer solution by acetone addition (Campbell and Anand 1972). This would provide either dry powder or acetone swollen particles to be coated. After removal of the supernatant, two coating dynamics are possible using supercritical technology: 1) the precipitated coating solution with the direct addition of coating material in a single injection or 2) simultaneous injection of polymer solution and coating solution unto the horn tip. A potential issue could be the precipitated nanoparticles are too large from the cyclohexane-acetone precipitate and block the injection nozzle; here a mixing device to help suspend the particles would be required prior to injection. Experiments of multiple component injection into supercritical conditions to evaluate the extraction properties of carbon dioxide are also suggested.

Future efforts of encapsulating materials within hydrogel nanoparticles include mesalamine's solubility in acid for improved encapsulation within the polymerized hydrogel nanoparticles, evaluation of improved mucoadhesion of the hydrogel nanoparticles by in vitro studies, and potential use of reactions of zinc acetate to zinc oxide within the hydrogel particles would be novel.

Future improvement for coating hydrogel particles are suggested for delaying hydration of hydrogel particles. Incorporation of ethylene glycol dimethacrylate (EGDM) in place of methylbisacrylamide (MBA) as a crosslinker in the polymerization process could contribute to better compatibility with a hydrophobic coating material. Surface

modifications of the hydrogel particles are suggested in favor of a more compatible foundation for coating adhesion as hydrophilic and hydrophobic material are not compatible. Surface impregnation of an amphiphilic compound need only be partial to improve physical adherence of a hydrophobic material for hydration protection.

Copolymers are alternatives to the coating materials attempted in this research. Combining PLA with PS, this coploymer was generated by Yuan and Favis (2004), could provide better hydration protection and dependent upon the ratio used improve biodegradability of polystyrene material, and minimization of PS content should be attempted as PS in the ground is not an environmentally-friendly solution to the prevention of hydrating a hydrogel.

A bottom-up method core-shell polymerization can be beneficial to create a hydrophobic coating that would otherwise be incompatible with the core material (Lee and Rudin 1992; Vanderhoff 1992; Bassett 2001; Ho 2010). This mandates placement of the initiator in with the core material itself such that polymerization occurs on the surface of the core material similar to that used to generate amphiphilic particles consisting of net-like structure over a polyacrylamide core (Li and Ruckenstein 1996).

Future research efforts to improve core-shell analysis are needed where the polymer-polymer combinations have elemental similarities and where the differentiation of material is difficult. For example, utilizing PVDC as a coating material, elemental analysis is possible with chlorine present for detection. The fact that polyacrylamide has an amide interferes with the nitrogen present with mesalamine to utilize elemental analysis. Characterization of particles with polystyrene would be straightforward on TEM as contrast issues are not anticipated. Ruthenium tetraoxide staining of PS on PS-PMMA particle slices after microtoming for visualization on transmission electron microscopy produced clear images (Lee and Rudin 1992).

8.0 REFERENCES

Adamsky, F. A. and E. J. Beckman (1994). "Inverse emulsion polymerization of acrylamide in supercritical carbon dioxide." Macromolecules **27** 312-314.

Al-Hilli, S. M. and M. Willander (2006). "Optical properties of zinc oxide nano-particles embedded in dielectric medium for UV region: Numerical simulation." Journal of Nanoparticle Research **8**: 79-97.

Allard, D. and C. Gombert (2001). Synergistically UV-photoprotecting triazine/silicone compositions. Societe L'Oreal S.A. United States. **6,171,579**.

Anton, N., J.-P. Benoit, et al. (2008). "Design and production of nanoparticles formulated from nano-emulsion templates - a review." Journal of Controlled Release **128**: 188-199.

Antonietti, M. and K. Landfester (2002). "Polyreactions in miniemulsions." Progress in Polymer Science **27**(4): 689-757.

Anzlovar, A., Z. C. Orel, et al. (2008). "Nanocomposites with nano-to-sub-micrometer size zinc oxide as an effective UV absorber." Polymeri **29**: 84-87.

Bahnemann, D. W., C. Kormann, et al. (1987). "Preparation and Characterization of Quantum Size Zinc Oxide: Fluoresence and Non Linear Optical Effects." J. Phys. Chem B **91**: 3789-3798.

Bajpai, S. K. and S. J. Sonkusley (2002). "Hydrogels for Colon-specific Oral Drug Delivery: An In Vitro Drug Release Study (II)." Iranian Polymer Journal **11**(3).

Bandi, N., R. Gupta, et al., Eds. (2004). Supercritical Fluid Technology for Drug Product Development. New York, Marcel Dekker.

Bassett, D. R. (2001). "Hydrophobic Coatings from Emulsion Polymers." The Journal of Coatings Technology **73**(912): 43.

Beckman, E. J. (2004). "Supercritical and near-critical CO2 in green chemical synthesis and processing." Journal of Supercritical Fluids **28**(2-3): 121-191.

Beckman, E. J. and R. D. Smith (1990). J. Phys. Chem. **94** 345.

Beckman, E. J. and R. D. Smith (1990). J. Supercrit. Fluids **3**: 205.

Blagodatkikh, I., V. Tikhonov, et al. (2006). "New Approach to the Synthesis of Polyacrylamide in Miniemulsified Systems." Macromolecular Rapid Communications **27**(22): 1900-1905.

Bleich, J., P. Kleinebudde, et al. (1994). "Influence of gas-density and pressure on microparticles produced with the ASES process." International Journal of Pharmaceutics **106**(1): 77-84.

Brinker, C. J. and G. W. Scherer (1990). Sol-Gel Science: The Physics and Chemistry of Sol-Gel Processing. . San Diego, CA, Academic Press Inc.

Broadhead, J., S. K. E. Rouan, et al. (1992). "The spray drying of pharmaceuticals." Drug Development and Industrial Pharmacy **18**(11): 1169-206.

Brock, T., M. Grotelaes, et al. (2000). European coatings handbook. Hannover, Germany, Vincent Verlag.

Bryden, A. M., H. Moseley, et al. (2006). "Photopatch testing of 1155 patients-results of the U.K. multicentre photopatch study group." British Journal of Dermatology **155**(4): 737-747.

Cai, W. and R. B. Gupta (2001). "Poly(N-ethylacrylamide) hydrogels for lignin separation. ." Ind. Eng. Chem. Res. **40**(15): 3406-3412.

Cai, W. and R. B. Gupta (2002). Hydrogels

Kirk-Othmer Encyclopedia of Chemical Technology (5th Edition) **13:** 729-754.

Campbell, A. N. and S. C. Anand (1972). "Phase Equilibria in the Systems Acetone - Methanol, Acetone - Cyclohexane, Methanol- Cyclohexane, and Acetone-Methanol- Cyclohexane " Canadian Journal of Chemistry **50**: 479

Cao, L., L. Chen, et al. (2008). "Synthesis of PNIPA/PDMS-g-PAA Core-Shell Composites in Supercritical Carbon Dioxide. ." Journal of Applied Polymer Science. **108** 3843-3850.

Cao, Z., Z. Zhang, et al. (2009). "Synthesis and UV shielding properties of zinc oxide ultrafine particles modified with silica and trimethyl siloxane." Colloids and Surfaces A: Physiochem. Eng. Aspects **340**: 161-167.

Capek, I. (2003). Designed Monomers and Polymers **6**(4): 399-409.

Catchpole, O. J., J. B. Grey, et al. (2000). "Fractionation of fish oils using supercritical CO2 and CO2+ ethanol mixtures. ." Journal of Supercritical Fluids **19**(1): 25-37.

Charbit, G., E. Badens, et al. (2004). Methods of particle production. Supercritical Fluid Technology for Drug Product Development. Y. Peter, B. K. Uday and S. Boris. New York, Marcel Dekker**:** 367-410.

Chattopadhyay, P. and R. B. Gupta (2002). "Protein Nanoparticles Formation Using Supercritical Antisolvent with Enhanced Mass transfer." AIChE J. **48**: 235-244.

Chattopadhyay, P., B. Y. Shekunov, et al. (2007). "Production of solid lipid nanoparticle suspensions using supercritical fluid extraction of emulsion (SFEE) for pulmonary delivery using the AERx system." Advanced Drug Delivery Reviews **59**: 444-453.

Cocero, M. J., A. Martin, et al. (2008). "Encapsulation and co-precipiation processes with supercritical fluids: Fundamentals and applications." J. Supercritical Fluids.

Cohen, R. D. (2006). "Review article: evolutionary advances in the delivery of aminosalicylatese for the treatment of ulcerative colitis. ." Ailment Pharmacology and Therapeutics. **24**: 465-74.

Consani, K. A. and R. D. Smith (1990). J Supercrit Fluids **3**: 51.

Cooper, A. (2000). "Polymer synthesis and processing using supercritical carbon dioxide." J. Material Chemistry **10** 207-234.

Cross, S. E., B. Innes, et al. (2007). "Human Skin Penetration of Sunscreen Nanoparticles: In-vitro Assessment of a Novel Micronized Zinc Oxide Formulation." Skin Pharmacology and Physiology **20**(3): 148-154.

Cutie, S. S., D. E. Henton, et al. (1996). "The Effects of MEHQ on the Polymerization of Acrylic Acid in the Preparation of Superabsorbent Gels." Superabsorbent Gel Preparation

Daniels, E. S., E. D. Sudol, et al., Eds. (1992). Polymer Latexes - Preparation, Latexes, and Applications. ACS Symposium Series. Washington, D.C., American Chemical Society.

Davies, O., A. Lewis, et al. (2008). "Applications of supercritical CO2 in the fabrication of polymer systems for drug delivery and tissue engineering." Advanced Drug Delivery Reviews. **60** 373-387.

Dobbs, J. M., J. M. Wong, et al. (1987). "Modification of supercritical fluid phase behavior using polar cosolvents." Ind. Eng. Chem. Res. **26**(1): 56-65.

Eckert, C. A., B. L. Knutson, et al. (1996). Nature **383**.

Elton, D. and R. B. Gupta WATER STABILIZATION USING MICROPARTICLES. PCT/US2008/009398. United States. **WO/2009/020594**.

Elvassore, N., A. Bertucco, et al. (2001). "Production of insulin-loaded poly(ethylene glycol)/poly(L-lactide) (PEG-PLA) nanoparticles by gas antisolvent techniques." Journal of Pharmaceutical Sciences **90**(10): 1628-1636.

Falk, R. F. and T. W. Randolph (1998). "Process variable implications for residual solvent removal and polymer morphology in the formation of gentamycin-loaded poly(L-lactide) micropaticles." Pharmaceutical Research **15**(8): 1233-1237.

FDA. (2009). "Food and Drug Administration. Radiation-Emitting Products - Sunscreen." Retrieved 3/2010, from http://www.fda.gov/Radiation-EmittingProducts/RadiationEmittingProductsandProcedures/Tanning/ucm116445.htm.

Florence, A. T., Ed. (2006). Nanoparticulates as drug carriers. Nanoparticle Flow: Implications for Drug Delivery. Danvers, MA, Imperial College Press.

Galehassadi, M., M. Mahkam, et al. (2007). "Synthesis and characterization of new macromolecule systems for colon specific drug delivery." e-Polymers **028**.

Gavini, E., P. Chetoni, et al. (2004). "PLGA microspheres for the ocular delivery of a peptide drug, nacomycin using emulusification/spray-drying as the prepartion method: in vitro/in vivo studies." European Journal of Pharmaceutical Science **57**: 207-212.

Giunchedi, P. and U. Conte (1995). "Spray-drying as a preparation method of microparticulate drug delivery systems: an overview." S.T.P.Pharmaceutical Sciences **5**: 276-290.

Goldschmidt, A. and H.-J. Streitberger (2003). BASF Handbook on Basics of Coating Technology. Hannover, Germany, BASF Coatings AG.

Gonen, M., D. Balkose, et al. (2009). "Supercritical Carbon Dioxide Drying of Methanol-Zinc Borate Mixtures." Industrial & Engineering Chemistry Research **48**(14): 6869-6876.

Gruening, R., D. J. Perschbacher, et al. (2005). Anti-infectious hydrogel compositions. I. Hydromer, USA. United States.

Guo, L., S. Yang, et al. (2000). "Synthesis and Characterization of poly(vinylpyrrolidone)-Modified Zinc Oxixde Nanoparticles." Chemical Materials **12**: 2268-2274.

Gupta, R. B. (2005). Supercritical Fluid Extraction. Encyclopedia of Chemical Processing, Marcel Dekker.

Gupta, R. B. (2006). Supercritical fluid technology for particle engineering. . Nanoparticle Technology for Drug Delivery. R. B. Gupta and U. B. Kompella, Drugs and the Pharmaceutical Sciences. **159** 53-84.

Gupta, R. B. and P. Chattopadhyay (2003). Method of forming nanoparticles and microparticles of controllable size using supercritical fluids with enhanced mass transfer. United States. **6620351**.

Gupta, R. B. and P. Chattopadhyay (2003). Method of forming nanoparticles and microparticles of controllable size using supercritical fluids with enhanced mass transfer. **US Patent 6620351.**

Gupta, R. B. and U. B. Kompella, Eds. (2006). Nanoparticle Technology for Drug Delivery. Drugs and the Pharmaceutical Sciences. New York, Taylor & Francis Group.

Gupta, R. B. and J.-J. Shim (2007). Solubility in Supercritical Carbon Dioxide. . Boca Raton, FL., Taylor & Francis Group.

Haishi, T., E. Sakamoto, et al. (1992). Flaky powder of zinc oxide and its composition for external use. United States.

Hanson, K. M., E. Gratton, et al. (2006). "Sunscreen enhancement of UV-induced reactive oxygen species in the skin." Free Radical Biology and Medicine **11**(8): 1205.

Hemingway, M. G., R. B. Gupta, et al. (2010). "Hydrogel Nanopowder Production by Inverse-Miniemulsion Polymerization and Supercritical Drying." Ind. Eng. Chem. Res.

Heneczka, M., J. Baldyga, et al. (2006). "Modeling of spray-freezing with compressed carbon dioxide." Chemical Engineering Sciences **61**: 2880-2887.

Hester, C. I., R. L. Nicholson, et al. (1990). Powder coating technology. Park Ridge, New Jersey, Noyes Data Corporation.

Ho, K., W. Li, et al. (2010). "Amphiphilic polymeric particles with core–shell nanostructures: emulsion-based syntheses and potential applications." Colloid & Polymer Science: 1-21.

Huang, Y., W. Leobandung, et al. (2000). "Molecular aspects of muco- and bio-adhesion: tethered structures and site-specific surfaces." J. Control. Release.

Huglin, M. B., M. M. A. M. Rehab, et al. (1986). "Thermodynamic interactions in copolymeric hydrogels." Macromolecules **19**(12): 2986-2991.

Hynd, M., J. A. Turner, et al. (2007). "Applications of hydrogels for neural cell engineering." J Biomater Sci. Polymer Edn **18**(10): 1223-1244

Jackson, S. J., D. Bush, et al. (2000). "Effect of resin surface charge on gastric mucoadhesion and residence time of cholestyramine." International Journal of Pharmaceutics **205**: 173-181.

Jayasundera, M., B. Adhikari, et al. (2009). "Surface modification of spray dried food and emulsion powders with surface-active proteins: A Review." Journal of Food Engineering **93**: 266-277.

Jing, L., Z. Xu, et al. (2001). "The surface properties and photocatalytic activities of ZnO ultrafine particles." Applied Surface Science **180**: 308-314.

John, S., S. Marpu, et al. (2010). "Hybrid zinc oxide nanoparticles for biophotonics." Journal of Nanoscience and Nanotechnology **10**(3): 1707-12.

Jounela, A., P. Pentikainen, et al. (1975). "Effect of particle size on the bioavailability of digoxin. ." Eur J Clin Pharmacol **8**(365-70).

Jouyban, A. R., M., B. Y. Shekunov, et al. (2002). "Solubility prediction in supercritical CO2 using minimum number of experiments." Journal of Pharmaceutical Science **91**(5): 1287-1295.

Jung, J. and M. Perrut (2001). "Particle design using supercritical fluids: literature and patent survey." Journal of Supercritical Fluids **20**: 179-219.

Junginger, H. E., J. C. Verhoef, et al. (2007). Drug Delivery: Mucoadhesive Hydrogels. Encyclopedia of Pharmaceutical Technology**:** 1169-1200.

Kapoor, Y. and A. Chauhan (2008). "Drug and surfactant transport in Cyclosporine A and Brij 98 laden p-HEMA hydrogels." Journal of Colloid and Interface Science **322**(2): 624-633

Kazarian, S. G., N. Sakellarios, et al. (2002). "High-pressure CO2-induced reduction of the melting temperature of ionic liquids." Chemical Communications(12): 1314-1315.

Kersten, B. S., T. Catalano, et al. (1991). "Ion-pairing high-performance liquid chromatographic method for the determination of 5-aminosalicyclic acid and related impurities in bulk chemical." Journal of Chromatography **588**: 187-193.

Kharb, V., M. Bhatia, et al. (2006). "Nanoparticle technology for the delivery of poorly water soluble drugs." Pharm Technol. **30**

Khrenov, V., M. Klapper, et al. (2005). "Surface Functionalized ZnO Particles Designed for the Use in Transparent Nanocomposites." Macromolecular Chemistry and Physics **206**(1): 95-101.

King, M. B. and T. R. Bott, Eds. (1993). Extraction of natural products using near-critical solvents. London, Blackie Academic & Professional (A&P).

Kiran, E., G. Brunner, et al. (2009). "The 20th anniversary of the Journal of Supercritical Fluids–A special issue on future directions in supercritical fluid science and technology." Journal of Supercritical Fluids **47**(3): 333-335

Klein, K. (2004). "Using zinc oxide in sunscreen products." Cosmetics & Toiletries **199**: 22-25.

Kriwet, B. and T. Kissel (1996). "Poly(acrylic acid) Microparticles Widen the Intercellular Spaces of Caco-2 cell monolayers: an examination by confocal laser scanning microscopy." European Journal of Pharmaceutics and Biopharmaceutics. **42**(4): 233-240.

Kriwet, B., E. Walter, et al. (1998). "Synthesis of bioadhesive poly(acrylic acid) nano- and microparticles using an inverse emulsion polymerization method for the entrapment of hydrophilic drug candidates." Journal of Controlled Release **56** 149-158.

Landfester, K. (2009). "Miniemulsion Polymerization and the Structure of Polymer and Hybird Nanoparticles." Angewandte Chemie International Edition **48**: 4488-4507.

Landfester, K., M. Willert, et al. (2000). "Preparation of Polymer Particles in Nonaqueous Direct and Inverse Miniemulsions." Macromolecules **33**: 2370-2376.

Lane, M. E., F. Brennan, S., et al. (2005). "Comparison of post-emulsification freeze drying or spray drying for the microencapsulation of plasmid DNA." Journal of Pharmacy and Pharmacology **57**(7): 831-838.

Lee, S. and A. Rudin (1992). Control of Core-Shell Latex Morphology. Polymer Latexes - Preparation, Characterization, and Applications. E. S. Daniels, E. D. Sudol and M. S. El-Aasser. Atlanta, GA, American Chemical Society. **492:** 234-254.

Leuenberger, H. (1987). Process of drying a particulate material and apparatus for implementing the process. US, 4,608,764.
Levine, K. L., J. O. Iroh, et al. (2004). "Synthesis and properties of the nanocomposite of zink oxide and poly(amic acid)." Applied Surface Science **230** 24-33.
Li, B., X. Zhu, et al. (2008). "Supercritical carbon dioxide-induced melting temperature depression and crystallization of syndiotactic polypropylene." Polymer Engineering & Science **48**(8): 1608-1614.
Li, H. and E. Ruckenstein (1996). "Amphiphilic particles with hydrophilic core/hydrophobic shell prepared via inverted emulsions." Journal of Applied Polymer Science **61**(12): 2129-2136.
Li, Q., S. L. Chen, et al. (2007). "Durability of nano ZnO antibacterial cotton fabric to sweat." Journal of Applied Polymer Science **103**(1): 412-416.
Liversidge, G. G. and K. C. Cundy (1995). "Particle size reduction for improvement of oral bioavailability of hydrophobic drugs: absolute oral bioavilability of nanocrystalline danzol in beagle dogs." Int J Pharm. **125** 91-97.
Majerik, V., G. Charbit, et al. (2007). "Bioavailability enhancement of an active substance by supercritical antisolvent precipitation." J. Supercritical Fluids **40** 101-110.
Martín, A., A. Bouchard, et al. (2007). "Mathematical modeling of the mass transfer from aqueous solutions in a supercritical fluid during particle formation." Journal of Supercritical Fluids **41**(1): 126-137.
Martin, T. M., N. Bandi, et al. (2002). "Preparation of budesonide and budesonide-PLA micropartilces using supercritical fluid precipitation technology." AAPS Pharm Sci Technol **3**(3).
Masters, K. (1991). Spray Drying Handbook. New York, John Wiley & Sons.
Mendez-Santiago, J. and S. Teja (1999). "The solubility of solids in supercritical fluids." Fluid Phase Equilibrium: 158-160; 501-510.
Merisko-Liversidge, E. M. and G. G. Liversidge (2008). "Drug nanoparticles: formulating poorly water-soluble compounds. ." Toxicol Pathol. **36** 43-8.
Merryman, H. T. (1959). Science **130**: 628-629.
Michiya, T., K. Matsuyama, et al. (2007). Oily particles containing zinc oxide particles, hydrogel particles containing the same, and manufacture thereof. E. P. Office.
Ming, H. Y. and X. S. Li (2003). "Fully Coupled Analysis of Failure and Remediation of Lower San Fenando Dam." Journal of Geotechnical and Geoenvironmental Engineering **129**(4): 336-349.
Mitchell, J. K., C. D. P. Baxter, et al., Eds. (1995). Performance of improved ground during earthquakes. Soil Improvement for earthquake hazard mitigation. Reston, VA, ASCE.
Mitchell, J. K., H. G. Cooke, et al. (1998). Design considerations in ground improvement for seismic risk mitigation. Geotechnical Special Publication. Conference on Geotechnical Earthquake and Soil Dynamics III. Part 1 (of 2), Seattle, Washington, ASCE.
Moyler, D. A. (1994). Extraction of flavours and fragrances with compressed CO2. Extraction of Natural Products Using Near-Critical Solvents. M. B. King and T. R. Bott. Glasgow, UK, Blackie Academic & Professional.

Mukhopadhyay, M. (2000). Natural Extracts Using Supercritical Carbon Dioxide. Boca Raton, FL, CRC Press.
Mukhopadhyay, M. and S. V. Dalvi (2004). "Mass and heat transfer analysis of SAS: effects of thermodynamic states and flow rates on droplet size." The Journal of Supercritical Fluids **30**(3): 333-348.
Muller, C. R., V. L. Bassani, et al. (2000). "Preparation and Characterization of Spray-Dried Polymeric Nanocapsules. ." Drug Development and Industrial Pharmacy. **26** (3): 343-347.
Nail, S. L. and L. A. Gatlin (1993). Freeze drying: principles and practice. New York, Marcel Dekker, Inc.
NIST. "National Institute of Standards and Technology." from webbook.nist.gov/chemistry/.
NNI. (2009). "National Nanotechnology Initiative." from www.nano.gov.
O'Neill, M. L., M. Z. Yates, et al. (1998). "Dispersion Polymerization in Supercritical CO2 with a Siloxane-Based Macromonomer " Macromolecules **31**(9): 2838-2847.
Ohde, H., C. M. Wai, et al. (2007). "The synthesis of polyacrylamide nanoparticles in supercritical carbon dioxide." Colloid & Polymer Science **285**(4): 475-478.
Packhaeuser, C. B., K. Lahnstein, et al. (2009). "Stabilization of Aerosolizable Nano-carriers by Freeze-Drying." Pharmaceutical Research **26**(1): 129-138.
Park, H. and J. R. Robinson (1985). J Controlled Release **2**: 257-275.
Park, H. and J. R. Robinson (1987). "Mechanisms of mucoadhesion of poly(acrylic acid) hydrogels." Pharmaceutical Research **4**(6): 457-64.
Pasquali, I., R. Bettini, et al. (2008). "Supercritical fluid technologies: An innovative approach for manipulating the solid-state pharmaceuticals." Advanced Drug Delivery Reviews **60**: 399-410.
Peppas, N. A., P. Bures, et al. (2000). "Hydrogels in pharmaceutical formulations. ." European Journal of Pharmaceutics and Bioplarmaceutics. **50**: 27-46.
Peppas, N. A. and P. A. Buri (1985). J Controlled Release **2**: 257-275.
Perrut, M. (2000). "Supercritical Fluid Applications: Industrial Developments and Economic Issues." Industrial Engineering Chemical Research. **39**(12): 4531-4535.
Perrut, M. (2000). "Supercritical fluid applications: industrial developments and economic issues." Ind. Eng. Chem. Res. **39**(12): 4531- 4535.
Perrut, M. (2003). "Supercritical fluids applications in the pharmaceutical industry." STP Pharma Sciences **13**(2): 83-91.
Pesika, N. S., Z. Hu, et al. (2002). "Quenching of Growth of ZnO Nanoparticles by Adsorption of Octanethiol " J. Phys. Chem. B **106** (28): 6985-6990.
Pikal, M. J. (2007). Freeze Drying. Encyclopedia of Pharmaceutical Technology. J. Swarbrick. Pinehurst, NC., Informa Healthcare USA, Inc. **1**.
Pinnell, S. R., D. Fairhurst, et al. (2000). "Microfine zinc oxide is a superior sunscreen ingredient to microfine titanium dioxide." Dermatologic Surgery - American Society for Dermatologic Surgery **26**(4): 309-14.
Quintero-Ortega, I., A. Vivaldo-Lima, et al. (2007). "Modeling of the Homogeneous Free-Radical Copolymerization Kinetics of Fluoromonomers in Carbon Dioxide

at Supercritical Conditions." Journal of Macromolecular Science w, Part A: Pure and Applied Chemistry **44**: 205-213.
Rasenack, N. and B. W. Muller (2002). "Dissolution rate enhancement by in situ micronization of poorly water-soluble drugs." Pharm Res. **19** 1894-900.
Reverchon, E. (1997). "Supercritical fluid extraction and fractionation of essential oils and related products." Journal of Supercritical Fluids **10**(1): 1-37.
Reverchon, E. and R. Adami (2006). "Nanomaterials and supercritical fluids. ." Journal of Supercritical Fluids **37** 1-22.
Reverchon, E., I. De Marco, et al. (2007). "Nanoparticles production by supercritical antisolvent precipitation: A general interpretation." J. Supercritical Fluids **43**: 126-138.
Rizvi, S. S. H., Ed. (1994). Supercritical fluid processing of Food and Biomaterials. London, Blackie Academic & Professional (A&P).
Robinson, J. R. and H. Park (1984). Int J Pharm. **19**: 107-127.
Roco, M. C. (1999). "Nanoparticles and nanotechnology research." J.ournal of Nanoparticle Research **1**(1): 1-6.
Rodríguez, E., M. C. Valbuena, et al. (2006). "Causal agents of photallergic contact dermitis diagnosed in the national institute of dermatology of Columbia." Photodermatol Photoimmunol Photomed **22**(4): 189-192.
Rodriguez, F., C. Cohen, et al. (2003). Principles of Polymer Systems. New York, New York, Taylor & Francis Books, Inc.
Sakohara, S. and K. Mori (2008). "Preparation of ZnO nanoparticles in amphiphilic gel network." Journal of Nanoparticle Research **10**(2): 297-305.
SCCP (2006). "Opinion on Benzophenone-3." European Commission - Scientific Committee on Consumer Products.
Seed, H. B. and I. M. Idriss (1982). Ground Motions and Soil Liquefaction During Earthquakes. EERI, UCB, Berkley, CA.
Seed, H. B., F. Makdisi, et al. (1975). Slides in the San Fernando Dams During the Earthquake of February 9,1971. ASCE Journal of the Geotechnical Engineering Division.
Seil and Webster (2008). Int J Nanomedicine **3**(4): 523-31.
Señoráns, F. J., A. Ruiz-Rodriguez, et al. (2003). "Isolation of brandy aroma by countercurrent supercritical fluid extraction. ." Journal of Supercritical Fluids **26** (2): 129-35.
Shekunov, B. Y., P. Chattopadhyay, et al. (2006). "Nanoparticles of Poorly Water-Soluble Drugs Prepared by Supercritical Fluid Extraction of Emulsions." Pharmaceutical Research **23**(1): 196-204.
Silebi, C. A. and J. G. DosRamo (1989). "Separation of submicrometer particles by capillary hydrodynamic fractionation (CHDF)." Journal of Colloid and Interface Science **130**: 14-24.
Smart, J. D. (2005). "The basics and underlying mechanisms of mucoadhesion." Adv. Drug Delivery Reviews **57**: 1556-1568.
Society, A. C. (2009, 2009). "Skin Cancer Facts." from www.acs.org.
Spanhel, L. and M. A. Anderson (1991). "Semiconductor clusters in the sol-gel process: quantized aggregation, gelation, and crystal growth in concentrated zinc oxide colloids." Journal of the American Chemical Society **113**(8): 2826-2833.

Stahl, E., K. W. Quirin, et al. (1987). Dense Gases for Extraction and Refining. Berlin. **Spring-Verlag**

Sutton, R. (2008). "CDC: Americans Carry Body Burden of Toxic Sunscreen Chemical - Environmental Working Group (EWG)." Environmental Working Group Science Analysis, from www.ewg.org/analysis/toxicsunscreen.

Sze Tu, L., F. Dehghani, et al. (2002). "Micronisation and microencapsulation of pharmaceuticals using a carbon dioxide antisolvent." Powder Technology **126**(132-149).

Takeuchi, H., H. Yamamoto, et al. (2001). "Mucoadhesive microparticulate systems fo peptide drug delivery." Drug Delivery Reviews **47**: 39-54.

Thairs, S., S. Ruck, et al. (1998). "Effect of dose size, food and surface coating on the gastric residence and distribution of ion exchange resin." Int J Pharm. **176**: 47-53.

Thakur, R. and R. B. Gupta (2005). "Rapid Expansion of Supercritical Solution with Solid Cosolvent (RESS-SC) Process: Formation of Griseofulvin Nanoparticles. ." Industrial & Engineering Chemistry Research **44**(19): 7380-7387.

Tom, J. W. and P. G. Debenedetti (1991). "Formation of bioerodiable polymeric microspheres and microparticles by rapid expansion of supercritical solutions." Biotechnol. Prog. **7**: 403-411.

Tom, J. W., X. Kwauk, et al. (1993). "Rapid expansion of supercritical solutions (RESS): fundamentals and applications." Fluid Phase Equil. **82**.

U.S. Food & Drug Administration, F. (2010). "Orange Book: Approved Drug Products with Therapeutic Equivalence Evaluations." Retrieved March 5, 2010, 2010, from www.accessdata.fda.gov.

Valderrama, J. O., M. Perrut, et al. (2003). "Extraction of Astaxantine and Phycocyanine from Microalgae with Supercritical Carbon Dioxide. ." Journal of Chemical and Engineering Data **8**(4): 827-830.

Vanderhoff, J. W., J. M. Park, et al. (1992). Preparation of Particles for Microvoid Coatings by Seeded Emulsion Polymerization. 201st National Meeting of the American Chemical Society, Atlanta, GA, ACS Symposium Series.

Verreck, G., A. Decorte, et al. (2006). "The effect of pressurized carbon dioxide as a plasticizer and foaming agent on the hot melt extrusion process and extrudate properties of pharmaceutical polymers." The Journal of Supercritical Fluids **38**(3): 383-391.

Wahab, R., A. Mishra, et al. (2010). "Antibacterial activity of ZnO nanoparticles prepared via non-hydrolytic solution route." Applied Microbiology and Biotechnology **87**(5): 1917-1925.

Wang, Y., R. N. Dave, et al. (2004). "Polymer coating-encapsulation of nanoparticles using a supercritical anti-solvent process." Journal of Supercritical Fluids **28**: 85-99.

Wang, Z. L. (2006). "Novel Zinc Oxide Nanostructures Discovery by Electron Microscopy." Journal of Physics: Conference Series **26**: 1-6.

Wang, Z. L., W. H. Finlay, et al. (2006). "Powder formation by atmospheric spray-freeze-drying." Powder Technology **170**: 45-52.

Werling, J. O. and P. G. Debenedetti (1999). "Numerical modeling of mass transfer in the supercritical antisolvent process." J. Supercritical Fluids **16**: 167-181.

WHO. (2010, 2010). "Ultraviolet radiation and the INTERSUN Programme." World Health Organization Retrieved 3/2010, from http://www.who.int/uv/en/.
Willert, M. and K. Landfester (2002). "Amphiphilic Copolymers from Miniemulsified Systems." Macromolecular Chem. Phys. **203**: 825-836.
Xu, Z. Z., et al. (2004). "Encapsulation of nanosized magnetic iron oxide by polyacrylamide via inverse miniemulsion polymerization." Journal of Magnetism and Magnetic Materials. **277**: 136-143.
Yadav, A. V. and V. B. Yadav (2008). "Improvement of physicochemical properties of mesalamine with hydrophilic carriers by solid dispersion (kneading) method." Research J. Pharm. and Tech. **1**(4).
Yamamoto, O., M. Komatsu, et al. (2004). "Effect of lattice constant of zinc oxide on antibacterial characteristics." Journal of Materials Science: Materials in Medicine **15**(8): 847-851.
Yasuji, T., H. Takeuchi, et al. (2008). "Particle design of poorly water-soluble drug substances using supercritical fluid technologies." Adv Drug Delivery Reviews **60** 388-98.
Yin, N. and K. Chen (2004). "Ultrasonically initiated emulsifier-free emulsion copolymerization of n-butyl acrylate and acrylamide. Part I: Polymerization mechanism." Polymer **45**: 3587-3594.
York, P. (1999). "Strategies for particle design using supercritical fluid technologies." Pharmaceut. Sci. Technol. Today **2**: 430-440.
Young, T. J., K. P. Johnston, et al. (1999). "Encapsulation of lysozyme in a biodegradable polymer by precipitation with a vapor-over-liquid antisolvent." Journal of Pharmaceutical Science **88**(6): 640-50.
Yuan, Z. and B. D. Favis (2004). "Macroporous poly(L-lactide) of controlled pore size derived from the annealing of co-continuous polystyrene/PLA blends." Biomaterials **25**: 2161-2170.
Zhang, D. and e. al. (2006). J. Phys. Chem B **110**: 9079-9084.

APPENDIX A. High Pressure Vessel Design

A.1. Vessel 1 – Large High Pressure Vessel with Windows

This vessel was designed by Melinda Hemingway and manufactured by Brian Schweiker the Chemical Engineering Department Machinist. The intent of this new vessel addition to the high pressure supercritical fluids laboratory is to enable two injections of solvent at one time while utilizing an ultrasonication horn for enhanced mass transfer as well as a larger volume capacity at 500 ml with windows to observe phenomenon occurring and increase product yield. Semi-continuous experiments were executed in Chapter 5 for the coating of hydrogel particles in a continuous flow of supercritical carbon dioxide.

An adaptation piece to account for the larger diameter vessel and the smaller diameter horn a novel design for usage of the ultrasonication horn was generated composed of the top, adapter, and main body pieces (Figure A.1-5). Some initial leak issues during pressure tests yielded modifications to initial design at Teflon o-rings locations. Required minimum applied torque when closing the vessel configuration to prevent significant pressure leaks in under investigation, and will soon be completed following a torch wrench purchase and final vessel ports installed. A structured base support has been designed to allow the option of a bottom port installed when required and to allow easier collection of powder material. Initial pressure tests and ultrasonication activation experiments were promising. This large vessel has been physically pressure tested to 4200 psi and withstood no significant leaks. An activation of ultrasonication while pressurized to 1600 psi and heated to 40˚C was promising with harmonics tolerable from 20% to 35% amplitude, typical operational parameters.

Figure A1. High Pressure Vessel.

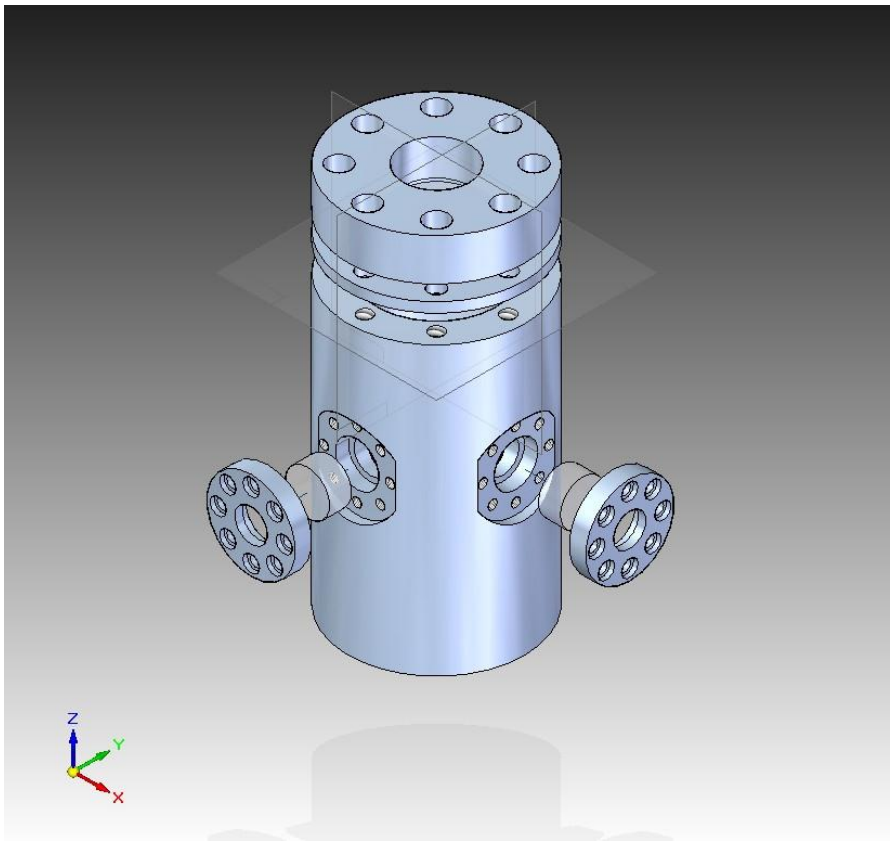

Figure A2. High Pressure Vessel in Solid Edge.

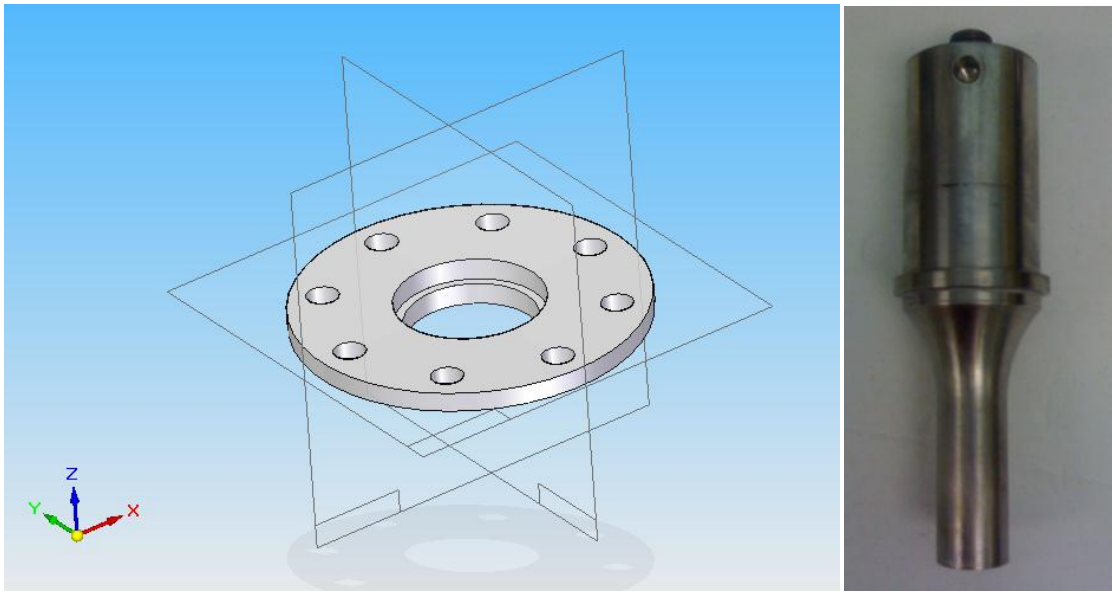

Figure A3. Adapter piece and the ultrasound horn that rests on the lip.

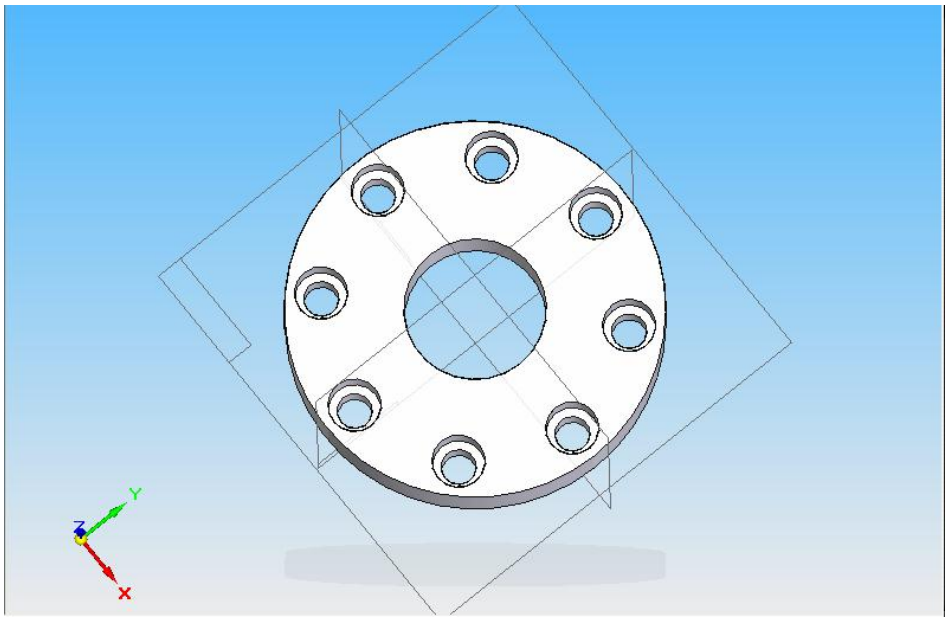

Figure A4. Top with screw holes.

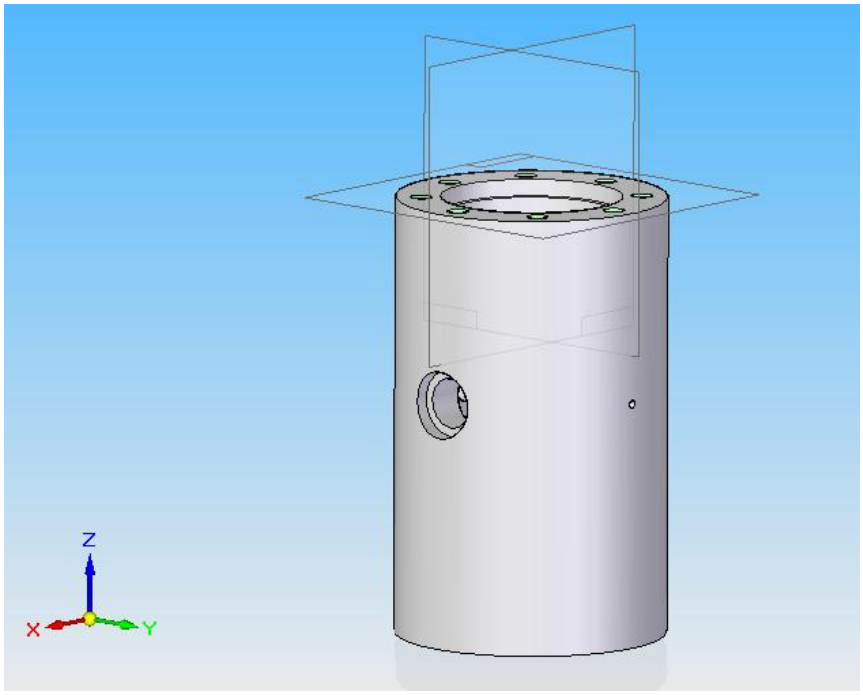

Figure A5. Main Body of Vessel.

The vessel dimensions were diagrammed in Solid Edge by Mr. Schweiker. The view sights were determined by aligning the windows to view the ultrasound horn's tip in the top ¼" of the windows diameter. Sapphire windows (1in. diameter by ½" thickness) were obtained instead of quartz based on pressure rating. The standard safety factor at room temperature is three. Sapphire window dimensions are ½" thick by 1" diameter which can withstand 16064 psi (Figure A6).

Dimensions (inches)		PRESSURE (psi)			
Diameter	Plate Thickness	SAPPHIRE	Quartz		
1.0	0.035	79	10		
1.0	0.075	361	45		
1.0	0.125	1004	126		
1.0	0.200	2570	321		
1.0	0.250	4016	502		
1.0	0.500	16064	2008		
2.0	0.035	20	#		
2.0	0.075	90	#	Design Stress (psi):	
2.0	0.125	251	31	Sapphire	20000
2.0	0.200	643	80	PCA	17500
2.0	0.250	1004	126	Quartz	2500

Figure A6. Maximum Allowed Pressure Limits for Circular Windows (Saphikon now Saint-Gobins Crystals)

A.2 Center of Gravity (COG) Calculations

Center of gravity calculations were executed to evaluate the proper location of welded holding arms to attach to the support base and frame. In the three types of calculations, the measurement is determined to be within a tolerable allowance to machining precision and human error in measurements. With the development of an axis of rotation supporting the weight of the larger vessel, the center of gravity was calculated for the best location of rotation to minimize forces on the joint in both an upright manner and in horizontal direction for collecting powder. A screw joint instead of solid weld was decided upon in this position. The center of mass or gravity, R, is defined as the average of positions, r_i, weighted by masses, m_i:

$$\mathbf{R} = \frac{\sum m_i \mathbf{r}_i}{\sum m_i}.$$

An integral is utilized to calculate the center of mass for a continuous distribution with mass density, ρ(r), and total mass, *M*, the sum becomes an integral:

$$\mathbf{R} = \frac{1}{M}\int \mathbf{r}\, dm = \frac{1}{M}\int \rho(\mathbf{r})\,\mathbf{r}\, dV = \frac{\int \rho(\mathbf{r})\,\mathbf{r}\, dV}{\int \rho(\mathbf{r})\, dV}.$$

Three numerical integration methods based on location (left weighted, right weighted, trapezoidal) were utilized to estimate the center of mass of the large high pressure vessel, then averaged to obtain the position of the rotating support.

	L	**R**	**Mid**
Sum(m*r)	2006.49	2007.621	1968.911
Sum Mass	613.43	613.43	613.43
COG	3.271	3.273	3.210

A-3. Vessel 2 – Small High Pressure Vessel Design

This vessel was designed by Melinda Hemingway and manufactured by a mechanical engineering masters student under the mentorship of Lewis Peyton. The intent of this new vessel addition to the high pressure supercritical fluids laboratory is to enable multiple experiments taking place in the laboratory while utilizing an ultrasonication horn for enhanced mass transfer. A semi-continuous state is planned as batch development of nanopowder in a continuous flow of supercritical carbon dioxide. The utilization of this manufactured vessel has lead to some insights on how to repair major leaks at juncture ports for high pressure tubing: utilizing two ferrules and Teflon tape around the gland produces a secure seal. This vessel (403/304 instead of 316 SS) has tendency to rust and routine preventative maintenance to remove is recommended. A Solid Edge version of the below sketch is available from mechanical engineering.

A-4. High Pressure Safety

High pressure operating conditions required of supercritical fluids warrant special safety precautions in place for mandatory protection of personnel. In the laboratory environment, this is indicative of wearing safety goggles and appropriate attire, placement of high pressure devices behind secondary enclosures, and proper ventilation. Carbon dioxide, although nonflammable, is a potential asphyxiation hazard if uncontrolled expulsion of the high pressure vessel. Preventative protective methods and extra precautions should be paramount in a routine work environment.

Appendix B. Detailed Polymerization Recipe for Polyacrylamide

Continuous Phase: cyclohexane 24 g, Span 80 (sorbitan monoleate) 0.75 g

Cool cyclohexane (CH) in refrigerator while weighing out disperse phase

Bubble N_2 for 2 min at 10 psi through chilled CH while weighing Span80

Disperse Phase: water 2.25-3.0 g, monomer acrylamide 2.25 g

N,N-methylenebisacrylamide (MBA) cross-linker 0.0225 g (1%) – 0.111 g (4%)

Place on shaker >#7 setting until MBA is dissolved (30 minutes)

For particle loading, add particles first, ultrasonicate sample (1 min 10%), then remaining components, ultrasonicate prior to dropwise addition (1 min 10%)

Mix continuous phase covered until Span 80 dissolved & golden color (30 minutes)

Add disperse phase to continuous phase drop wise at a rate of at 1 drop / 5 sec

#4 Thermix magnetic stirrer around 15 minutes minimum

Allow to mix for 1 hr at this rate covered with teflon tape on rim of 140 ml glass flask glass plate, al foil and parafilm around to secure vessel and prevention evaporation

Ultrasonicate = horn (1/2" default tip) tip in with Al foil & parafilm

10% Amplitude, 15 min total sonication time, pulsed 5sOn/5sOff (take 30 min)

Chilled water bath around flask T=14˚C

Nitrogen Purge = 2 min ~5psi no stirring occurred

Cover with aluminum foil, paraffin, and glass cover

Initiator AIBN added 75 mg directly, 150 rpm

Flask hovered over hot water bath at 65°C with plastic shelf underneath

Continue to purge ~10 psi for 5 min

Added flask to heat at 65˚C (start timer), purge for 5 min at 10 psi

At 10 min into reaction, adjust to 2 psi purge bubbles

After 15 min into reaction, turn N_2 tank off

Allowed reaction to continue until completion (2 hrs default)

Run POLY sample on DLS (estimate 5 drops in 10 ml CH, intensity 300-500 kHz)

Appendix C. Materials of Interest.

Chemical CAS #	Structure	MW (g/mol)	T_m (˚C) T_g (˚C)	Water Solubility	Abbre.
Acrylamide 79-06-1	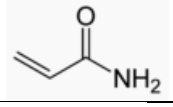	71.08	T_m 84.5	2.04 kg/L (25˚C)	AM
Poly (acrylamide) 9003-05-8	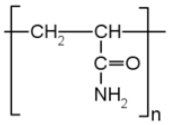		Cross-linked	Highly Absorbs	PAM
Acrylic Acid	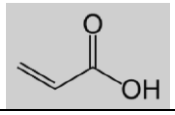	72.06	T_b 139 T_m 14	Miscible	AA
Mesalamine 89-57-6	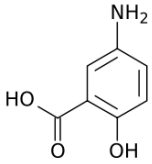	153.13	T_m 283	0.8 mg/ml (20°C)	MSM
Zinc Oxide 1314-13-2	$(Zn^{+2})(O^{-2})$	81.408	T_m 975 T_g 2360	0.16mg/ 100ml (30˚C)	ZnO
Poly(vinyl acetate) 9003-20-7	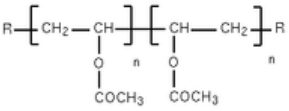	100,000	T_g 30		PVAc
Polysulfone 25135-51-7	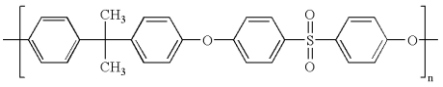	M_w 35000 M_n 16000	T_g 185		PSF
Polylactide 26161-42-2	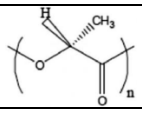	50000	T_g 60 T_m 175		PLLA
Poly(hydroxybutyrate) 26063-00-3	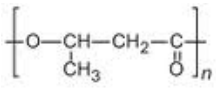	M_w 437,000 M_n 300,000			PHB
Gelucire (50-13)	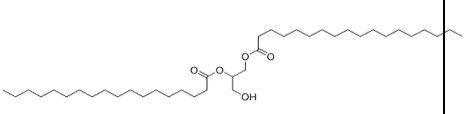				

Appendix D. Supplementary Information on Chapter 2 Experiments

D-1. Surfactant Effect and Ultrasound Effect on Polymerization

The effects of varying surfactant amounts through direct experimentation were investigated with three amounts (1%, 2%, and 5%) utilized, all other factors held constant. Surfactant percentages were determined based on monomer weight. As expected through previous emulsion studies, the more surfactant amount utilized the smaller the particle size (number-weighted mean diameter-NMD) as the surface tension is lessened. The surfactant quantity is based on weight percentage to monomer is not approaching the critical micelle concentration that is utilized in typical emulsion polymerizations with zero surface tension. These experiments were prior to lowering the quantity of water in disperse phase from 3 g to 2.25 g which increased the ratio of surfactant to monomer disperse phase to obtain smaller particles with similar surface tension as the initial 5% Span 80 with 3 g water in disperse phase.

NMD	Span 80 1%	Span 80 3.3%	Span 80 5%
Peak 1	135.1 – 97%	92.5 – 97.1%	75.7 – 98.3%
Std Dev	18.5 – 13.7%	11.4 – 11%	9.3 – 12.3%
Peak 2	876.4 – 3%	278.7—2.9%	254.2 –1.7%
Std Dev	66.9 – 7.6%	40.9 – 14.1%	29.9 – 11.8%

The effect of ultrasonication horn tip diameter was examined. For these experiments only the three phase system was utilized of cyclohexane (24 g), water (3 g), and surfactant Span 80 (0.75 g equivalent to 3.3 % mentioned previously). The same ultrasonication amplitude of 10 % was employed on both solutions in a pulse output of 5 s On-Off intervals for a total of 15 minutes. The 0.50 in. horn tip with less surface area at the same energy input generated slightly smaller particles at 316 nm, whereas the 0.75 in. tip produced 436 nm particles intensity-weighted mean diameter (IMD).

IMD	US tip 0.5in	US tip 0.75in.
nm	316.4	435.7
Std Dev nm	133.2	250.5
Std Dev %	42.1	57.5
VMD	342.5	547.7
Std Dev nm	133.2	250.5
Std Dev %	42.1	57.5
NMD	138.3	94
Std Dev nm	58.2	54
Std Dev %	42.1	57.5

The swelling percentage for hydrogels can be calculated by the difference of the initial weight of sample, m_1, from a fully water saturated of the same sample m_2:

$$\% \text{ swelling} = (m_2 - m_1) / m_1 \qquad \text{(Eq. 1.4)}$$

The swelling diffusion mechanism in hydrogel can change from Fickian to non-Fickian when the cross-linker content is increased and when co-polymers are used. Fickian diffusion relates the rate (flux) a substance will move through another substance, or mass transfer, in relation to the concentration gradient. (Cai and Gupta 2001)

$$J_i = -\frac{Dc_i}{RT}\frac{\partial \mu_i}{\partial x} \qquad \text{(Eq. 1.5)}$$

where J is the diffusion flux (mol/m^2·s), D is the diffusivity (m^2/s), the index i is indicative of the ith species, c is the concentration (mol/m^3), μ is the chemical potential (J/mol), R is the gas constant (J/(K mol), T is temperature (K), and x is the direction of the gradient change. This equation typically describes mass transfer and concentration gradients in one direction.

D-2. Water Solubility Calculations in $scCO_2$

Calculations were performed to evaluate a basis for the limiting step in the supercritical drying of the miniemulsion polymerization, water removal. The knowledge of this data assisted in optimization of the system flow rates of $scCO_2$ and the miniemulsion injection. These calculations suggested initial flow rate parameters, lower injection flow rate 0.25 ml/min to higher CO_2 flow rate 15+ ml/min, based on injecting only water into the vessel.

Defined Constants. CO_2 density at 4°C

Temp C	Pressure	CO2 density	MW CO2	Water Sol in CO2	MW H2O
40	1500	0.96	44	0.00428	18

Water solubility in CO_2 at T 313.2K: mol% and mg/ml% (Gupta and Shim 2007) Referenced and extrapolated.

P bar	mol water/ mol CO2	mg water/ ml CO2
101.3	4280	0.00428
111.5	4400	0.0044
126.7	4670	0.00467
152	5070	0.00507
177.3	5430	0.00543
202.7	5800	0.0058

Calculation % of water in injected miniemulsion

Polymerization Components			Volumetric ml	% by vol
Cyclohexane	24	g	30	0.888689
Water	3	g	3	0.088869
Span 80	0.75	g	0.757576	0.022442
Total	27.75	g	33.75758	
Dry (assume dissolves with no impact on volume)				
AM	2.25	g		
MBA	0.0225	g		
AIBN	0.075	g		

Volume of vessel	100	ml
	0.1680873	ml
To reach water in POLY	0.5287071	ml

Flow rate balance of scCO2 solving ability and injected water content

Balance	**Water 8.89%**	**40C, 101.3bar**		
ml/min	**Inj**	**0.25**	**0.5**	**1**
CO2	Water ml/min	0.022217	0.044434	0.088869
5	0.0084044	0.013813	0.03603	0.080465
10	0.0168087	0.005409	0.027626	0.07206
12	0.0201705	0.002047	0.024264	0.068698
15	0.0252131	-0.003	0.019221	0.063656
18	0.0302557	-0.00804	0.014179	0.058613
20	0.0336175	-0.0114	0.010817	0.055251
24	0.0403409	-0.01812	0.004094	0.048528

*Balance Calculated by Inj-CO_2

Flow rate balance of water content injected and available $scCO_2$ solving power

The addition of cyclohexane and Span 80 in the miniemulsion system was not expected decrease the quantity of water removed; however, the presence of Span 80 and cyclohexane showed an increase effect on the water content removed. Solubility studies of sorbitan monooleate and the mixture in $scCO_2$ are suggested for future work to elucidate the actual solubility effects of the components on the mixture.

D-3. HPLC Calibration of Sorbitan Monooleate - Span 80

A large quantity of time and energy was spent optimizing and reviving the Waters HPLC system to obtain readable consistent peak areas and retention times. Technical skills required mastery of this HPLC system to obtain results. Multiple mobile phase ratios were attempted to separate sorbitan monooleate peaks (85:15, 75:25, 70:30, 60:40) from the other components.

This 60-40 (volume %) of IPA and water mobile solvent separated the crosslinker methylbisacrylamide (MBA) and concentrated IPA injected solution from the sorbitan monooleate peaks. The mono-and di-ester peaks were much stronger than the tri- and tetra-esters that are present in the commercial Span 80 purchased. This is due to the manufacturing process and usage not requiring as pure product for applications. The diester peaks were the basis for Span 80 content.

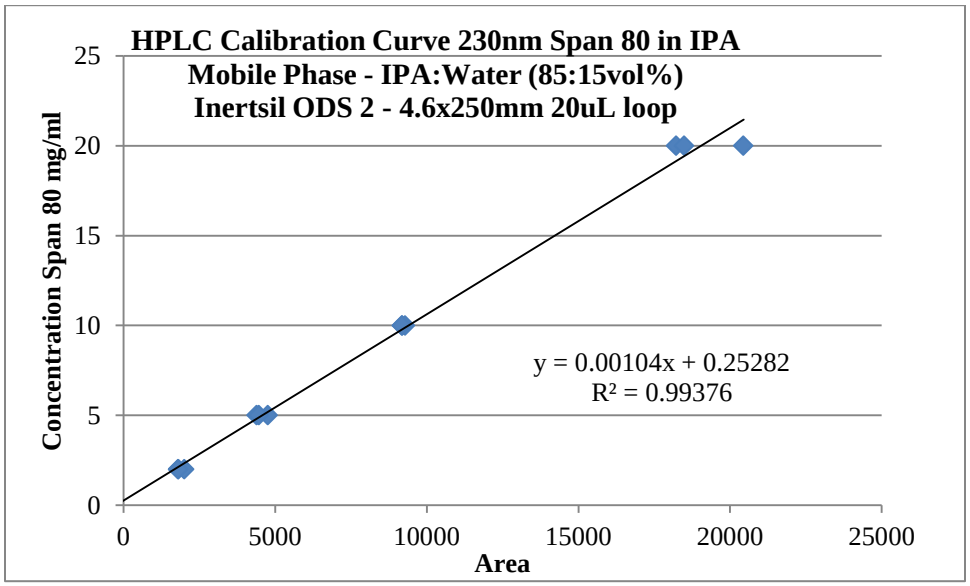
HPLC Calibration Curve 230nm Span 80 in IPA
Mobile Phase - IPA:Water (85:15vol%)
Inertsil ODS 2 - 4.6x250mm 20uL loop
Concentration Span 80 mg/ml
Area
y = 0.00104x + 0.25282
R² = 0.99376
0
5
10
15
20
25
0
5000
10000
15000
20000
25000

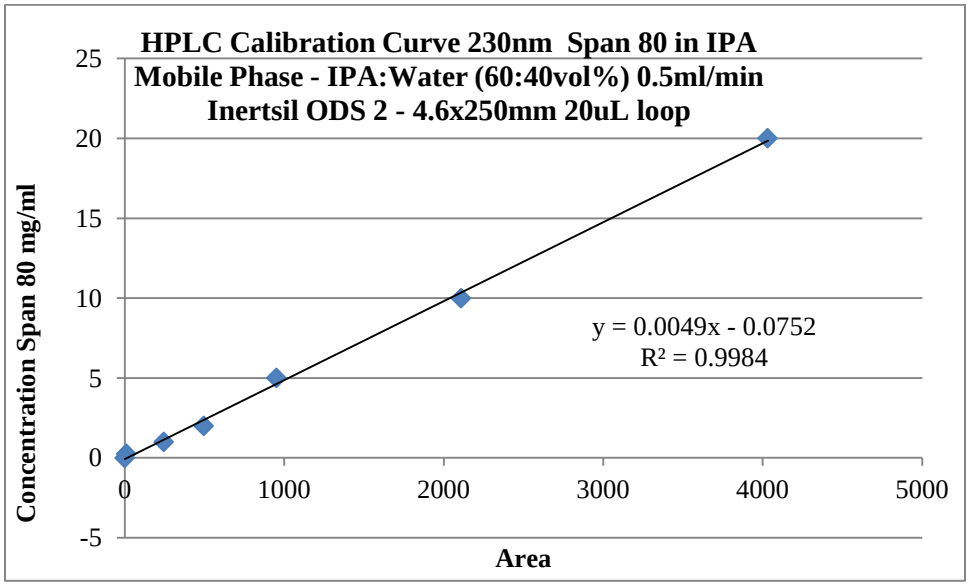
HPLC Calibration Curve 230nm Span 80 in IPA
Mobile Phase - IPA:Water (60:40vol%) 0.5ml/min
Inertsil ODS 2 - 4.6x250mm 20uL loop
Concentration Span 80 mg/ml
Area
y = 0.0049x - 0.0752
R² = 0.9984
-5
0
5
10
15
20
25
0
1000
2000
3000
4000
5000

Appendix E. Mesalamine HPLC

E.1 Calibration Curve and Data

For mesalamine encapsulation analysis, an HPLC method was developed based on Kersten's work (Kersten 1991). A mobile phase of KH_2PO_4 and heptanoic sulfuric sodium salt (890 ml), methanol (50 ml), and acetonitrile (30 ml) was flowed at 1.2 ml/min through a Hypersil C8 column, 50 µL aliquots were injected, and analyzed by UV at 220 nm wavelength. Calibration curve was established for mesalamine (eluted at a 33-35 minute retention time) from 1 to 100 ppm in a 10% 1*N* HCl solution and potential residual interferences (monomer, crosslinker, initiator, surfactant, and polymer) were evaluated. The calibration curve was generated by dissolving 40.43 mg mesalamine in 5 ml 1*N* HCl following diluting with desired amount of water. Inject volume for each sample was 50µl. Mesalamine concentrations were obtained by extracting mesalamine from the hydrogel powder using 1*N* HCl, centrifuging (2 min at 3400 rpm), and filtering (0.2 µm syringe filter), and these processed solutions run on the HPLC.

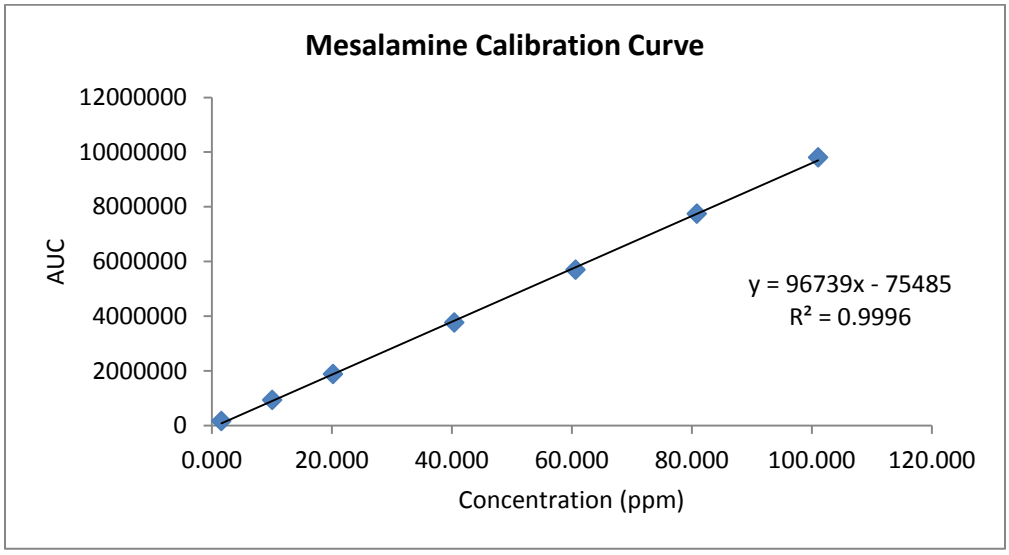

		Peak Areas					
Conc (ppm)	**1.617**	**10.108**	**20.215**	**40.430**	**60.645**	**80.860**	**101.075**
1	155887	919156	1877162	3772011	5695217	7739588	9787182
2	154225	920499	1880571	3746081	5689892	7732080	9809800
Mean	**155056**	**919827.5**	**1878867**	**3759046**	**5692555**	**7735834**	**9798491**
S.D	1175.21	949.64	2410.53	18335.28	3765.34	5308.96	15993.34
RSD	**0.7579**	**0.1032**	**0.1283**	**0.4878**	**0.0661**	**0.0686**	**0.1632**

	1N MES Stability 100ppm			
	in water	**in 1N Hcl**	**After a day**	
Date Run		18-Sep	19-Sep	4-Oct
1	9641713	9358119	9552297	9869936
2	9629967	9361830		
Mean	9635840	9359975	9552297	9869936
S.D	8305.676	2624.073		
RSD	0.086196	0.028035		
Assay	**98.34**	**95.52**	**97.49**	**100.73**

Stability of mesalamine in 1*N* HCl was found to be within tolerable range. Mesalamine standard 100 ppm was made September 19 and evaluated next day and periodically thereafter. Polyacrylamide displayed no peaks in the mesalamine retention time (H5 and 141). Mesalamine alone with the shorter extraction time recovered 93% of expected mesalamine (H6 and 143). Control samples of known mesalamine content were physically mixed with polyacrylamide. Using a shorter extraction time of 1.5 hrs, concentrations obtained were low at 77% recovery (H7, 142, and Expt. 9). Using a longer extraction time overnight and stronger acid content, recovery from the physically mixed mesalamine and PAM was 100% (C1).

CONTROLS PAM	Peak Areas 10% 1 N HCl: MeOH			
	H5	141	H5 2nd day	141 2nd day
1	No Peak	No Peak	No Peak	No Peak
2	No Peak	No Peak	No Peak	No Peak
Mean	---	---	---	---
S.D	---	---	---	---
RSD	---	---	---	---

CONTROLS	Peak Areas 10% 1 N HCl: MeOH			
	H6	143	H6 2nd day	143 2nd day
1st Day	MES Alone (2.5mg/ml)	MES Alone (1mg/ml)	MES Alone (2.5mg/ml)	MES Alone (1mg/ml)
1	3255666	1276270	3346007	1300909
2	3262931	1270566	3351848	
Mean	**3259298.5**	**1273418**	**3348927.5**	**1300909**
S.D	5137.13	4033.34	4130.21	---
RSD	**0.1576**	**0.3167**	**0.1233**	**---**
Conc	34.47	13.94	35.40	14.23
D.F	66.67	66.67	66.67	66.67
Final Conc (mg/ml)	**2.298**	**0.930**	**2.360**	**0.949**
Expected	2.51	1	2.51	1
%	**91.56**	**92.96**	**94.02**	**94.85**

CONTROLS PAM+MES Physical mix	Peak Areas					
	75% 1 N HCl:water overnight	10% 1 N HCl: MeOH 1.5 hrs				
	C1	**142**	**142 2nd day**	**H7**	**H7 2nd day**	**Expt 9 PAM NP**
1	2728588	1052409	1199734	2719673	2802386	1197096
2	2716241	1054937	1200219	2721678		1194397
Mean	**2722414.5**	**1053673**	**1199976.5**	**2720675.5**	**2802386**	**1195747**
S.D	8730.65	1787.57	342.95	1417.75	---	1908.48
RSD	**0.3207**	**0.1697**	**0.0286**	**0.0521**	---	**0.1596**
Conc	28.92	11.67	13.18	28.90	29.75	13.14
D.F	10.00	66.67	66.67	66.67	66.67	66.67
Final Conc (mg/ml)	**0.289**	**0.778**	**0.879**	**1.927**	**1.983**	**0.876**
Expected	0.2875	1	1	2.5	2.5	1
%	**100.60**	**77.81**	**87.90**	**77.08**	**79.33**	**87.61**

SAMPLE IV	Peak Areas				
	Samples (20mg/4ml) 50:50 1N HCl in (MeOH or water) Overnight				100mg/5ml 1.5hr 10% 1N HCl:MeOH
	Expt-4 (MeOH)	**Expt-4 (MeOH)**	**Expt-4 (water)**	**Expt-4 (water)**	**Expt-4**
	0.4 to 1 ml dilution	**As Such**	**0.4 to 1 ml dilution**	**As Such**	**0.03/2**
1	1031016	2575228	957355	2527704	118335
2	1026176	2617961	957290	2515118	121022
Mean	**1028596**	**2596594.5**	**957322.5**	**2521411**	**119678.5**
S.D	3422.40	30216.79	45.96	8899.65	1900.00
RSD	**0.3327**	**1.1637**	**0.0048**	**0.3530**	**1.5876**
Conc	11.41	27.62	10.68	26.84	2.02
D.F	2.50	1.00	2.50	1.00	66.67
Final Conc (mg/ml)	**0.029**	**0.028**	**0.027**	**0.027**	**0.134**
Expected	0.25	0.25	0.25	0.25	1
% Efficiency	**11.41**	**11.05**	**10.68**	**10.74**	**13.45**

SAMPLE V	Peak Areas		
	(20mg/4ml) 50:50 1N HCl:MeOH/water Overnight		100mg/5ml 10% 1N HCl:MeOH 1.5hr
	Expt-5 (water)	**Expt-5 (water)**	**Expt-5**
	0.4 to 1 ml dil	**As Such**	**0.03ml to 2ml**
1	5155417	13010675	713517
2	5184245	13047555	710913
Mean	**5169831**	**13029115**	**712215**
S.D	20384.47	26078.10	1841.31
RSD	**0.3943**	**0.2002**	**0.2585**
Conc	54.22	135.46	8.14
D.F	2.50	1.00	66.67
Final Conc (mg/ml)	**0.136**	**0.135**	**0.543**
Expected	0.25	0.25	1
% Efficiency	**54.22**	**54.19**	**54.28**

SAMPLES VI & VII & III	Peak Areas					
	(20mg/4ml) 50:50 1N HCl (MeOH/H20)	100mg/5ml 1.5hr 10% 1N HCl:MeOH		20mg/4ml (3ml 1N HCl:water) overnight		
	Expt-7 (water)	**Expt-6**	**Expt-7**	**Expt 7**	**Expt 6**	**Expt 3**
	As Such	**1N HCl**	**1N HCl**	**As Such**	**As Such**	**As Such**
1	1328790	No Peak	717465	1300013	11046	0
2	1326994	No Peak	71572	1310817	15124	0
Mean	**1327892**	**---**	**394518.5**	**1305415**	**13085**	
S.D	1269.96	---	456715.32			
RSD	**0.0956**	**---**	**115.7652**			
Conc	14.51	---	4.86			
D.F	1.00	5.00	5.00			
Final Conc (mg/ml)	**0.015**	**---**	**0.024**	**0.009**	**0.022**	**0.002**
Expected	0.25	1	1	0.25	0.25	0
% Efficiency	**5.80**	**---**	**2.43**	**3.60**	**8.80**	**---**

E.2. HPLC Chromatographs Examples

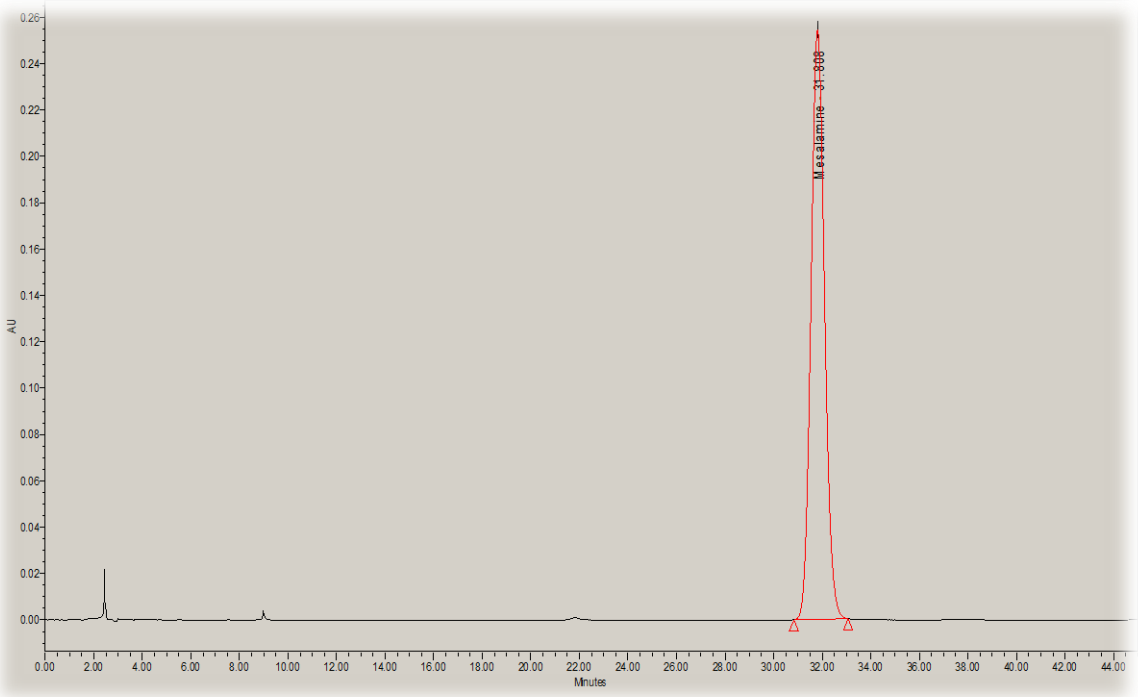

Mesalamine Standard – 100 ppm

Potential Interference Components

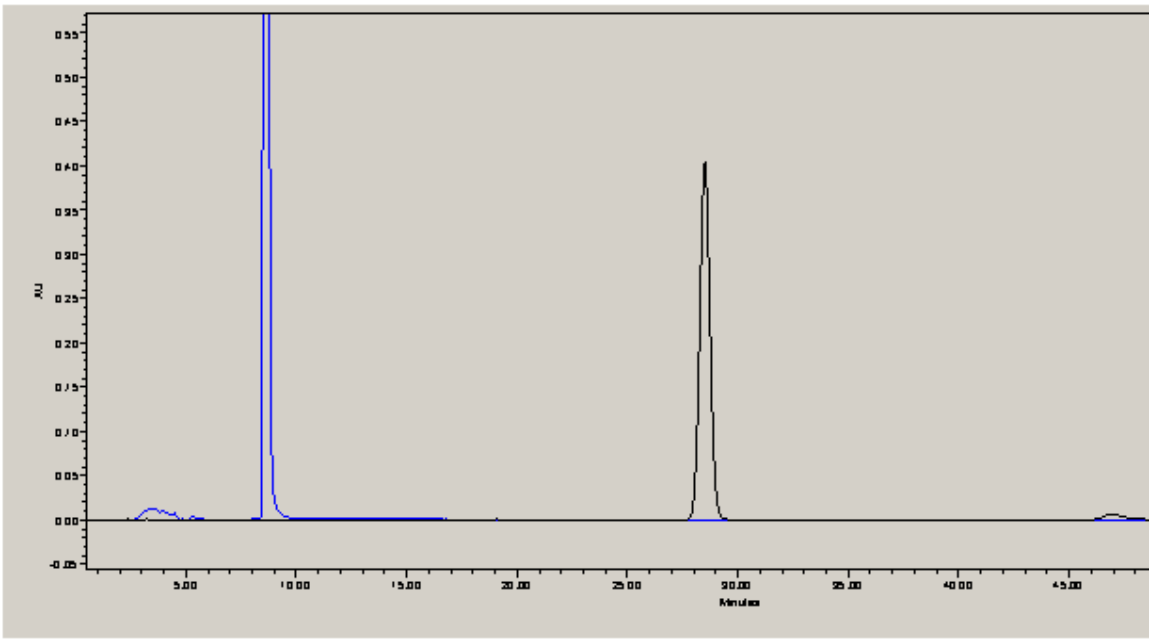

Methylbisacrylamide (MBA) + Mesalamine (black)

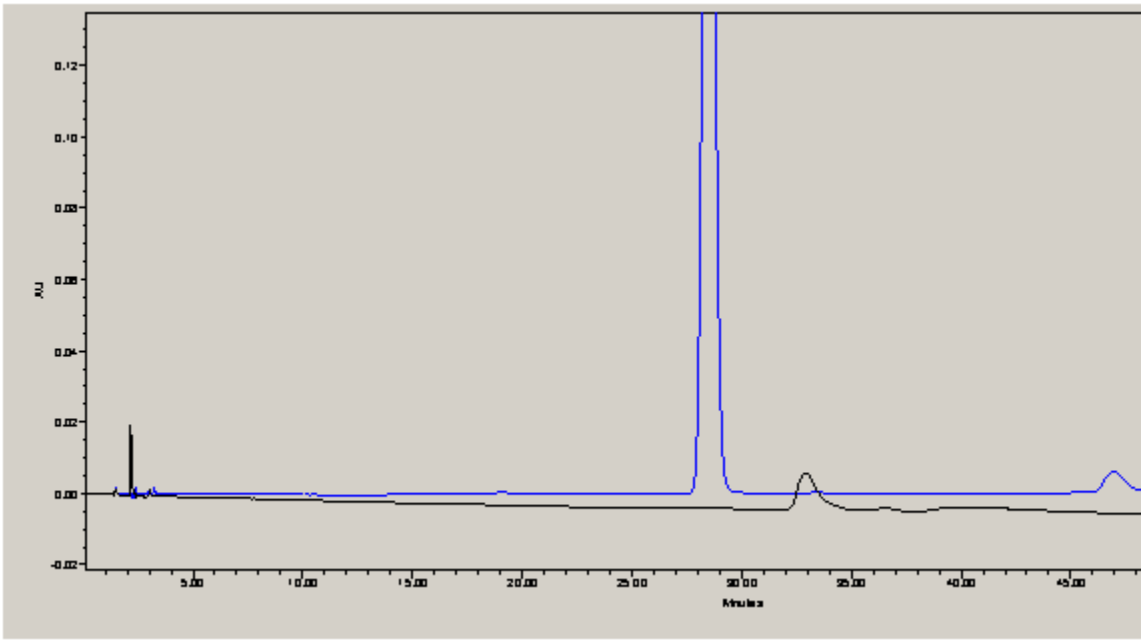

AIBN + Mesalamine (blue)

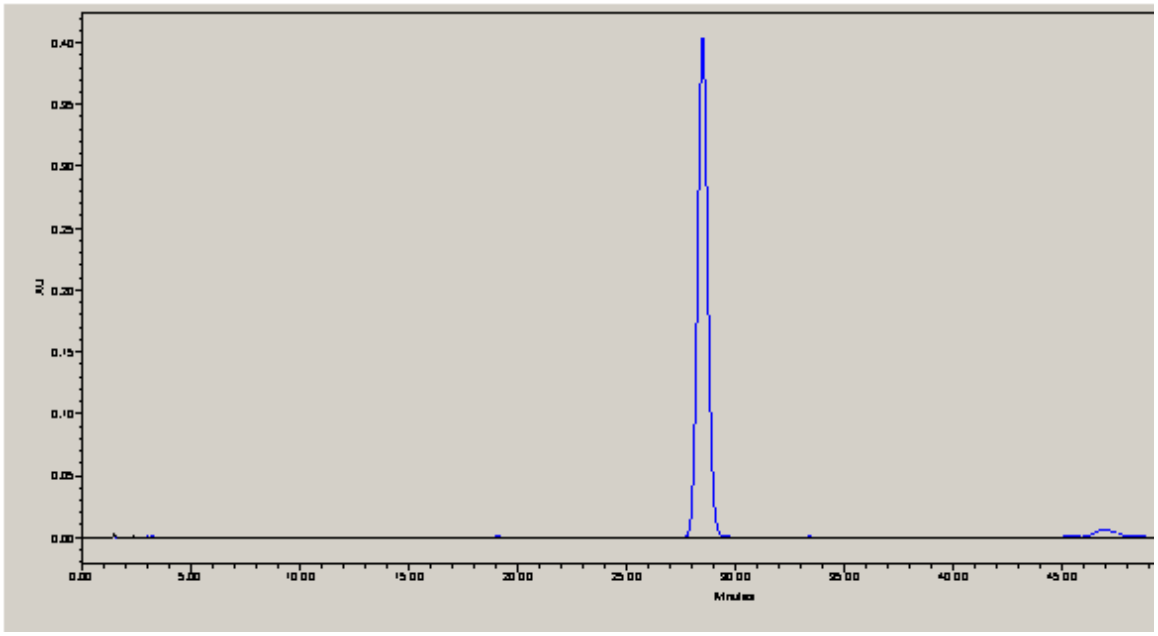

Span 80 + Mesalamine (blue)

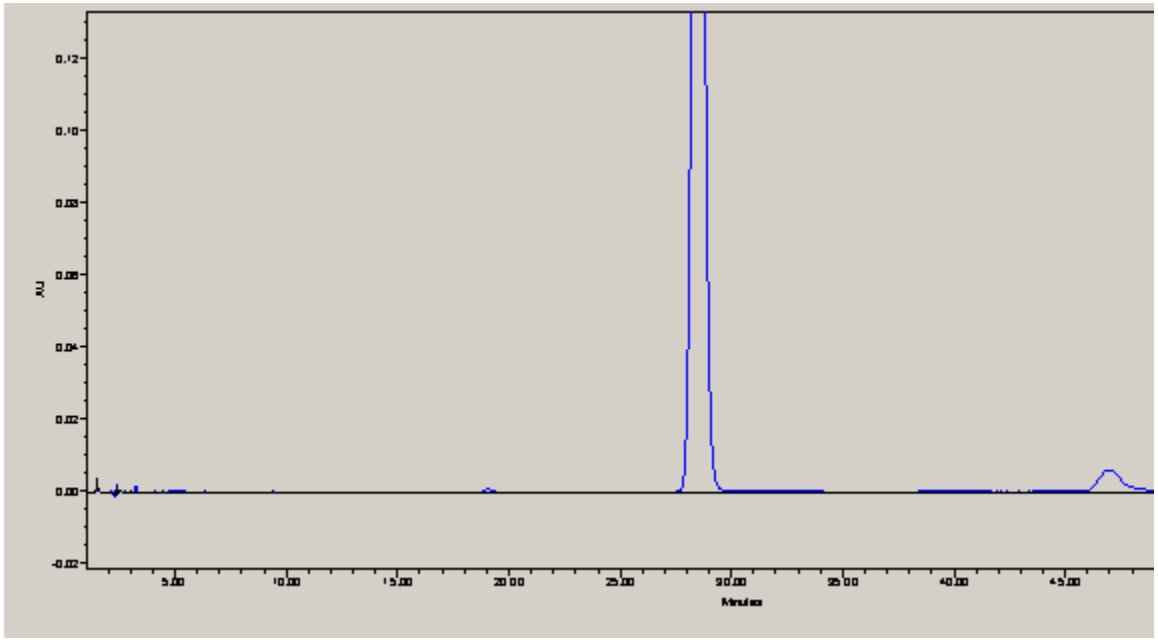

Span 80 (black) + Mesalamine (blue) (ZOOM)

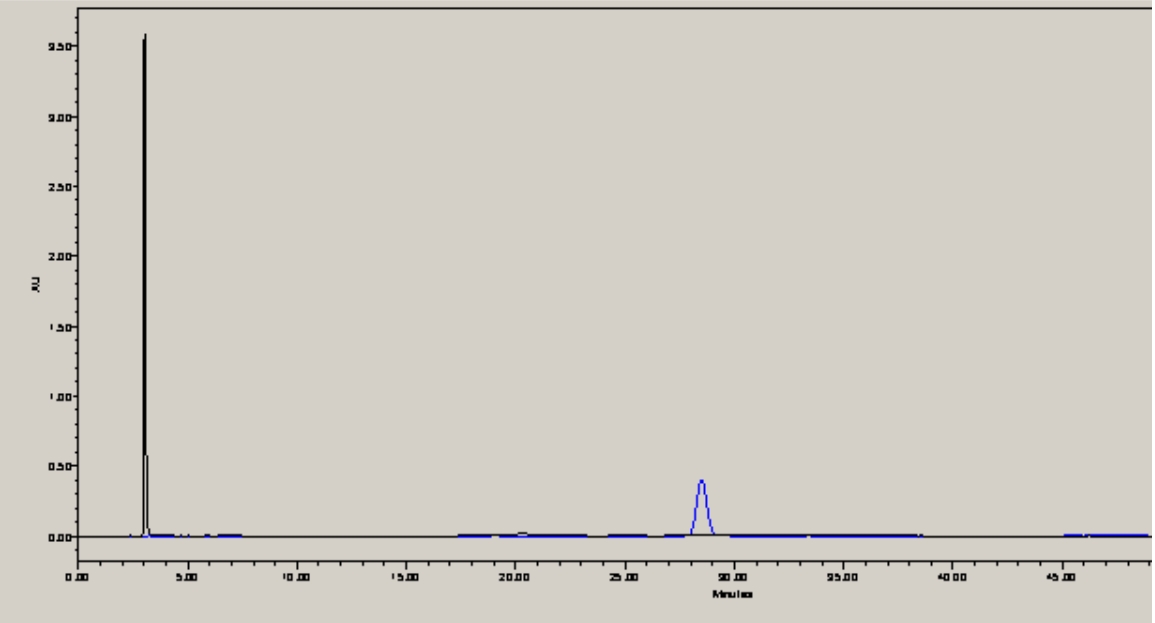

Acrylamide (black) + Mesalamine (blue)

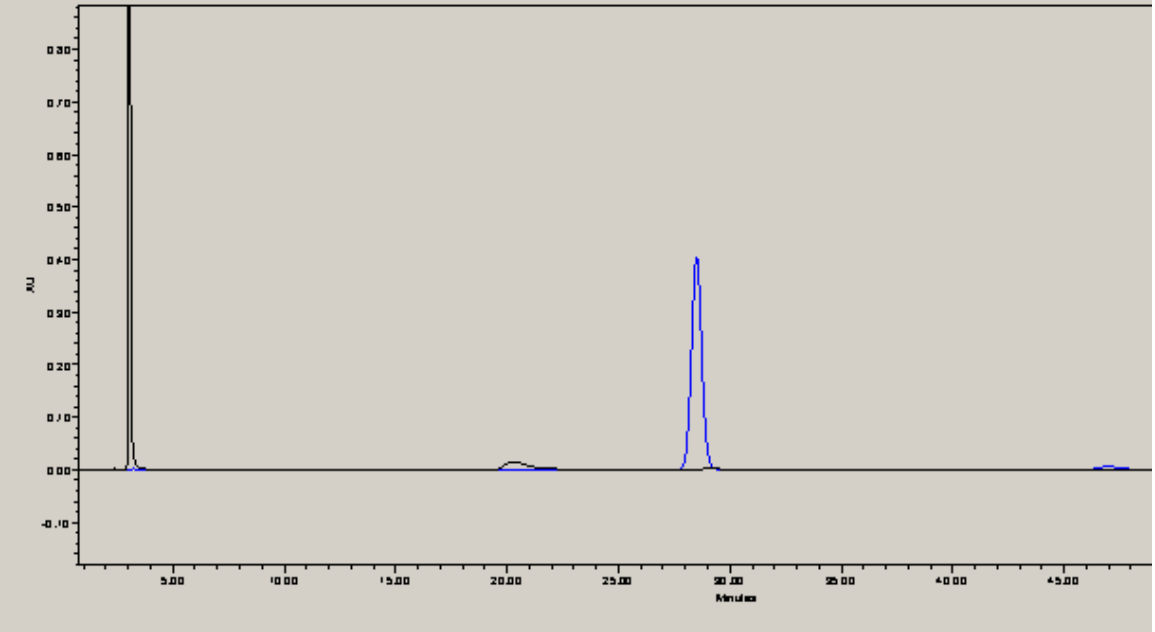

Acrylamide (black) + Mesalamine (blue) (ZOOM)

Examples of Experimental Samples

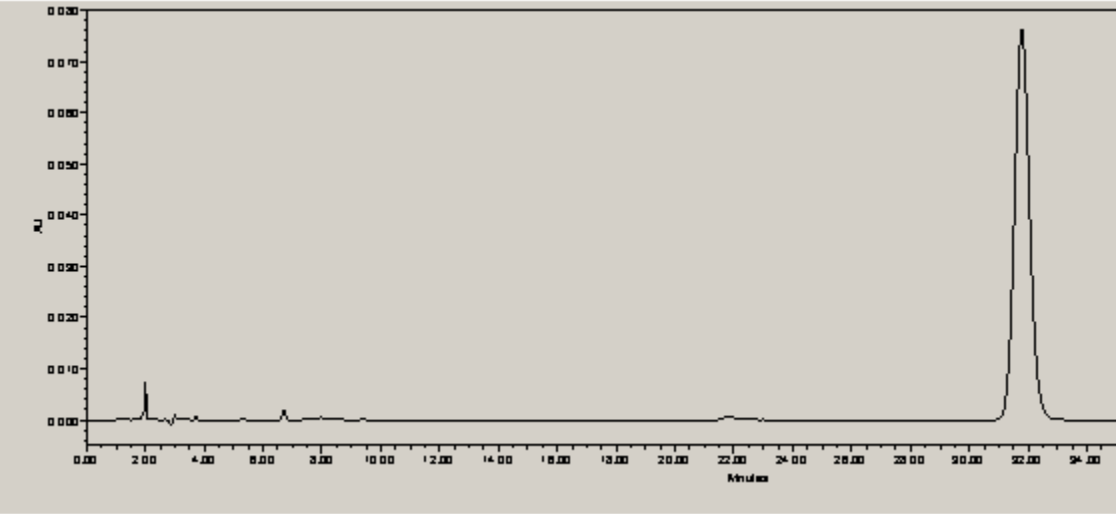

C1

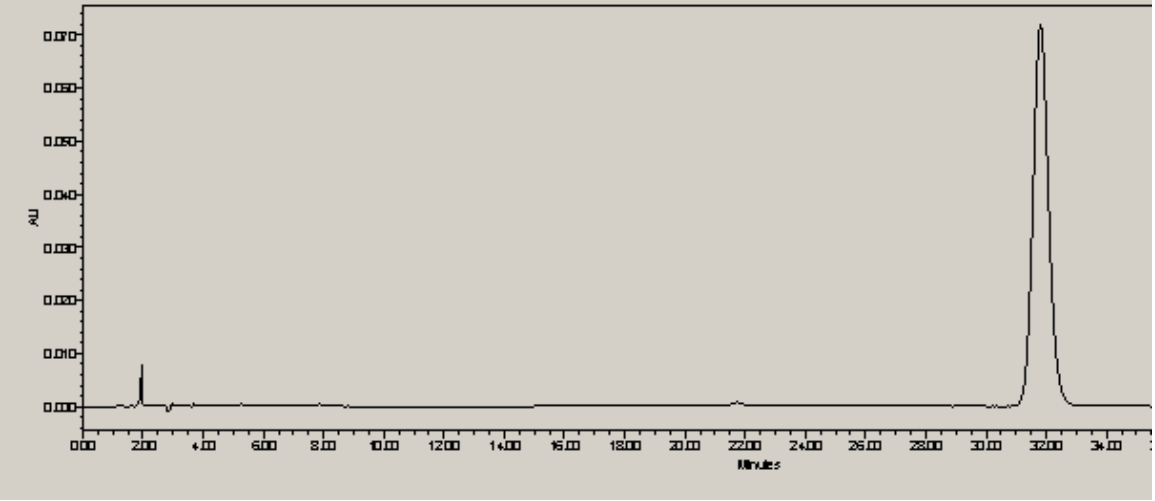

C3

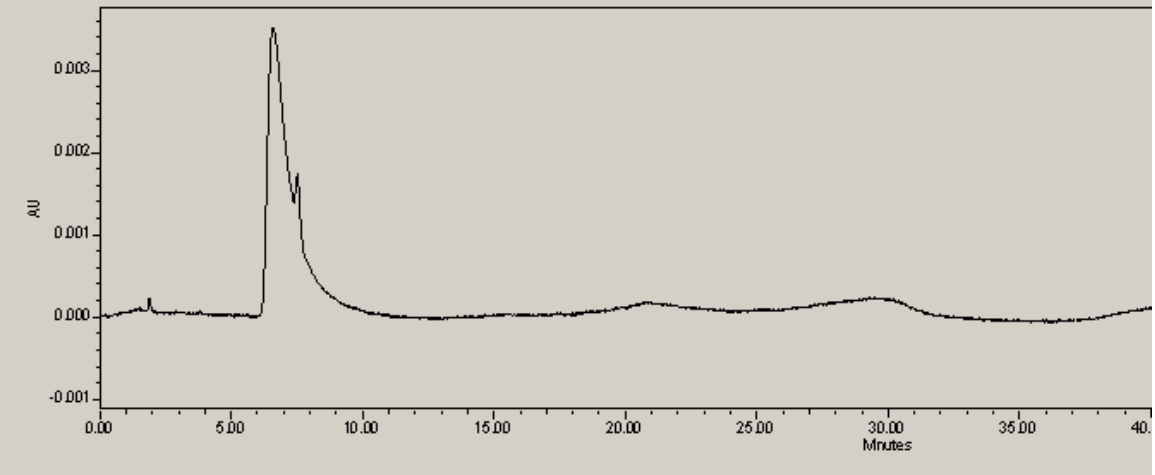

Experiment II – Polyacrylic acid

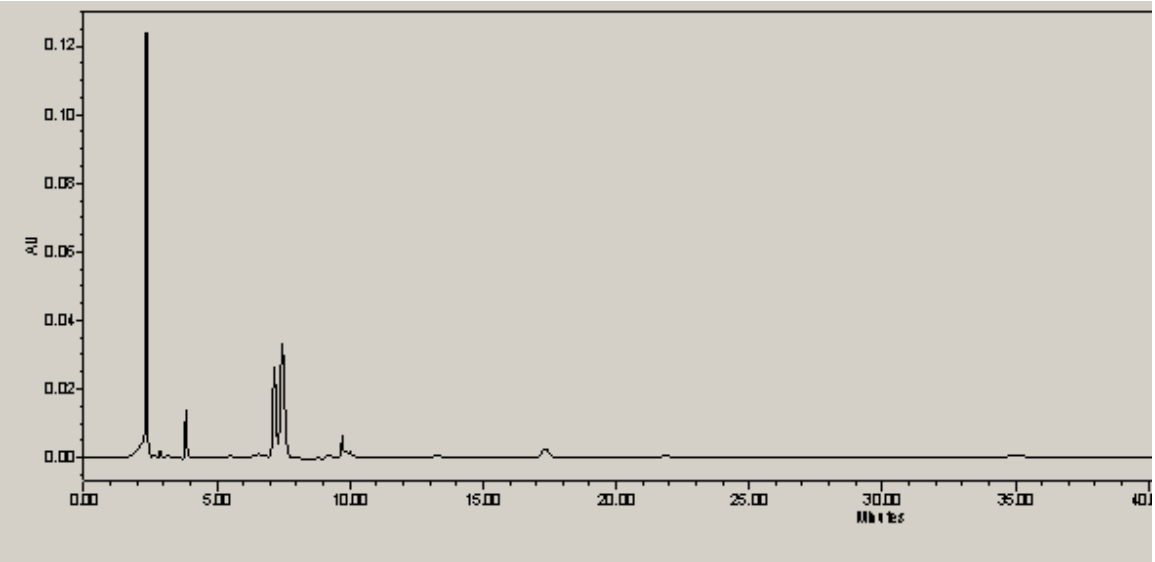

Experiment III - Copolymer

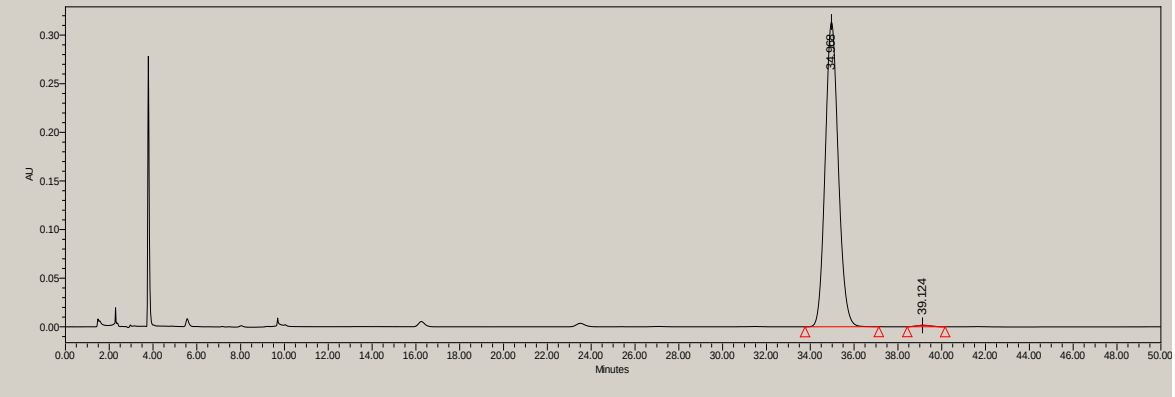

Experiment V

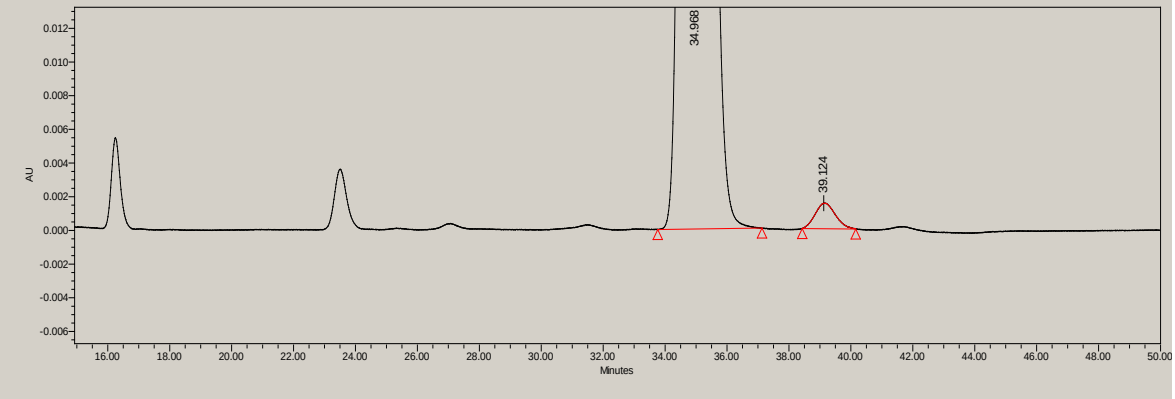

Experiment V (Zoom)

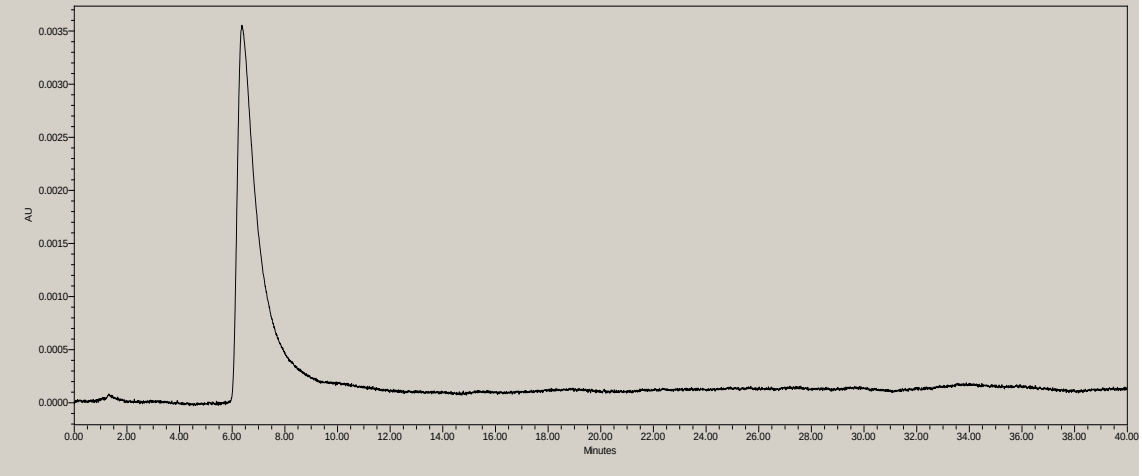

Experiment VI

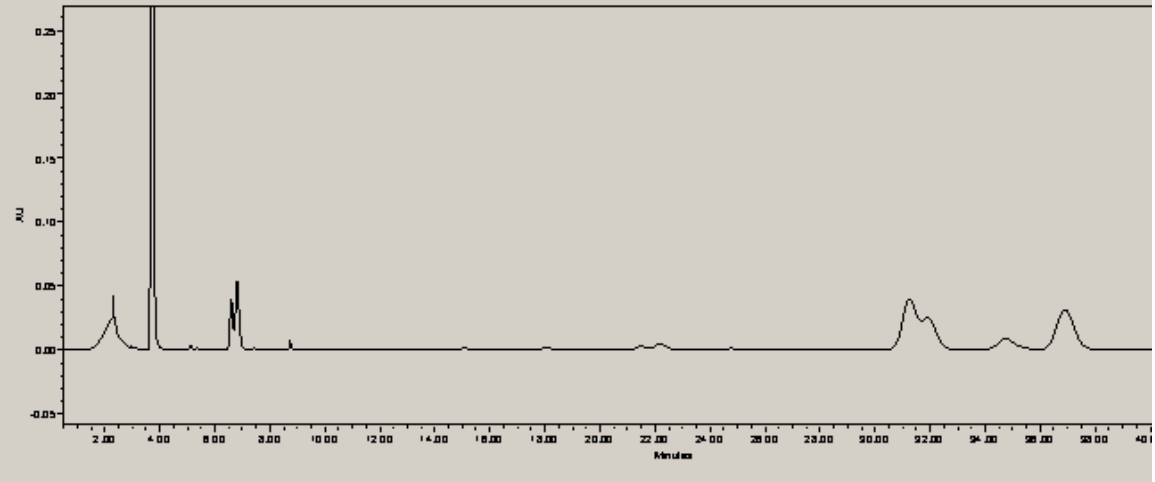

VI-C (Zoom) Copolymer-MSM

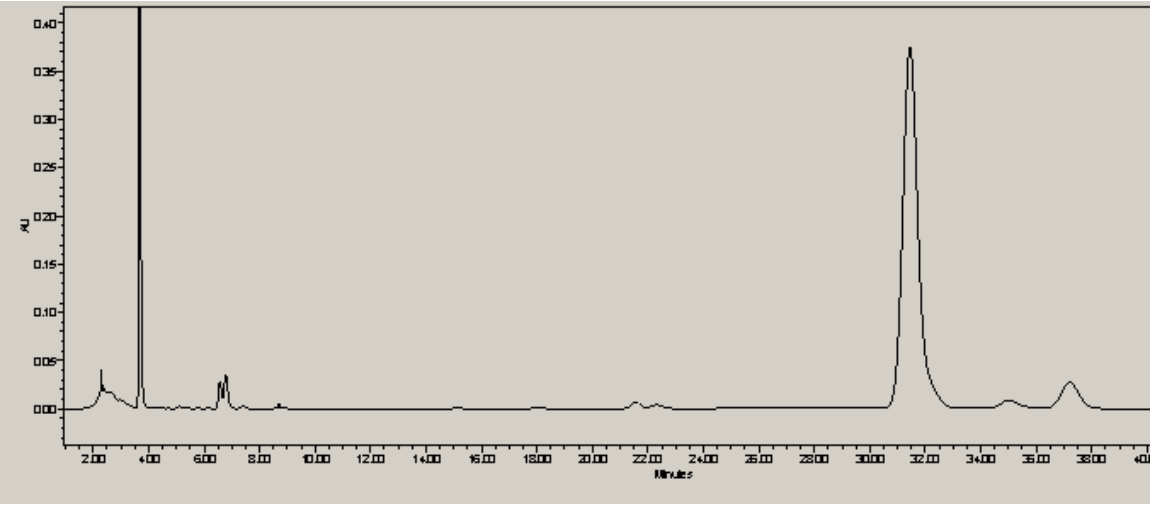

Experiment VI filter (zoom)

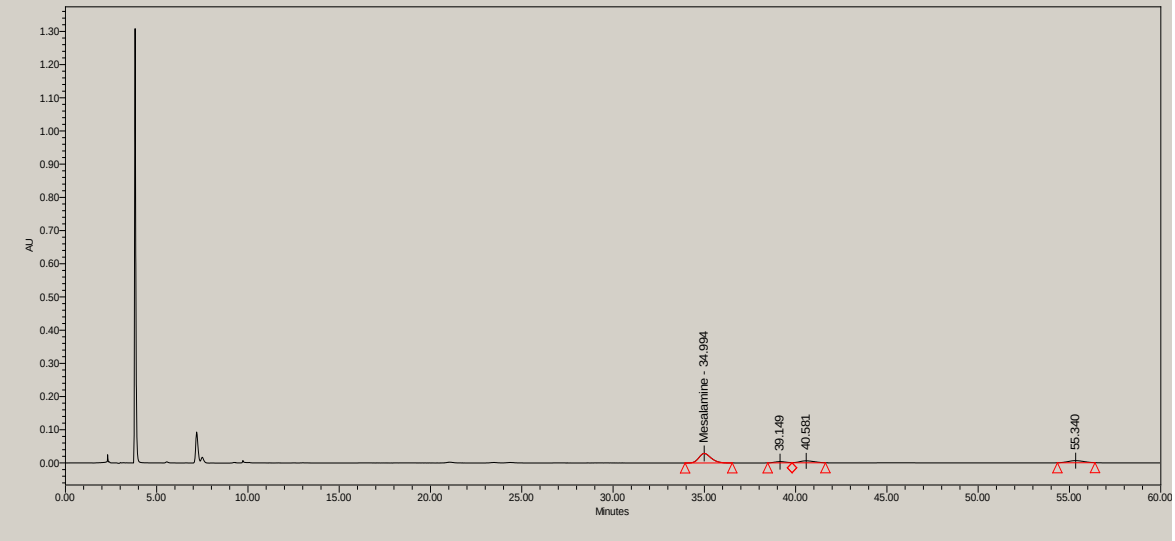

Experiment VII

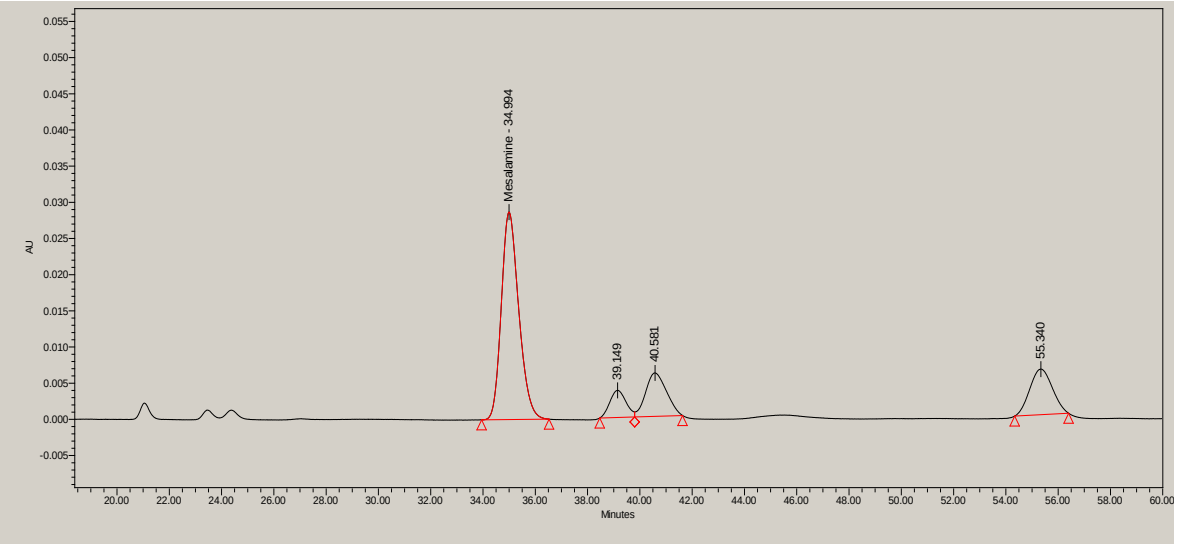

Experiment-VII (zoom)

E-3. Mesalamine Particle Calculations

NANOFLAKES		thickness	length
cylinder	nm	100	900
short cylinder SA = A flat surface + B cylinder			
A 2 circles			
r=	500	450	400
(2pi r^2) A=	1570796.3	1272345	1005310
B Cylinder	h=	100	
r=	500	450	400
(2pi*r*h) B=	314159.27	282743.3	251327.4
SA_{tot} = A + B	1884955.6	1555088	1256637
		AVG (nm^2)	**1.57E+06**
Volume	h=	100	
r=	500	450	400
(pi*h*r^2) V=	78539816	63617251	50265482
		AVG (nm^3)	**6.41E+07**

GROUND PARTICLES		width	length
	nm	225	350
2 sphere halves + cylinder			
A Sphere			
r=	112.5	110	100
(4pi r^2) A=	159043.1	152053.1	125663.7
B Cylinder		r= 112.5	
h=	125	130	150
(2pi*r*h) B=	88357.29	91891.59	106028.8
SA_{tot} = A + B	247400.4	243944.7	231692.5
		AVG (nm^2)	**2.41E+05**
Volume			
A Sphere			
r=	112.5	110	100
(4*pi*r^3)/3 A=	5964117	5575280	4188790
B Cylinder		r= 112.5	
h=	125	130	150
(pi*r^2*h) B=	4970098	5168902	5964117
V_{tot} = A + B	10934215	10744181	10152908
		AVG (nm^3)	**1.06E+07**

Appendix F. Commercial PAM – Design of Automated Grinding

An IKA® –WERKE M20 grinder with a cooling jacket and 4-edged blade was used to grind commerical polyacrylamide. Two systems were developed to chill the water pumped to the cooling jacket: a chiller finger to 15˚C and ice to 4-10˚C. A total of 15 minutes grinding time was accomplished, with 20 seconds grinding time and 60 - 90 second average rest times between each 20 second grind session. Every 5 minutes of grind time, a 5 minute break was taken to allow the grinder motor to cool and to allow for the addition of more ice.

After grinding the powder, it is transferred to a USA Standard Sieve tower with 75 µm (No. 200), 45 µm (No. 325), and 25 µm (No. 500) sieve diameters. The sieve tower was placed on a Retsch AS 200 Sieve Shaker for 50 minutes at 70% amplitude and settled for 30 minutes before collecting the powder from the different sieve trays refining the size ranges of ground polyacrylamide as <25 µm, 25-45 µm, 45-75 µm, and >75 µm. The 25-45 µm and <25 µm were used for further testing in evaluating coating applications.

In the process of coating polyacrylamide, the commercial product was ground to a size suitable for experimental usage after sieving. In this process, a water bath cooled grinder required manual activation of a button for an extended duration period. The optimized grinding series was obtained by guiding undergraduate students: Craig James Smith, Michael O'Guin, and Stacy Sommerfeld. The execution of multiple grinding sessions to supply civil engineering the hydrogel powder consists of hard work with assistance by these undergraduate students and visiting doctoral student Jin Heyang.

An automatic system to override the manual push button was developed with assistance from Brian Schweiker with time allotments for supplying energy (ON) and holding time (OFF). The adjustable designed automated system is set-up for a 2min wait time and 20s grind time and counts the number of cycles (ON/OFF) that has occurred. Currently, 15-20 cycles are executed prior to checking the temperature and adding more ice to the system. If the system is allowed to heat from excessive use, the polyacrylamide batch was deemed unusable and was not provided to civil engineering. The entire grinding session for 25-30 g PAM batches consists of 4-5 runs of the 15-20 cycles for a total

grinding time of 20-33 minutes over the course of 2.33hrs to 4 hrs not including break times for preventative machine overheating. Placement with the automated grinding system for set active grinding time and rest time is diagrammed below. Two dials establish the time duration for each active and rest period: active on the top and rest time on the bottom. Selection is determined by both the letter and dial number between minimum and maximum. Cycles are counted as one active time and one pause time. Setting used was for the active period (D, 5) and rest period (H, 8.5). Approximately 15 cycles are executed before adding more ice to the cold water bath (chiller finger broke). The forms generated to track grinding and collection of powder are also below.

Minimum time $= 15\text{cycles} \times 20\text{s} \times \frac{1\text{min}}{60\text{ s}} \times 4\text{runs} = 20\text{minutes grinding/2hrs hold time}$

Maximum time $= 20\text{cycles} \times 20\text{s} \times \frac{1\text{min}}{60\text{ s}} \times 5\text{runs} = 33\text{minutes grinding/3.33hrs hold time}$

SELECT TIME RANGE			
	MIN	MAX	units
A	0.6	2.5	sec
B	1.5	5	sec
C	2.5	10.5	sec
D	5	21	sec
E	10	42	sec
F	0.4	1.4	min
G	0.7	2.8	min
H	1.5	5.5	min
I	3	11	min
J	5.5	22.5	min
K	11	45	min
L	0.4	1.5	hr
M	0.8	3	hr
N	1.5	6	hr
O	3	12	hr
P	6	24	hr

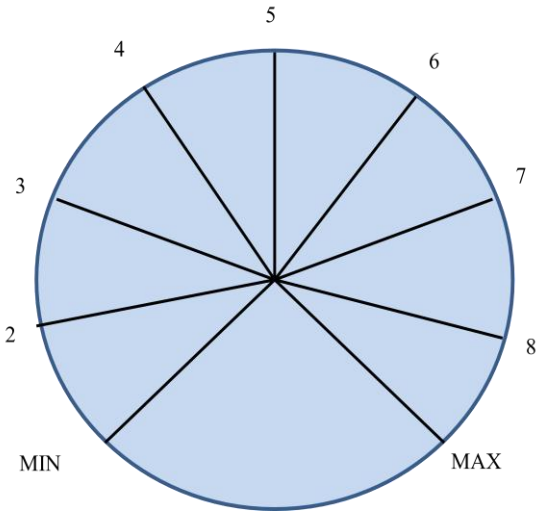

Face on the Automated Grinding Instrument

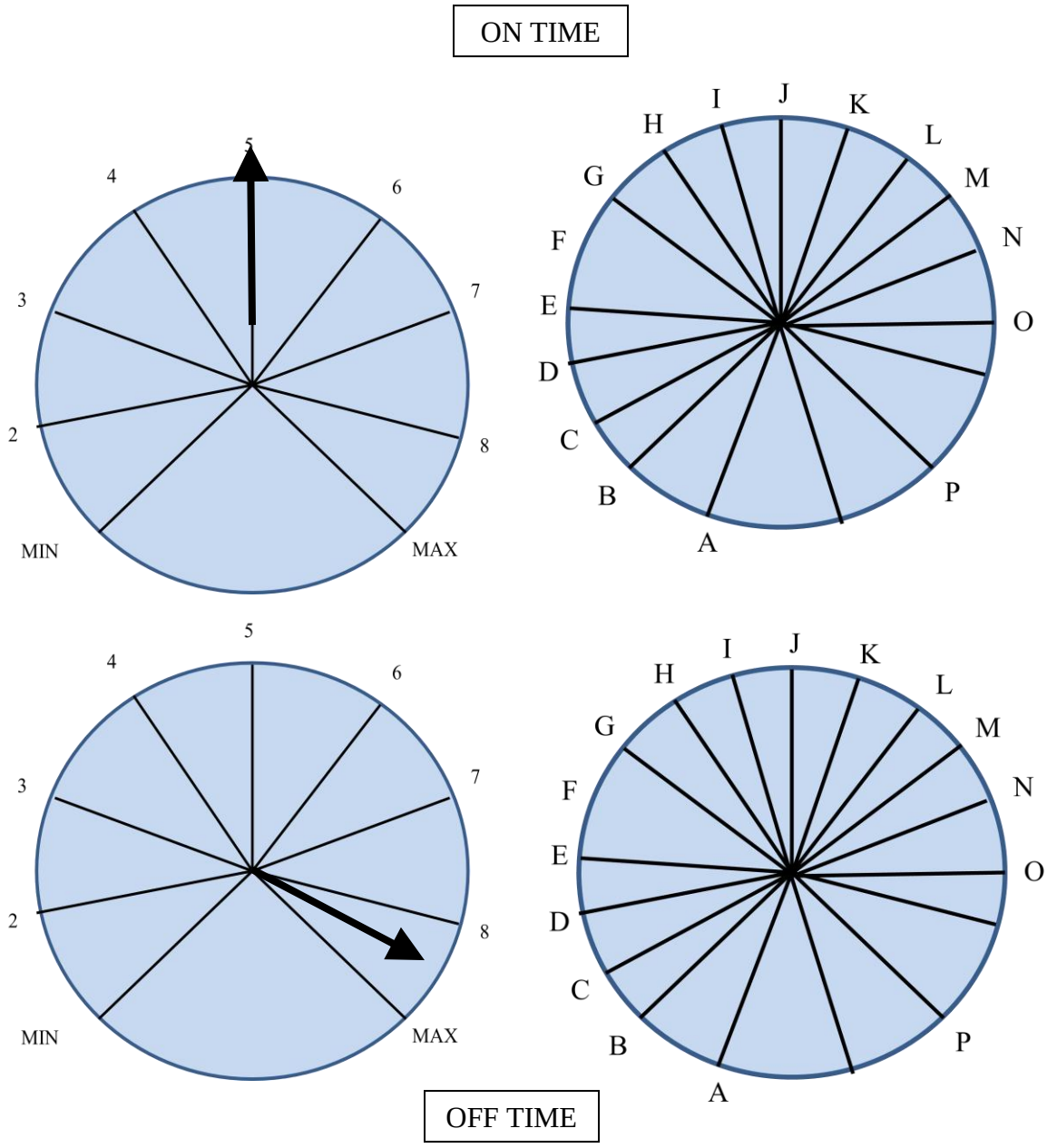

Grinder Form

Date:

Sample:

Sample Amt.:

Cooling Method:

	Grind Time	Rest Time	Water Bath Temp		Grind Time	Rest Time	Water Bath Temp
1				31			
2				32			
3				33			
4				34			
5				35			
6				36			
7				37			
8				38			
9				39			
10				40			
11				41			
12				42			
13				43			
14				44			
15				45			
	Break Time:						
16							
17					Average Grind Time:		
18					Average Rest Time:		
19					Average Temp:		
20					Total Grind Time:		
21							
22					Vial, g	Vial+Powder, g	Powder, g
23				>75			
24				25-45			
25				45-75			
26				<25			
27							
28							
29							
30							
	Break Time:						

IKA Automated Grinder Form

Date: _____

Sample Label: _____

Sample Amount (g):

1 Settings

On Time (Grinding)			Off Time			# of Cycles
Letter	Mark #	Time	Letter	Mark #	Time	

Water Bath T (˚C)

Method	Before	During Grinding	After

2

Break Time	Water Bath T (˚C)				# of Cycles
	Method	Before	During Grinding	After	

3

Break Time	Water Bath T (˚C)				# of Cycles
	Method	Before	During Grinding	After	

4

Break Time	Water Bath T (˚C)				# of Cycles
	Method	Before	During Grinding	After	

5

Break Time	Water Bath T (˚C)				# of Cycles
	Method	Before	During Grinding	After	

6

Break Time	Water Bath T (˚C)				# of Cycles
	Method	Before	During Grinding	After	

Average Temperature:
Total Grind Time:

Sieving

	Time	Amp%

Sample Collection Date:

(g)	Vial	Vial+Pow	Powder
>75			
25-45			
45-75			
<25			

Appendix G. Synopsis of PCT/US2008/009398 - Liquefaction Prevention

A sandy soil environment can be vastly simplified to be composed of mixed sand and water. As an earthquake progresses and shakes, this once homogenous mixture begins to separate as the water in between the sand particles mobilize. This effect is defined as liquefaction, or in chemical engineering terms, fluidization of the soil, and concrete blocks are not well supported on water. Liquefaction results in large ground displacements. If this occurs underneath buildings, large loss of property and potentially even life can occur from liquefaction. Liquefaction typically occurs within minutes after the initial major shock wave; many people standing in doorways feeling relief of surviving are shocked when the foundation of their building starts to collapse or sink. The liquefaction effect is well documented and well-known in civil engineering. For example, the 1971 San Fernando, CA, earthquake caused liquefaction failure of the San Fernando Dam was analyzed by many resulting in information and design procedures for predicting liquefaction susceptibility (Seed 1975; Seed and Idriss 1982; Mitchell 1995; Ming and Li 2003).

Several remediation procedures proposed and executed for high liquefaction susceptibility sites are discussed by Mitchell et al. (1995; 1998). Current remediation efforts mostly consist of treating the soil *before* construction or treating soil outside the building footprint after construction. Applicable areas are those prone to liquefaction include loose, sandy saturated soils including where seismic activity occurs. Higher prone areas are near fault lines and plates tectonic junctures, typically near coastal regions, such as the western coasts of the Americas. Application in earthen or embankment dams is also potential of this proposed technology. A safe method to treat liquefiable soil underneath existing buildings is needed to immobilize the water around the sand particles by hydration of hydrogels (Elton and Gupta).

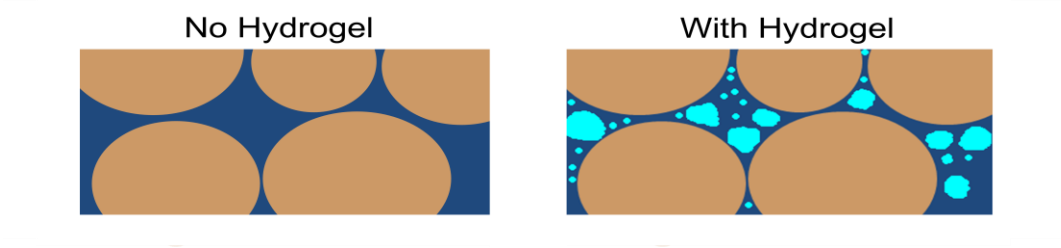

Figure G-1 Diagram of hydrated sand (L) no hydrogel and (R) with hydrogel in the pores.

Hydrogels hydrate in the presence of water to form a gel. The total volume of hydrogel and water remains similar to the original volume as to not affect the foundation of existing buildings. This hydration of hydrogel immobilizes the sand particles. For transport of the hydrogel nanoparticles into existing soil, the polyacrylamide must be protected initially from the water content to prevent hydration. In this state, the crosslinked hydrogel will also be the smallest as a dry powder. Producing and protecting the hydrogel nanoparticles with a coating is a critical step to this project and is discussed in Chapter 2 for production of the hydrogel nanoparticles and in Chapter 5 for coating hydrogel.

Two encapsulation designs can be employed to produce a new microparticle with a nanoscale protective "time-release" coating to stabilize groundwater. This coating should prevent premature hydrogel hydration during installation. Either a group of hydrogel molecules or singular nanoparticles are encapsulated by a layer of hydrophobic polymer. Once the particles have been transported into the voids of the soil, the coating must degrade, exposing the hydrogel to the pore water for hydration. Coating thickness and material are varied to adjust the degradation time. From this basis, adjustments should be made for the required time for installation.

Particle settling velocity, *v*, is given by Stokes' law

$$v = \frac{d^2 g(\rho_s - \rho_l)}{18\mu_1} \quad \text{(Eq. 5.1)}$$

as where, *g* is gravitational acceleration (9.8 m/s^2 at sea level), ρ_l is liquid density (997 kg/m^3 for water), μ_l is dynamic viscosity (0.00089 Pa-s for water). Settling velocities for various particle diameters (*d*), are shown in Table G for hydrogel (solid density, ρ_s, 1700 kg/m^3) and shows displacements for particles of varying sizes in water at 15°C (typical groundwater temperature). Thermal (Brownian) fluctuations resist particle settlement. According to Einstein's fluctuation dissipation theory, average Brownian displacement *x* in time *t* is

$$x = \sqrt{\frac{2k_B T t}{\pi \mu d}} \quad \text{(Eq. 5.2)}$$

where, k_B is Boltzman's constant (1.38×10 J K), and *T* is temperature in Kelvin. Table G shows displacements for particles of varying sizes in water at 15°C (typical groundwater temperature). The Brownian displacement of 1000 nanometer-size particles in water is 1,687 nm/s, which is more than the settling velocity of 430 nm/s. Hence, these particles are too small to settle by themselves and are not likely to float merely due to Brownian motion. This imparts an important property to small particles: they can be easily kept suspended in groundwater at any solid density. So, for this work, the target particle size will be kept at 1000 nanometers, or lower, so that density matching of solids to groundwater is not a concern. The particles will stay where they are placed, suspended in the water.

Table 4. Particle settling velocities and Brownian displacement

Particle diameter (nm)	Settling velocity (nanometer/second)	Brownian displacement (nanometers) in 1 second
1	0.00043	53,332
10	0.043	16,865
100	4.30	5,332
1,000	430	1,687
10,000	43005	533

Table G. Particle settling velocities and Brownian displacement (Elton and Gupta).

Appendix H. Chapter 5 Coating Hydrogel Supplements

H.1 Annealing of polymers (PLA, PSF, PVAc)

Drops of polymer solutions previously mentioned were air dried on microscope slides, viewed, placed in oven at varying temperatures (65˚C, 85˚C, 100˚C) for three hours to see if the polymers changed morphology. The idea behind this is to minimize or even eliminate pores that water has been able to penetrate through to the hydrogel. Once some water reaches the hydrogel and initiates swelling, the shell-coating is displaced and rapid increase in hydration. Polyvinyl acetate remained a clear film regardless of annealing. No visible detection was visible on the microscope except for PSF at 100˚C for 3 hours. This incorporated with the polyacrylamide nanoparticles would most likely yield a bigger clump of PSF with nanoparticles within unless suspension while heating was achieved.

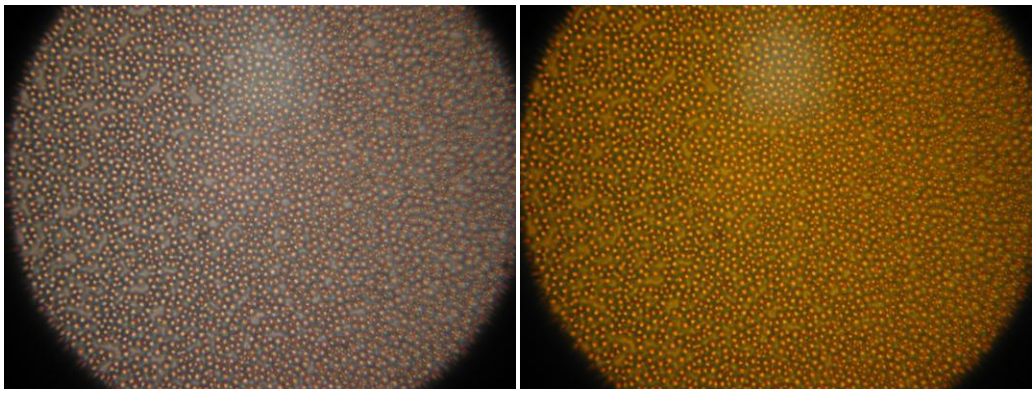

Figure H-1. PLA (not annealed) - Magnification:40X10

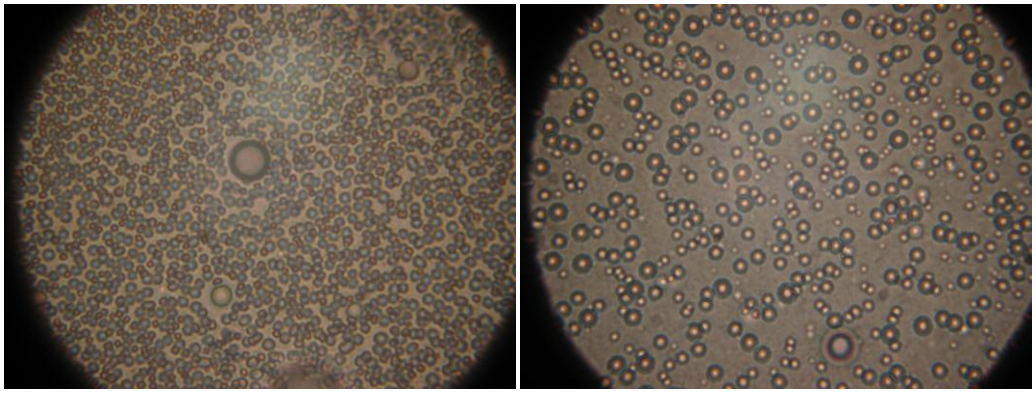

Figure H-2. PLA 1&2 annealed at a)65°C and b)85°C - Magnification:100X10

Figure H-3. PLA annealed at a) 85°C b) 100˚C Magnification:100X10

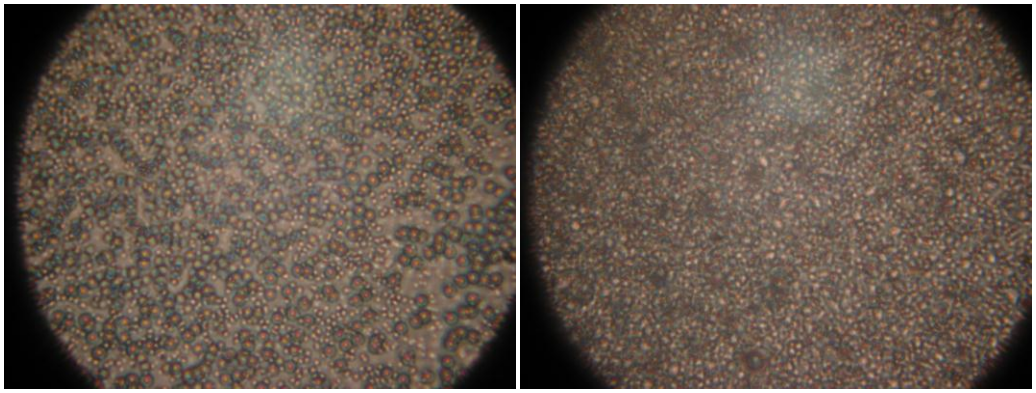

Figure H-4. Polysulfone (PSF) (annealed at a) 65°C and b) 85°C - Magnification:100X10

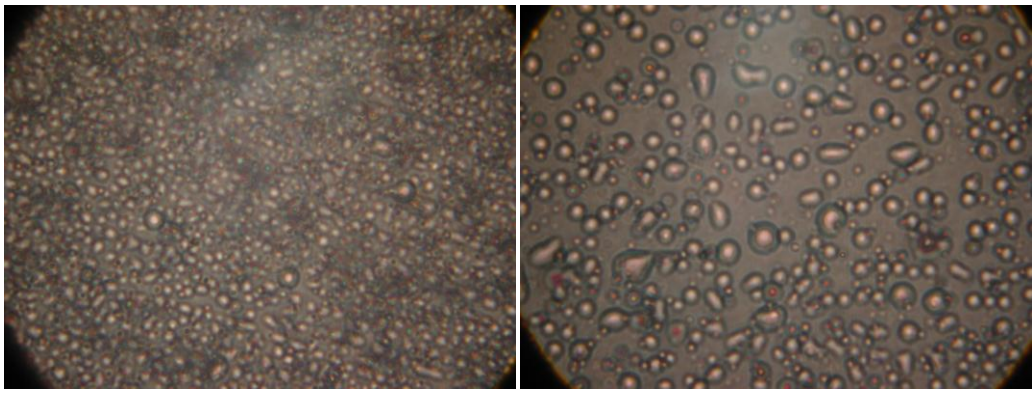

Figure H-5. PSF annealed at a)85°C b)100˚C - Magnification:100X10

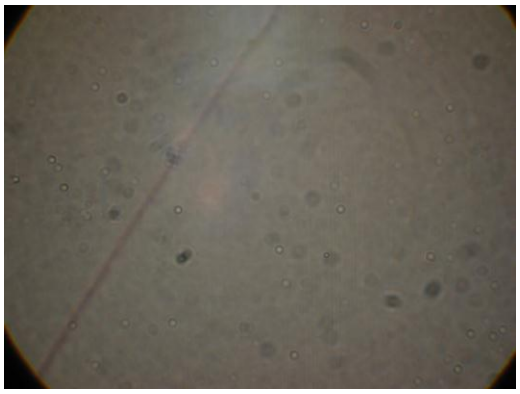

Figure H-6: PVAc 3 (edge) annealed at 100˚C Magnification:100X10

H.2 Refractometer

Using a Fisher Scientific refractometer, the index of refraction was considered a potential tool for coating analysis. This method was considered as only 1 µl of sample is required. Hydrated hydrogel with water does not have a different index of refraction than water 1.333 with an accuracy ±0.002 units.

H.3 Coating Thickness

Effective coating thickness for coverage of particles needs to be estimated to help optimize using the following equation:

$$Mass\ ratio\ (core{:}\ shell) = \frac{\rho_{core}}{\rho_{shell}} \times \frac{1}{\left(\frac{r_o}{r_i}\right)^3 - 1}$$

which utilizes the mass ratio of core and shell material, the density of core particle ρ_{core}, density of shell material ρ_{shell}, average particle size r_{o}, and the coating thickness r_{i}. This calculation was utilized to estimate the target thickness produced and the amount of injected coating solution required in milliliters, or the average thickness generated by the milliliters of coating solution injected. All injected amounts were lower than the required quantities to achieve a thickness of 5 µm for a 25 µm particle. A 1 to 3 ratio (PVAc:PAM) and was the highest core-shell utilized in SAS-EM coating.

H.4 Hydrophilic-Lipophilic Balance

The Hydrophilic-Lipophilic Balance (HLB) is commonly used to measure surfactant tendency to water or lipophile and predicts properties as a surfactant. Samples that are very lipophilic will have a 0 and those that are hydrophilic have a 20 on this arbitrary scale. This number can be determined by a variety of methods.

Appendix I. Supplementary Supercritical Carbon Dioxide Technologies

I.1 Supercritical Fluid Chromatography

The development and research in supercritical fluids has drastically increased as evident by the numerous publication journals produced in the last 20 years (Kiran 2009). Supercritical technology chromatography (SFC) has also started to penetrate the chromatography industry, replacing the organic solvents commonly used to make the process more environmentally friendly, or "green". Supercritical carbon dioxide is also being utilized for supercritical fluid chromatography replacing the more commonly used organic solvents. This application of SCF gained momentum due to shortages of acetonitrile due to the cascading effect of gasoline and crude oil shortages of the previous decade.

I.2 Supercritical Fluid Fractionation

Supercritical fluid fractionation (SFF) based on the highly selective nature of the supercritical fluid has uses in polymer fractionation, polyunsaturated fatty acids, pollution abatement, etc. Supercritical fluid can also be used to impregnate a compound that is soluble in the supercritical fluid into porous materials, such as deacidification and reinforcements in books, loading drugs into medical devices or patches, and aromas in food products (Perrut 2000). Multiple chemical reactions can also be executed in supercritical fluid media foregoing the volatile organic solvents (VOCs). Particle and extraction supercritical technologies are discussed in following sections.

I.3 Supercritical Fluid Extraction

Supercritical fluid extraction was the first large scale application of supercritical technology, for example the German food industry in the 1980s. Most notably was the encouragement in research and development of natural products (Stahl 1987; King and Bott 1993). The United States, France, and Italy picked up the technology in the following two decades. At the turn of the century Asia, supercritical technology utilization in industry was growing with phytopharmaceuticals preparation in Korea and

China and spices and aromas (Señoráns 2003) extractions in India. (Rizvi 1994; Reverchon 1997)

In industry, the carbon dioxide stream is commonly cycled back through after separation of the extractant. The inlet stream is fed into a high pressure extractor and the soluble compound dissolves in supercritical carbon dioxide. Then pressure is reduced by a reduction valve and sent into a low pressure separator. Here, as pressure decreases the extracted compound from the carbon dioxide stream precipitates as a change in density precipitates the extract as solubility is lowered. The extract is collected as the carbon dioxide is recycled and repressurized back into the high pressure extractor.

Typical extracted natural compounds include fragrances and spices as seen in Figure 1.2 below, and percent yields from supercritical CO_2 are on average at least double the extraction of steam distillation. The benefits of utilizing carbon dioxide include an oxygen-free system preventing oxidation of the extracts, minimal thermal degradation from low operation temperature, asceptic extracts as microbes and spores are not soluble, organic solvent-free extraction as CO_2 is gas at ambient temperature. (Gupta 2005) Extraction of carotenoids and phytochemical separation from microalgae produces good yields (Valderrama 2003). Sometimes simple slight depressurization to adjust the density will greatly affect the solubility allowing the extractant to precipitate adding greater ease for separation.

A more commonly recognized application of supercritical carbon dioxide extraction is decaffeinating coffee beans through extraction. Hops resins extractions and decaffeination of coffee were the first industrial processes of supercritical fluids in Germany. A typical coffee bean decaffeination process, primarily performed on black tea or coffee beans, consists of wet coffee beans introduce into a high pressure separator, then carbon dioxide is counter-currently flowed to extract the caffeine. Carbon dioxide and caffeine are then separated with water in an absorber; this water is commonly the base for caffeinated beverages (e.g. colas).

Natural Substance	Steam distillation (% yield)	Supercritical CO_2 (% yield)
Aniseed	2.1-2.8	7
Carrot	0.2-0.5	3.3
Cumin	2.3-3.6	14
Ginger	1.5-3.0	4.6
Garlic	0.06-0.4	4.6
Oregano	3-4	5
Pepper	1.0-2.6	8-18
Rosemary	0.5-1.1	7.5
Sage	0.5-1.1	1.0

Table I-1. Comparison of % yields of fragrance and flavor extracts of natural products (Moyler 1994; Mukhopadhyay 2000; Gupta 2005)

Economics are of utmost consideration after proving laboratory scale success when advancing to scale-up of a supercritical fluid system. Perrut (2000) developed equation 1.2 correlates unit price and system parameters to a logarithmic relation based on his expertise of numerous pilot- and industrial-scale SFE/SFF, online SFE/impregnation (SFI), and particle atomization (PA) units: $PI = A(10V_T Q)^{0.24}$ with a dimensionless price index *PI*, solvent flow *Q*, column volume V_T, and a constant *A*. The column volume is directly related to total extractors. This equation applies for a large range of facilities types from the bench scale (0.5-L autoclave) to the industrial scale (500-L autoclave), underestimates the smaller bench scale equipment (0.2-L autoclave) process costs, and overestimates the industrial scale units, like those mentioned earlier for hops or coffee extractions. However, some special process design systems that can affect the overall cost in either positive or negative aspects, for example SFE and impregnation system for good manufacturing practices (GMP) in adherence to Food and Drug Administration (FDA) standards can increase costs. Innovative design systems that are also cost effective are a valuable asset of this industry (Perrut 2000).

I.4 Polymerizations in Supercritical Fluid

Polymerization technology has combined with supercritical fluid processing. Inverse emulsion polymerization of acrylamide in supercritical ethane and propane mixture was carried out at 65°C (Beckman and Smith 1990; Beckman and Smith 1990). Polymerization of polyacrylamide was successful in supercritical carbon dioxide with a synthetic fluoro-surfactant (Adamsky and Beckman 1994) and sodium bis(2-ethylhexyl) sulfosuccinate (Ohde 2007). Consani and Smith (1990) demonstrate that conventional alkyl-functional ionic surfactants have poor solubility in $scCO_2$, and nonionic ethoxylated alcohol surfactants have high solubility in $scCO_2$ but their water uptake was appreciably low and capability of supporting acrylamide emulsion polymerization poor (Beckman and Smith 1990). Supercritical carbon dioxide commonly involves fluoro-compounds as suspension media for polymerizations of fluoromonomers (Quintero-Ortega 2007) and highly coagulated particles with issues of steric stabilization (O'Neill 1998).

I.5 Nanoparticle Formation with Supercritical Carbon Dioxide

A solute's solubility in supercritical fluid carbon dioxide can aide in selecting which supercritical technique, antisolvent (discussed in Chapters 1 & 3) or solvent, to produce micronized or nanosized particles. Drug solubility can be related to CO_2 density by the temperature and pressure. Three important factors regulate drug solubility in supercritical CO_2: the vapor pressure of drug, drug–CO_2 interaction, and density of CO_2. (Gupta and Kompella 2006) Drug vapor pressure is a function of temperature (*T*), and CO_2 density is a function of pressure (*P*) and temperature (*T*), Mendez–Santiago and Teja (1999) observed that the solubility (y_2 mmol/mol CO_2) can be estimated using this in the following equation:

$$y_2 = \frac{10^6}{P} \exp\left(\frac{A}{T} + \frac{B\rho_1}{T} + C\right) \qquad \text{(Eq. 1.3)}$$

where *P* is in bars, *T* is in Kelvin, ρ_1 is CO_2 density in moles per milliliter. Constants *A*, *B*, and *C* can be found in Table 1.3 for a few compounds (Gupta and Kompella 2006).

An extensive collection of solubilities of compounds can be located in the book Solubility in Supercritical Carbon Dioxide (Gupta and Shim 2007).

Drug	***A***	***B***	***C***
Biphenyl	-10,200	132,800	25.75
Capsaicin	-7,172	70,830	19.54
D(-)-Fructose	-871.2	10,740	-4.29
D(+)-Glucose	847.1	2,471	-9.12
Ketoprofen	-12,090	157,500	24.72
Naproxen	-9,723	122,900	18.11
1-Octanedecanol	-17,290	141,000	45.32
Penicillin V	-6,459	73,730	13.29
Piroxicam	-10,560	18,130	17.57
Progesterone	-12,090	21,040	23.43
t-Retinol	-8,717	168,900	16.60
Testosterone	-14,330	238,300	26.42
Theophyline	-6,957	94	760
Vanillin	-7,334	136,500	14.53

Table I-2. Values for constants of Mendez-Santiago & Teja solubility equation. (Gupta and Kompella 2006)

Rapid expansion of supercritical solution/suspensions (RESS) has been employed for particle formation of organic substances, especially polymers and polymer–drug composites (Tom 1993; Jung and Perrut 2001; Thakur and Gupta 2005). In RESS, supercritical fluid passes through a chamber, dissolves the component, and then is rapid depressurized in another chamber forming particles. Although RESS utilizes no organic solvents, RESS is restricted to low polarity compounds. In the processes of RESOLV and RESAS, a supercritical solution that has a dissolved desired component is sprayed

into a liquid solvent (RESOLV) or aqueous solution containing stabilizers (RESAS) for prevention of growth and stabilization of particles.

To prevent low solubility and growth by coagulation in RESS, a solid cosolvent, such as menthol, can be added in rapid expansion of supercritical solution with solid cosolvent (RESS-SC) (Figure 1.7) (Thakur and Gupta 2005). The solid is removed by a lyophilization step carried out separately after expansion from the nozzle. Examples of solid cosolvents are those that are solid at the exit nozzle conditions but easily sublime in lyophilization, such as menthol. For successful RESS and RESS-SC, the drug needs good solubility in supercritical CO_2, ($scCO_2$), solid at nozzle exit condition (5–30˚C), good vapor pressure for easy removal by sublimation, should be nonreactive with drugs or CO_2, and inexpensive (Thakur and Gupta 2005; Gupta 2006).

I.6 Nanoparticles formed from Supercritical Antisolvent Method

Drug nanoparticles not involving hydrogels were produced using the Supercritical Anti-Solvent (SAS) process. Drug solutions were injected into supercritical CO_2, rapidly extracting the solvent, and causing the drug to precipitate as nanoparticles. An additional CO_2 was used to flush the high pressure vessel to remove solvent. The high pressure vessel is slowly depressurized, and drug nanoparticles are collected. Drug solutions has varying solvents and concentrations: insulin (9.82 mg/ml concentration) in dimethylsulfoxide (DMSO), ampicillin (1.6 mg/ml) in methanol-acetone (1:2 by volume), and drugs with acetate bases Drug-1 (20 mg/ml) & Drug-2 (8.75 mg/ml) in methanol. Scanning electron micrographs of the SAS produced drug nanoparticles are shown below.

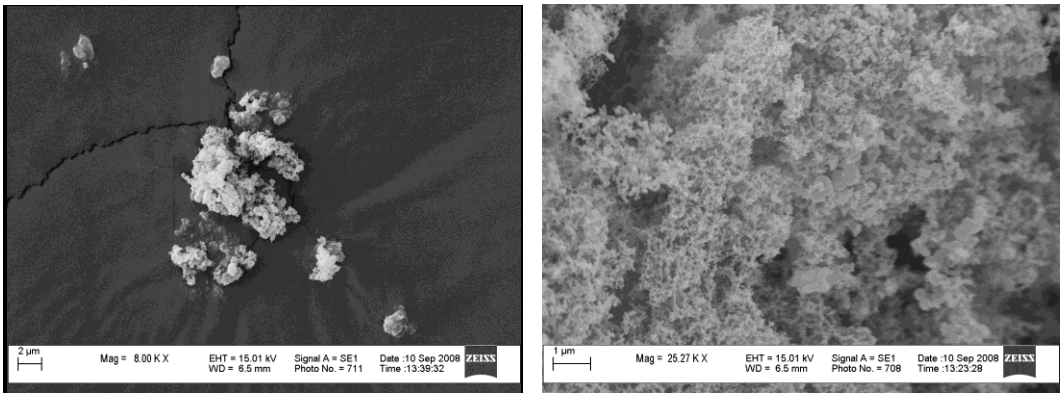

Figure I-1. Ampicillin (left) and Insulin (right) Nanoparticles produced through supercritical antisolvent process.

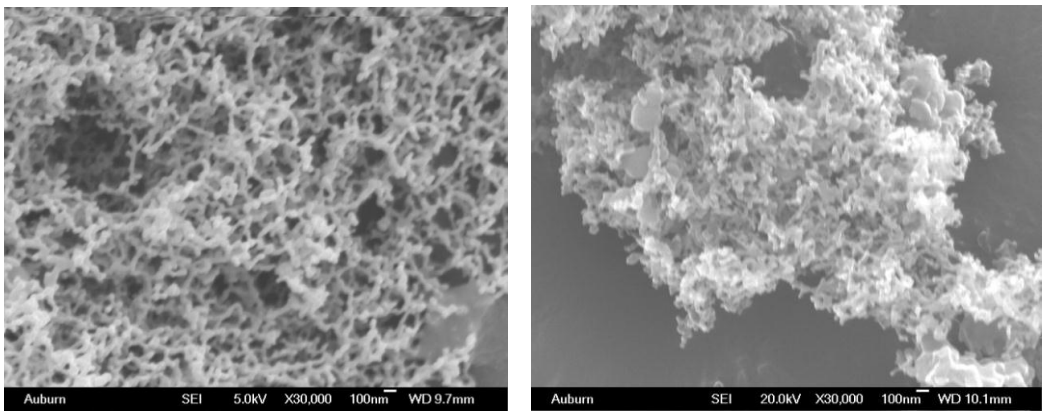

Figure I-2. Scanning electron micrograph of Drug-1 (left) and Drug-2 (right) nanoparticles produced from supercritical antisolvent process.